Evaluation of Striatin as a novel Microtubule Modulator

Dissertation

Zur Erlangung des Doktorgrades (Dr. rer. nat.)
der
Mathematisch-Naturwissenschaftlichen Fakultät
der
Rheinische Friedrich-Wilhelms-Universität Bonn

vorgelegt von

Linda Förster
aus
Köln

Bonn 2022

I Thesis origin and declaration

The work presented in this thesis was performed between February 2017 and June 2021 in the laboratories of Prof. Dr. Oliver Gruß and Prof. Dr. Walter Witke in the Institut für Genetik, which are part of the Mathematisch-Naturwissenschaftliche Fakultät, from the Rheinische Friedrich-Wilhelms-Universität Bonn in Germany. This work has been independently produced and written by myself. There are no other sources than the ones from the supplemented appendix and nothing else as the here mentioned resources and tools had been used. At the date when this thesis is submitted it has not been published somewhere else.

Promotionsgesuch eingereicht am: 24.08.2022

Tag des Kolloquiums: 13.01.2023

Erscheinungsjahr 2023

Die Arbeit wurde angeleitet von Prof. Dr. Oliver Gruß und angefertigt mit Genehmigung der Mathematisch-Naturwissenschaftlichen Fakultät der Rheinischen Friedrich-Wilhelms-Universität Bonn.

Prüfungskommission:

Vorsitzender: Prof. Dr. Peter Dörmann,

Gutachter/Betreuer: Prof. Dr. Oliver Gruß,

Gutachter: Prof. Dr. Walter Witke,

weiteres Mitglied: Prof. Dr. Gabriel Schaaf

II Index

Contents

III List of figures

IV List of tables

V Abbreviations

A	Ampere
A. nidulans	*Aspergillus nidulans*
Abb	Abbreviation
AcOH	Acetic acid
anti-ms	anti-mouse-Fc secondary antibody
anti-rb	anti-rabbit-Fc secondary antibody
Amp	Ampicillin
APC	Adenomatous-polyposis-coli
APC/C	Anaphase-promoting complex / cyclosome
APEX	Ascorbate peroxidase
APS	Ammoniumperoxodisulfat
ARPP19	CAMP regulated phosphoprotein 19
ATG	Methionin start codon
ATP	Adenosintriphosphat
AURKA	Aurora kinase A
AURKB	Aurora kinase B
BD	Binding domain
BIOID	Biotinylation IDdentification assay
BLAST	Basic local alignment search tool
BLOSUM	Blocks substitution matrix
bp	Base pairs
BRB80	Brinkley renaturing buffer 80
BUB1	Budding uninhibited by benzimidazoles 1 protein kinase
BUBR1	Mitotic spindle checkpoint protein kinase; budding uninhibited by benzimidazoles 1
BSA	Bovines serum albumin
Ca^{2+}	Calcium ion
C. elegans	*Caenorhabditis elegans*
CAM	Calmodulin (binding domain)
CAMKII	Calmodulin–dependent kinase II
CAN	Calcineurin
CCAN	Constitutive centromere-associated network
CCD	Charged-coupled device
CCT8	Component of the chaperonin-containing T-complex (TRiC)
cDNA	complementary DNA
CDC14	Cell division cycle protein 14,dual specificity potein phosphatase
CDC20	Cell-division cycle protein 20, initiates chromatid separation and entrance into anaphase as APC/C^{CDC20}
CDC25	Cell division cycle 25A,dualspecificityphosphatase
CDC55	PPP2R2A Serine/threonine-protein phosphatase 2A 55 kDa regulatory subunit B α isoform
CDH1	APC/C activator in the budding yeast *Saccharomyces cerevisiae*
CDK1	Cyclin-dependend kinase 1
CDK5RAP2	CDK5 regulatory subunit associated protein 2
CENP	Centromere protein
CEP	Centrosomal protein
CH	Calponin homology
CHO	Chinese hamster ovary
CKA	Connector of kinase to AP-1
CKAP / CH-TOG / XMAP215	Cytoskeleton associated protein 5
CLASP	CLIP-associated proteins
CLIP	Cytoplasmic linker protein
CM1	Centrosomin motif 1
CMM3 / PDCD10	Cerebral cavernous malformations 3 protein / programmed cell death 10
CMV	Cytomegalovirus over expression promoter
CNS	central nervous system
Co-IP	Co-immunoprecipitation
Conc	concentration
COPD	Chronic obstructive pulmonary disease
CPAP	Centrosomal protein 4.1-associated protein
CRISPR/Cas9	Clustered regularly interspaced short palindromic repeat/Cas9 complex
CSF	Cytostatic factor
CSPP1	Centrosome and spindle pole associated protein 1
CTTNBP2	Cortactin binding protein 2
Cy3	Cyanine dye 3
3D	Three dimensional
D. melanogaster	*Drosophila melanogaster*
ddH_2O	double-distilled water
DMEM	Dulbecco's modified eagle's medium
DAPI	4',6-Diamidino-2-phenylindole, nuclear staining
DMS	Dimethyl suberimidate
DMSO	Dimethylpimelimidate
DNA	Deoxyribonucleic acid
DPBS	Dulbecco's phosphate buffered saline (without $Ca^{2+}$and Mg^{2+})
DTT	Dithiothreitol
Dyna	Dynabeads
E. coli	*Escherichia coli*

EB	End binding protein
ECL	Enhanced chemiluminescence
EDTA	Ethylendiamintetraacetat
EGFP	Enhanced green fluorescent protein
EGTA	glycol-bis(β-aminoethyl ether)-N,N,N′,N′-tetraacetic acid
EM	Electron microscopy
EMBL	European molecular biology laboratory
EMI2	Early mitotic inhibitor 2, also known as FBXO43 or XERP1 in *Xenopus*
EMT	epithelial-mesenchymale transition
ENSA	Endosulfineα
ER	Endoplasmic reticulum
EST	Expressed sequence tag
et al.	*et altera*, and others
EtBr	Ethidiumbromide
etc.	*et cetera*
EtOH	Ethanol
e-value	Expected value, significance
FCS	Fetal calf serum
FDR	False discovery rate
fw	forward
g	gravity
gRNA	Guide RNA
G418	Geneticin
GCK	Germinal centre kinase
GCP	γ-ring complex protein
gDNA	Genomic DNA
Genta	Gentamicin
GFP	Green fluorescent protein
gp	Guinea pig
GS	Goat serum
GSK3B	Glycogen synthase kinase 3 β
GTP	Guanosintriphosphat
GW	Greatwall kinase (MASTL, Microtubule-associated serine/threonine kinase like)
h	Hour(s)
HASPIN	Histone H3 associated protein / haploid germ cell-specific nuclear protein kinase
HCG	Human choriongonadotropin
HCl	Hydrogenchlorid
HEPES	4-(2-hydroxyethyl)-1-piperazineethanesulfonic acid
HSS	High speed supernatant
hTERT RPE-1	Telomerase reverse transcriptase-immortalized retinal pigment epithelial cell line
HRP	horseradish peroxidase
HUGO	Human gene nomenclature committee
h.s./ h. sapiens	*homo sapiens*
ID	Immunodepletion
Ident	Identity
IF	Immunofluorescence
IgG	Immunoglobulin G unspecific antibody
IP	Immunoprecipitation
IPTG	Isopropyl-β-D-thiogalactopyranosid
IKBKE	Inhibitor of nuclear factor kappa-B kinase subunit epsilon
IMR-90	human embryonic lung fibroblast cell line
JNK	Core kinase from c-Jun N-terminal kinase (JNK) pathway
k-fiber	kinetochore fiber
Kana	Kanamycin
kB, kBP	Kilo base, kilo base pair
kDa	Kilo dalton
KD	Knock down
KIF	Kinesin family member
KMN	network of protein KNL1, MIS12, and NDC80
KNL1	Kinetochore-null protein 1
KO	Knock out
KT	Kinetochore protein complex
M-phase	In cell division (mitosis or meiosis)
MACF	microtubule-actin crosslinking factor
MAD1	Mitotic arrest deficiency 1
MAP	Microtubule-associated protein
MASTL	Microtubule associated serine/threonine kinase like (GW)
MCAK	Mitotic centromere-associated kinesin (KIF2C)
MEM	Minimum essential medium
MeOH	Methanol
MIB1	Mindbomb E3 ubiquitin protein ligase 1
min	Minute(s)
MINK1	Misshapen-like kinase 1
MIS12	MIND Kinetochore complex component homolog
mKate2	Monomeric kate2 fluorescent protein
MOB4	Mps one binder kinase activator-like 4
MP	Milk powder
MPF	Maturation promoting factor

MPS1	Monopolar spindle 1 kinase,
mRNA	messenger RNA
M. musculus	*Mus musculus*
MBS	Modified barth's saline buffer
MBT	Mid-blastula transition
MCS	Multiple cloning side
M	molar
mM	millimolar
MMR	Marc's modified ringer's buffer
mL	milliliter
MP	Milk powder
ms	mouse
MS	Mass spectrometry
MT	Microtubule(s)
MTOC	microtubule organizing center
MZT1	Mitotic spindle organizing protein 1 / Mozart1
NaOH	Sodium hydroxide
NEDD1	Neural precursor cell expressed developmentally down-regulated protein 1
Neo	Neomycin
NDC80	Kinetochore Complex Component Homolog/ HEC1 Highly expressed in cancer
NEB	Nuclear envelope breakdown
nm	Nanometer
NME7	Non-metastatic cells 7, protein expressed in (nucleoside-diphosphate kinase)
NP-40	Octoxinol 9 or nonidet P-40
NPL4	Nuclear protein localization 4 homolog (*S. cerevisiae*)
NUP	Nucleoporin
NTPs	Nucleotide triphosphate mixture containing adenosine, guanidine, uridine and cytosine
L	Liter
lacO	Lac-operon
LATS	Large tumor suppressor kinase
LC-MS/MS	Liquid chromatography–mass spectrometry/ mass spectrometry
LSS	Low speed supernatant
OD	Optical density
ORF	Open reading frame
ori	Origin of replication
p. a.	*pro analýzu*
PBS	Phosphate buffered saline
PCM1	Pericentriolar mass / material protein 1
PCNT	Pericentrin
PCR	Polymerase chain reaction
pH	*potential hydrogenii*
PIPES	piperazine-N,N′-bis(2-ethanesulfonic acid)
PFA	Paraformaldehyde
PMSF	Phenylmethylsulfonylfluorid
PMT	Photomultiplier tube
PLK	Polo-like kinase
PO	Peroxidase
POI	protein of interest
PolyA	Polyadenylation
ProtA	Protein A
PP1	Protein phosphatase 1
PP2A	Protein phosphatase 2 A
PP4	Protein phosphatase 4
PPI	Protein-protein interaction
PRC1	Protein regulator o fcytokinesis 1
PSP	Protein serine/threonine phosphatase
PT3	T3 Promoter
PT5	T5 Promoter
PT7	T7 Promoter
PTM	Posttranslational modification
RAN	RAS-related nuclear protein
RANBP	RAN binding protein
RAS	G-protein RAS (rat sarcoma)
rb	rabbit
RCC1	Regulator of chromosome condensation 1
rev	reverse
RHAMM	Hyaluronan-mediated motility receptor (HMMR), or RHAMM (receptor for haluronan mediated motility)
RIPA	Radioimmunoprecipitation assay buffer
RNA	Ribonucleic acid
(si)RNA/RNAi/shRNA	(small interfering) Ribonucleic acid depletion, small hairpin RNA
rpm	Revolutions/rounds per minute
RSA	Regulator of spindle assembly
RT	Room temperature
S. cerevisiae	*Saccharomyces cerevisiae*
S. pombe	*Schizosaccharomyces pombe*
SAC	Spindle assembly checkpoint
SAS	Spindle assembly protein

SDS-PAGE	sodium dodecyl sulfate-polyacrylamide gel electrophoresis
sec	Second(s)
SG_2NA	STRN3/Cell cycle S/G_2nuclear autoantigen
SGO2	Shugoshin2
SIKE1	Suppressor of IKBKE 1
siRNA	Small interfering RNA
sgRNA	Small guide RNA
SLMAP	Signaling lymphocytic activation molecule-associated protein
S. m.	*Sordaria macrospora*
SMC2	Structural maintenance of chromosomes 2
sol	Solvent, solution
SPD	Spindle defective protein
SSX2IP	Synovial sarcoma, X breakpoint 2 interacting protein
STIM	Stromal interaction molecule
Strep	Streptomycin
Strept	Streptavidin
STRIP1/2	Striatin-interacting protein 1/2
STRIPAK	Striatin-interacting phosphatase and kinase complex
STRN	Striatin
STRN3	Striatin3 / SG_2NA /SG2NA
STRN4	Striatin 4 / Zinedin
SV40 ST	simian vacuolating virus 40 small tumor antigen
T20	Tween® 20
TAE	Tris-acetat-EDTA
TBS	Tris-buffered saline
TEMED	Tetramethylethylendiamin
TFA	Trifluoroacetic acid
THOC	THO Transcription factor/nuclear export complex
+TIPs	Plus end tracking proteins
TNF	Tumor necrosis factor
TNIK	TRAF2 and NCK-interacting protein kinase
TOG	Tumor overexpressing gene
TRAF2	TNF receptor-associated factor 2
Tris	Tris(hydroxymethyl)-aminomethan
TPX2	Targeting protein for Xklp2
TUBA1A	Tubulin α-1A chain
TUBB	Tubulin β chain
TUBG1	Tubulin γ 1
TX-100	Triton X-100
WB	Western blot
WD repeats	Tryptophan-aspartate repeat domain
WDR8/WRAP73	WD repeat-containing protein WRAP73
WNT	Wg (wingless) int-1 signaling pathway
UFD1	Ubiquitin recognition factor in ER-associated degradation 1
UV	Ultraviolet
xl / X. laevis	*Xenopus laevis*
XL-177	*Xenopus laevis* skin keratinocytes
xt / X. tropicalis	*Xenopus tropicalis*
XB	*Xenopus* buffer
YAP	Yes-associated protein
ZIN	Striatin 4 / STRN4/Zinedin
γ-TURC	γ-tubulin ring complex
µL	microliter
µm	micrometer

VI Acknowledgements

I am deeply thankful to Prof. Dr. Oliver Gruß and Prof. Dr. Walter Witke. Both facilitated my work at the Institut für Genetik. They provided the foundation stones for the biological hypothesis for my *Ph. D.* thesis. Numerous scientific discussions and their many constructive comments have greatly improved this work. Foremost I would like to thank Oliver, who guided me through the topic's complexity. He was consistently patient, forgave mistakes, did the numerous corrections and he saw the potential of each individual result, even when it did not correspond to the expectation. Without his guidance, support and good nature, I would never have been able to fulfill this task and interpret the complexity of my topic. He helped me to master this important and future determinative time of my life. Furthermore I am incredible thankful to all the members of the Institute, alumni and even the students with lab rotation. All the people I met showed endless positive attitude to help each and every student. I want to emphasize the great work of the postdocs Dr. Maximilian Schilling and Dr. Pietro Pilo Boyl. Both of them invest a lot of time to explain complex scientific relationships from the bottom multiple times. All members of the Institute sacrificed their time in order to help me. Special thanks are regarded to Christoph Peter and Zhenzhen Chu, who had the same difficulties and were really encouraging and guiding persons during the whole project. I still feel guilty for all the days without a good functional frog egg extract and am really incredibly grateful that both of you kept calm and moved on. Moreover I would like to thank Gerd Landsberg who guided newcomers and managed the major task of the lab routine. Without his effort the lab would have never been able to function the way it did. A warm word of thanks also goes to the students I supervised, namely Nathalie Rieder and Chiara Schockhoven. Especially in the last year of my thesis their hard work encouraged me to manage this project. Last but not least I would like to thank my family, my friends and my boyfriend Sebastian. Their permanently cheering and backing helped me to manage this really striking period.

The more you know, the more you know you don't know.

Aristotle (384–322 BC)

VII Abstract

The dynamics of the cell cycle and cell division are governed by tubulin polymers, *i. e.* microtubules (MTs). Defects of MT assembly or disassembly lead to pathogenic cellular conditions, negatively affecting cell viability, cell shape, migration and genomic stability. Previously, our lab established a screen for so far unknown mitotic and meiotic MT modulators. In this project, I distinguish, characterize and localize novel MT associated proteins (MAPs) and MT modulators, including Striatin (STRN).

STRN is described as a regulating platform subunit in a kinase and phosphatase-harbouring complex called STRIPAK (Striatin phosphatase and kinase complex). A key component of this complex, Protein Phosphatase 2 A (PP2A), is known to play a major role in cell division progression also as MT dynamics regulator. In association with PP2A, STRN could function as a regulatory PP2A subunit for a tight posttranslational modification (PTM)-switch of yet unknown STRN interactors that function as MAPs. An interaction partner analysis by co-immunoprecipitation and binding partner analysis by mass spectrometry might address this question.

Indeed, the STRN interactome in my work shows multiple partnerships to known MAPs. I further compare *in vivo* models, like the embryonic IMR-90 fibroblasts cell line with cell cycle-arrested *Xenopus leavis* egg extracts and find STRN-related similarities. I analyze the consequences of the lack of STRN in both models and in different cell cycle stages. STRN depletion in mitotic *Xenopus laevis* extracts stabilizes spindle structures. In human embryonic lung fibroblasts a CRISPR knock out (KO) of STRN decelerates mitotic progression and the cells stay longer in G_2/M-, pro- and especially in metaphase. Together with my results various facts suggest STRN has different roles in the cell regarding MT dynamics and ciliogenesis.

1. Introduction

1.1 Microtubules (MTs) are essential for cell division

Eukaryotes complex cellular functions, such as cell division, are governed by dynamic cytoskeletal elements. A main cytoskeleton component, the microtubules (MTs), are responsible for nuclear positioning, assembly of cilia (ciliogenesis), corresponding cellular signaling, and segregation of chromosomes during cell division. Altered MT dynamics can lead to cell division defects, aneuploidy, reduced fitness, a longer generation time and cell death.

In 1835 Hugo von Mohl was the first one to observe cell division in green alga and in 1882 Walther Flemming, for the first time, termed the mitotic phases from observations in salivary gland cells[1,2]. An elaborate cell division includes prophase, prometaphase, metaphase, metaphase-anaphase-transition, anaphase, telophase and cytokinesis. In terms of my work, I speak of cell division in general, which is why I sum up mitosis and meiosis to 'M-phase'. In order to simplify or to categorize my results I declare G_2/M-transition, prophase, prometaphase and metaphase as M-phase entry, while metaphase-anaphase-transition, anaphase, telophase and cytokinesis sum up to M-phase exit.

In interphase, most MTs arise from the MT organizing center (MTOC), in which they are anchored on their minus ends. These organizing centers can have different forms like the animal centrosome, with centrioles or basal bodies, *i. e.* cylindrical tubulin structures. The pericentriolar material, PCM, assembles around centrioles. PCM and centrioles form the centrosome. The interphasic MTOC is generally close to the nucleus. From here, MTs can arrange to higher ordered structures that are reduced at the cellular periphery. In contrast, M-phase requires a completely rearranged MTOC and MT protein network. The objective of cell division is to split up the duplicated DNA from one cell into two cells.

At the time of DNA replication, the MTOC duplicates in most animal cells. When cell division starts, a cell arranges its previously duplicated MTOC as opposite-wise centrosomes. The centrosome is a cell organelle that consists of a dense matrix of centrosomal proteins. The centrioles are part of centrosomes and embedded in the centrosomal protein network, also known as pericentriolar material (PCM). Experimental data shows that centrosomes are not necessarily required for cell division[3]. So which role do centrosomes play? Mutants of *D. melanogaster* that do not have centrosomes can develop into morphologically normal adults[3].

In somatic cells the centrioles form cilia. The formation of cilia, ciliogenesis, occurs during G_1-phase of the cell cycle, whereas ciliary shortening and disassembly occurs at later steps in the cell cycle. Non-motile, primary cilia serve as antenna of the cell and can be used for sensing. Motile, secondary cilia play an important function *e. g*. in cleaning the respiratory system[4]. After centriole disassembly, the centrioles are duplicated in preparation for cell division. The older, *i. e*. mother centriole can be identified by its small appendages. The mother centriole always organizes more PCM than its orthogonally arranged daughter centriole. Centriole numbers are under tight control[5]. Within a centrosome, centrioles control cell polarity and asymmetric cell division[6]. Dysregulation of centromatrix proteins, for example upon mutation of their respective genes, can lead to proliferative abnormalities (cancer) or microcephalic phenotypes. At the primary structure level, many centromatrix proteins show structural similarities and often contain coiled-coil domains[7–13].

1.2 The microtubule-organizing center (MTOC) is responsible for the organization of microtubular structures

The centrosome as MTOC controls MT dynamics. The mitotic spindle and astral MTs nucleate from the two mitotic centrosomes. However, not all cellular divisions are depending on the existence of a centrosome. Both MTs and chromatin are restructured during cell division. It is believed that the essential role of spindle organization can be taken over by proteins and protein complexes of centrosomes even in the absence of a structured platform of a fully assembled centrosome.

MT-associated proteins (MAPs) play a major role in the PCM. This network matures and assembles during cell division, expands and increases in density for M-phase entry. A mitotic spindle forms as a bipolar structure, of which the poles are defined by the PCM, which regulates organelle trafficking, protein degradation and spindle assembly. For example, it consists of proteins that serve as nucleation seed for the start of MT growth. The best known nucleator of MTs is γ-tubulin. Since the mature PCM contains a dense, concentrated amount of MTs, it also houses a high concentration of MT dynamics controlling proteins. Purified tubulin has the capability to spontaneously nucleate on its own. There are multiple known and unknown factors that influence seed formation *in vitro*, like polymer growth, branching behavior and growth speed. MT tuning can occur in short, transient intervals during the cell cyle[14,15]. For cellular processes MT can constantly grow and shrink in an assembly-disassembly cycle known as dynamic instability[16]. MAPs can accelerate or decelerate this process. MAPs describe all proteins that bind to either monomer subunits of α- or β-tubulin or polymerized MT. Multiple processes are covered by tight MAP control, like ciliogenesis, DNA congression and nuclear positioning. These proteins control and organize tubulin poly- and depolymerization. As one can imagine, the whole network of interacting MAPs plays a crucial role in fine tuning of MT dynamics. They are tightly regulated by a number of mechanism, (including PTMs), to ensure the appropriate dynamics of the system[17–19].

However, our knowledge about regulation of MAP and consequently MT dynamics is still full of gaps, and one does not know if PTM modulators or which ones (kinases? phosphatases?) activate MAPs and consequently control MT dynamics. Although a number of mitotic MAPs have been identified, many more remain to be discovered. Proteomics help to identify novel MAPs, to address how they are regulated and to characterize their role in MT dynamics. Moreover, many MT modulators in interphase and mitosis are spatially and temporally regulated. When a protein is suspected to have a MT modulating function, interaction and localization studies during cell cycle processes give insight into its potential role as MAP. A crucial factor for MTs growth and rearrangement in M-phase is the cell cycle dependent modulation of MAPs. Not only the protein level of MTs ‘tuner’ increases during centrosomal maturation, but also the special modification that improves MAP ‘fitness’, like activity and substrate specificity. The MAPs are therefore targeted by posttranslational modifications (PTM).

The PTMs are responsible for allosteric control of protein function, checkpoint signaling, and initiation of signaling cascades. PTMs comprise phosphorylation, polyadenylation, ubiquitinylation, SUMOylation and *vice versa* the removal of these modifications[20]. Phosphorylation is one of the major mechanisms how cells modulate molecular entities and activities. A phosphorylating protein is called kinase, while a dephosphorylating protein is called phosphatase. The phosphatases follow several structural folds and catalytic mechanisms, while the kinases work with one single structurally defined mechanism.

1.3 MTs dynamics are controlled by phospho-regulation of Microtubule-associated proteins (MAPs)

Phospho-modification generally occurs at hydroxyl groups of amino acids, mostly serine and threonine. Not as common as amino modifying kinases are lipid kinases and carbohydrate kinases. The phosphatase cleaves a terminal phospho-ester of an amino acid and bond energy can be released. Phosphorylation is a less favorable reaction because kinases are mostly driven by the ATP/ADP ratio within cells[21]. Since the phosphate group contains negative charges, phosphorylation can cause drastic sterical changes and thereby alter protein-protein binding. Together, kinases and phosphatases guarantee a tightly controlled interplay of phospho-modification. Conformational changes are essential for the manifold interplay that handles the restructuration during cell cycle and cell division progression. Thus, protein serine/threonine kinases and phosphatases can switch between an ‘on’ and an ‘off’ state of target phospho-proteins.

Many kinases and phosphatases are adjustable screws and thus also critical elements in checkpoints and rate-limiting processes. Most mitotic proteins undergo regulation in preparation for mitosis, often governed by reversible modification. In 2019, 89 protein phosphatases and 518 kinases were documented in humans[22,23]. Obviously, these numbers are growing rapidly, and cellular mechanisms are controlled by a higher number of kinases than phosphatases. A large range of kinases are counteracted by a few phosphatases. The kinases often are highly substrate specific while the phosphatases cover a broad range of targets[23,24].

Many kinases and phosphatases are vital and classified as tumor suppressors while others are classified as oncogenes. Their tight linkage for cell cycle control mechanisms leads to the risk for cancerogenic cell transformation. Activation of oncogenes or the inactivation of tumor-suppressor genes lead to cellular degeneration. Both phosphatases and kinases are thus promising therapy drug targets since their active sites can be manipulated by chemicals that can serve as promoters or inhibitors.

For example, protein phosphatases PP1 and PP2A are examined as targets for therapies against Alzheimer's disease, asthma, cancer, tumor, chronic obstructive pulmonary disease (COPD) and Crohn's disease[25–28]. Both, PP1 and PP2A are crucial players in mitotic entry and exit. The phosphatase enzyme family specificity, time-dependent localization and fine tuning of target phosphorylation state has been described in recent research by the Saurin lab[29–31]. The authors found that PP1 and PP2A have complementary functions during the mitotic entry and exit. Major cell cycle-related phosphatase actions in mammals are accomplished by the four phosphoprotein phosphatases (PPP family), including PP2A, PP1, PP4 and PP6[32–34]. Already in 2000 Hiraga *et al*. observed that PP2A co-sediments with polymerized MT[35]. Inhibition of PP2A destabilizes MTs and leads to premature mitosis in neuronal cells[36]. PP1 and PP2A show different phospho-dependency and regulation requirements at the kinetochore complex[29], *i. e.* the interaction platform of MT and chromatids in mitosis (see below).

The counteractor of the phosphatases are the kinases. They include calcium-calmodulin–dependent kinase II (CAMKII), CDK (cyclin-dependent kinase 1 and 2), Aurora (A and B), PLK (polo-like kinase) family, BUB1, HASPIN and MPS1. While AURKA mainly acts in mitotic entry, AURKB partly manages mitotic exit. Some kinases act over a variety of cell cycle stages, like PLK1, which controls different set screws of M-phase entry and exit[7-10]. Several kinases modulate MAPs, and the MAPs regulate MTs dynamics during M-phase. In M-phase entry the MTs pull the DNA to the spindle equator, known as congression. Tight yet highly dynamic control of important cell cycle regulators for this process play an essential role in cytoskeletal organization, and thereby have an effect onto the behavior of the MTs[41].

In order to guarantee an even distribution of genetic information after cell division, the chromatin DNA fibers change their conformation by being folded into consecutive higher-order-structures. This process is controlled by kinase and phosphatase PTM. Genome condensation includes the chromosome folding pentameric protein complexes condensin and cohesin that form ring structures around the DNA.

Another MAP family that is controlled by kinase and phosphatase PTMs are the motor-proteins. They actively move under ATP-consumption within cells. Motor-proteins are responsible for cargo transport or flagella motion. One motorprotein family, the kinesins form a subgroup called chromokinesins. Chromokinesins are known to have a DNA-binding domain. Without the PTM-driven kinesin superfamily protein 4 (KIF4) chromosomes lose their characteristic 'X' shape M-phase morphology[42–45]. During DNA congression HASPIN kinase phosphorylates histone H3, thereby Aurora B kinase (AURKB) is recruited to the inner M-phase spindle[46]. During spindle assembly, AURKB hyperphosphorylates multiple substrates in the spindle midzone, like NDC80 (or HEC1). This decreases NDC80's affinity to MTs. All chromosomes are bioriented and aligned at the metaphase plate. This describes the morphology when MTs reach from centromeres (and kinetochores) with their plus ends to minus ends at centrosomes.

The kinetochore complex is a disc-shape supramolecular structure. It assembles around the centromere of the condensed chromosomes in a final step of prometaphase. Kinetochore assembly is controlled by kinases and phosphatases. The final function of kinetochore assembly peaks in metaphase when all pairs of sister chromatids have paired, and a complete bipolar mitotic spindle has formed. The MT minus ends are anchored at the centrosome and the plus ends at the kinetochore protein complexes. With progressing to segregation, the MT k-fibers are shortened, and the sister chromatids move towards to the poles while maintaining attachment to the kinetochore complex. Often the mitotic spindle is then further elongated. In flies, worms and yeast the MAP kinesin-5 (KIF11 or EG5) regulate spindle elongation by restricting the rate of pole–pole separation[47–50]. A phospho-dependent mechanism allows AURKB, and its antagonizing phosphatases PP2A and PP1 to control correct k-fiber MTs attachment[51,52]. The spindle midzone is stabilized by a kinetochore-associated AURKB phosphorylation gradient. The gradient is counteracted by phosphatase PP1 and PP2A.

Dephosphorylation leads to metaphase-anaphase transition. In *Xenopus laevis* cell free extracts, removal of AURKB by the ubiquitin ligase complex ATPase P97, UFD1 and NPL4 is required for the release of metaphase state and anaphase progression[53]. The sister chromatid segregation marks the beginning of M-phase exit with the activation of phosphatases, chromosome decondensation and nuclear envelope reassembly.

1.4 Protein Phosphatase 2 A (PP2A) is a master regulator of the cell cycle

The PP2A phosphatase is one of the most complex serine/threonine phosphatase family members, that is involved in neuronal stabilization, cardiac muscle function and MT-arranged cycle activities[54]. Special subunit-depending isoforms are discussed being involved in chromosome decondensation[55]. The holoenzyme is a trimeric complex, which consists of a structural subunit PP2A A, a catalytic subunit PP2A C, and a regulatory subunit PP2A B[56,57]. The PP2A A and PP2A C domains only consist of an α- or β-variant, while the PP2A B subunit is a variable building block consisting of four different groups B, B', B'' and B'''. The schematic figure 1 shows each B-subunit has several gene products that have their own regulatory interactions. The latter B''' variant includes the here discussed STRN family members, as part of the PP2A complex.

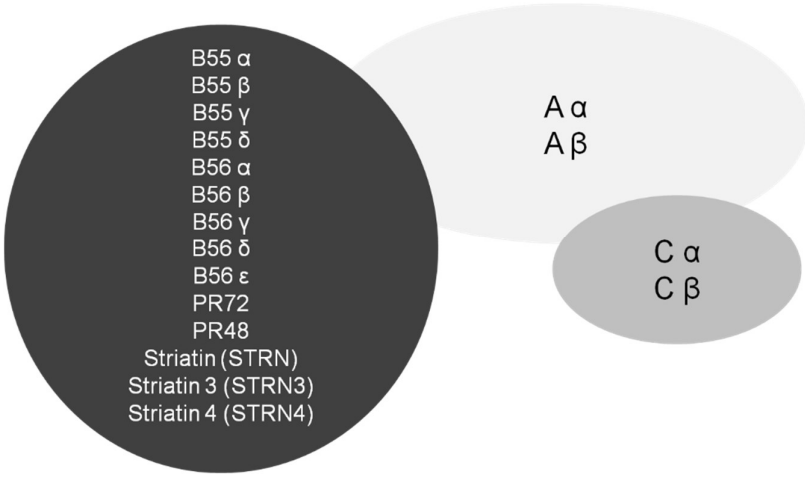

Figure 1: The PP2A complex and its different variable subunits. The holoenzyme of PP2A consists of a regulatory B, catalytic C, and scaffold A subunit. The 65 kDa A and the 36 kDa C subunit form the core enzyme[58]. The highly variable B subunit enables the high substrate specificity for a broad range of targets. The B subunits differ considerably in their primary amino acid sequences and expression levels are tissue specific[59,60]. The STRN family members are categorized as PP2A B''' subunit and they split up into several splicing-related isoforms[61].

PP1 and PP2A are suspected to antagonize M-phase kinase CDK1, *e. g*. by dephosphorylation of lamins in nuclear envelop reassembly during mitotic exit[62,63]. The kinase CDK1 is a key player in cell cycle regulation. Its regulatory subunit, the protein cyclin controls progression of a cell through the cell cycle by activating cyclin-dependent kinase (CDK). Research in *Schizosaccharomyces pombe* found a feedback loop mechanism, in which CDK1 inactivates WEE1. In regard to maintain interphase as a G_2/M-phase checkpoint, WEE1 is a kinase that phosphorylates CDK1. This inhibits the entry into mitosis[64].

As a CDK1 antagonist, the WEE1 kinase checkpoint verifies if the cell is fit (DNA damage) and well developed (cell size) enough for entering the division phase. PP2A B55 dephosphorylates two kinases: WEE1 and MASTL, keeping both inactive for mitotic progression[65,66]. Depletion of PP2A B55 regulatory subunit or scaffolding subunit PP2A Aα leads to failed chromatid segregation and delayed mitotic exit[62]. In yeast, mitotic entry PP2A B55 is inhibited by phosphorylation of CDK1[67,68]. In vertebrates PP1, PP4 and PP2A B55 are known to counteract phosphorylation of CDK1[69]. Similar to other feedback loops, inactivation of CDK1 leads to PP2A B55 activation for mitotic exit. PP2A B55 is part of centrosome separation, centriole duplication and centrosome disassembly[70–72].

In this case, Cyclin B (mitotic cyclin) concentration remains on a high level and CDK1 activity is maintained[73,74]. CDK1 has a broad range of substrates that control cell cycle events via their PTM[75]. Proteasomal degradation of Cyclin B deactivates the M-phase specific kinase CDK1. In interphase CDK1 is located in the nucleus. In the germ cell development preceding fertilization, *i. e*. meiosis, oocytes are stimulated by hormones and perform a maturation process that includes transcriptional silencing and germinal vesicle breakdown (GVBD).

In mitosis the activity of CDK1 increases by the progression of the nuclear envelope breakdown (NEBD). In both, GVBD and NEBD the nucleus is disassembled and the DNA exposed to the cytosol[76]. CDK1-Cyclin B interaction was first defined by Masui and Markert as cytoplasmic activity in *Xenopus laevis* eggs[77]. In frog oocytes the complex is known as maturation promoting factor (MPF). The MPF describes an activity that causes complete maturation of oocytes and cell cycle arrest. The mature ovum is arrested in metaphase of the second meiotic division. The very first cell division is the first mitotic division after fertilization. Multiple aspects of embryonal cell division are still enigmatic.

Another phosphorylation target of CDK1 is the securin-separase complex. When phosphorylation by the kinase stops due to anaphase-promoting complex/cyclosome (APC/C) Cyclin B degradation, the complex is not maintained. The APC/C is the responsible ubiquitin-ligase that ubiquinylates cell division specific proteins. Securin will be labeled by APC/C for proteasomal degradation. The protein securin releases and thereby activates separase, a protease that degrades the cohesin rings that link the two sister chromatids[78]. APC/C also labels Cyclin B for proteasomal degradation and the cell cycle can progress to interphase. Thereby the conserved APC/C enzyme is responsible for the M-phase exit[79–81].

The E3 ubiquitin ligase APC/C is activated and the cell is released from metaphase to the mitotic exit and anaphase, and two new genetically identical cells arise[82]. By this the cell reactivates phosphatases, which initiate metaphase-anaphase transition and M-phase exit. The separated sister chromatids move from the center of the spindle in the metaphase plate towards opposite poles of the cell. In budding yeast, chromatid segregation is driven by the phosphatase CDC14. The dual-specific enzyme CDC14 manages dephosphorylation of the CDK1/Cyclin B complex and kinetochore and spindle-associated proteins[83–86]. While CDC14 plays an essential role in yeasts, it is available but not necessary in vertebrates. Some higher plants, rhodophytes, and slime molds even lost the gene completely[87].

The so called spindle assembly checkpoint (SAC) is tightly linked to the kinetochore protein complex and inhibits the APC/C as long as the checkpoint criteria are not fulfilled[88]. This inhibition maintains the metaphase state and sister chromatids stay coherent. Together the SAC and APC/C are known as mitotic checkpoint complex (MCC). In this complex APC/C is blocked by SAC dependent modulation. When MTs are unattached to the kinetochore, the SAC protein complex MAD1-MAD2 inhibits ubiquitinylation by the APC/C[89–92]. In order to guarantee a highly dynamic progression the APC/C has co-activators which facilitate the recruitment of substrates. A central APC activator is CDC20, which in its active form is known as APC/C^{CDC20}. When the SAC criteria are fulfilled and all MT attach to the kinetochore, MAD2 releases from MAD1 and then fails to bind and to inhibit CDC20[91,92].

Regarding mitotic entry, it is known that the mitotic checkpoint kinase BUBR1 together with PLK1 recruits the PP2A B56 subunit for chromosome congression and kinetochore-localization[54,93,94]. The ring's degradation is inhibited and the sister chromatids keep together during mitosis[95]. Recent literature has suggested PP2A B56 interaction to the protein shugoshin2 (SGO2), known as the protector of centromeric cohesin, which stabilizes the metaphase plate[30,96]. While PP2A B56 is an important regulatory subunit for spindle stabilization and localized at the kinetochore complex, PP2A B55 (or CDC55, SUR-6, B55) is important for metaphase-anaphase transition and mitotic exit, and found at the spindle poles[97].

PP2A B55 is hypothesized to target many regulators of centrosomal assembly and disassembly such as CDK5 regulatory subunit-associated protein 3 (CDK5RAP2), CEP192 (SPD-2 in *C. elegans*), PLK1, and Aurora A kinase[72,98,99]. In the embryonic system of *Xenopus laevis* (meaning the first cell divisions after fertilization of the egg) PP2A B55 dephosphorylates CDK1 and Cyclin B is released for APC/C ubiquitinylation and proteasomal degradation[68].

Observation in the embryonic nematode *C. elegans* showed that the centrosomal proteins SPD-5, RSA-2 and RSA-1 form a complex and recruit the PP2A complex to centrosomes, where PP2A accumulates[100]. The depletion of PP2A B55 slows down the post-mitotic degradation of centrosomal scaffold integrated SPD-5 in the worm embryos and does not change SPD-5 overall concentration, as SPD-5 levels are relatively constant throughout the cell cycle[72,101]. During mitotic entry PP2A B55 generates motor protein dynein-mediated force with centrosome-nuclear envelope cohesion[70]. MT-mediated pulling forces are essential for chromosome segregation and destabilize the SPD-5 PCM clusters[72].

Previously, our lab found the PP2A B subunit STRN upregulated in *Xenopus laevis* M-phase arrested embryonic egg cytosolic extracts. This fact gives reason to assume a STRN regulated cell division process in early embryogenesis[102]. The following section will outline why the previously discussed (embryonal) cell cycle and division-control mechanisms of PP2A might be true for PP2A B subunit STRN.

1.5 Striatin (STRN) is a B regulatory subunit of PP2A

The protein STRN and its family members are known under the HUGO (Human Gene Nomenclature Committee) symbol STRN. The other two members are S/G_2 nuclear autoantigen known as SG_2NA (STRN3) and Zinedin (STRN4 or ZIN). The protein family name is referred to its first discovery in the dorsal striatum of complex eukaryotes.

During cell division the interphase MT reorganize into the mitotic spindle. Organization of this assembly and controlled spindle scaling is still poorly understood and STRN or superior STRN-associated complexes could enable defined tuning of essential MAPs.

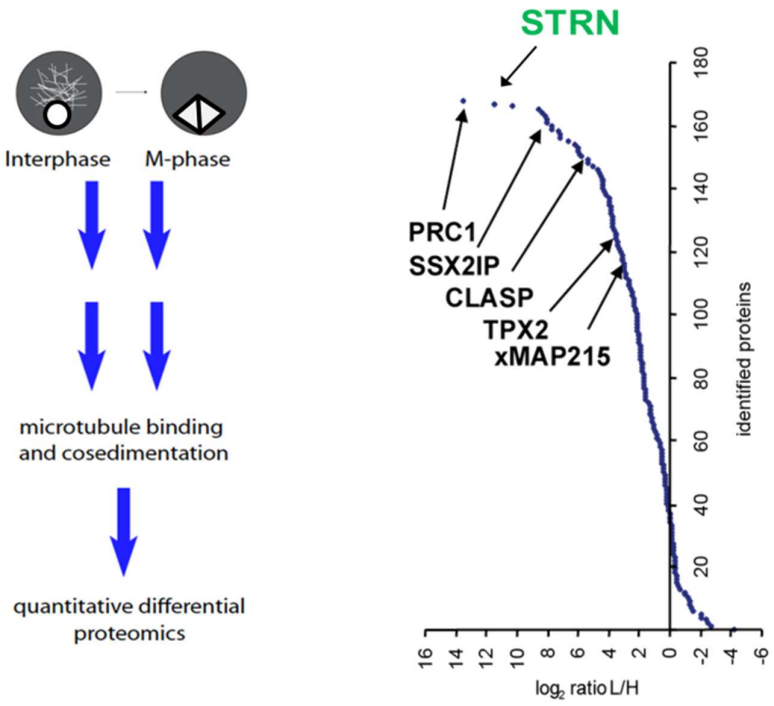

Figure 2: A cell cycle stage comparative analysis for novel MT associated proteins (MAPs) revealed STRN as putative candidate. Results from previous work found STRN upregulation in *Xenopus* CSF extracts upon M-phase remodeling. On the left the plot shows the workflow how potential novel MAPs can be found: Native MT co-sedimentation and purification was performed here for a MAP-specific screening with mass spectrometry analysis. On the right the plot shows the results from a five times repeated mass spectrometry screen. In this list of known and unknown MAP candidates STRN yielded the second highest score[102].

In previous work of my lab a method to pellet polymerized MT was used in order to analyze the MAP co-sediment[102]. This screening was done in a comparative manner between *Xenopus laevis* stage VI oocyte extract, which is arrested in late Interphase (G_2), and mature M-phase-arrested CSF egg extract[103]. Our lab made use of differential protein labeling in combination with standard mass-spectrometry analysis in order to quantify the two distinct cell cycle stages.

The taxol treated extracts stabilize the MT cytoskeleton against depolymerization because of a conformational change in the preformed MT lattice. This allowed co-sedimentation of MT and natively bound MAPs. The MAP proteome showed a rearrangement and upregulation of proteins to control MT behavior (shown in figure 2). An upregulation of centrosomal factors was detectable in the acentrosomal system like the *Xenopus laevis* egg extract[102]. The analysis from our earlier paper revealed potential MAP candidates for further analysis[102]. The plot in figure 2 summarizes five measurements and shows that STRN is a top-candidate for MT modulation.

Table 1: STRN transcripts splice variants and isoform alignments. Each transcript listed here encodes a human STRN family member protein. The human genome has 17 different predicted coding possibilities for STRN family members. The protein of interest in this work is upper STRN-1. The table shows all possible relatives of STRN-1 aligned to it in order to show the similarities between the family members. The main family members STRN, STRN3 and STRN4 show a strong conservation among each other.

Human splice variant ensembl-ID	UniProt Protein-ID	Length &mass	Alignment to STRN-1
STRN-1 **ENSP00000263918** **ENST00000263918**	**O43815-1**	**780 aa** **86,1 kDa**	
STRN-2 ENSP00000368513 ENST00000379213	O43815-2	731 aa 80,8 kDa	Query cover 100% Evalue 0 Identity 94%
SG_2NA STRN3-1 ENSP00000350071 ENST00000357479	Q13033-2 $SG_2NA\beta$	797 aa 87,2 kDa	Query cover 62% Evalue 0 Ident 71%
STRN3-2 ENSP00000347909 ENST00000355683	Q13033-1 $SG_2NA\alpha$	713 aa 77,7 kDa	Query cover 96% Evalue 0 Ident 65%
STRN3-3 ENSP00000452092 ENST00000556577	H0YJT2	172 aa 18,6 kDa	Query cover 35% Evalue $2x10^{-40}$ Ident 43%
STRN3-4 ENSP00000452542 ENST00000554991	H0YJZ4	139 aa 14,6 kDa	Query cover 25% Evalue $2x10^{-36}$ Ident 45%
STRN3-5 ENSP00000451233 ENST00000555152	G3V3G7	112 aa 12,8 kDa	Query cover 17% Evalue $5x10^{-47}$ Ident 68%
ZIN STRN4-1 ENSP00000263280 ENST00000263280	Q9NRL3-1	753 aa 80,6 kDa	Query cover 93% Evalue 0 Ident 51%
STRN4-2 ENSP00000375777 ENST00000391910	Q9NRL3-3	760 aa 81,3 kDa	Query cover 93% Evalue 0 Identity 51%
STRN4-3	Q9NRL3-2	257 aa 28,1 kDa	Query cover 33% Evalue10^{-36} Ident 38%
STRN4-4 ENSP00000440901 ENST00000539396	F5GYK2	634 aa 68,6 kDa	Query cover 86% Evalue 0 Ident 48%
STRN4-5 ENSP00000471354 ENST00000593979	M0R0P4	139 aa 15,3 kDa	Query cover 13% Evalue $5x10^{-36}$ Ident 64%
STRN4-6 ENSP00000469279 ENST00000596012	M0QXN2	73 aa 8,4 kDa	Query cover 9% Evalue 10^{-29} Ident 66%
STRN4-7 ENSP00000470040 ENST00000597063	M0QYS2	115 aa 12,7 kDa	Query cov 13% Evalue $2x10^{-36}$ Ident 64%
STRN4-8 ENSP00000472429 ENST00000597021	M0R2A7	103 aa 11,6 kDa	Query cover 12% Evalue 10^{-36} Ident 64%
STRN4-9 ENSP00000470634 ENST00000594287	M0QZM0	317 aa 34,2 kDa	Query cover 39% Evalue $2x10^{-58}$ Ident 58%

STRN4-10 ENSP00000472938 ENST00000600615	M0R317	198 aa 20,9 kDa	Query cover 40% Evalue 10^{-84} Ident 84%

The relationship of the STRN family members was discovered in 2000 with expressed sequence tag (EST) data bases, antibody based techniques and Ca^{2+}-dependent PP2A and CAM-related analysis[104,105]. Various papers showed STRN orthologues in fungi (STRA, PRO11), nematodes (CASH-1), and fruit fly (CKA)[106–108] while STRN orthologues in prokaryotes are not known so far.

The highly homologous STRN family members are not known to have an intrinsic catalytic activity. It is rather suggested that STRN family members serve as scaffold binding platforms and regulatory units for several intervening active enzymes. Proteins that serve as anchors for binding partners are common in regulated cellular processes, like the kinetochore complex component MIS12, a protein essential for chromosome alignment and segregation[109]. In a kinase cascade phosphorylation AURKB phosphorylates MPS1 kinase, which then can activate KNL1[110]. Only active KNL1 can bind to MIS12 platform protein and form the kinetochore. An analogue phosphatase-related process might be hypothesized for STRN binding partners.

All STRN family members are highly conserved and share four domains with characteristic protein-protein interactions: As figure 3 shows, they consist of a caveolin-binding domain, a coiled-coil domain, a calmodulin (CAM)-binding domain, and a tryptophan-aspartate (WD)-repeat domain[104,111]. The CAM-binding domain makes them Ca^{2+}-ion concentration sensitive. They exhibit MAP typical features, like conserved structure, coiled coil domain-dependent interactions, and coiled coil domain-dependent homo-, di- or oligomerization.

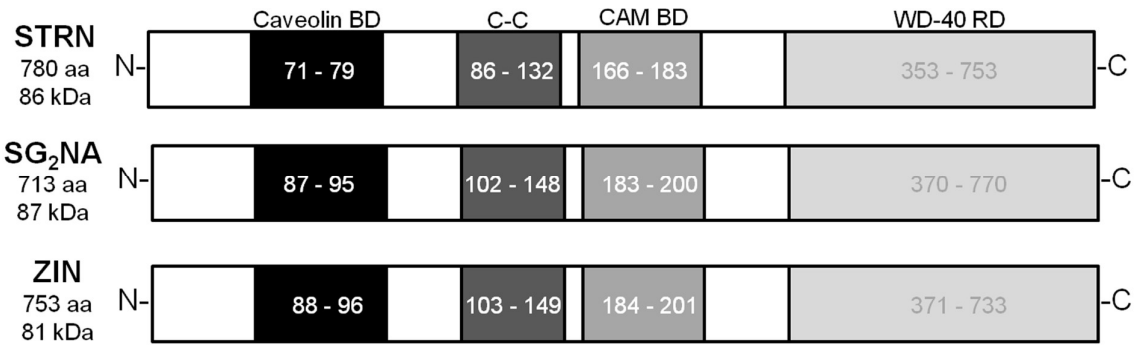

Figure 3: STRN family members and the STRN protein. The STRN family includes STRN, SG_2NA (STRN3) and ZIN (Zinedin/STRN4). Each member consists of several isoforms resulting from alternative splicing and mRNA editing[112,113]. All family members are conserved, consist of the same protein domains and show similar interaction partners. In recent studies, STRN3 is described as organizing center of the STRIPAK complex formation[114]. BD = Binding domain, C-C = coiled coil, CAM = Calmodulin, WD-40 RD = tryptophan-aspartic acid (W-D) dipeptide repeat domain.

Table 1 describes several STRN family member transcripts and isoforms. Most of them arise from alternative splicing. It is not clear which of them result in stable proteins or if a specific isoform occurs only short-lived[115]. Already published experimental data indicates the importance of STRN family members: For example, depletion of STRN family members can alter tight junction protein interaction of ZO-1 and F-actin localization in epithelial PC12 cells[116].

One close relative of STRN is STRN3, or SG_2NA, with 71% sequence identity to STRN in humans. This protein is upregulated from S- to G_2-phase during the cell cycle[117,118]. Recent studies show that SG_2NA can protect the mitochondrial membrane from oxidative damage and that it is involved in maintaining endoplasmic reticulum (ER) homeostasis[119,120]. The protein SG_2NA is known to be ubiquitously expressed in higher concentrations in a wide spectrum of tissues and is thereby the best described STRN family member with multiple functions. Previously published data have already verified that STRN3 dysregulation has an effect on cell cycle duration: Downregulation of SG_2NA with shRNA in mouse NIH3T3 cell line showed G_1-phase extension while over expression of STRN3 extended G_2-phase[121]. The molecular mechanism behind this effect is still enigmatic. It is likely that STRN concentration change has a similar effect.

The third family member STRN4 or Zinedin (named after a famous soccer player) is primarily described to be in high concentration in brain tissue. Data from proteinatlas.org shows a ubiquitous expression pattern of low STRN4 levels in broad spectra of tissues. A publication of 2017 found STRN4 to be upregulated in dendritic spines, when synaptic ion receptor activation is induced[122]. There is 51% sequence similarity between human STRN and STRN4.

Early publications described STRN to be predominantly expressed in the central nervous system (CNS)[123]. One of the first STRN-related experiments with oligonucleotide gene silencing showed, when STRN is downregulated, a dysregulated growth of dendrites, but not neurons in rats[124]. Other studies found that STRN downregulation results in increased dendritic complexity and an increased density of dendritic spines[125]. Therefore, STRN is known as regulator of neuronal development in striatal neurons. Aside from the brain, STRN could be also found in tissues like lung, liver, kidney, skeletal and cardiac muscle, testis, B and T lymphocytes, and fibroblasts[104,105,123,126].

STRN is primarily a cytosolic protein but also has the potential to occur membrane-bound. Published data shows that STRN localizes in organelles like the endoplasmic reticulum (ER), the nuclear envelope, the autophagosomes and (suggesting MT modulation) the centrosomes[106,107,127]. In 2018, in scope of a bioinformatical mass screening from human gene expression omnibus data, key genes, micro RNAs and transcription factors show that STRN down-regulation influences neuron projections and generates intracranial aneurysm[128]. A study in human and heterozygous mice shows STRN dysregulation is associated with salt sensitive blood pressure. The paper claims that STRN activates the mineralo corticoid receptor, which maintains sodium and water homeostasis[129]. Another study in breeded boxer dogs found frequent association of 8 bp deletion in the 3′ UTR of the STRN gene with dilated cardiomyopathy[130].

Further literature described that STRN co-localizes with MT in HEK293T cells. The research of Kaźmierczak-Barańska *et al*. shows STRN under representation leads to MAP2 phosphorylation and MT depolymerization. This caused the cells to stay in G_0/G_1-phase[131,132]. A direct interaction between STRN and MAP2 has not been confirmed yet. In the scope of the microscopy experiments of Kaźmierczak-Barańska *et al.* different STRN staining patterns could be observed depending on agent addition, like nocodazole[131]. Nocodazole is known to interfere with the polymerization of MT by binding to β-tubulin and stimulating its GTPase activity. The cell enters mitosis but MT cannot form metaphase spindles and the cell does not cross the spindle assembly checkpoint. This causes the cell to arrest in prometaphase[133]. No correlation between MT polymerization and STRN is described yet.

Ponniah *et al.* created a $STRN^{(-/-)}$ conditional floxed KO in mice. This KO restricts their perception by having an effect on their hearing. The authors suspect a STRN-PP2A regulatory function and suspect STRN lack disrupts the phosphorylation patterns that are essential for the cochlea and the organ of Corti. A previous paper already explained the significance of phosphorylation patterns in the sensory hearing organ[134–136]. In wild type mice, the authors were able to verify Adenomatous-polyposis-coli (APC) and epithelial cell-cell tight junction protein ZO-1 interaction to STRN. Both play a role in the WNT/β-Catenin signal transduction pathway and actin cytoskeleton management and both are phosphorylation-sensitive in a PP2A-dependent manner[116,137,138].

The WNT/β-Catenin signaling pathway includes manifold proteins and is essential for embryonal development. In the publication of Ponniah *et al.* STRN4 was not upregulated in the STRN KO mice. Although all STRN family members are known to interact with PP2A, it is not known if they are interchangeable regarding the compensation of defects.

1.6 STRN serves as a platform for protein complexation

STRN tends to form a high molecular weight complex with distinct binding partners[56]. The STRN family members interact with PP2A subunits and are themselves a regulatory subunit PP2A B'''. In 2009, Goudreault's tandem affinity purification experiment verified not only STRN as part of the PP2A complex, but also described for the first time STRIPAK components as part of a superordinate interaction network[139]. All STRN family members are known to serve as a platform for STRN-interacting phosphatase and kinase (STRIPAK) complex assembly[56,139–142]. Which STRN family member is integrated as STRIPAK component appears to be time and tissue specific.

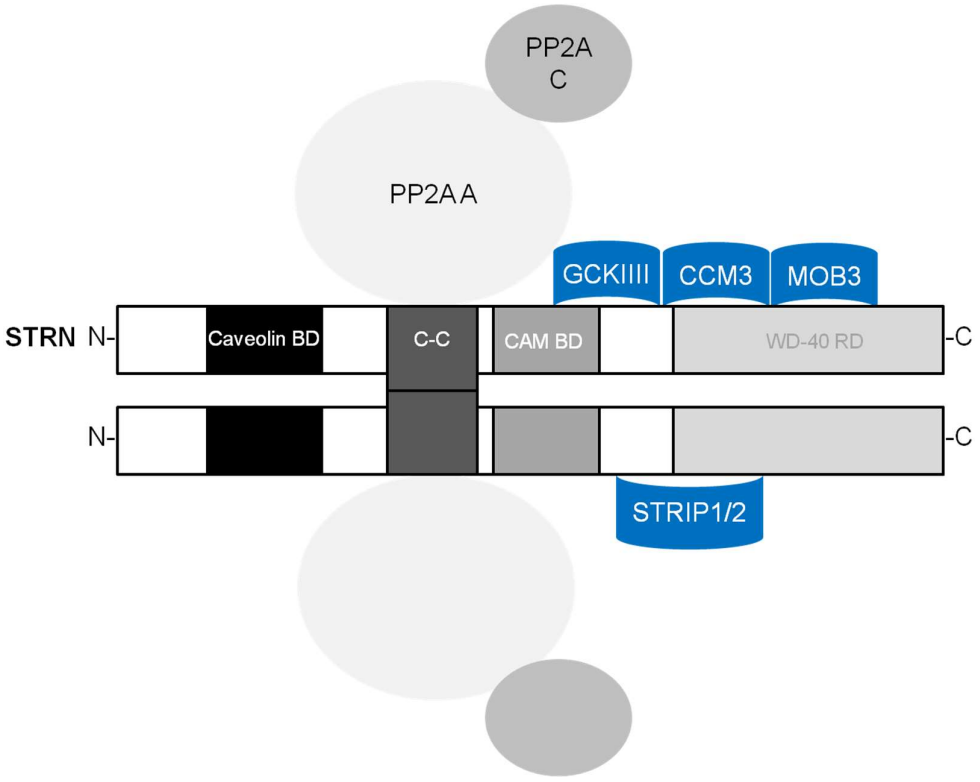

Figure 4: The STRIPAK (STRN-interacting phosphatase and kinase) complex and its core components[56]**.** This thesis focuses on STRN. STRN is described as binding platform for several kinases (like GCKIIIs) and PP2A phosphatase scaffold with its catalytic subunit. This fascinating interaction delivers a putative mechanism how the cell cycle progression could be precisely and specifically regulated in space and time.

Subsequent publications confirmed many of the proteins they found. STRIPAK core components include a STRN family member, the cell cycle controlling core phosphatase PP2A (A and C subunit), different kinases from the GCK family and other binding partners, such as STRIP1/2, CTTNBP2, SIKE1, TRAF3IP3, CMM3, and MOB4[56,139,140]. These findings caused several labs to check the regulation, activation, inhibition and dysfunction of this interaction network. The advantage of complex formation is a proximate interplay and sensitive specific regulation[143,144]. A detailed list of currently known STRIPAK components is presented in table 2.

One of the major STRIPAK and STRN family associated proteins is STRIP (Striatin-interacting protein). In human there are two STRIP genes (STRIP1 and STRIP2), while in yeast, worm and fruit fly only one is found. A mass spectrometry screen of proteomic interaction networks in 2012 found an interaction between STRIP1 and KATNAL2[145]. KATNAL2 (Katanin p60) is a MAP that is important for ATP-depended MT severing[146].

Together with STRIP, MOB4 was one of the first identified interaction partners of STRN. The MPS1 binder kinase activator (MOB) family includes for example MOB1, MOB2, MOB3, MOB4 and MOBp. Previous experiments showed that together with MOB4 STRN might be able to regulate membrane trafficking, intracellular vesicular transport, clathrin-dependent endocytosis and MT organization[131,147–149]. Similar to STRN family members MOB family members share high sequence homology and are known to regulate protein kinase activity.

In budding yeast *S. cerevisiae* MOB1P is phosphorylated by MPS1. The protein MPS1 is a kinase associated with both the SAC and the duplication of MTOC[17]. The fruit fly homologue MOB4 is known to be involved in spindle pole organization, kinetochore-fiber focusing and mitotic centrosome separation, but not duplication[151]. Trammel *et al.* used RNAi for MOB4 depletion in *D. melanogaster* S2 cells. The MOB4 downregulation leads to abnormal centrosome number and monopolar and bipolar defocused spindles. A similar function for MOB4 has not been proven yet. PP2A inhibition is known to cause STRN, STRN3 and MOB4 hyperphorphorylation[36]. If STRN family members have a similar function as the MOB family members in the STRIPAK complex is not clear yet.

In 2012 Hyodo *et al.* found direct interaction between STRN4 and misshapen like kinase 1 (MINK1) in HeLa and 293T cells. Together with STK3, STK4 and STK25, MINK1 belongs to the mammalian germinal center kinases (GCKs). In mammals GCKs regulate cell growth, polarization, apoptosis, migration, neuronal differentiation, and stress responses[152,153]. STK3/4, commonly known as hippo pathway-associated MST1/2, and STK25 (or MST4), are sub-grouped as GCKIII family members, while MINK1 is categorized as GCKIV member[143].

STRIPAK is a negative regulator of the hippo pathway, which is involved in cancer pathologies[141,154,155]. In first publications GCKIIIs were known to closely interact and to be recruited to STRIPAK by CCM3[139,144,156], whereas one GCKVI, namely MINK1 was able to directly bind STRN[143,144]. Recent discoveries in *Sordaria macrospora* verified direct interaction of the GCKIIIs to STRN as well[157]. In support of the hypothesis that STRN plays a role in mitotic progression, STRIPAK associated kinase MINK1 is required for abscission of the intercellular bridge during cytokinesis[143].

In the paper by Hyodo *et al.* an anti-MINK1 and anti-STRN4 co-immunoprecipitation could be verified. They showed STRN4 depletion leads to defects in cell division and

generates multinucleated HeLa cells[143]. The authors also found MINK1 is phosphorylated by CDK1 during mitosis. They suspect MINK1 to be auto-phosphorylated and targeted by PLK1. In this paper decreased kinase activity of MINK1 could be verified by recombinant PP2A (both PP2A A + C complex and PP2A A + B + STRN4) addition[158,159].

Table 2: The STRIPAK complex components and their nomenclature. The other species nomenclatures (when the protein was identified or available) are from studies with yeasts and other fungi, fruit fly and worms.

	HUGO Protein name in human	also known as	Protein name in other species	Corresponding origin
Protein phosphatase 2 A catalytic subunit C	PP2A Cα PP2A Cβ	PPP2CA PPP2CB	PPH21 PPH3 PPH22 MTS PP2A-28D PPA3 SmPP2Ac1	*Saccharomyces cerevisiae* *Saccharomyces cerevisiae* *Saccharomyces cerevisiae* *Drosophila melanogaster* *Drosophila melanogaster* *Schizosaccharomyces pombe* *Sordaria macrospora*
Protein phosphatase 2 scaffold subunit A	PP2A Aα PP2A Aβ	PPP2R1A PPP2R1B	TPD3 PP2A-29B PAA1 SmPP2AA	*Saccharomyces cerevisiae* *Drosophila melanogaster* *Schizosaccharomyces pombe* *Sordaria macrospora*
Protein phosphatase 2 regulatory subunit B	PP2A B56γ PP2A B56β PP2A B55α PP2A B55β PP2A B56δ PP2A B56ε PP2A B56α PP2A PR72 PP2A PR48 PP2A B55γ PP2A B55δ	PPP2R5C PPP2R5B PPP2R2A PPP2R2B PPP2R5D PPP2R5E PPP2R5A PPP2R3A PPP2R3B PPP2R2C PPP2R2D	RTS1 CDC55 TWS PP2A-85F	*Saccharomyces cerevisiae* *Saccharomyces cerevisiae* *Drosophila melanogaster* *Drosophila melanogaster*
Striatin (PP2A B‴)	**STRN**	**STRN-1**	CASH-1 **FAR8** **STRA** **PRO11** **CKA** **CSC3**	***Caenorhabditis elegans*** ***Saccharomyces cerevisiae*** ***Aspergillus nidulans*** ***Sordaria macrospora*** ***Drosophila melanogaster*** ***Schizosaccharomyces pombe***
S/G_2 nuclear auto antigen	STRN3	SG_2NA		
Zinedin	STRN4	ZIN		
MOB (MPS1 binder) family member, phocein	MOB4	MOB1 MOB3 PHOCN MOBKL3 PREI3	MOB4 / DMOB4 MOB1P SmMOB3	*Drosophila melanogaster* *Saccharomyces cerevisiae* *Sordaria macrospora*
Suppressor of IKBKE1; fibroblast growth factor receptor 1 oncogene partner 2	SIKE1	FGFR1OP2	FGOP2 FAR3/7 CSC4P	*Drosophila melanogaster* *Saccharomyces cerevisiae* *Schizosaccharomyces pombe*
Striatin interacting protein 1 /family with sequence similarity 40, member A	STRIP1	FAM40A	FAR11 STRIP FARL11	*Saccharomyces cerevisiae* *Drosophila melanogaster* *Caenorhabditis elegans*
Striatin interacting protein 2 /family with sequence similarity 40, member B	STRIP2	FAM40B	FAR11 STRIP FARL11	*Saccharomyces cerevisiae* *Drosophila melanogaster* *Caenorhabditis elegans*
Cortactin binding protein 2	CTTNBP2	KIAA1758 CORTBP2	NAUS CG10915	*Drosophila melanogaster* *Drosophila melanogaster*
Programmed cell death 10 cerebral cavernous malformations 3 protein	CCM3	PDCD10 TFAR15	CG5073	*Drosophila melanogaster*
TNF receptor associated factor 3 interacting protein 3; sarcolemma associated protein	TRAF3IP3	SLMAP T3JAM		
Serine/threonine kinase 4; mammalian STE20-like protein kinase 1, hippo)	STK4	MST1 KRS2	HPO SmKIN3 SmKIN24	*Drosophila melanogaster* *Sordaria macrospora* *Sordaria macrospora*
Serine/Threonine Kinase 3; mammalian STE20-like protein kinase 2)	STK3	MST2 MST3 STK24	PRK-9 SID-1 HPO SmKIN3 SmKIN24	*Saccharomyces cerevisiae* *Saccharomyces cerevisiae* *Drosophila melanogaster* *Sordaria macrospora* *Sordaria macrospora*
Serine/threonine kinase 25 sterile 20/oxidant stress-response kinase 1; misshapen	STK25	MST4 MASK STK26 YSK1 SOK1	MSN	*Drosophila melanogaster*
Mitogen-activated protein kinase kinase kinase kinase 4	MAP4K4	HGK, KIAA0687 NIK MEKKK4		
Misshapen Like Kinase 1; misshapen	MINK1	B55 MAP4K6 ZC3 YSK2 MEKKK6		
TRAF2 and NCK interacting kinase	TNIK	MRT54	SHK1	*Schizosaccharomyces pombe*

Later analysis found different other STRIPAK interactors like the kinase MAP4K4[160]. MAP4K4 is known to activate the c-JUN N-terminal kinase (JNK) signaling pathway[161] and LATS1/2 (YAP1), which targets MST1/2, a hippo pathway component. MST1/2 controls cell proliferation and apoptosis[162]. Recent studies show that downregulation of MAP4K4 in HEK cells leads to cell degeneration and epithelial-mesenchymal transition (EMT)[160].

The MAP4K4 interaction with STRIPAK components is enhanced in the presence of polyomaviruses SV40 ST (simian virus 40 small tumor antigen), which is suspected to be carcinogenic[160]. In this context the authors found ST-promoted PP2A-dephosphorylation of MAP4K4 in a STRN4-including STRIPAK complex. Similar to MINK1, this dephosphorylation could play a role at metaphase-anaphase transition.

Identification of protein-protein interactions (PPIs) plays a key role to explain unknown molecular mechanisms, within living cells and tissues. The number of proteomic techniques to identify interactions is rapidly increasing and all have their pros and cons. When discussing results of these techniques one should never rely on one approach and model organism only. The strength of proteomic approaches (especially for dense protein matrices like the centrosome) for the analysis of cytoskeletal structures has been demonstrated in several studies[12,14,163–168]. The analysis of proteins that form the mitotic spindle is still challenging, because mitosis is a transient cell cycle stage. Nondurable proteins are difficult to meaningfully verify. In order to answer if proteins play a role in cell cycle dynamics, one model of choice can be the *Xenopus laevis* egg model system.

1.7 The *Xenopus laevis* cell free embryonal model is a appropriate tool for proteomics

The *Xenopus laevis* frog egg extract is a powerful tool for proteomic studies. Each single step of cell cycle stages can be monitored includingspindle assembly and chromatid segregation in meiosis and mitosis. After a seasonal hormone impulse or injection, follicle cells release progesterone, which induces oocyte transition from prophase I to metaphase II, *i. e.* to a mature ovum in the process of meiotic maturation (later seen in figure 10). The frogs begin to lay eggs of $^{+}/_{-}$1,2 mm in diameter. The eggs can be easily and gently crushed by centrifugation (see figure 5).

In previous research, immunoprecipitation, MS analysis, addition of recombinant proteins, activators or inhibitors or other manipulation has been done with the resulting concentrated cytosolic lysate[169,170]. The fertilization of one single complete haploid egg can create a new diploid life, resulting in an embryo. It takes the fertilized embryo 3 - 5 h until midblastula-transition when its recombined embryonal genes start to get transcribed[171].

The concentrated cytosol of mature amphibian eggs, known as low speed supernatant (LSS) or cytostatic factor (CSF) extract, has the advantage that it is arrested in metaphase of the second meiotic division awaiting fertilization[172]. The CSF state corresponds to a stable balance in the cytosol waiting to enter from an embryonic system into a somatic cell cycle[77,173]. The chromosomes are stuck at the metaphase plate. Multiple factors, protein complexes, particularly a positive feedback loop between MPF and CSF are responsible for the stable arrest[174].

One responsible protein for the CSF stationary state is the protein EMI2 (in *Xenopus* also known as XERP1). During G_2/M transition the APC/C is inhibited by PP2A B56 dependent dephosphorylation of EMI2[175]. Dephosphorylated EMI2 causes metaphase II arrest in unfertilized vertebrate eggs. CAMKII initiates mitotic exit by phosphorylating EMI2 beside others. EMI2 phosphorylation can be triggered by Ca^{2+} influx. A second-step phosphorylation of EMI2 is done by PLX1 (PLK1 in *Xenopus*)[176,177]. Thereby EMI2 degrades and the APC/C the E3 ubiquitin ligase activates. The mitosis marker protein Cyclin B is ubiquinylated and degraded by the proteasome[176–178].

The hyperphosphorylated protein EMI2 can be recognized by E3 ubiquitin ligases and labeled for proteasomal degradation[177]. Thereby CAMKII is able to induce spindle exit without APC/C activation[179]. In ascidians the phosphatases CAN and PP2A, but not kinase CAMKII, are necessary for fertilization of the egg and meiotic exit, whereas fertilized mouse eggs are essentially depending on CAMKII phosphorylation during meiotic exit[180–183].

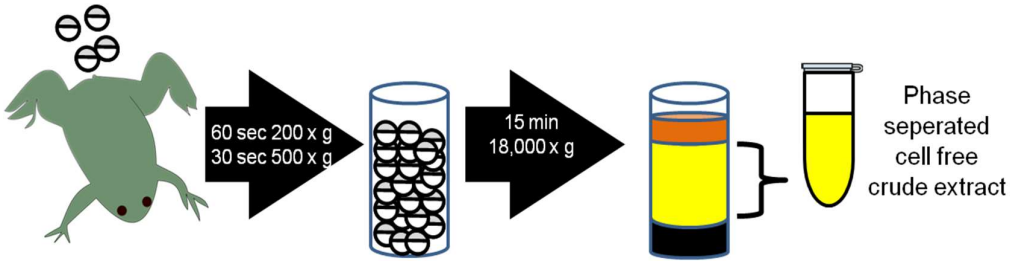

Figure 5: Production of cell free M-phase egg extract. The frog eggs of *Xenopus laevis* are an ideal source for proteomic studies. The eggs are first packed tightly and second gently crushed by centrifugation. The resulting lysates form a gradient of lipids, cytosol, the highly concentrated crude extract and pigments. The recovered crude extract is ready for assays.

Xenopus laevis M-phase extracts do not transcribe genes and proceed with a stationary stock of mRNAs. Only cell division and fertilization relevant proteins are translated. Even without fertilization the *Xenopus* egg extract is capable of describing cell division in almost all common division processes. Experiments showed addition of isolated sperm nuclei can replicate up to 100% of DNA when added to the CSF extract[184].

At the beginning of mitosis (simultaneously to NEBD) MAPs are accumulated for centrosomal nucleation, known as centrosome maturation[185,186]. When speaking of an embryonal system, the egg typically loses the centrosome during oocyte maturation. There are organisms where the sperm reintroduces the centrosome to the fertilized egg, but it is not a rare case that several early cell divisions can be performed even without the organelle[3,187].

The analysis of Maheshwari *et al.* gave reason to suspect STRN being a centrosomal candidate since they found STRN concentrated at the centrosomes of *C. elegans* germline stem cells during mitosis[107]. It is not clear how the centrosomes (including the MTOC and PCM) are reestablished after fertilization for further cell division. The way how the centrosome is reassembled in later embryonal development and the factors responsible for it still have to be decoded. New centrosome assembly from paternal and maternal centrosomes in vertebrate and its importance in embryonic mitosis is still enigmatic.

During gametogenesis *Xenopus laevis* eliminate their male and female centrosomes. After oocyte sperm fusion their centrosomal components complement each other and reestablish a functional zygotic centrosome. Mouse embryos are initially acentriolar until centrioles are created *de novo* at the pachytene 64 cell stage[188]. Whereas a somatic cell rapidly disassembles its PCM during mitotic exit of each cell cycle and the centrioles persist[72,189–193]. The factors described in the following section definitely play a role in this process, since all of them are present in the acentrosomal embryonal cell division.

A mechanism how an embryonal dividing cell of *C. elegans* breaks down PCM components in a PP2A-dephosphorylation dependent fashion was suggested by Enos *et al.* in 2018[72]. While PLK1 phosphorylation of SPD-5 leads to PCM assembly[194], this study shows PCM disassembly through PP2A dephosphorylation of SPD-5. Similarly, several phosphorylation processes during M-phase entry initialize PCM maturation and thereby γ-tubulin recruitment, complex formation and nucleation activation[195–198].

Even without centrioles γ-tubulin is vital to form a bipolar spindle, and is not only present in the spindle poles, but also on the spindle[199,200]. The protein, present in all eukaryotes, forms the γ-tubulin small complex (γ-TUSC), which further assembles to the γ-tubulin ring complex (γ-TURC). Both complexes have different functions and fine-tuning mechanism but are still MT nucleators. Beside the γ-TURC, regulation, positioning and correct spindle assembly is supported by several other proteins from the PCM.

One MAP that was first discovered in the embryonal *X. laevis* system is targeting protein for XKLP2, known as TPX2. Recombinant TPX2 can bind purified α/β-tubulin dimers and induce MT nucleation *in vitro*[201]. In *Xenopus laevis* egg extracts phosphorylated TPX2 is bound to importin. The GTP-bound form of G protein RAS-related nuclear protein, RAN, in its GTP conformation, can bind importin and TPX2 is released as active MT nucleator for spindle assembly, while secondarily the NEBD and γ-TURC can be activated in somatic cells[202,203]. Early experiments in *Xenopus laevis* egg lysates show that RAN is essential for spindle formation and is considered as MT nucleator[204–207]. Active RANGTP addition drives MT nucleation and organization into asters.

To form the γ-TUSC two molecules of γ-tubulin bind to the C-terminal domains of γ-ring complex protein (GCP) 2 and 3. Second additional GCPs (4, 5, and 6) and the proteins NEural precursor cell expressed Developmentally Down-regulated 1 (NEDD1), mitotic spindle organizing protein 1 and 2 (MOZART1/2, MZT1/2), and nucleoside diphosphate kinase 7 (NME7) complete the small complex to the γ-TURC. One of the first discovered essential factors of the PCM is pericentrin (PCNT).

1.8 The centrosome harbors the majority of MAPs

Correct PCNT localization is controlled by pericentriolar material 1 protein (PCM1), one of the very first known so called centriolar satellite proteins. Satellite proteins are dense granules scattered around the centrosome protein network[208]. The centrosomal components PCTN, CDK5RAP2 and SPD-5 are phosphorylated by PLK1. A mutation of PLK1 shows a lack of supramolecular scaffold PCM assembly[209–214]. Phosphorylation is the initial step for centrosome maturation and spindle formation[215,216]. In cooperation with the Schiebel lab (ZMBH Heidelberg, Germany) our lab found monomeric G-actin incorporated into the γ-TURC[217]. The G-actin function is still unsolved.

The ring complex components NEDD1 and MZT1 link the γ-TURC to the N-terminal centrosomin motif 1 (CM1) domain of CDK5RAP2[218]. The centrosomal protein NEDD1 is hyper-phosphorylated for mitosis[196]. NEDD1 protein contains WD40 repeat domains, that leads NEDD1 to the centrosome[218,219]. WD40 repeat domains are also part of the here discussed STRN protein. Studies in *C. elegans* showed a centrosomal accumulation of the orthologue of STRN's tightly linked partner protein STRIP in meiotic metaphase oocytes. The STRIP depletion resulted in infertile worms[107]. STRN is suspected to stabilize STRIP proteins[220]. NEDD1 is targeted by Aurora A kinase[221].

Similar to AURKB, AURKA controls length of k-fiber MT and therefore the stability of the assembling mitotic spindle[222]. The centrosome maturation in *C. elegans* embryos can be stopped by AURKA knock down (KD). This experiment inhibited the recruitment of γ-tubulin and XMAP215 (CKAP5 in human)[223]. XMAP215 is a processive MT polymerase that can increase the MT growth rate up to 10-fold[224,225].

An overrepresentation of γ-TURC component CDK5RAP2 leads to accumulation of PCM. A combination of overrepresented CDK5RAP2 and MT-disrupting conditions (by nocodazole) results into MT-nucleating clusters in the cytosol. The protein CDK5RAP2 is a γ-tubulin, γ-TUSC and γ-TURC independent MT nucleator. Liquid-liquid phase separation of CDK5RAP2 accelerates MT polymerization[214,226,227]. Phosphorylated PCTN can target CDK5RAP2 and prepares CDK5RAP2 for complex formation.

In fruit fly embryos CDK5RAP2 concentration determines the PCM expansion radius[228]. CDK5RAP2 reduction does not disassemble the γ-TURC in the here cited paper[229]. A combination of a MT seed nucleating function for CDK5RAP2 is not known yet, however it has an interaction to end binding protein 1 (EB1 or MAPRE1 in human). Together CDK5RAP2 and EB1 addition results in accelerated MT elongation[230,231]. EB1 is known to stabilize XMAP215 accumulation at the plus ends, where XMAP215 accelerates MT elongation, by recruiting tubulin dimer building blocks for polymerization[232].

Table 3: Proteins discussed in this work and their (putative) role as MT modulators. The previously described STRIPAK complex components are listed because some of them are already described MT modulators. My work describes STRN in context of MT modulation.

APC/C	E3 ubiquitin ligase	spindle assembly checkpoint, ubiquitinylates many targets for mitotic exit	176,233,234
ARRP19	PP2A-B55, MASTL	Mitotic progression	66,97,235,236
AURKA	kinase	multiple functions, mitotic entry	222,237–239
AURKB	kinase	multiple functions, mitotic exit	38,239–241
BUBR1	kinase	spindle assembly checkpoint	93,242,243
CAMKII	kinase	Ca^{2+} signaling, mitotic progression	179,244–246
CCM3	STRIPAK	proliferation, apoptosis, migration, golgi assembly	23,61,126–128,130,138,139,142,144,147,149,70,218,220,233,240,74,84,86,91,97,102,115
CDK1	kinase	Multiple functions, forms MPF with Cyclin B	31,181,251
CEP152 /ASL	PLK1	centrosome, ciliogenesis, spindle assembly	9,170,228
CEP192 / SPD-2	PP1, AURKA, PLK4	centrosome, ciliogenesis, spindle assembly	196,210,213
CEP215 / CDK5RAP2	NME7	γ-TURC component, MT nucleation, spindle assembly, +TIP, MT elongation	195,197,217,229,230,248
CKAP5 / XMAP215		MT nucleation, elongation, +TIP	214,232,248,252
CLASP1		MT nucleation, elongation, +TIP	248,253
CLIP1 / CLIP170		MT nucleation, elongation, +TIP	248,254,255
CPAP / SAS4	AURKA, PLK1	centrosome, ciliogenesis, spindle assembly	3,189,256
CTTNBP2	STRIPAK	Regulator of actin cytoskeleton	23,61,126–128,130,138,139,142,144,147,149,70,218,220,233,240,74,84,86,91,97,102,115
EB1 / MAPRE1		MT nucleation, elongation, +TIP	248,254,255,257–259
ENSA	PP2A-B55, MASTL	Mitotic progression	66,97,235,236
KIF10 / CENPE	BUBR1	DNA congression, kinetochore assembly	260
KIF11 / EG5		MT nucleation, elongation, spindle assembly	260,261
KIF18B		MT motor protein golgi-to-ER retrograde transport, MT depolymerization, spindle disassembly	260,262
KIF2C /MCAK		+TIP MT depolymerization, spindle disassembly	260,262
KIF4		MT motorproteingolgi-to-ER retrograde transport	42,260
MAP4K4	STRIPAK kinase	JNK signaling pathway, proliferation, embryonic development, apoptosis.	23,61,126–128,130,138,139,142,144,147,149,70,218,220,233,240,74,84,86,91,97,102,115
MASTL/GW	kinase	Mitotic progression	66,97,235,236
MINK1	STRIPAK kinase	activator of JNK and MAPK14/p38 pathways	23,61,126–128,130,138,139,142,144,147,149,70,218,220,233,240,74,84,86,91,97,102,115
MOB4	STRIPAK	Membrane trafficking, golgi assembly, spindle focusing	23,61,126–128,130,138,139,142,144,147,149,70,218,220,233,240,74,84,86,91,97,102,115
MZT1	NME7	γ-TURC component, MT elongation, spindle assembly	195,197,217,229,230,248
NEDD1	NME7	γ-TURC component, MT elongation, spindle assembly	195,197,217,229,230,248
NME7	kinase	γ-TURC component phosphorylation	195,197,217,229,230,248
PCM1	MIB1, GSK3B	centrosome, ciliogenesis, spindle assembly, recruits PCTN to the centrosome	263,264
PCNT	MIB1 E3 ubiquitin ligase, PLK1	centrosome, ciliogenesis, spindle assembly, recruits CDK5RAP2 to the centrosome	210,265
PLK1	kinase	multiple functions, mitotic entry, progression, centrosome	39,40,95,210,212
PLK4	kinase	multiple functions, mitotic entry, centrosome	71,170,263,266
PP1	phosphatase	multiple functions, mitotic exit	29,34,63,69,267
PP2A	STRIPAK phosphatase	multiple functions, mitotic entry and exit	23,61,126–128,130,138,139,142,144,147,149,70,218,220,233,240,74,84,86,91,97,102,115
PP4		multiple functions	34,69,268
PRC1	CDK1, CDK2, PLK1	Mitotic exit, cytokinesis	248
RAN		GTPase, MT nucleation, spindle assembly, protein/mRNA nucleus inport/export	202,203,221,269,270
RANBP2 / NUP358		Centrosome, protein/mRNA nucleus inport/export	202,203,205,221,269,270
RCC1		MT nucleation, spindle assembly, protein/mRNA nucleus inport/export	203,206,207
SGO2	PP2A	DNA congression, protects centromeric cohesion complexes until mitotic exit	30,31
SIKE1	STRIPAK	Multiple signaling pathways	23,61,126–128,130,138,139,142,144,147,149,70,218,220,233,240,74,84,86,91,97,102,115
SSX2IP		Centrosome, ciliogenesis, spindle assembly	102,248,271,272

STK25/26 (GCKIII)	STRIPAK kinase	Hippo pathway	23,61,126–128,130,138,139,142,144,147,149,70,218,220,233,240,74,84,86,91,97,102,115
STK3 (GCKIII)	STRIPAK kinase	Hippo pathway	23,61,126–128,130,138,139,142,144,147,149,70,218,220,233,240,74,84,86,91,97,102,115
STK4 (GCKIII)	STRIPAK kinase	Hippo pathway	23,61,126–128,130,138,139,142,144,147,149,70,218,220,233,240,74,84,86,91,97,102,115
STRIP1/2	STRIPAK	Membrane trafficking, golgi assembly	23,61,126–128,130,138,139,142,144,147,149,70,218,220,233,240,74,84,86,91,97,102,115
STRN	**STRIPAK**	**signaling, PP2A regulation**	**23,61,126–128,130,138,139,142,144,147,149,70,218,220,233,240,74,84,86,91,97,102,115**
STRN3	STRIPAK	signaling, PP2A regulation	23,61,126–128,130,138,139,142,144,147,149,70,218,220,233,240,74,84,86,91,97,102,115
STRN4	STRIPAK	signaling, PP2A regulation	23,61,126–128,130,138,139,142,144,147,149,70,218,220,233,240,74,84,86,91,97,102,115
TNIK	STRIPAK kinase	WNT signaling JNK signaling	23,61,126–128,130,138,139,142,144,147,149,70,218,220,233,240,74,84,86,91,97,102,115
TPX2	AURKA, AURKB	MT nucleation, elongation, branching, spindle assembly, protein/mRNA nucleus inport/export, +TIP, nucleus envelop breakdown	248,273,274
TRAF3IP3	STRIPAK	JNK signaling	23,61,126–128,130,138,139,142,144,147,149,70,218,220,233,240,74,84,86,91,97,102,115
TUBG1		γ-TURC core component, MT nucleation, elongation, spindle assembly	195,197,217,229,230,248
WDR8		Centrosome, ciliogenesis, spindle assembly	102,271,272

Analysis in *D. melanogaster* S2 cells shows that EB1 is not essential for creating a MT network in interphase but is a vital factor to create a dense MT bipolar spindle in cell division[275]. XMAP215 and EB1 share the same protein functional class. They belong to the so called +TIPs MAPs that bind to the MTs plus end and frequently share the short polypeptide motif Ser-x-Ile-Pro (SxIP).

Other proteins with a SxIP motif include the already mentioned tumor suppressor protein APC, the MT-actin crosslinking factor (MACF), the cytoplasmic linker protein (CLIP1), CLIP-associated proteins (CLASP family), the STromal Interaction Molecule-1 (STIM1), the motorprotein dynactin subunit p150glued, and the mitotic centromere-associated kinesin (MCAK)[232,256,276–278]. In contrast to EB1's interaction to XMAP215, MCAK interacts with KIF18B and depolymerizes MT[262,279]. Depletion of MCAK results in reduced spindle stretch, delayed chromosome congression, alignment defects, and severe missegregation of chromosomes in Chinese hamster ovary (CHO) cells[280].

Which factors are important to form spindles without centrosomes during meiosis? In this work I focus on the putative MAP STRN since this protein showed a significant upregulation during a interphase/M-phase comparative MAP purification[102].

1.9 Aim of my thesis project

Proper mitotic progression requires a bulk of proteins to be phosphorylated and dephosphorylated. Therefore, specific and precise kinases and phosphatases are crucial for proper timing of cell division. Interplay between phosphorylation states is possible by a complex protein assembly. This could be given by STRN as binding platform. STRN is known to regulate PP2A-dependend dephosphorylation in different model organisms. The protein STRN was found in maturing *Xenopus leavis* egg extract[102]. In context of my thesis project, I aimed to analyze the role of STRN as a putative MAP. I intended to examine STRN's localization and to characterize its role and the mechanism during cell division.

In this context, I also aimed to verify if STRN is upregulated during meiosis in comparison to interphase. To understand STRN's interaction behavior I used the *Xenopus laevis* cell-free mitotic extract. The localization pattern within the synchronous STRN-depleted egg lysates can be monitored using altered behavior of tubulin polymerization and immunofluorescence microscopy in different cell lines.

I examined potential interaction partners, also including transient interactions, from respective immune complexes. I aimed to answer the question which cell cycle and cell division related function STRN has in the embryonal system.

2 Materials and methods

○ 2.1 Chemicals and enzymes

All used chemicals were *p. a.*-quality. The enzymes, chemicals, kits and materials were ordered from Sigma-Aldrich (Steinheim), Roche Diagnostics (Mannheim), Carl Roth (Karlsruhe), Merck (Darmstadt), GE Healthcare (Solingen), Agilent Technologies (Waldbronn), QIAGEN (Hilden) and Invitrogen, Thermo Fisher Scientific or Life Technologies (Schwerte). Restriction enzymes, T4-DNA-Ligase, Antarctic phosphatase and Q5™ High Fidelity DNA-polymerase were purchased from New England Biolabs (Frankfurt am Main).

○ 2.2 Solutions, buffers, media, primer, strains, cultures and antibody

4x Laemmli[281] protein sample buffer pH 6,8 (HCl/NaOH), stored at -20 °C

200 mM tris
400 mM DTT
8% SDS
0,4% bromophenol blue
40% glycerol

BRB80[282] pH 8,8 (HCl/KOH), stored at 4 °C

80 mM PIPES
1 mM $MgCl_2$
1 mM EGTA

CSF[283] pH 7,7 (HCl/KOH), prepared fresh

XB-CSF
100 mM KCl
0,1 mM $CaCl_2$
2 mM $MgCl_2$
5 mM EGTA
50 mM sucrose
10 mM HEPES

CSF salts
100 mM KCl
10 mM HEPES
2 mM $MgCl_2$

CSF$^+$ stringent washing
250 mM KCl
2 mM $MgCl_2$
10 mM HEPES
0,1% triton X-100

MBS salts pH 7,8 (HCl/NaOH), autoclaved, stored at RT

88 mM NaCl
1 mMKCl
5 mM HEPES
2,5 mM $NaHCO_3$

MBS pH 7,8 (HCl/NaOH), prepared fresh
MBS salts supplemented with 0,41 mM $CaCl_2$

MMR pH 7,8 (HCl/NaOH), autoclaved, stored at RT

100 mM NaCl
2 mM KCl
1 mM $MgSO_4$
2 mM $CaCl_2$
5 mM HEPES (pH 7,8)
0,1 mM EDTA

Dejelly solution, prepared fresh
0,25 x MMR with 2% L-cysteine, pH 7,7 (HCl/KOH)

Extract fixative, stored at -20 °C
MMR supplemented with
48% glycerol
11% formaldehyde
5 µg/mL DAPI

XB salts pH 7,7 (HCl/KOH), filter sterilized, stored at 4 °C

100 mM KCl
0,1 mM $CaCl_2$
2 mM $MgCl_2$

XB pH 7,7 (HCl/KOH), prepared fresh
XB salts supplemented with
50 mM sucrose
10 mM K-HEPES

PBS pH 7,4 (HCl/NaOH), autoclaved, stored at RT

NaCl 137 mM
KCl 2,7 mM
Na_2HPO_4 10 mM
KH_2PO_4 1,8 mM

For PBS-TX100 + 0,1% triton X-100, stored at RT
For PBS-TW20 + 0,05% tween-20, stored at RT

Ni-NTA lysis and wash buffer, stored at 4 °C
PBS supplemented with
8,7% glycerol
150 mM NaCl
20 mM Imidazole
1 mM DTT
Ni-NTA eluation buffer, stored at 4 °C
PBS supplemented with
8,7% glycerol
150 mM NaCl
400 mM Imidazole
1 mM DTT

RIPA, pH 7,6, stored at -20 °C

25mM tris
150mM NaCl

1% NP-40
1% sodium deoxycholate
0,1% SDS

Running/Blotting buffer, stored at RT

192 mM glycine
50 mM tris
(1% SDS for SDS-PAGE)

TAE pH 8,0, stored at RT

40 mM tris
20 mM acetic acid
1 mM EDTA

TBS pH 7,5 (HCl/NaOH), autoclaved, stored at RT

50 mM tris
150 mM NaCl

Bacteria growth media
LB[284,285] (luria broth) pH 7,2 (HCl/NaOH), autoclaved, stored at RT

For 1L
9 g Bacto-tryptone
4,5 g yeast extract
4,5 g NaCl

+ 1,5% Agar for petri dishes

2xYT pH 7,2 (HCl/NaOH), autoclaved, stored at RT

For 1L
16 g Bacto-tryptone
10 g yeast extract
5 g NaCl

Cell Culture Media, media stored at 4 °C, supplements stored at -20 °C

DMEM (HeLa) + 10% FCS + 1xPen/Strep stock
MEM Eagle (IMR-90) + 10% FCS+ 1xPen/Strep stock
DMEM F12 (hTERT RPE-1) + 10% FCS+ 1xPen/Strep stock+ 2 mM L-glutamine
Leibovitz (XL-177) + 10% FCS+ 1xPen/Strep stock

Table 4: Devices and laboratory equipment.

Acculab Sartorius Atilon 13N	Sartorius Biotech GmbH, Göttingen
Beckman Coulter J2-21	Beckman Coulter, Krefeld
Biometra T gradient thermocycler	Biometra GmbH, Göttingen
Biophotometer	Eppendorf, Hamburg
Criterion™ blot chamber system	BIO-RAD, München
Criterion™ cell SDS gel chamber	BIO-RAD, München
Dry incubator for bacteria B6120	Heraeus-Holding, Hanau
Eppendorf centrifuge 5415R	Eppendorf, Hamburg
Eppendorf Thermomixer comfort	Eppendorf, Hamburg
EPS 300 power supply	Amersham Pharmacia, GE Healthcare GmbH, Solingen
Fluorescence microscope Keyence BZ-X800E	Keyence Deutschland GmbH, Neu-Isenburg
Fluorescence microscope Zeiss Axiophot with AxioCamMrm and HBO100 lamp	Carl Zeiss Microscopy GmbH, Jena
Fluorescence microscope Leica DM5500B with Leica DFC 420C camera and LED lamp	Leica Microsystems GmbH, Wetzlar
Fluorescence microscope motic AE31 with moticam pro and MH6100B lamp	Motic Europe, SLU, Barcelona
Gel doc XR+ geldocumentationsystem	BIO-RAD, München
GFL 3013 seesaw	GFL Labortechnik, Burgwedel
HeidolphDuomax 1030	Heidolph Instruments GmbH, Schwabach
IKA combimag RET heated magnetic stirrer	IKA®-Werke GmbH & CO. KG, Staufen
IKA mag REO magnetic stirrer	IKA®-Werke GmbH & CO. KG, Staufen
Image Quant LAS 4000 mini	Amersham Pharmacia, GE Healthcare GmbH, Solingen
Incubator CO_2-auto-zero	Heraeus-Holding, Hanau
Innova 4230 refrigerated incubator shaker	New Brunswick™, Eppendorf, Hamburg
JA-10 fxed angle rotor	Beckman Coulter, Krefeld
JA-20 fixed angle rotor	Beckman Coulter, Krefeld
JS-13.1 swinging bucket rotor	Beckman Coulter, Krefeld
Laboratory balance Kern DMS580	Husch & Röhrig GbR,H&R, Köln
M3 Rotilab® mini magnetic stirrer	Carl Roth, Karlsruhe
Microwave micromat NE1027	Panasonic Europe, Hamburg
Multitron AJ 112/6 shaker	Infors AG, Bottmingen
NanoVue plus spectrophotometer	GE Healthcare GmbH, Solingen
pH-meter TFK325 SenTix 41	WTW InoLab, Xylem Analytics Germany Sales GmbH, Weilheim
Photometer UV-1600PC	VWR International GmbH, Darmstadt
Sartorius analytic	Sartorius Biotech GmbH, Göttingen
Scotsman ice crusher AF 103	Scotsman Ice Srl, Pogliano Milanese
SepatechMegafuge 1.0	Heraeus-Holding, Hanau
Sprout minicentrifuge	Biozym, Oldendorf
Tabletop ultracentrifuge Optima Max	Beckman Coulter, Krefeld
Test tube rotator 34528	Snijders Labs, Tilburg
Tissue culture dishes	Greiner Bio-One Labortechnik GmbH, Kremsmünster
TLA-120.2 rotor	Beckman Coulter, Krefeld
TLS-55 rotor	Beckman Coulter, Krefeld
Vortex mixer VTX-3000L	LMS Consult GmbH & Co. KG Laboratory and Medical Supplies,Brigachtal
Water bath M20	LAUDA Dr. R. Wobser GmbH & CO. KG,Lauda-Königshofen

Table 5: Bacteria strains and cell types.

Bacteria for expression		
***Escherichia coli* DH5α**	F⁻*endA1 glnV44 thi-1 recA1 relA1 gyrA96 deoRnupG Φ80dlacZ* ΔM15Δ*(lacZYAargF)U169 hsdR17* ($r_K^- m_K^+$) λ^-	Hanahan, 1983[286]
***Escherichia coli* BL21 (DE3)**	F⁻*ompT gal dcmlonhsdS*$_B$($r_B^- m_B^-$)*λ*(DE3 *[lacI lacUV5-T7 gene 1 ind1 sam7 nin5])*	Studier & Moffatt, 1986[287]
***Escherichia coli* Rosetta™(DE3)**	F⁻ *ompThsdS*$_B$($r_B^- m_B^-$) *gal dcm*(DE3)pRARE (Cam^R)	Novagen (Merck)
***Escherichia coli* ArcticExpress (DE3) RP**	F⁻ *ompThsdS*($r_B^- m_B^-$)*dcm*$^+$*Tet*^{R}*galλ*(DE3)*endAHte [cpn10 cpn60* Gent^R*] [argUproLStrr]*	Agilent Technologies
***Escherichia coli* ArcticExpress (DE3) RIL**	F⁻ *ompThsdS*($r_B^- m_B^-$) *dcm*$^+$*Tet*^{R}*galλ*(DE3) *endAHte [cpn10 cpn60* Gent^R*] [argUileYleuWStrr]*	Agilent Technologies
***Escherichia coli* SoluBL21™**	F⁻ *ompThsdSB*($r_B^- m_B$ $^-$) *gal dcmλ*(DE3 *[lacIlacUV5- T7 gene1 ind1 sam7 nin5])*	Genlantis
***Escherichia coli* TG1**	F' *[traD36 proABlaclqZ*ΔM15*] supE thi-1* Δ*(lac-proAB)* Δ*(mcr$_B^-$hsdSM)5,* ($r_K^- m_K^-$)	iCARTAB biomedical co. LTD
***Escherichia coli* QIAexpress M15**	F⁻*Φ80Δlac*M15*, thi, lac⁻, mtl⁻, recA⁺,* Km^R	QIAGEN
***Escherichia coli* OverExpress™ C43(DE3)**	F⁻*ompThsdSB*($r_B^- m_B^-$) *gal dcm*	Lucigen
Cell lines and frogs		
hTERT RPE-1	Human adherent retina epitelium	ATCC® CRL-4000™
IMR-90	Wild type, human adherent fetal lung fibroblast	ATCC® CCL-186™
IMR-90 STRN KO	eSpCAS9(1.1)-Puro CRISPR/CAS9 STRN KO, short term, puromycin selection	This work

IMR-90 STRN-EGFP	pcDNA3.1 stable cell line, G418 selection	This work
IMR-90 HA-MiniID-P2A-mKate2	pcDNA3.1 stable cell line, BIOID control, G418 selection	This work
IMR-90 HA-TurboID-P2A-mKate2	pcDNA3.1 stable cell line, BIOID control, G418 selection	This work
IMR-90 HA-STRN-MiniID-P2A-mKate2	pcDNA3.1 stable cell line, STRN-BIOID, G418 selection	This work
IMR-90 HA-STRN-TurboID-P2A-mKate2	pcDNA3.1 stable cell line, STRN-BIOID, G418 selection	This work
HeLa	Wild type, human adherent adenocarcinoma	ATCC® CCL-2™
HeLa STRN-EGFP	BAC clone stable cells, G418 selection	ReberLab
HeLa PP2Ac-EGFP	BAC clone stable cells, G418 selection	ReberLab
XL-177	*Xenopus laevis* skin keratinocytes	EMBL Heidelberg
Xenopus laevis	2yo females*; Xenopus laevis* oocytes (stage I-VI) and mature eggs purified sperm nuclei	This work, obtained at Nasco, Wisconsin; Liu and Schiebel (ZMBH Univesität Heidelberg) Antonin (IBMC, RWTH Aachen)
Xenopus tropicalis	*Xenopus tropicalis* mature eggs and fertilized embryos	Prof. Dr. Dietmar Schmucker and Dr. Gabriela Edwards Faret (LIMES Universität Bonn)

Table 6: Plasmid list and cloning strategy.

pBluescriptKS(+) EB1	Synthesized source for *homo sapiens* EB1 PCR template; codon optimized to get rid of internal restriction sites	Biocat, this work	SAL1,HINDIII/ BAMH1,SPH1
pBluescriptKS(+) STRN	Synthesized source for *mus musculus* STRN PCR template; codon optimized to get rid of internal restriction sites	Biocat, this work	SAL1,HINDIII/ BAMH1,Sph1
pBluescriptKS(+) *xl*TPX2	Synthesized source for *Xenopus laevis*TXP2 PCR template; codon optimized to get rid of internal restriction sites	Biocat, this work	SAL1,HINDIII/ BAMH1,SPH1
miniTurbo-His6_pET21a (MiniID)	Bacterial expression of BirA mutant (*E. coli* BirA^{aa1-63} deleted; Q65P, I87V, R118S, E140K, Q141R, S150G, L151P, V160A, T192A, K194I, M209V, I305V), C-terminal 6xHis tag	Addgene #107178 Branon *et al.* (2018)[288]	
TurboID-His6_pET21a	Bacterial expression of BirA mutant (*E. coli*BirA Q65P, I87V, R118S, E140K, Q141R, S150G, L151P, V160A, T192A, K194I, M209V, M241T, S263P, I305V), C-terminal 6xHis tag	Addgene#107177 Branon *et al.* (2018)[288]	
pET21a HA-STRN-TurboID-His	Bacterial expression of STRN-TurboID fusion	This work	NHE1-HF / BAMH1-HF
pET21a HA-STRN-MiniID-His	Bacterial expression of STRN-MiniID fusion	This work	NHE1-HF / BAMH1-HF
pET21a HA-EB1-TurboID-His	Bacterial expression of EB1-TurboID fusion	This work	NHE1-HF / BAMH1-HF
pET21a HA-EB1-MiniID-His	Bacterial expression of EB1-MiniID fusion	This work	NHE1-HF / BAMH1-HF
pET21a HA-*hs*TPX2-TurboID-His	Bacterial expression of *hs*TPX2-TurboID fusion	This work	NHE1-HF / BAMH1-HF
pET21a HA-*hs*TPX2-MiniID-His	Bacterial expression of *hs*TPX2-MiniID fusion	This work	NHE1-HF / BAMH1-HF
pET21a HA-*xl*TPX2-TurboID-His	Bacterial expression of *xl*TPX2-TurboID fusion	This work	NHE1-HF / BAMH1-HF
pET21a HA-*xl*TPX2-MiniID-His	Bacterial expression of *xl*TPX2-MiniID fusion	This work	NHE1-HF / BAMH1-HF
pQE80L	Bacterial expression, encodes a laclq repression module, N-terminal 6xHis tag	QIAGEN, Hilden	
pQE80-CAMKII$^{aa1-290}$	Bacterial expression, of human CAMKII$^{aa1-290}$, N-terminal 6xHis tag	Rebere*t al.* (2008)[179,245]	
pQE32-RAN^{Q69L}	Bacterial expression, of dog mutant RAN^{Q69L}, N-terminal 6xHis tag	Grusse*t al.* (2001)[203,269,270,289]	
pQE70 *hs*TPX2	Plasmid source for *homo sapiens* TXP2 PCR template;	Grußet *al.* (2001)[203]	
myc-BIOID2-MCS	Mammalian expression of BIOID2-N-terminal fusions, pcDNA3.1 backbone	Addgene #74223 Kim *et al.* (2016)[290] Backbone from Invitrogen (cat. V79020)	
MCS-BIOID2-HA	Mammalian expression of BIOID2-C-terminal fusions, pcDNA3.1 backbone	Addgene #74224 Kim *et al.* (2016) Backbone from Invitrogen (cat. V79020)	
pcDNA3.1 HA-TurboID	Mammalian expression of recloned TurboID, from addgene #107177;forbiotinylation assay in cells	This work	NHE1-HF / KPN1-HF
pcDNA 3.1 HA-MiniID	Mammalian expression of recloned MiniID, from addgene #107178; for biotinylation assay in cells	This work	NHE1-HF / KPN1-HF

pcDNA 3.1 HA-STRN-TurboID	Mammalian expression of STRN-TurboID, for transient cell transfection and biotinylation assay	This work	NHE1-HF / KPN1-HF
pcDNA 3.1 HA-STRN-MiniID	Mammalian expression of STRN-MiniID, for transient cell transfection and biotinylation assay	This work	NHE1-HF / KPN1-HF
pcDNA3.1 HA-EB1-TurboID	Mammalian expression of EB1-TurboID, for transient cell transfection and biotinylation assay	This work	NHE1-HF / KPN1-HF
pcDNA3.1 HA-EB1-MiniID	Mammalian expression of EB1-MiniID, for transient cell transfection and biotinylation assay	This work	NHE1-HF / KPN1-HF
pcDNA3.1 HA-*hs*TPX2-MiniID	Mammalian expression of *hs*TPX-MiniID, for transient cell transfection and biotinylation assay	This work	NHE1-HF / KPN1-HF
pMCS5-5'HA-mKate2	Source for P2A-mKate2 PCR template	Provided by the Witke lab, thanks to Michael Reinke	MoBiTec
pcDNA3.1 HA-TurboID-P2A-mKate2	Mammalian expression of TurboID, for stable cell transfection and biotinylation assay	This work	XHO1 / ECORV
pcDNA3.1 HA-MiniID-P2A-mKate2	Mammalian expression of MiniID, for stable transfection and biotinylation assay	This work	XHO1 / ECORV
pcDNA3.1 HA-STRN-TurboID-P2A-mKate2	Mammalian expression of STRN-TurboID, for stable cell transfection and biotinylation assay	This work	XHO1 / ECORV
pcDNA3.1 HA-STRN-MiniID-P2A-mKate2	Mammalian expression of STRN-MiniID, for stable cell transfection and biotinylation assay	This work	XHO1 / ECORV
pcDNA3.1 HA-EB1-TurboID-P2A-mKate2	Mammalian expression of EB1-TurboID, for stable cell transfection and biotinylation assay	This work	XHO1 / ECORV
pcDNA3.1 HA-EB1-MiniID-P2A-mKate2	Mammalian expression of EB1-MiniID, for stable cell transfection and biotinylation assay	This work	XHO1 / ECORV
pcDNA3.1 HA-*hs*TPX2-MiniID-P2A-mKate2	Mammalian expression of *hs*TPX2-MiniID, for stable cell transfection and biotinylation assay	This work	XHO1 / ECORV
pCS2+8	Mammalian expression vector for *in vitro* transcription, CMV promoter, T7, SP6; with additional 8 bp cutter restriction enzymes (ASCI, PACI, FSEI, ASISI)	Addgene #34931 Gokirmak ***et al.*** (2012)[291] (pCS2+ from RZPD)	
pCS2+8 HA-STRN	Mammalian expression vector for *in vitro* transcription and STRN rescue	This work	BAMH1-HF / ECOR1-HF
pCS2+8 HA-TurboID	Mammalian expression vector for *in vitro* transcription and biotinylation in CSF extract recloned TurboID, from addgene #107177	This work	ECOR1-HF / XBA1
pCS2+8 HA-MiniID	Mammalian expression vector for *in vitro* transcription and biotinylation in CSF extract; recloned MiniID, from addgene#107178	This work	ECOR1-HF / XBA1
pCS2+8 HA-STRN-TurboID	Mammalian expression vector for *in vitro* transcription and biotinylation in CSF extract	This work	PAC1 / XHO1
pCS2+8 HA-STRN-MiniID	Mammalian expression vector for *in vitro* transcription and biotinylation in CSF extract	This work	PAC1 / XHO1
pCS2+8 HA-EB1-TurboID	Mammalian expression vector for *in vitro* transcription and biotinylation in CSF extract	This work	ASC1 / XHO1
pCS2+8 HA-EB1-MiniID	Mammalian expression vector for *in vitro* transcription and biotinylation in CSF extract	This work	ASC1 / XHO1
pCS2+8 HA-*x*/TPX2-TurboID	Mammalian expression vector for *in vitro* transcription and biotinylation in CSF extract	This work	BAMH1-HF / ECOR1-HF
pCS2+8 HA-*x*/TPX2-MiniID	Mammalian expression vector for *in vitro* transcription and biotinylation in CSF extract	This work	BAMH1-HF / ECOR1-HF
pSpCAS9(BB)-2A-Puro (PX459) V2.0	CAS9 from *S. pyogenes* with 2A-Puro, and cloning backbone for sgRNA (V2.0)	Addgene #62988	BBS1-HF

Table 7: Primer and RNA list, sequences and purpose.

21STRN fw	5'-GATCGCTAGC ATGTACCCATACGATGTTCCAGATTACGCTATGGACGAGCA GGCGG-3' T_M= 60 °C	Forward PCR for NHE1-HF / BAMH1-HF pET21a-HA-STRN-TurboID/MiniID-His and NHE1-HF / KPN1-HF pcDNA3.1 HA-STRN-TurboID/MiniID
21STRN rev	5'-GATCGGATTCTACAAAGACCTTAGCCAGGGCG-3' T_M= 60 °C	Reverse PCR for NHE1-HF / BAMH1-HF pET21a HA-STRN-TurboID/MiniID-His
21EB1 fw	5'-GATCGCTAGCATGTACCCATACGATGTTCCAGATTACGCTAT GGCAGTGAACGTATACTCAACGTC-3' T_M= 60 °C	Forward PCR for NHE1-HF/ BAMH1-HF pET21a HA-EB1-TurboID/MiniID-His and NHE1-HF / KPN1-HF pcDNA3.1 HA-EB1-TurboID/MiniID
21EB1 rev	5'-GATCGGATTCCTCCTCCTGTGGGCCCC-3' T_M= 60 °C	Reverse PCR for NHE1-HF / BAMH1-HF pET21a HA-EB1-TurboID/MiniID-His
21*x*/TPX2 fw	5'-GATCGCTAGC ATGTACCCATACGATGTTCCAGATTACGCT ATGGCAGACGCGCAGG-3' T_M= 60 °C	Forward PCR for NHE1-HF / BAMH1-HF pET21a HA-*x*/TPX2-TurboID/MiniID-His and NHE1-HF / KPN1-HF pcDNA3.1 HA-*x*/TPX2-TurboID/MiniID
21*x*/TPX2 rev	5'-GATCGGATTCGCACTTAAACCTGTCCGAGAAGTTAGG-3' T_M= 60 °C	Reverse PCR for NHE1-HF / BAMH1-HF pET21a HA-*x*/TPX2-TurboID/MiniID-His
21*hs*TPX2 fw	5'-GATCGCTAGC ATGTACCCATACGATGTTCCAGATTACGCTATGTCACAAGTT AAAAGCTCTTATTCCTATGATG-3' T_M= 59 °C	Forward PCR for Nhe1-HF / BAMH1-HF pET21a HA-*hs*TPX2-TurboID/MiniID-His and NHE1-HF / KPN1-HF pcDNA3.1 HA-*hs*TPX2-TurboID/MiniID
21*hs*TPX2 rev	5'-GATCGGATTCGCAGTGGAATCGAGTGGAGAATTTG-3' T_M= 59 °C	Reverse PCR for NHE1-HF / BAMH1-HF pET21a-HA-*hs*TPX2-TurboID/MiniID-His
cDNATurboIDfw	5'-GATCGCTAGCATGTACCCATACGATGTTCCAGATTACGCTAT GAAAGACAATACTGTGCCTCTGAAG-3'	Forward PCR for NHE1-HF / KPN1-HF pcDNA3.1 HA-TurboID-

	T_M= 59 °C	
cDNATurboID rev1	5'-GATCGGTACCGTGCGGCCGCAAGC-3' T_M= 60°C	Reverse PCR for NHE1-HF/ KPN1-HF pcDNA3.1 HA-TurboID
cDNATurboID rev2	5'-GATCCTCGAGGTGCGGCCGCAAGC-3' T_M= 60 °C	Reverse PCR for NHE1-HF / XHO1 pcDNA3.1 HA-X-TurboID fusion constructs
cDNAMiniIDfw	5'-GATCGCTAGC ATGTACCCATACGATGTTCCAGATTACGCTATGATCCCGCTG CTGAACG-3' T_M= 60 °C	Forward PCR for NHE1-HF/ KPN1-HF pcDNA3.1 HA-MiniID-
cDNAMiniID rev1	5'-GATCGGTACCTCTTTTCGGCAGACCGCAG-3' T_M= 60 °C	Reverse PCR for NHE1-HF/ KPN1-HF pcDNA3.1 HA-MiniID-
cDNAMiniID rev2	5'-GATCCTCGAGTCTTTTCGGCAGACCGCAG-3' T_M= 60 °C	Reverse PCR for NHE1-HF / XHO1 pcDNA3.1 HA-X-MiniID fusion constructs
P2AmKate2 fw	5'-GATCCTCGAGGGATCCGGAAGCGGAGCTAC-3' T_M= 60 °C	Forward PCR for XHO1 /ECORV pcDNA3.1 HA-X-XID-P2A-mKate2
P2AmKate2 rev	5'-GATCGATATCCTATCTGTGCCCCAGTTTGCTAGG-3' T_M= 60 °C	Reverse PCR for XHO1 /ECORV pcDNA3.1 HA-X-XID-P2A-mKate2
pCSTurboIDfw	5'-ATCCACTAGTGGCGCGCCTACCCATACGATGTTCCAGATTA CGCTATGAAAGACAATACTGTGCCTCTGAAG-3' T_M= 59 °C	Forward PCR for ASC1 /XHO1 pCS2+8 HA-TurboID
pCSTurboID rev	5'-GATCCTCGAGTCAGTGGTGGTGGTGGTGG-3' T_M= 57 °C	Reverse PCR for ASC1 /XHO1 pCS2+8 HA-TurboID
pCSMiniIDfw	5'-ATCCACTAGTGGCGCGCCATGTACCCATACGATGTTCCAGA TTACGCTATGATCCCGCTGCTGAACG-3' T_M= 60 °C	Reverse PCR for ASC1 /XHO1 pCS2+8 HA-MiniID
pCSMiniID rev	5'-AGAGGCTCGAGTCTTTTCGGCAGACCGCAG-3' T_M= 60 °C	Reverse PCR for ASC1 /XHO1 pCS2+8 HA-MiniID
pCSSTRN-TurboIDfw pCSSTRN-MiniIDfw	5'-ATCCACTAGTGGCGCGCCTTAATTAAGGCCGGCCATGTACC CATACGATGTTCCAGATTACGCT-3' T_M= 60 °C	Forward PCR for PAC1 /XHO1 pCS2+8 HA-STRN-TurboID pCS2+8 HA-STRN-MiniID
pCSSTRN-TurboID rev pCSEB1-TurboID rev pcs*x*/TPX2-TurboID rev	5'-GAGGCTCGAGTGCGGCCGCAAGCTTCTTTTC-3' T_M= 60 °C	Reverse PCR for PAC1 /XHO1 pCS2+8 HA-STRN-TurboID pCS2+8 HA-EB1-TurboID pCS2+8 HA-*x*/TPX2-TurboID
pCSSTRN-MiniID rev pCSEB1-MiniID rev pCS*x*/TPX2-MiniID rev	5'-TCTAGAGGCTCGAGTCTTTTCGGCAGACCGCAG-3' T_M= 60 °C	Reverse PCR for PAC1 /XHO1 pCS2+8 HA-STRN-MiniID pCS2+8 HA-EB1-MiniID pCS2+8 HA-*x*/TPX2-MiniID
pCSEB1-TurboID fw pCSEB1-MiniID fw	5'-CACTAGTGGCGCGCCATGTACCCATACGATGTTCCAGATTA CGCTATGGCAGTGAACGTATACTCAACG-3'T_M= 60 °C	Forward PCR for ASC1 /XHO1 pCS2+8 HA-EB1-TurboID HA-EB1-MiniID
pCS*x*/TPX2-TurboID fw pCS*x*/2TPX2-MiniID fw	5'-TGCAGGATCCATGTACCCATACGATGTTCCAGATTACGCTAT GGCAGACGCGCAGG-3' T_M= 60 °C	Forward PCR for BAMH1-HF /XHO1 pCS2+8 HA-*x*/TPX2-TurboID HA-*x*/TPX2-MiniID
KO sgRNA1 sense	5'-CACC G AACAACCACCCGGGCGCCGG-3' T4 PNK annealing	Forward for BBS1-HF PX459 STRN CRISPR KO
KO sgRNA1 antisense	5'-AAAC CCGGCGCCCGGGTGGTTGTTC-3' T4 PNK annealing	Reverse for BBS1-HF PX459 STRN CRISPR KO
siRNA1 STRN KD Silencer™ Select	Ambion™ Thermofisher s13587	STRN KD
siRNA2 STRN KD Silencer Select	Ambion™ Thermofisher s13588	STRN KD
siRNA MAD2	MAD2L1-HSS106243	MAD2 KD

Table 8: Antibodies and chemical staining reagents.

Primary antibodies						
STRN antibody rabbit	Proteintech	21624-1-AP		1 : 500	1 : 800	No, polyclonal
Anti-STRN rabbit	Prestige Antibodies® Powered by Atlas Antibodies	HPA017286	RALLGFSSDVTDREDDKNQDSVVNG TEAEVKETAMIAKSELTDSASVLDNFK FLESAAADFSDEDEDDDVDGREKSVI DTSTIVRKKALPDSGEDRDTKEALKE FDFLVTSEEGDNESRSAGDGTDWEK EDQC *hs*STRN$^{aa20-152}$	1 : 500	1 : 800	Yes, polyclonal
STRN-AB0 Purified mouse anti-STRN clone 6	BD Transduction Laboratories™	610838	TFPPSSGKSFIMGADEALESELGLGE LAGLTVANEADSLAYDIANNKDALRK TWNPKFTLRSHFDGIRALAFHPIEPVL ITASEDHTLKMWNLQKTAPAKKSTSL DVEPIYTFRAHKGPVLCVVMSSNGEQ CYSGGTDGLIQSWSTTNPNV ratSTRN$^{aa450-600}$	1 : 1000	1 : 1000	Yes, monoclonal
STRN-AB1 rabbit *newly generated*	CASLO ApS		(107)**QHE**WARFEVERAQWEVER(124), (137)**ERK**GQENLKKDLVRR(151) and (160) **KQE**RAKYHKLKYGTE (174) 3 mixed human peptides for 2 rabbits	1 : 500	1 : 800	No, polyclonal
STRN-AB2rabbit *newly generated*	Davids Biotechnologie		(290) **AAA**DFSDEDEDDDVDGREK (308) and (386) **YKK**ERKGKKGVKRPNRS (402) 2 mixed human peptides 2 rabbits	1 : 500	1 : 800	Yes, polyclonal
STRN-AB3 rabbit *newly generated*	Seramun Diagnostica GmbH		(386) **YKK**ERKGKKGVKRPNRS (402) Multiple organisms (conserved peptide) 1 human peptide for 2 rabbits	1 : 500	1 : 800	Yes, polyclonal
Anti-EB1 rabbit	Sigma	E3406	C-terminus, synthetic peptide *hs*EB1$^{aa252-268}$	1 : 500	1 : 1000	polyclonal
Anti-*x*lSSX2IP rabbit	Bärenz *et al.*[102]		*Xenopus laevis x*lSSX2IP	1 : 500	1 : 800	polyclonal
Anti-*hs*SSX2IP rabbit	Bärenz *et al.*[102]		human SSX2IP	1 : 500	1 : 800	polyclonal
Anti-*x*lTPX2 rabbit	Gruß *et al.*[203]		*Xenopus laevis x*lTPX2	1 : 500	1 : 800	polyclonal
Anti-*hs*TPX2 rabbit	Gruß *et al.*[203]		human TPX2	1 : 500	1 : 800	polyclonal
Anti-α-tubulin mouse	Sigma	T5168	human TUBA4A (tubulin α 4a)	1 : 1000	1 : 1000	monoclonal
Anti-α-tubulin rat clone YOL 1/34	Millipore Sigma	CBL270	human TUBA4A$^{aa414-422}$	1 : 1000	1 : 1000	monoclonal
Anti-acetylated-tubulin (Lys40) mouse	Proteintech®	66200-1-lg	synthesized peptide derived	1 : 1000		monoclonal
Anti-γ-tubulin mouse	Sigma	T6557	synthetical γ-tubulin peptide, KLH conjugated	1 : 2000	1 : 1000	monoclonal
Anti-HA rabbit	Sigma	H6908	YPYDVPDYA	1 : 1000	1 : 1000	polyclonal
Anti-GRP78 rabbit	MyBio Source	MBS854638	synthesized peptide derived from human GRP78	1 : 1000	1 : 1000	polyclonal
Anti-GAPDH mouse	Sigma	CB1001	Purified rabbit muscle	1 : 1000	1 : 1000	monoclonal
Anti-Paxillin mouse clone PXC-10	Sigma	P1093	C-terminal part of recombinant chicken paxillin$^{aa305-559}$	1 : 1000	1 : 1000	monoclonal
Anti-Vinculin mouse clone hVIN-1	Sigma	V9131	Purified human uterus	1 : 1000	1 : 1000	monoclonal
Anti-*x*lRHAMM rabbit	Jacopo *et al.*[202]		recombinant *Xenopus* GST-RHAMM-CT (corresponding to the last 137 aa) and affinity purified	1 : 1000	1 : 1000	polyclonal
Anti-*hs*SMN rabbit	Husedzinovic *et al.*[292]			1 : 800	1 : 1000	polyclonal
Anti-MPM2 mouse	abcam	ab14581	tissue/ cell preparation (mitotic human HeLa cell cytosolic lysate).	1 : 1000	1 : 1000	monoclonal
Anti-*x*lCyclin B guinea pig	Reber *et al.*[179]			1 : 300	1 : 500	polyclonal
Anti-GFP rat (1A5)	bioacademia		Recombinant GFP protein	1 : 1000	1 : 1000	monoclonal

Anti-GFP mouse IgG1κ (clones 7.1 and 13.1)	Roche	11814460001	purified immunoglobulin	1 : 1000	1 : 1000	monoclonal
Anti-ARL13B rabbit	Proteintech®	17711-1-AP	ARL13B fusion protein Ag12015 derived		1 : 1000	polyclonal
Secondary antibodies						
Goat Anti-rabbit HRP	abcam	ab6721	rabbit IgG H&L, whole molecule	1 : 10000		polyclonal
Goat Anti-mouse HRP	sigma	A0168	mouse IgG Fc specific	1 : 10000		polyclonal
Goat Anti-rabbit IgG H&L Cy3 ®	abcam	ab6939	full length native rabbit IgG		1 : 1000	polyclonal
Goat Anti-Rabbit IgG H&L Cy2 ®	abcam	ab6940	full length native rabbit IgG		1 : 1000	polyclonal
Goat Anti-mouse IgG H&L Cy3 ®	abcam	ab97035	full length native mouse IgG		1 : 1000	polyclonal
Goat Anti-mouse IgG H&L Cy2 ®	abcam	ab6944	full length native mouse IgG		1 : 1000	polyclonal
Donkey anti-rabbit IgG Alexa Fluor 594	Invitrogen™	A-21207	γ-immunoglobins heavy and light chains		1 : 1000	polyclonal
Donkey anti-mouse IgG Alexa Fluor 594	Invitrogen™	R37115	γ-immunoglobins heavy and light chains		1 : 1000	polyclonal
Goat anti-rabbit IgG Alexa Fluor 488	Invitrogen™	A32731	γ-immunoglobins heavy and light chains		1 : 1000	polyclonal
Donkey anti-mouse IgG Alexa Fluor 488	Invitrogen™	R37114	γ-immunoglobins heavy and light chains		1 : 1000	polyclonal
Goat anti-rat IgG Alexa Fluor 488	Invitrogen™	A-11006	γ-immunoglobins heavy and light chains		1 : 1000	polyclonal
Goat anti-rat Alexa Fluor 594	abcam	ab150160	Synthetic peptide corresponding to IgG		1 : 1000	polyclonal
Labeling (bio)reagents						
Hoechst	abcam	ab228551	DNA, nucleus	1 µg/mL		chemical
Streptavidin-488	Invitrogen™	S11223	biotinylation, Biotin	1 : 1000		Recombinant protein
Streptavidin-HRP	Rockland Inc	S000-03	biotinylation, Biotin	1 : 40000		Recombinant protein

○ 2.3 Molecular cloning procedure

The cloning of full length *strn, eb1, egfp*, *mkate2* and different *bioid* coding sequences (CDS) was performed with Q5 DNA polymerase (New England Biolabs). The oligos were purchased at Integrated DNA Technologies, Inc. (IDT, Leuven) and designed with respective 5' prime overhang for desired restrictions enzymes and case-specific tags. The template, PCR-product, digestion-product and plasmid concentration was measured with a NanoVue Plus™ Spectrophotometer (GE Healthcare). Each time I prepared a fresh TAE (tris based acetic acid EDTA) agarose gel electrophoresis, which is especially used for separation and purification (visible by addition of 0,5 µg/mL ethidium bromide) of nucleic acids such as DNA or RNA. By applying an electric charge, nucleic acids move through an 1% agarose in TAE matrix field.

Pipetting scheme for Q5® High-Fidelity DNA Polymerase

5-100 ng template DNA10 µL 5x Q5 reaction buffer (New England Biolabs)
10 µL 5x GC Enhancer (necessary for *strn* cDNA amplification (New England Biolabs))
1 µL dNTP-Mix (10 mM Life Technologies)
2,5 µL forward primer (10 pmol/µL Integrated DNA Technologies, Inc.)
2,5 µL revers primer (10 pmol/µL Integrated DNA Technologies, Inc.)
0,5µL Q5 High-Fidelity DNA Polymerase (New England Biolabs)

- Add to 50 µL with ddH_2O

Following program was used for gene amplification:

Table 9: Thermocycler program for DNA amplification.

Initial denaturation	98 °C	30 sec
25 - 35 cycles	98 °C 50 – 72 °C *(Primer-specific T_M)* 72 °C	10 sec 30 sec 30 sec/kB
Final extension	72 °C	2 min
Hold for cooling	4 °C	unlimited

The PCR products were purified with FastGene's PCR protocol (Nippon Genetics). 2 µg of purified products were overnight digested with high fidelity endonuclease and CutSmart® buffer. Digested fragments were purified with FastGene's gel extraction protocol (Nippon Genetics).

For ligation reaction I used 200 ng total DNA in a 1:3 (insert : vector) relation with 2 U of T4 DNA Ligase (NEB). The DNA fragments were fused for 2 h at RT or overnight at 16 °C.

Table 10: Antibiotics, immunochemicals and toxins for selection.

Reagent	Abb.	Stock Conc.	Working Conc.	Notes/usedfor…
Ampicillinsodiumsalt	Amp	100 mg/mL	100 µg/mL	plasmid selection in bacteria
Chloramphenicol	Cam	20 mg/mL	20 µg/mL	plasmid selection in bacteria; only candidate that required EtOH and not H_2O as solvent
Geneticindisulfatesalt	G418	100 mg/mL	300 - 500 µg/mL	Used for plasmid selection in cell culture
Gentamicinsulfate	Gen	20 mg/mL	20 µg/mL	plasmid selection in *E. coli* ArticExpress cryostocks
Kanamycinsulfate	Kana	25 mg/mL	25 µg/mL	plasmid selection in bacteria
Penicillin G	Pen	100x	50 u/mL	the prevention and elimination of bacterial contaminants in cell culture
Puromycin	Puro	10 mg/mL	2 µg/mL	plasmid selection in cell culture
Streptomycin sulfate	Strep	60 mg/mL 100x	60 µg/mL	plasmid selection in *E. coli* ArticExpress cryostocks and prevention and elimination of bacterial contaminants in cell culture

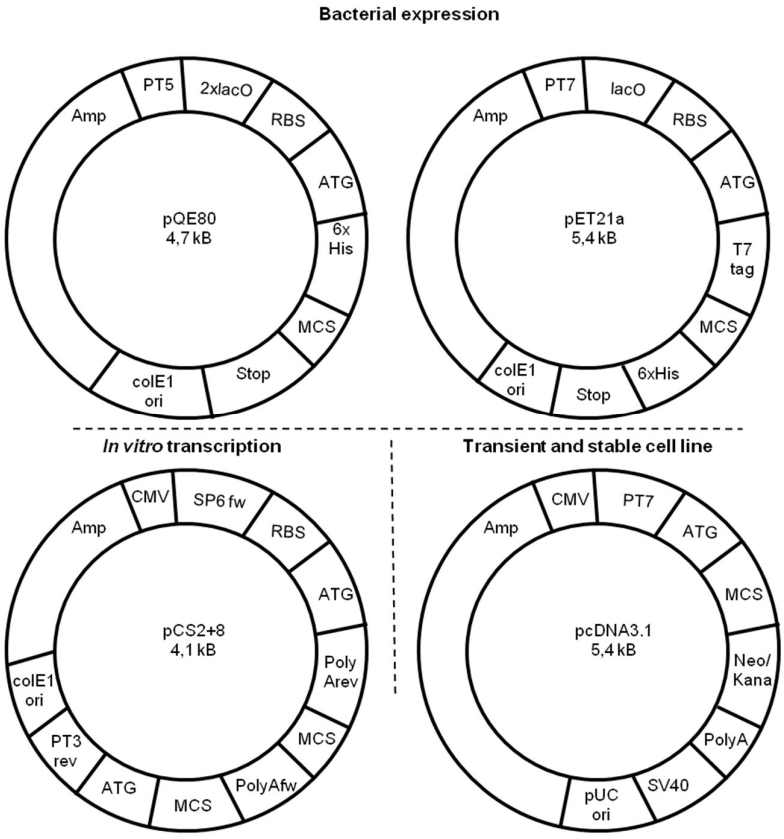

Figure 6: Scheme of the here used plasmid vectors, differences and their purpose. The here seen empty vectors were the base for the here used cloning strategy. The previous table 6 shows the vector matrices for the cloned inserts. The upper ones were used for bacterial expression of recombinant protein (like CAMKII$^{aa1\text{-}290}$) in different *E. coli* strains (table 5). The lower two plasmids were used for two different purposes in human cell culture: The eSpCAS9 vector contains the coding for the CRISPR/CAS9 protein. A specific cut in the genomic DNA is produced with a cloned STRN KO guide oligo. The linearized pcDNA3.1 was transfected into IMR-90 cells. This was done transient and under selection for genomic stable cells.

In order to amplify plasmid or to transform it into bacteria strains for protein expression, I used the heat shock transformation protocol according to Hanahan *et al.*[286]. For the DNA amplification of the in figure 6 seen plasmids, a single colony was selected from agar plates. Overnight bacterial cultures were set up for mini-preparation using the protocol from Birnboin and Doly[293]. Positive clones were verified with enzymatic digestion according to the cloning strategy. In a last step I re-transformed positive clones and re-cultured them in midi-pure grade with PureLink™ HiPure Plasmid Filter Maxiprep Kit (Life Technologies).

2.4 SDS page and immunoblotting

The analytical and preparative sodium dodecyl sulfate polyacrylamide gel electrophoresis (SDS PAGE) was performed as published in Laemmli 1970[281]. The gel percentage and recipe composition is found in following table 11. The gel's mesh density was adapted as required.

Table 11: Recipes for here used protein gel electrophoresis.

4 mL of 6% stacking gel	10 mL of 8% separating gel	10 mL of 10% separating gel
2,7 mL H_2O	4,7 mL H_2O	4,1 mL H_2O
0,8 mL acrylamide (30%)	2,7 mL acrylamide (30%)	3,3 mL acrylamide (30%)
0,5 mL 1M tris (pH 6,8)	2,5 mL 1,5 M tris (pH 8,8)	2,5 mL 1,5 M tris (pH 8,8)
20 µL SDS (20%)	50 µL SDS (20%)	50 µL SDS (20%)
40 µL APS (10%)	100 µL APS (10%)	100 µL APS (10%)
4 µL TEMED	10 µL TEMED	10 µL TEMED

An electroblot was performed in order to transfer proteins from gel to nitrocellulose membrane. For wet blotting I used Amersham™ Protran® Western blotting nitrocellulose membrane (GE Healthcare) and blotted for 2 h at 400 mA. Blotting was verified with PonceauS and blocked with PBS with 0,05% tween-20 and either 5% milk powder or 1% BSA for 20 min at RT. Primary antibody binding was performed with overnight incubation with gently shaking at 4 °C. Secondary antibody binding was done for 1-3 h shaking at RT. For *Xenopus laevis* egg extract samples I diluted the extract in an 1:10 relation with 4x sample buffer (200 mM tris [pH 6,8], 400 mM DTT, 8% SDS, 4% bromophenol blue, 40% glycerol) and loaded 0,25 µL -1 µL pure extract onto the gels.

○ 2.5 Expression and purification of recombinant proteins

The expression protocol of recombinant proteins was adapted to the different expressing *E. coli* strains used in this study. The soluble recombinant proteins of CAMKII$^{aa1\text{-}290}$ and RAN^{Q69L} were obtained like previously described[179,245,273,289]. Every bacteria strain was induced with 0,2 mM IPTG. The expression culture was supplemented with 1 mM PMSF. For STRN (fusion) constructs I tested different expression strains (table 5), protocols and plasmids according to the manufacturer's recommended procedures. All proteins were purified according to the expression strain manufacturer protocol or Porath *et al.*[294]. All pre-cooled purification buffers were supplemented with 1 mM PMSF, 1x cOmplete™, EDTA-free protease inhibitor cocktail (Roche) and. 10 mM DTT. For purification His-tagged proteins were bound to Ni-NTA agarose (Jena Bioscience) beads, washed and eluated with PBS containing 400 mM imidazole. The purified proteins were dialyzed against CSF salt buffer, they were concentrated with a Vivaspin 6 (10 kDa MWCO, Sartorius) column and their concentration was checked with a BSA gradient on a Coomassie (InstantBlue® by abcam) gel and they were fractionated, snap-frozen in liquid nitrogen and stored at - 80 °C.

○ 2.6 Antibodies and labeling reagents

The peptide antibodies against the conserved STRN protein were produced in rabbits by CASLO ApS (STRN-AB1), Davids Biotechnologie GmbH (STRN-AB2) and Seramun Diagnostica GmbH (STRN-AB3). STRN is conserved between species. The first and the second (CASLO ApS and Davids Biotechnology) antibody came as mixed serum. Purification from rabbit serum was performed with an antigen coupled SulfoLink™ coupling resin (Thermo Fisher Scientific) according to the manufacturer's protocol. The STRN-AB3 antibody was delivered as purified fraction. Every ordered peptide antibody was diluted with 50% glycerol and stored at – 20 °C. The commercial antibodies were fractionated, snap-frozen in liquid nitrogen and stored at – 80 °C. All of the here generated peptide antibodies were suitable to be used in human and frog cells. The STRN antibodies were selectively optimized, in order to guarantee higher substrate specificity and isoform distinction, the higher the AB-number the better the antibody. The most specialized anti-STRN antibody was STRN-AB3.

2.7 Immunofluorescence staining and microscopy

Indirect immunofluorescence microscopy is a powerful tool to analyze intracellular antigene localization in cell culture monolayers or tissues. The human cell lines (IMR-90, IMR-90 stable clones, hTERT RPE-1, HeLa, HeLa stable clones or XL-177) were cultured onto cover slips to a confluence of 60 – 90%. The cells were washed with PBS and fixated with either ice-cold 100% methanol (MeOH) for 10 min at - 20 °C or PBS with 4% PFA for 20 min at RT. After fixation the samples were washed 3 times with PBS. The permeabilization was done with PB + 0,5% TX100 for 5 min. For blocking I used 5% goat serum or ROTI® Immunoblock (Roth) in PBS for 30 min at RT. Primary antibodies were diluted in PBS and incubated for 1 h at RT. The same was done with the secondary antibodies, after a further 3 times PBS washing step. All chemical reagents like DAPI or labeled streptavidin were incubated simultaneously with the secondary antibody. In the end the cover slips were mounted with Fluoromount-G™ (Thermo Fisher Scientific) onto a microscope slide.

For the *Xenopus laevis* egg extract fixated samples, I used 0,2 mg/mL Cy3-labeled tubulin in order to visualize MT dynamics. For a statistical meaningful verification 4 samples (each 1,5 µL fixated extract) of each condition were analyzed. Distinct MT structures were counted with the 40x and 63x air objective for magnification.
For documentation of immunofluorescence microscopy a Zeiss Axiophot, the Leica DM5500B and Keyence BZ-X800E were used to localize specific signal in defined optical sectional planes. Comprehensive analysis and image processing were ensued using Zeiss ZEN Blue 2012, Leica LAS AF and the BZ-X software package. For further processing Adobe® Photoshop® CS6 and Fiji/ImageJ were used. The statistical analysis and plotting was done in MS Excel 2003, PSPP (GNU-project) by matched-pair student's t-test and gnuplot 5.4.1[295].

2.8 Preparation of *Xenopus laevis* oocytes and eggs

For stage VI oocytes I surgically removed the ovary of adult *Xenopus laevis* females. The tissue was treated with 1,5 h in 0,1 mg/mL liberase (Roche) in 1x MBS buffer (80 mM NaCl, 1 mM KCl, 1 mM $MgSO_4$ x $7H_2O$, 50 mM HEPES, 25 mM $NaHCO_3$, pH 7,8 adjusted with NaOH; plus 0,7 mM $CaCl_2$ freshly added)[296,297]. The separation of largest or mature oocytes was first done with sieves (Hobby 21630 aquaristics with > 300 nm, > 560 nm and for stage VI oocytes > 900 nm) and second by eye-selection. The selected oocytes were washed with CSF buffer and gently crushed to extracts as previously done[172]. All oocyte extracts were compared with egg extracts by Coomassie (InstantBlue® by abcam) and Western blot (anti-α-tubulin, anti-*xl*TPX2).

Preparation of *Xenopus laevis* egg extracts and functional assays in *Xenopus* egg extracts CSF-arrested (M phase) were prepared as described previously[172]. The energy mix, leupeptin, pepstatin, chymostatin (LPC) or protease inhibitors were omitted because it would not change the results significantly. A view crude extract samples were provided by P. Liu and E. Schiebel (ZMBH Heidelberg, Germany). The mitotic arrest and aster formation of CSF extracts was checked via addition of 10 nM RAN^{Q69L} and 0,2 mg/mL Cy3-labeled tubulin.

A full cell cycle was allowed, and the system was rearrested in M-phase using CSF extract as described previously[203,298,299]. Spindle assembly was monitored by adding < 500 nuclei/µL of *X. laevis* sperm nuclei and 0,6 mM $CaCl_2$[299–302]. Sperm nuclei were provided by W. Antonin (Institute of Biochemistry and Molecular Cell Biology, RWTH Aachen, Germany). The workflow to generate complete bipolar spindles is seen in figure 7.

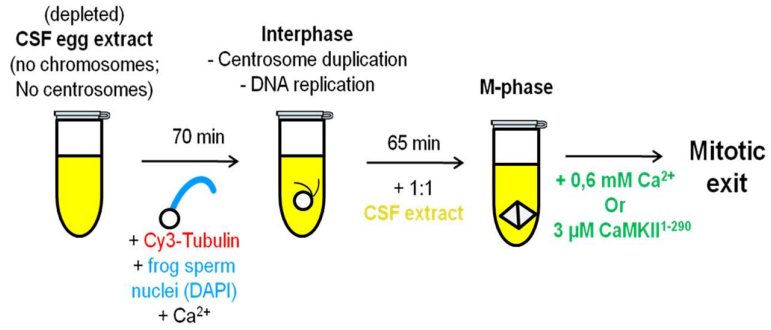

Figure 7: Setup for spindle assembly and chromatid segregation assay. The *Xenopus laevis* egg extract can be cycled through one round of the cell cycle by addition of Ca^{2+} and sperm nuclei. The nuclei provide chromosomes and centrosomes that can be replicated in interphase. When this cycled extract is diluted 1:1 with mitotic extract, it finds its way back into a mitotic stage. The here as M-phase referred condition has the advantage to form bipolar spindles. These can be observed by addition of fluorescent labeled Cy3-tubulin. Differences between non-depleted and STRN-depleted extracts can be analyzed and chromatid segregation deficiencies determined.

In order to assay mitotic MT assembly and metaphase to anaphase transition, CSF extracts were activated and incubated for 60-90 min at 20 °C to reach interphase. Addition of mitotic extract 1:1 (vol/vol) and 40-65 min incubation recovered metaphase. Spindle reactions were preserved by squashing under a coverslip with fixation buffer (48% glycerol, 1x MMR [100mM NaCl, 2 mM KCl, 1 mM $MgSO_4$, 2 mM $CaCl_2$, 5 mM HEPES (pH 7,8), 0.1 mM EDTA], 11% formaldehyde, and 5 µg/mL DAPI)[303]. Mitotic exit samples were generated by adding further 0,6 mM $CaCl_2$ or 3 µM of $CAMKII^{aa1-290}$ to the complete spindle mitotic extract[179,245].

2.9 Immunodepletion in *Xenopus laevis* egg extracts

Co-immunoprecipitation (co-IP) in cell lysates and cell-free extracts, like the CSF-arrested mitotic *Xenopus laevis* egg extract, is a common way to catch the protein or antigen of interest (POI) and purify it through specific antibodies[304]. In case of co-IP the antibody can be coupled to protein A bound magnetic beads and the immune complex can be precipitated easily. Optimization like chemical coupling of the antibody to the beads and higher stringency of washing buffer with detergent and high salt concentration are possibilities to get rid of false binding partners. This method is highly depending on the antibody specificity and the interactome to one distinct time point[305]. Weak and transient interactions (like the rapid kinase/phosphatase PTM shift) are not covered.

For STRN and control Δmock/anti-IgG depletion in egg extract I bound 50 µg affinity purified antibody to 50 µL protein-A Dynabead slurry (Life Technologies). Therefore the magnetic beads were equilibrated with PBS containing 0,1% triton X-100. The washed beads were diluted in antibody and filled up with PBS-TX100 to 300 µL. The binding of the antibodies to the protein-A was done under rotation and 4 °C over night. Unbound excess antibody was removed by washing 2 times with PBS-TX100. The antibody-bead mix was equilibrated for the egg extract by washing it with CSF buffer (100 mM KCl, 2 mM $MgCl_2$, 10 mM HEPES, pH 7,8 with KOH). For depletion the buffer was removed and the extract gently mixed with semi-dry antibody-bead mix. The antibody binding to the frog egg extract (with anti-STRN or anti-IgG) was done for 45 min on ice. The beads were resuspended every 20 min for proper distribution of bead-coupled antibody.

The beads were washed 4 times with CSF^+ (250 mM KCl, 2 mM $MgCl_2$, 10 mM HEPES, 0,1% TX100) and two times with PBS-TX100. The immune-bound proteins were eluated with 50 µL of 100mM glycine (pH 2.5). After 15 min rotation at room temperature the bead-free supernatant was used for cold iso-propanol protein precipitation. The pellet was air dried and resuspended in SDS Laemmli sample buffer. This IP fraction was used for analysis by Coomassie, silver staining (protocol according to Kerényi[306]), WB and MS . The STRN and IgG-depleted extract was cycled for bipolar spindle assembly and chromatid segregation assay (figure7)[302].

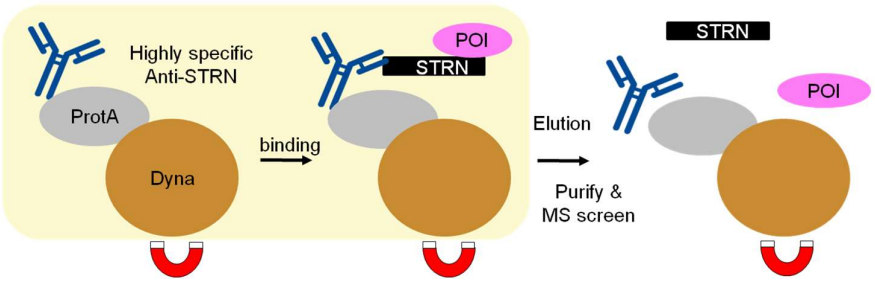

Figure 8: Immunodepletion and immunoprecipitation concept. The strategy is based from a method published in 1986[307]. Recombinant 45 kDa protein A is covalently coupled to 2,8 µm super paramagnetic beads. Because of protein A, these commercially available so called Dynabeads™ (Thermo Fisher Scientific) can be linked to a highly specific anti-STRN antibody. This bead-antibody complex is suitable for STRN, and STRN-interactor fishing in protein rich mitotic *Xenopus laevis* egg extracts. After stringent washing the eluate is used for mass spectrometry.

Proteins from rabbit sera could lead to false positives in IP mass spectrometry, since they also interact with the *X. laevis* LSS (low speed supernatant).In later experiments I covalently coupled the antibody to the magnetic protein-A beads. Covalently coupling enables harder washing of the antibody and proteins from immunogenization and serum-purification can be rejected. As previously the antibody-protein-A Dynabeads were washed with PBS-TX100 after overnight binding. The beads were washed two times with 100 mM sodium borate, pH 9.

The crosslinking was done by adding 5,2 mg DMP/mL buffer under rotation for 30 min at RT. The reaction was stopped by washing two times with 200 mM ethanolamine, pH 8,0. A second wash was done under rotation for 30 min at RT. Next the not covalently crosslinked proteins or excess proteins were removed by washing 2 times < 2 min with 100 mM glycine, pH 2,5. Finally the beads were washed two times with PBS-TX100 and were ready for previous depletion protocol. I used 100 mM glycine, pH 2,5 for elution. This method should be able to natively pull down STRN associated complexes from the protein lysates. Since the corresponding Western blots and Coomassie verification gave no adequate signal for STRN, I switched to the non-crosslinked antibody for MS analysis.

2.10 Sucrose gradient centrifugation of *Xenopus laevis* egg extracts

In order to check if STRN is assembled as supramolecular complex with other proteins, I fractionated the *X. laevis* egg extract by protein size, density and shape, their so called Svedberg units. This is done by a sucrose gradient with and without high salt using the HSS. Since the stage VI oocytes have a low STRN concentration, a cell cycle specific verification (interphase/M-phase) was done with *Xenopus tropicalis* eggs and fertilized embryos as well. I got this cells and blastocysts from Prof. Dr. Dietmar Schmucker and Dr. Gabriela Edwards Faret from the LIMES institute of Universität Bonn. The embryos were not older than 4 h (64 cell stage maximum). They were prepared as previously described[172].

I made high-speed supernatant (HSS) by 1 h, 100.000x g, 4 °C centrifugation. The clear supernatant was directly loaded on top of a 10 - 40% linear sucrose gradient (with and without 1 M NaCl) buffered with CSF-salts buffer. Centrifugation was performed in a TLS-55 rotor at 100.000x g for 2 ½ h at 4 °C. Fifteen fractions of 550 µL each were collected from top to bottom of the gradient and tested by immunoblotting.

2.11 Purification of MAPs from oocyte and egg extracts

The *Xenopus laevis* stage VI oocytes and egg extracts were produced as previously described[172]. For MAP purification one could use already nitrogen-frozen extracts. The high speed supernatant (HSS) extracts were won by 1 h centrifugation at 100.000x g with a TLA120.2 rotor at 4 °C. The clarified supernatant was preincubated for 5 min at 20 °C with 8% pentadiol. The MTs were polymerized by addition of 1 mM GTP, 10 µM cytochalasin D and 50 µM taxol at 20 °C. The control was 50 µM nocodazole instead of taxol at 4 °C. The mixture was incubated for 30 min and diluted 1 :2 (vol/vol) with BRB80 (80 mM K^+-PIPES, 1 mM EGTA, 1 mM $MgCl_2$, pH 6,8) with 1 mM GTP and respectively 50 µM taxol (20 °C) or 50 µM nocodazole (4 °C). The samples were loaded onto 2x volume buffer cushion (dilution buffer, with toxins and 25% glycerol) and centrifuged 10 min at 100.000x g with a TLA120.2 rotor.

The pellet was resuspended in dilution buffer with toxins and loaded onto the buffer cushion a second time. A second centrifugation washed the MT pellet. The pellets were resuspended in 4x laemmli buffer, cooked and loaded on gel. As before all oocyte extracts were quality checked by comparing them with egg extracts with Coomassie (InstantBlue® by abcam) and Western blot (anti-tubulin loading control, anti-*xl*TPX2, anti-*xl*SSX2IP).

Alternately to gel and blot analysis the taxol pellet was resuspended in PME (100 mM K^+-PIPES pH 6,9; 2 mM EGTA, 1 mM $MgSO_4$, 1 mM DTT, 0,1 mM GTP) according to the protocol by Sloboda[308]. After addition of 3,5 M NaCl the MAPs dissociate from the hyperstabilized tubulin. The tubulin polymers are pelleted by centrifugation and the MAP supernatant transferred into a dialysis tube. After desalting this sample could be used for IP, precipitation, gel and blot analysis.

2.12 Cell culture, transfection of linearized plasmids and generation of stable cell lines

All cell culture media, sera and reagents are acquired from Gibco™ (Thermo Fisher Scientific) PAN-Biotech. Embryonal IMR-90 lung fibroblasts were cultured in MEM Eagle supplemented with 10% fetal calf serum (FCS) containing 50 units/mL penicillin, and 50 µg/mL streptomycin in a humidified 5% CO_2 incubator. When reaching 80% to 90% confluence, cells were split. They were washed once with DPBS (Gibco) and detached by incubation of 5 min in 0,25% trypsin/EDTA at 37 °C. To stop the trypsinization, complete culturing media was added at a ratio of 5:1. Finally, cells were diluted >1:10, depending on the experiment. Mycoplasma testing was not performed before experiments and the DAPI signal implies no contamination during all experiments. The *Xenopus laevis* XL-177 cells were cultured under RT and all solutions for their maintenance were 20 °C during their usage.

In order to check the ciliogenesis, cells were starved for 72 h. The usual media was replaced with serum free media. Cell cycle analysis of IMR-90 cells synchronized in mitosis by either 100 nM nocodazole treatment for 8 h or (Aurora A kinase inhibitor) 4 µM MK-5108 (also known as VX-689)[309] treatment for 24 h. The late G_2/Prophase arrest was released by PBS wash and replaced with media without toxins for 80 min at 37 °C. An interphasic (S-phase) arrest was accomplished by culturing the cells in media supplemented with 2 mM thymidine.

In the regrowth experiment cell plates were incubated 60 min on ice to depolymerize the MT. Afterwards the cells were moved back onto a 37 °C heating plate for 4 min and directly MeOH fixated for IF staining.

Transient transfection was performed with eSpCAS9 (for STRN KO) and linearized pcDNA3.1 (for stable cell lines) plasmids. The plasmids were KPN1-HF restriction endonuclease digested and purified with FastGenegel/PCR Extraction Kit (Nippon Genetics). 1 µg of this DNA was transfected with 3,2 µL/mL Lipofectamine 2000 transfection reagent (Life Technologies) diluted in Opti-MEM I reduced serum media (Gibco, Life Technologies) following to the manufacturers recommendations.

For STRN KD experiments cells got transfected with 25 pmol Lipofectamine RNAiMAX (Life Technologies) Silencer™ Select siRNA (Ambion™ Thermofisher) following to the manufacturers recommendations. In both transfection strategies the media was replaced after 24 h. A stable genome integration of pcDNA3.1-transfected cells was achieved by 500 µg/mL G418 selection. Positive clones were recognized and single IMR-90 cells sorted by the mKate2 or EGFP reporter gene fluorescent signal.

For cryopreservation the trypsinized cell suspension was pelleted at 1000 rpm for 2 min. Cells were resuspended in 4 °C cold MEM Eagle supplemented with 20% FCS and 10% DMSO. The cryopreservation tubes were slowly cooled down to - 80 °C. For long-term storage, the frozen cells were transferred to liquid nitrogen. To thaw cells, the cryopreservation suspension was defrozen at room temperature and cells were washed once in MEM with additives and seeded on 10 cm plate.

2.13 Biotinylation assay with synchronized stable cells

An alternative promising method to study interaction proteomics came up in 2012: BIOID not only fishes for current interaction partners, but generates a cloud of near-natural potential candidates[310]. In this method a biotin ligase can be fused to a protein of choice and expressed or recombinantly added to a proper model like cell culture, cell free extract or stably integrated into the genome. After substrate addition the ligase labels proximate proteins of the region of destination within the cell. This technique has three advantages: First, very weak and transient interactions are covered, second, purification of biotinylated proteins can be easily done with streptavidin-based purification and, third, biotinylation is a rare PTM within the cell, which endogenous almost only occurs in context of rare carboxylation[311].

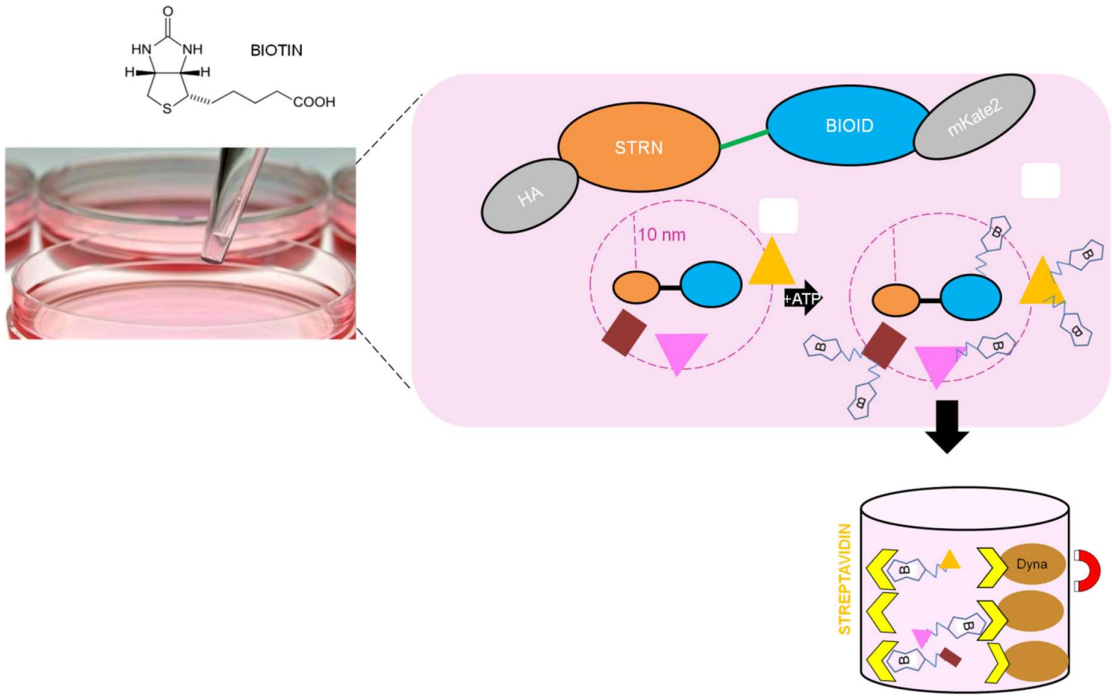

Figure 9: BIOID principle in cell culture. In this work I make use of an engineered faster version of the frequently described BIOID method, namely TurboID and MiniTurbo (here MiniID). In brief a transfected cell line expresses a fusion construct of your protein of interest (POI, here STRN). The fusion protein can be ubiquitous or is transported to its predetermined location in the cell. When biotin is added the biotin ligase starts to biotinylate proximate putative interaction partners in a range of around 10 nm. Thereby even transient interactions can be screened. This process is time and substrate concentration dependent. The biotinylated proteins can easily and stringently be separated by Streptavidin-based affinity purification. With optimized conditions a highly specific interactome can be deduced after mass spectrometry analysis.

The biotinylation distance of the here used BIOID biotin ligase is supposed to be around 10 nm. The higher the substrate concentration and the longer the incubation times, the more false targets are biotinylated[290]. During the last years several biotin ligases were tested, mutations were integrated and deletions were made in order to get a very fast, stable and small ligase tag, with minimum false labeling and maximum speed. Two inventions from engineering over the last years are TurboID and MiniTurbo (here MiniID)[288]. These fusion tags are already tested in multiple systems like yeast, fruit fly and nematodes[288].

On top of that they seem to be currently the fastest fusion tags. They are already tested at room temperature (RT, 20 °C) and their fast labeling which are two favorable aspects for using this technique in the *Xenopus laevis* embryonic extract model system, since it offers a highly concentrated protein amount (>100 µg of protein) for mass spectrometry. Here I use the human IMR-90 stable cell line at 37 °C for this assay, as a complementary analysis in a different model organism.

In order to get an appropriate amount of protein mass I cultured cells in two 15 cm plates to a confluence of 75% one day before the assay is done.
For the biotinylation assay I used different substrate concentration and incubation times, in order to determine the optimal concentration of exogenous biotin required for efficient labeling in IMR-90 cells. Biotinylation efficiency could be verified with Western blot. Since milk could contain free biotin the blot was blocked with 1% BSA. For detection I bound recombinant streptavidin peroxidase (streptavidin-horseradish peroxidase/HRP, Rockland) conjugate in a 1:20.000 dilution for 1h at RT.

The saturation point for biotinylation by BIOID or C terminal BIOID-fusions at 37 °C was reached with 150 µM biotin in 80 min. Just like the original publication showed MiniID and its fusions have a lower labeling efficiency, but generate less false positive background[288]. I used the same labeling conditions for MiniID as for TurboID and respective fusion constructs.

The extracellular biotin was removed by washing the cells with DPBS and trypsinized them as previously described. The cells were centrifuged and the pellet resuspended in 100-300 µL 4 °C cold RIPA lysis buffer (50 mM tris pH 8, 150 mM NaCl, 0.1% SDS, 0.5% sodium deoxycholate, 0,5% triton X-100, 0,5% NP-40) supplemented with 1x cOmplete™, EDTA-free protease inhibitor cocktail (Roche), 1 mM PMSF and 1 mM DTT. The lysates were incubated 5 min on ice and subsequently clarified with centrifugation at 4 °C for 16.000x g for 10 min.

The supernatants were transferred to a fresh tube. In order to stop the labeling reaction, I got rid of intracellular biotin in the lysates through Sephadex® G-25 gelfiltration (Sigma-Aldrich). The filtration media was solved in PBS excess and swelled over night at RT. Afterwards an appropriate amount (+/- 2 mL) loaded onto an empty PD-10 column (GE Healthcare). The G-25 media was equilibrated with PBS, supplemented with 1x cOmplete™, 1 mM PMSF and 1 mM DTT. The clarified RIPA lysates could be loaded onto the column, re-buffered to PBS (with previous additives) and biotin-free fractions collected. I checked in which fractions the biotinylated protein eluate by streptavidin-HRP Western blot and pooled them.

For purification of biotinylated targets I used MyOne™ streptavidin C1®-coupled magnetic dynabeads (Life Technologies) and equilibrated them with PBS supplemented with 1x cOmplete™, EDTA-free protease inhibitor cocktail (Roche), 1 mM PMSF and 1 mM DTT. The binding was done over night at 4 °C under rotation. The next day I checked the supernatant for unbound proteins and purified the beads: I washed the beads with 3x 1 mL PBS, 1 mL of 1 M KCl, 100 mM Na_2CO_3, 1 mL of 2 M (fresh) urea in 10 mM tris (pH 8) and again 2x 1 mL PBS. For purification and yield control the biotinylated proteins were eluted in 50 µL 4x laemmli sample buffer and verified by gel staining and streptavidin-HRP Western blot.

2.14 Synthesis of capped mRNA

For the *in vitro* transcription and later *ex vivo* translation in *Xenopus laevis* egg extract, I synthesized mRNA with 5'-Cap with them mMESSAGEmMACHINE™ SP6 transcription kit (Invitrogen) according to the manufacturers protocol. The template pCS2+8 plasmid was overnight digested with KPN1-HF and purified with phenol/chloroform extraction protocol with ROTI®Phenol/ Chloroform/ Isoamyl alcohol (Roth)[312].

Pipetting scheme for mMESSAGEmMACHINE™ SP6 mRNA Transcription

1 µg linearized plasmid template
20 µL 2x NTP/CAP
4 µL 10x reaction buffer — Incubated for 2 h at 37 °C
4 µL SP6 enzyme mix
Add to 40 µL with nuclease free water

The reaction was stopped and purified with LiCl precipitation with the Kit included solution and protocol. The pelleted mRNA was afterwards resuspended in 15 µL nuclease free water and quality checked with 1% agarose gel electrophoresis with 0,5 µg/mL ethidium bromide. For translation I used empirically dilutions of the purified mRNA templates in the egg extract (1:10, 1:50). The agarose gel resulted in positive mRNA transcription but the Western blot of the translation reaction no positive protein expression could be observed. Therefore this strategy was not followed any further and I focused onto previous discussed alternative methods.

2.15 Mass spectrometry and proteomic analysis

For identification of STRN-interaction partners I used the LC-MS/MS screening service done by the core facility for mass spectrometry & proteomics (CFMP) at the Zentrum für molekulare Biologie at the Heidelberg University (ZMBH) and the core facility for mass spectrometry from Institute of Biochemistry and Molecular Biology at the Bonn University (IBMB). The Coomassie (InstantBlue® by abcam) gel was run ¼ into a Criterion™ TGX™ precast gel (BIO-RAD). Each lane was cut out, reduced, alkylated and digested with trypsin according to their in-gel digestion protocol. Proteins were analyzed by sensitive Orbitrap-MS systems.

Data analysis was done with Scaffold (version 4.10.0). Unknown proteins (especially not curated ones in *Xenopus laevis*) were blasted against NCBI's blastp and UniProt database containing human reference proteome sequences[313,314]. When possible, the RefSeq sequence was used. The list of EntrezIDs got subtracted from candidates that are typical false positives (*e. g*. human keratin), and that were found in the control (anti-IgG or standalone BIOID). A GO term based analysis was done in STRINGdb and Reactome database.

3 Results

The experiments described here serve the purpose to figure out the function of STRN as a putative novel MAP. The primary interest was to evaluate the protein's localization in the cell, its behavior in context of cell-cycle dependent down- and upregulation and its interaction partners. This was done first with different model organisms and second in different stages of the cell cycle.

3.1 *In silico* analysis of STRN family members and comparison to known MAPs

The family member STRN (or STRN1) was found to be upregulated in the screen for MAPs in meiotic maturation by Bärenz *et al.*[102]. It is known that STRN1, STRN3 and STRN4 share similar protein-protein interaction domains[104]. At the beginning of the experimental part, I focus on the different STRN family members and variants that appear as isoforms. In January 2022, 1582 STRN related genes and 2679 transcript entries from different species were noted in the ensemble database. The database listed 10 STRN related gene and 52 transcript entries in human. Besides STRN family members these also include proteins with related STRN nomenclature like STRiatin Interacting Protein (STRIP).

Table 12: Homology and orthology of STRN, STRN3 and STRN4 in human (*hs*) and frog (*xl*). Comparing alignments of mRNA (NM) and protein (NP). Each entry shows the e-value and %-identity of the blastn and blastp result (NCBI's BLOSUM-62 default search). The gray box shows the RefSeq mRNA or protein Entrez identifier.

	***hs*STRN**	***xl*STRN**	***hs*STRN3**	***xl*STRN3**	***hs*STRN4**	***xl*STRN4**
***hs*STRN**	NM_003162 NP_003153	**NM**Evalue 0 **NM**Ident76% **NP**Evalue 0 **NP**Ident 79%	**NM**Evalue 1x10^{-137} **NM**Ident 69% **NP**Evalue 0 **NP**Ident 65%	**NM**Evalue 4x10^{-98} **NM**Ident 67% **NP**Evalue 0 **NP**Ident 62%	**NM**Evalue 2x10^{-56} **NM**Ident 78% **NP**Evalue 0 **NP**Ident 51%	
***xl*STRN**	**NM**Evalue 0 **NM**Ident76% **NP**Evalue 0 **NP**Ident 79%	NM_001094152 NP_001087621	**NM**Evalue 1x10^{-167} **NM**Ident 70% **NP**Evalue 0 **NP**Ident 63%	**NM**Evalue 5x10^{-90} **NM**Ident 77% **NP**Evalue 0 **NP**Ident 62%	**NM**Evalue 2x10^{-48} **NM**Ident 70% **NP**Evalue 0 **NP**Ident 49%	
***hs*STRN3**	**NM**Evalue 1x10^{-137} **NM**Ident 69% **NP**Evalue 0 **NP**Ident 65%	**NM**Evalue 1x10^{-167} **NM**Ident 70% **NP**Evalue 0 **NP**Ident 63%	NM_001083893.2 NP_001077362.1	**NM**Evalue 0 **NM**Ident 75% **NP**Evalue 0 **NP**Ident 81%	**NM**Evalue 1x10^{-40} **NM**Ident 69% **NP**Evalue 0 **NP**Ident 53%	
***xl*STRN3**	**NM**Evalue 4x10^{-98} **NM**Ident 67% **NP**Evalue 0 **NP**Ident 62%	**NM**Evalue 5x10^{-90} **NM**Ident 77% **NP**Evalue 0 **NP**Ident 62%	**NM**Evalue 0 **NM**Ident 75% **NP**Evalue 0 **NP**Ident 81%	XM_018232187.1 XP_018087674.1	**NM**Evalue 4x10^{-66} **NM**Ident 65% **NP**Evalue 0 **NP**Ident 51%	
***hs*STRN4**	**NM**Evalue 2x10^{-56} **NM**Ident 78% **NP**Evalue 0 **NP**Ident 51	**NM**Evalue 2x10-48 **NM**Ident 70% **NP**Evalue 0 **NP**Ident 49%	**NM**Evalue 1x10^{-40} **NM**Ident 69% **NP**Evalue 0 **NP**Ident 53%	**NM**Evalue 4x10^{-66} **NM**Ident 65% **NP**Evalue 0 **NP**Ident51%	NM_013403.3 NP_037535.2	
***xl*STRN4**						Not described in *X. laevis*

As seen in table 12, the protein of interest, STRN, shows sequence identities between different species at mRNA and protein level. The list displays aligned STRN family member mRNAs and proteins. All STRN family members can function as a PP2A regulatory B''' subunit and can be component of the STRIPAK complex[105,140]. In addition, most of the STRIPAK components are highly conserved. STRN family member STRN1 is the most conserved family member. STRN1 reaches up to 80% homology between orthologues of human and frog. High sequence homology is an indicator of conserved functions and interactions. This would be essential for evolutionary immutable processes like a MT modulation during cell division. The data so far shows that no STRN4 or similar protein had been described in *Xenopus laevis*. The present data has its gaps and limitations which is why it is important to clarify individual differences.

In order to verify individual differences between the species, a similar comparison of already described proteins can be meaningful. Candidates for comparability can be MAPs like EB1 and TPX2, since their functions and major interactions are known and our lab has tools for them available[202,203,315]. These proteins take care of crucial cellular processes, which are evolutionary conserved between eukaryotes. Besides STRN analysis, I therefore evaluated the mutual alignments for these already well described MAPs. The list shows the comparison between mRNA and protein NCBI Reference Sequence (RefSeq) entries.

Table 13: Interspecies mRNA and protein homology of STRN and established MAPs, EB1 and TPX2. Similar to table 12 the alignments listed here show interspecies similarities and document conserved sequence orthology indicating a likely similar cellular function. Besides STRN, I also listed mRNA and protein comparison for EB1 and TPX2. I chose those two because they are well known and described M-phase related MT modulating activities.

%Query identityof…	*Homo sapiens*	*Xenopus laevis* S	*Mus musculus* CL57BL6	*Drosophila melanogaster*
STRN mRNA				
Homo sapiens	NM_003162	Evalue 0 Ident 76%	Evalue 0 Ident 85%	Evalue $5x10^{-25}$ Ident 70%
Xenopus laevis S	Evalue 0 Identity 76%	NM_001094152	Evalue $3x10^{-13}$ Ident 90%	Evalue $7x10^{-270}$ Ident 68%
Mus musculus CL57BL6	Evalue 0 Ident 85%	Evalue $3x10^{-13}$ Ident 90%	NM_011500	Evalue $3x10^{-290}$ Ident 68%
Drosophila melanogaster	Evalue $5x10^{-25}$ Ident 70%	Evalue $3x10^{-290}$ Ident 68%	Evalue $7x10^{-270}$ Ident 68%	NM_001273292 (isoform G)
EB1/MAPRE1 mRNA				
Homo sapiens	NM_012325	Evalue $7x10^{-95}$ Ident 76%	Evalue 0 Ident 84%	Evalue 10^{-41} Ident 70%
Xenopus laevis S	Evalue $7x10^{-95}$ Ident 76%	NM_001088741	Evalue $5x10^{-90}$ Ident 75%	Evalue $3x10^{-48}$ Ident,71%
Mus musculus CL57BL6	Evalue 0 Ident 84%	Evalue $5x10^{-90}$ Ident 75%	NM_007896	Evalue $6x10^{-38}$ Ident 70%
Drosophila melanogaster	Evalue 10^{-41} Ident 70%	Evalue $3x10^{-48}$ Ident 71%	Evalue $6x10^{-38}$ Ident 70%	NM_001273605 (isoform G)
TPX2 mRNA				
Homo sapiens	NM_012112	Evalue $5x10^{-106}$ Ident 68%	Evalue 0 Ident 82%	Evalue 0,6 Ident 86%
Xenopus laevis S	Evalue $5x10^{-106}$ Ident 68%	NM_001093282	Evalue $6x10^{-81}$ Ident 65%	Evalue 0 Ident 85%
Mus musculus CL57BL6	Evalue 0 Ident 82%	Evalue $6x10^{-81}$ Ident 65%	NM_001141975.1	Evalue 0 Ident 86%
Drosophila melanogaster	Evalue 0,6 Ident 86%	Evalue 0 Ident 85%	Evalue 0 Ident 86%	TPX2 orthologue supposedly SSP1/MEI-38^{316} (no AURKA binding domain) NM_130566
STRN protein				
Homo sapiens	NP_003153	Evalue 0 Ident 79%	Evalue 0 Ident 97%	Evalue $2x10^{-166}$ Ident 61%
Xenopus laevis S	Evalue 0 Ident 79%	NP_001087621	Evalue 0 Ident 79%	Evalue $2x10^{-164}$ Ident 61%
Mus musculus CL57BL6	Evalue 0 Ident 97%	Evalue 0 Ident 79%	NP_035630	Evalue $5x10^{-166}$ Ident 62%
Drosophila melanogaster	Evalue $2x10^{-166}$ Ident 61%	Evalue $2x10^{-164}$ Ident 61%	Evalue $5x10^{-166}$ Ident 62%	NP_001260221 (isoform G)
EB1/MAPRE1 protein				
Homo sapiens	NP_036457	Evalue $2x10^{-168}$ Ident 75%	Evalue 0 Ident 97%	Evalue 10^{-110} Ident 54%
Xenopus laevis S	Evalue $2x10^{-168}$ Ident 75%	NP_001082210	Evalue $8x10^{-160}$ Ident 74%	Evalue $4x10^{-109}$ Ident 52%
Mus musculus CL57BL6	Evalue 0 Ident 97%	Evalue $8x10^{-160}$ Ident 74%	NP_031922	Evalue $2x10^{-111}$ Ident 54%
Drosophila melanogaster	Evalue 10^{-110} Ident 54%	Evalue $4x10^{-109}$ Ident 52%	Evalue $2x10^{-111}$ Ident 54%	NP_001260734 (isoform G)
TPX2 protein				
Homo sapiens	NP_036244	Evalue 0 Ident 52%	Evalue 0 Ident 79%	Evalue 0 Ident 23%
Xenopus laevis S	Evalue 0 Ident 52%	NP_001086751	Evalue 0 Ident 50%	Evalue 0 Ident 46%
Mus musculus CL57BL6	Evalue 0 Ident 79%	Evalue 0 Ident 50%	NP_001135447	Evalue 0 Ident 35%
Drosophila melanogaster	Evalue 0 Ident 23%	Evalue 0 Ident 46%	Evalue 0 Ident 35%	TPX2 orthologue supposedly SSP1/MEI-38^{316} (no AURKA binding domain) NP_569922

The here described table 13 shows mRNA and protein alignment between STRN, EB1 and TPX2. Looking at different identities between different species, STRN achieved the highest values (always > 60% and up to 97%) for both mRNA and protein. The proteins EB1 and TPX2 show higher sequence differences between the model species. In all candidates, the highest evolutionary conserved sequences were found between the mammalian species human and mouse. The multiple sequence alignment tool Clustal Omega (EMBL-EBI) of the STRN protein primary structure compared to typical MAP candidates (TPX2, EB1, SSX2IP) gave no result of identical MAP characteristic sequence motifs.

The analysis of highly conserved proteins such as STRN allows the use of respective sequences from almost any model organism. As a mouse cDNA clone was readily available, I used mouse cDNA as a template for the production of recombinant protein with the final goal to generate antibodies against the highly conserved STRN protein.

In order to analyze its molecular function, the first attempt was to generate recombinant, purified protein of the full-length mouse STRN protein. The creation of different fusion constructs within different expression vectors was successful. During bacterial cultivation and induced expression all STRN products (full protein, fragments, fusions, urea refolding) became insoluble. This was true for optimized expression strains and protocols, including *Escherichia coli* OverExpress™ C43(DE3)[317], Rosetta™(DE3) (Sigma), SoluBL21™ (Genlantis), ArcticExpress™ (DE3)RIL/RP[318], M15 (Qiagen) and TG1 (Lucigen). From literature STRN is known to sub-fractionate in the membrane insoluble samples of HEK293T and MDCK cellular lysates[319].

3.2 Optimization and experimental outcome of anti-STRN antibody in *Xenopus* egg extract

An alternative to recombinant expressed proteins for immunization and antibody production is peptide synthesis of epitopes with predicted high immune response. A peptide antibody can be even used to monitor and localize STRN by immune fluorescence microscopy of *Xenopus laevis* egg extracts. Several optimization experiments showed that a second generated STRN antibody was purer and gained higher peptide specificity than of a first attempt.

Table 14: The here used different anti-STRN antibodies and their interspecies detection potential between frog and human.

			STRN protein *Homo sapiens*	STRN protein *Xenopus laevis*
STRN-AB0 Purified Mouse Anti-Striatin Clone 6/Striatin *commercial*	BD Transduction Laboratories™ rat STRN aa. 450-600	TFPPSSGKSFIMGADEA LESELGLGELAGLTVAN EADSLAYDIANNKDALR KTWNPKFTLRSHFDGIR ALAFHPIEPVLITASEDH TLKMWNLQKTAPAKKS TSLDVEPIYTFRAHKGP VLCVVMSSNGEQCYSG GTDGLIQSWSTTNPNV	Query cover 100% Evalue $2x10^{-108}$ Ident 97%	Query cover 100% Evalue $2x10^{-100}$ Ident 91%
STRN-AB2 *newly generated*	Davids Biotechnologie 2 human peptides	(290) **AAA**DFSDEDEDDDVDG REK (308) and (386) (purification peptide "AAA") **YKK**ERKGKKGVKRPNR S (402) (purification peptide "YKK")	AAA Query cover 100% AAA Evalue $3x10^{-18}$ AAA Ident 100% YKK Query cover 100% YKK Evalue $6x10^{-16}$ YKK Ident 100%	AAA Query cover 100% AAA Evalue $1x10^{-7}$ AAA Ident 47% YKK Query cover 100% YKK Evalue $6x10^{-16}$ YKK Ident 100%
STRN-AB3 rabbit *newly generated*	Seramun Diagnostica GmbH human peptide	(386) **YKK**ERKGKKGVKRPNR S (402) sensitive against multiple organisms STRN (conserved peptide)	Query cover 100% Evalue $6x10^{-16}$ Ident 100%	Query cover 100% Evalue $6x10^{-16}$ Ident 100%

Already 21 years ago Castets *et al.* described a Western blot signal pattern for the different STRN family members[104]. They showed discrepancies between the predicted molecular weight and the running behavior on SDS-gels. According to their paper STRN runs at 114 kDa, STRN4 (Zinedin) at 100 kDa and their STRN3 (SG_2NA) antibody generated multiple signals at 112, 102 and 94 kDa. In contrast, our newly generated antibodies STRN-AB2 and STRN-AB3 can differentiate between STRN family members (see table 14). The 2 peptide-antibodies are made from sequences with identities of 47% (AAA peptide) and 100% (YKK peptide) between human and frog.

The ordered peptide antibodies were tested for human and frog STRN antigene recognition. I checked if lysates in different cell cycle stages yielded in a different STRN Western blot pattern. The depictured figure 10 shows different developmental stages of *Xenopus laevis* oocytes, mature eggs and fertilized embryos. The late oocytes contain an enormous mass of mRNAs, while no DNA is transcribed, known as transcriptional silencing[320]. Transcription is reactivated after mid-blastula transition. During the very fast first divisions of embryogenesis the embryo does not grow in size. It internally divides into new cells. The depicted embryo stage describes a frog embryo prior to mid-blastula-transition. This transition takes place after 13 division cycles in *Xenopus laevis* and slows down the division rate dramatically[321].

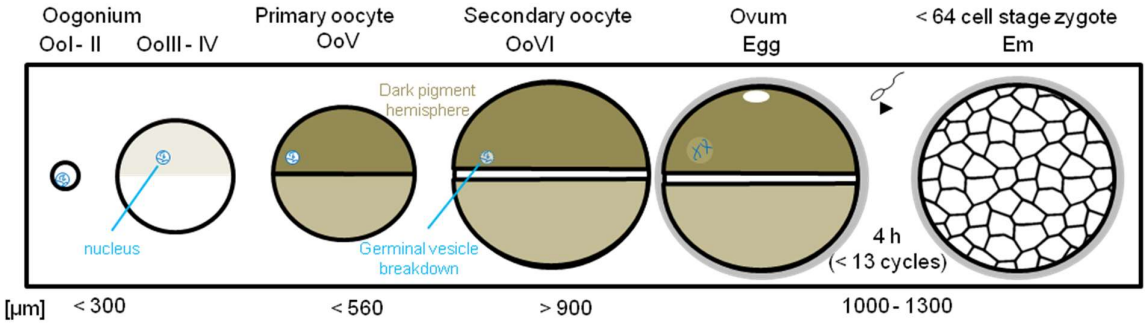

Figure 10: Oogenesis and early embryogenesis in *Xenopus laevis*. The oocytes are separated by their diameters. They are sieved through different mesh sizes. Thereby I define a categorization of different stages for analysis used here. All oocytes, mature eggs and fertilized embryos (in 64 cell stage maximum) are crushed by centrifugation to generate homogenous high-protein lysates.

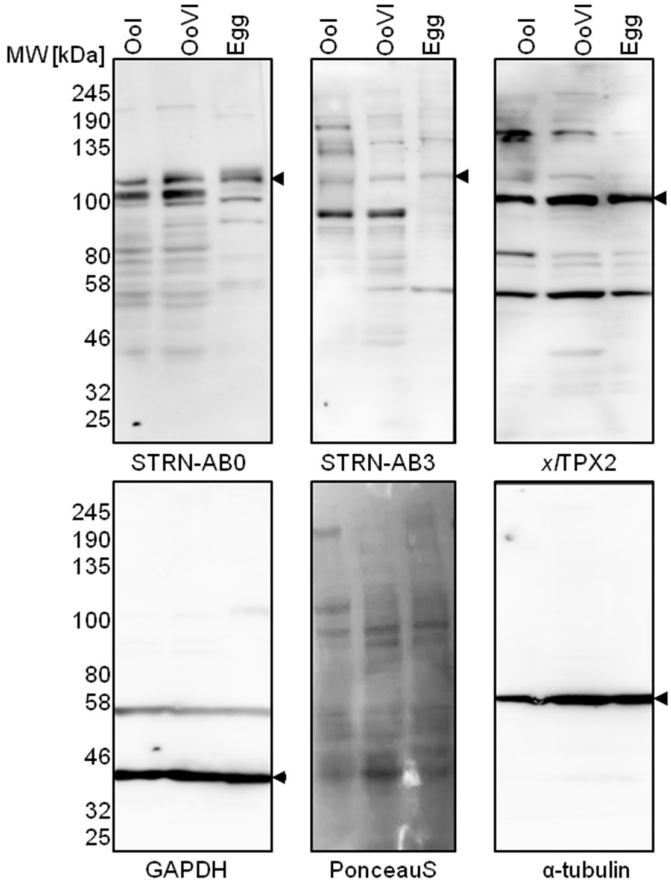

Figure 11: Western blot STRN antibody signals in oocyte and egg. The pictures show Western blots of early and late oocyte, resembling interphase and mature egg extract, resembling metaphase. The blot was developed by adding ECL™ Select or Amersham ECL. I compare commercial STRN-AB0 to newly generated STRN-AB3. The oocyte maturation was controlled by an *xl*TPX2 antibody (Gruß *et al.* 2001[203]). GAPDH, PonceauS and α-tubulin serve as loading control. The black arrows indicate the expected migration behavior for the individual proteins (STRN at 110 kDa, TPX2 at 100 kDa, GAPDH at 36 kDa, α-tubulin at 50 kDa).

The depicted figure 11 shows a comparison between different oocyte and egg extract lysates of *Xenopus laevis*. All STRN antibodies generate a line at 110 kDa. Some signals of the unspecific anti-STRN signals change during the maturation process while the signal of interest stayed equal. Although the STRN-AB2 and STRN-AB3 are derived from similar immunization peptides, the STRN-AB3 antibody produced less background of unspecific signal. The loading control of anti-GAPDH and anti-α-tubulin and the PonceauS staining indicates equal protein amounts. Frog lysates were further analyzed via an additional TPX2 blot. TPX2 has been shown to be upregulated during oocyte maturation processes[322].

This is not the case in the blot of figure 11, neither for TPX2 nor for STRN. Previous literature showed a clear upregulation within late interphase oocytes and eggs for both of them[102]. The difference is that the paper showed upregulation in MS of MT and MAP co-sediments. Possibly, a Western blot of total lysates is not the method of choice to proof this. The anti-STRN detection in lysates was highly dependent on the quality of the lysates and the loading amount. The detection in frog was promising enough to use STRN-AB3 for verification of immunodepletion and immunoprecipitation via Western blot.

The sheer number of identified interaction candidates from previous literature suggests the potential of STRN to form supramolecular complexes. This has been described in previous literature[140]. The authors point out that STRN might serve as anchor platform for multiple proteins or protein complexes. One well known complex is the PP2A trimeric protein phosphatase. Alternatively, the diverse STRIPAK complex components might be constituents of the STRN platform.

One method to further analyze STRN complex formation in a native environment is given by sucrose gradients of cell free lysates. Thanks to the lab of Prof. Dr. Dietmar Schmucker and Dr. Gabriela Edwards Faret from the LIMES institute of Universität Bonn, our lab received fertilized frog egg samples of a closely related species to *X. laevis*, namely *Xenopus tropicalis*. This frog species is preferred for *Xenopus* genetics since animals are diploid although otherwise highly similar to *X. laevis*. An alignment of *X. laevis* and *X. tropicalis* STRN using NCBIs blastp tool results in 96% identity, a query cover of 100% and an e-value of 0.

I am able to visualize STRN's molecular complex formation in different cell cycle stages in the depicted sucrose gradient of figure 12. This was achieved with the STRN-AB3 antibody (S3) in M-phase arrested eggs and fertilized embryos of *Xenopus tropicalis*. To make this analysis comparable to previous documentation I check the gradient also in unfertilized egg extracts of *Xenopus laevis*. The fertilized frog embryos are prior to mid-blastula-transition, *i. e.* maximum 4 h old, 64 cell stage blastocysts. These embryos are not fully synchronized anymore and show a mixture of all cell cycle stages. On top of that sedimentation of protein complexes is compared under normal and high salt conditions.

High ionic strength changes protein-protein interactions. Thereby the supramolecular assembled complexes can break apart. The Western blot in figure 12 shows cell free M-phase egg and embryo extract of *Xenopus tropicalis* and *Xenopus laevis* with and without 1 M NaCl (+N) addition. In all cases, I use γ-tubulin (γT) as control, since its running behavior under normal and high slat conditions in sucrose gradients is well known from previous literature[323,324]. Each signal peak is reduced to 3 out of 15 lanes (white marking in figure 12).

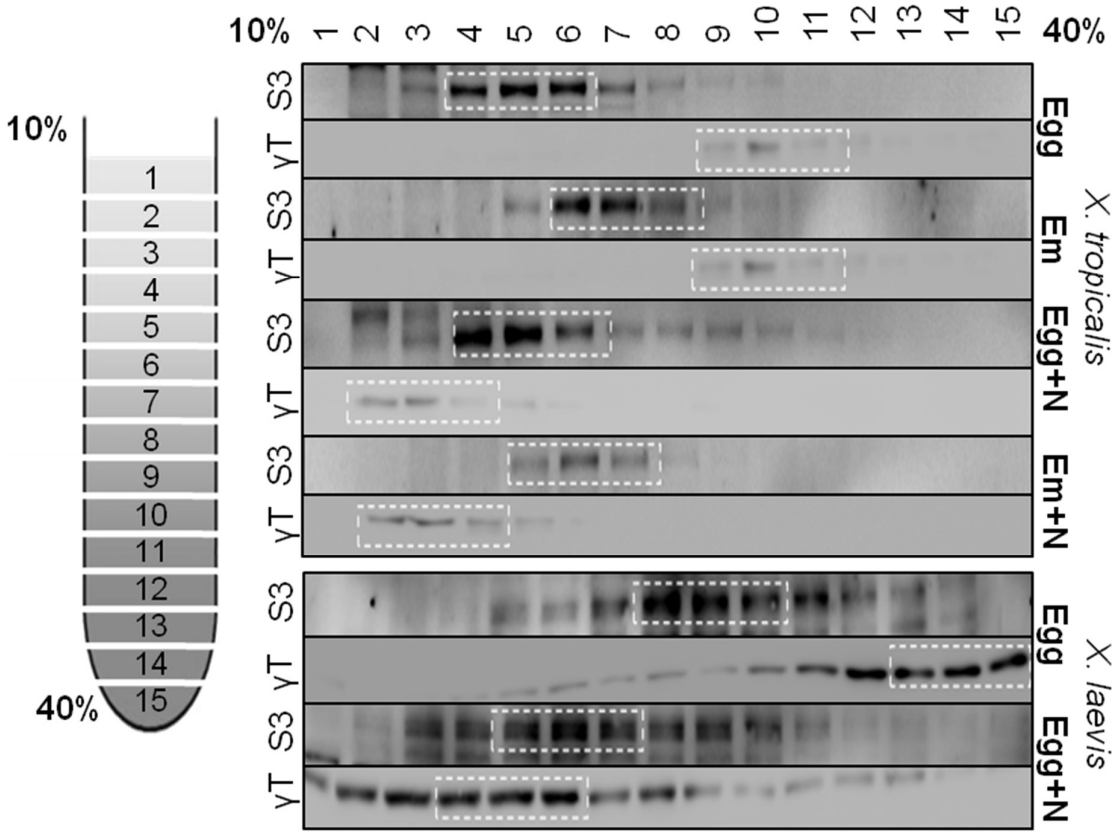

Figure 12: Western blot of the 10% - 40% sucrose density gradient fractions in different frog species. The left side shows the STRN-AB3 (S3 at 110 kDa) signal and the right side the anti-γ-tubulin (γT at 55 kDa) signal. The white dotted line frames the 3 lanes of the signal peak. The blots suggest a different role of STRN within the embryonic extracts of the closely related species *Xenopus laevis* and *Xenopus tropicalis*. The peak shifts by salt addition. In *X. laevis* it shifts 3 lanes while there is minor effect in *X. tropicalis*.

The blot shows all fractions (1 [10%] to 15 [40%]) of the sucrose gradients, in which proteins and protein complexes were separated according to their sedimentation velocity. The sedimentation for each protein is quantitatively described by its Svedberg unit value. On the left side the blots show STRN-AB3 signals and on the right side blots show anti-γ-tubulin signals. Similar to the STRN alignment, the γ-tubulin protein alignment between *X. laevis* and *X. tropicalis* resulted in 99% identity, a query cover of 100% and an e-value of 0. The γ-tubulin sedimentation between *X. laevis* and *X. tropicalis* shows differences. While the signal in *X. laevis* is similar to the prospective one of the human γ-tubulin ring complex, *X. tropicalis* behaves like a smaller or differently shaped complex. The salt addition indicates disassembly of the γ-TuRC.

For the anti-STRN signal a shift by one fraction can be observed upon salt addition. Furthermore, similar to the γ-tubulin signal, a species-dependent signal shift can be observed also for STRN: While the STRN signal in untreated egg extract of *X. tropicalis* peaks within fractions 4-6, it appeared in fractions 8-10 in *X. laevis*. The 4% different sequence identity is unlikely to be the reason for this mass shift. The more probable explanation would be species-depended different interactions or complex assembly.

Earlier results already showed an accumulation of STRN within pelleted purified MTs of *Xenopus laevis* mitotic eggs[102]. MT hyper stabilization by taxol addition and pellet centrifugation is analyzed via Western blot in figure 14 A. The procedure to receive the samples is shown in figure 13. The photos of figure 13 indicate that an adequate amount of MTs is pelleted while hardly anything is found in the nocodazole control. The following blot of figure 13 approves accumulated tubulin in the taxol pellet and a negligible signal in the nocodazole control.

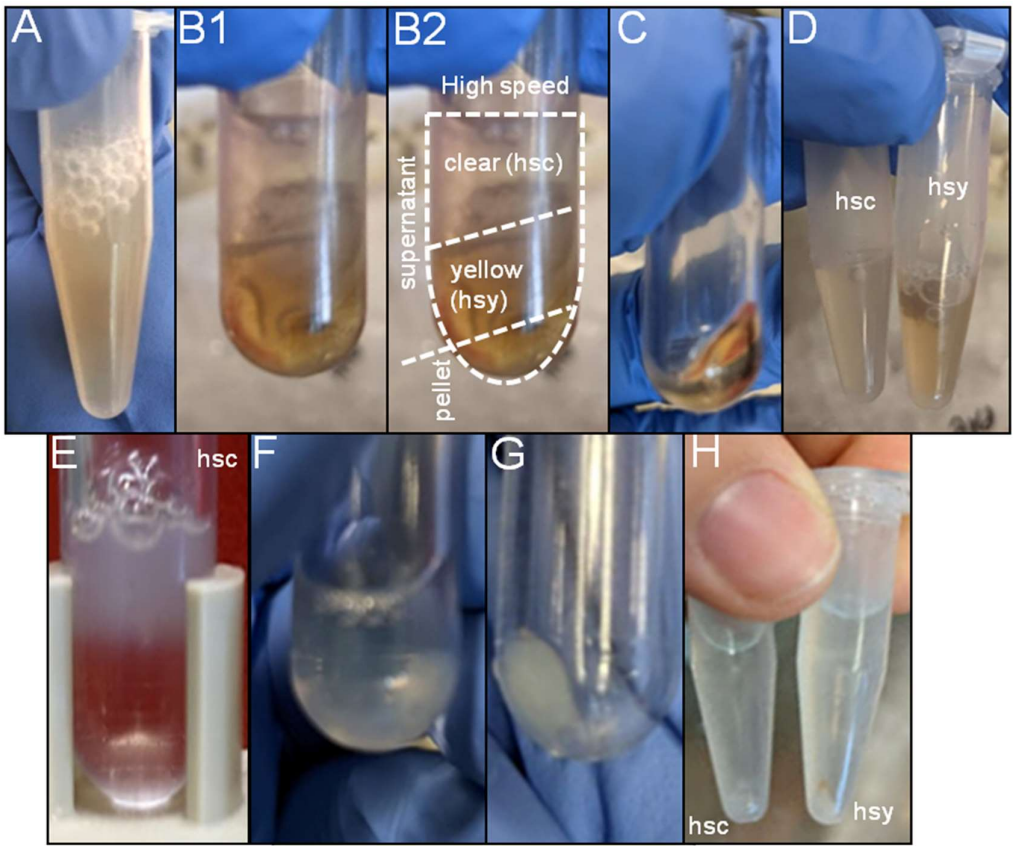

Figure 13: Step-by-step procedure of MAP pelleting of *Xenopus laevis* CSF egg extract. A) 1,2 mL thawed and pooled CSF egg extract B1&2) the high speed supernatant after centrifugation. The viscous cytosol separates into clear soluble cytosol (hsc), yellowish membrane, organelle enriched light fraction (hsy) and heavy fraction with pigments (C). E) supplemented, incubated and diluted clear fraction loaded onto the centrifugation cushion F and G) Clear soluble fraction after taxol induced MT polymerization and centrifugation (pelleted MT and MAPs). The taxol pellet was used for anti-STRN co-IP. H) shows the eluted protein precipitate for mass spectrometry.

In figure 14 A) I analyze the MAP pellet via Western blot analysis. The blot suggests STRN pelleted with tubulin after taxol addition. I use two different antibodies to clarify this question, and both generate a signal at 110 kDa. The pellet is desalted and used for immunoprecipitation. This sample should generate a less complex interactome result than previously and should be limited to the MT-related interactions of STRN. The process continues to use this sample for the blot in figure 14 B). The immunoprecipitation of STRN with STRN-AB3 from the MT pellet is seen in figure 14 picture B). As before, two different STRN antibodies are used for detection in order to clarify the question if, first, STRN is in the pellet and, second, if it can be purified via co-IP.

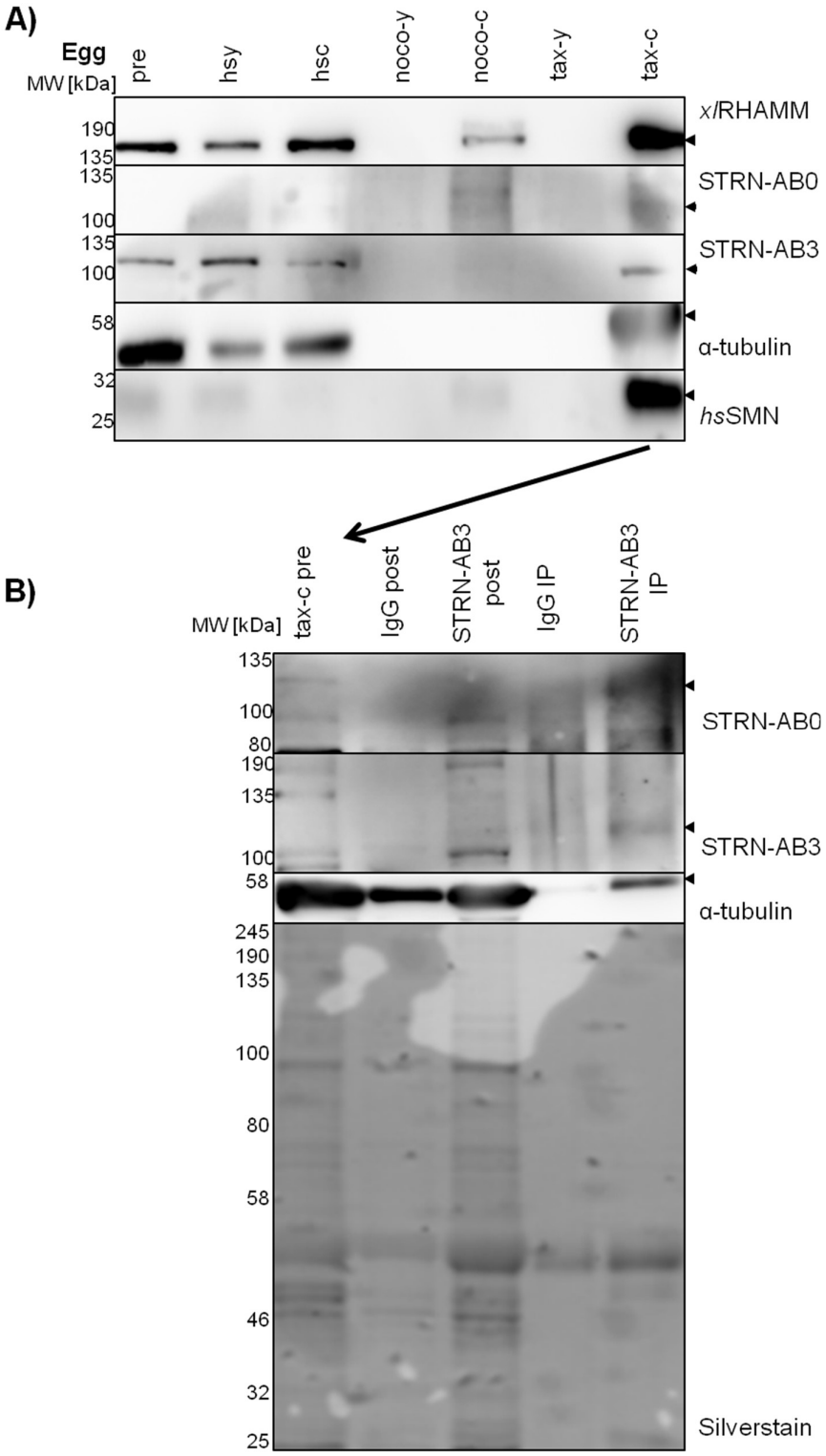

Figure 14: MT polymerization induced MAP pelleting and pellet co-IP. Picture A) shows the Western blots of different antibodies that play a role in MT dynamics and the blots of the putative candidate STRN: In all blots the respective protein accumulates in the polymerized MT pellet while STRN detection in the taxol MAP pellet remained unclear. This can mean the epitope is covered in these samples. B) Immunoprecipitation of the taxol pellet with STRN

antibody makes this epitope visible again. The black arrow indicates the expected height of STRN at 110 kDa, α-tubulin at 50 kDa.

While proteins like RHAMM are well known to associate with MTs, I newly discovered MT association of SMN (Survival of Motor Neuron, see below for proteomic ID approaches). Recently, our lab showed SMN's colocalization to MTs in intact human cells[325]. Therefore, the sample tax-c was the sample of choice for proceeding with a STRN antibody IP.

The blot depicted in figure 14 B) argues for a STRN-MT interaction, since the STRN antibody IP generates a tubulin signal. This is the case for MT/MAP-pellet STRN co-IP but not for IP from mixed lysate. A corresponding mass spectrometry of a first taxol MAP pelleting and second STRN antibody IP is still pending. This would be a highly specific possibility for MAP/MT-related STRN characterization. Furthermore, blot analysis of the MAP-pellet IP for potential STRN interactors RHAMM, SSX2IP, CSPP1 from this thesis or previous literature (STRIPAK components) can be meaningful.

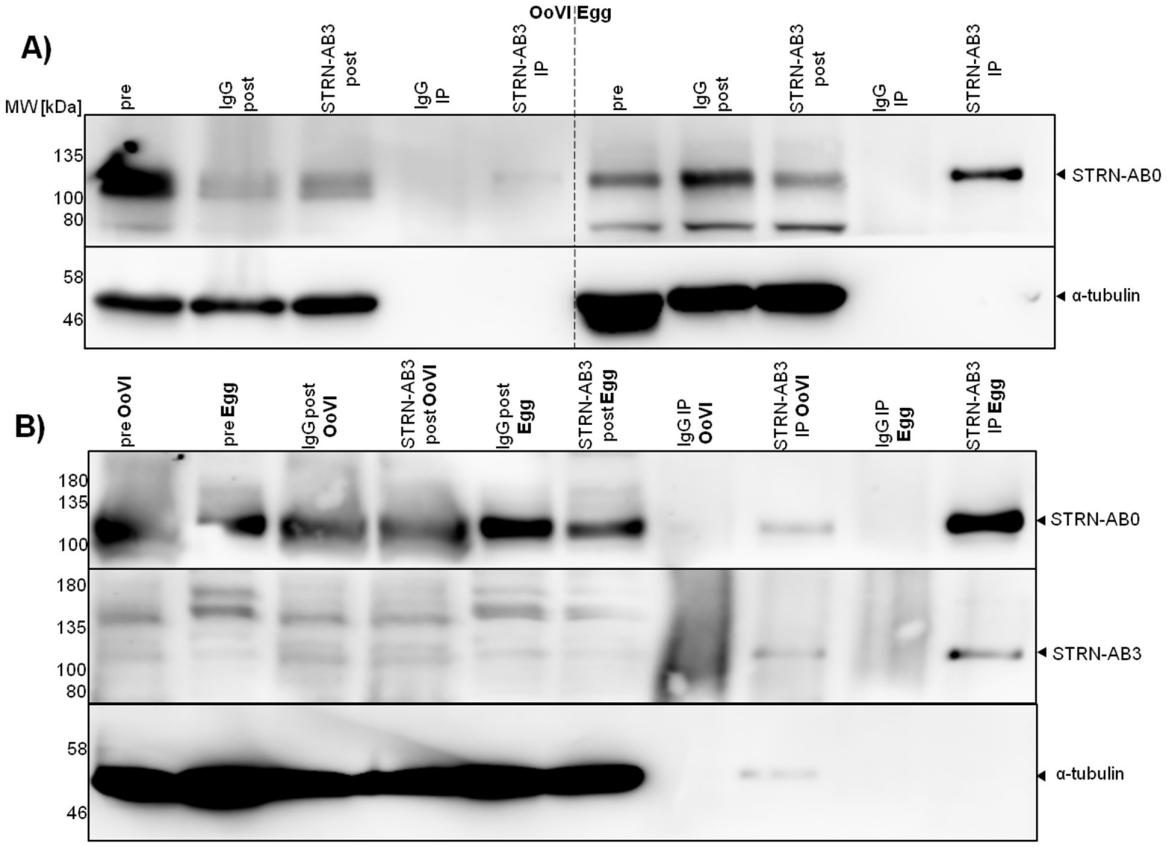

Figure 15: Western blot proofs STRN upregulation in *Xenopus laevis* mature eggs. Stage VI oocytes resemble late interphase lysates while mature eggs correspond to metaphase lysates. The anti-STRN antibody for the protein A Dynabeads-based immunodepletion and immunoprecipitation is the STRN-AB3 purified rabbit antibody. A) shows a direct comparison of the co-IP fractions of stage VI oocytes and CSF egg extract shows no accumulated STRN in mitotic egg samples. This becomes visible when analyzing it as in B) next to each other. The lower blots show the anti-α-tubulin loading control. A PonceauS analysis (not shown) indicated similar protein mass between egg and oocyte. The lysates proof a sequential reduction of STRN (also seen in figure 16). The black arrows resemble the protein mass of STRN at 110 kDa and α-tubulin at 50 kDa.

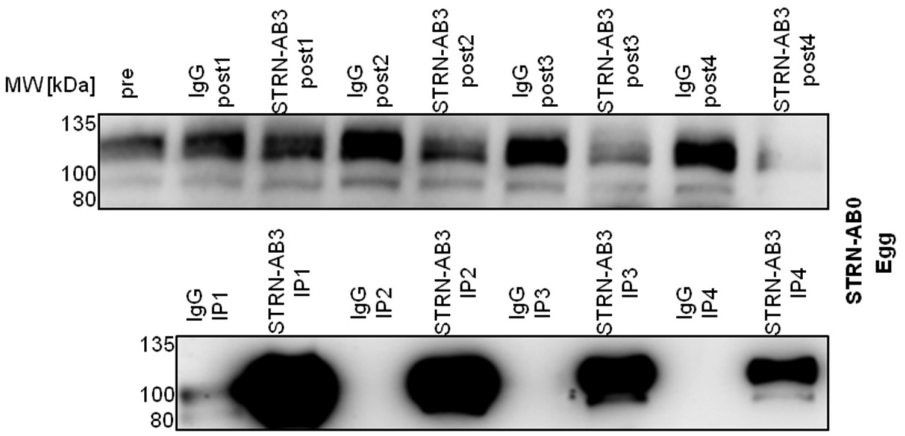

Figure 16: Sequential reduction of STRN in immunodepleted lysates and corresponding immuno precipitation. The upper blot shows the successive reduction of STRN within the mixed protein lysates. The lower blot shows the corresponding stepwise pull down. Even though I use same amounts of antibody and beads, the pull down signal reduces in each round. The extract does not compensate STRN shortage with translation processes. A complete STRN-immunodepleted egg extract is not functional anymore since this procedure requires many pipetting steps and is time consuming.

Using the STRN antibody I compare immunoprecipitation and immunodepletion of STRN in (late G_2 stage VI) oocytes and mature *Xenopus laevis* egg lysates. The blots depicted in figure 15 and 16 show two different experiments. In figure 15 the comparison of oocyte to egg shows high variation of the STRN 110 kDa signal in complex protein lysates. STRN was reduced after treatment with the bead coupled antibody. The blot shows that 18x more STRN got precipitated from the mature egg extract in comparison to the stage VI late oocyte extract. Figure 16 gives information that a sequential STRN depletion can be performed. After four rounds a decreased STRN concentration in the anti-STRN depleted extract can be verified compared to the anti-IgG control.

Consistently, the associated co-IP fractions show a stepwise reduced amount of STRN immuno-complexes. The problem with this sequential method is that the egg extract's potential to cycle through the first round of the cell cycle and to produce a bipolar spindle suffers from each round of treatment and the resulting number of structures becomes too low for quantification.

A problem with higher antibody-bead concentration for STRN reduction is that the relatively large beads lead to a reduced spindle forming potential as well. As a compromise I therefore use two rounds of depletion. In a total of 11 different experiments an overall average reduction of down to 35% residual STRN in the depleted lysates can be verified (figure 17 left graph). The probability of a random correlation is below 9%.

3.3 STRN deficiency in CSF extract extends metaphase

To study the functional consequences of STRN depletion I use two rounds of depletion in order to verify mitotic deficiencies specifically resulting from STRN depletion. Cell cycle irregularities are observed under the microscope and are depicted in figure 17 (untreated) and 18 (Ca^{2+} and $CAMKII^{aa1\text{-}290}$ treated). Calcium is a second messenger that has multiple functions in the cell[326]. A defined Ca^{2+}-concentration can trigger metaphase-anaphase transition. Two Ca^{2+}-sensitive proteins are the cell cycle associated phosphatase calcineurin (also known as CAN or PP2B) and the kinase CAMKII. Both CAMKII and CAN have calmodulin (CAM) binding domains. During *Xenopus* sperm initiated egg fertilization, a resulting Ca^{2+} wave activates both CAMKII and CAN[327]. In order to reactivate cell cycle progression Ca^{2+} binds to calmodulin (CAM). This binding activates ion channels, protein kinases, adenylyl cyclases, protein phosphatases and phosphodiesterases[328]. In *Xenopus laevis* CAMKII initiates meiotic exit by phosphorylating XERP1 (also known as EMI2). Thereby XERP1 degrades and the APC/C the E3 ubiquitin ligase activates. The mitosis marker protein Cyclin B is ubiquinylated and degraded by the proteasome[176–178]. CAM-binding dependent kinases are increased during *Xenopus laevis* oocyte maturation, meiotic spindle formation and activated prior to chromatid segregation[179,245].

The difficulty of using calcium only to induce mitotic exit is the direct STRN calcium sensitiveness due to its calmodulin binding domain. The more proper alternative to only-calcium is the treatment of the arrested *in vitro* spindles under addition of recombinant purified $CAMKII^{aa\text{-}1\text{-}290}$. The kinase is designed bearing amino acids (aa) 1-290 without its C terminal domain and thereby constitutively active[245]. For this reason, $CAMKII^{aa1\text{-}290}$ can trigger mitotic progression without calcium.

Following graphs show the behavior of the spindle forming potential of control immunodepleted IgG-treated (Δmock) and anti-STRN-treated (ΔSTRN) extracts. In each sample (2 µL extract per slide) I count the numbers of bipolar spindles first and the number of sperm nuclei second. The spindle forming potential is obtained by dividing the total number of spindles per slide by the total number of sperm nuclei per slide. 100% corresponds to the highest achieved result or spindle forming potential within all experiments. The right graph of figure 17 shows that the upper 25% quartile to the lower 25% quartile (the major group of counted spindle forming units) ranges from ca. 10% - 40% for both control and STRN depletion.

The difference of STRN depleted extract is visible within the upper whisker to the maximum. It is around 20% higher compared to the non-depleted extract. This suggests a more stable group of bipolar spindles in extracts lacking STRN. The statistical difference between IMR-90 wildtype endogenous STRN and STRN depleted extract regarding the number of a fully cycled first mitotic bipolar spindle is $p = 0{,}183$. Since the complete spindle is the requirement for subsequent chromosome segregation, the statistics regarding number of experiments and samples for this observation is unquestionable.

There is no obvious difference between spindle forming unit and spindle morphology and for both conditions (depleted and non-depleted) the same conditions are used as starting point. For the segregation (figure 18) I focus on samples with exactly same time points and treatment. They have to be normal distributed for the paired t-test. The p-values are mentioned for significant differences.

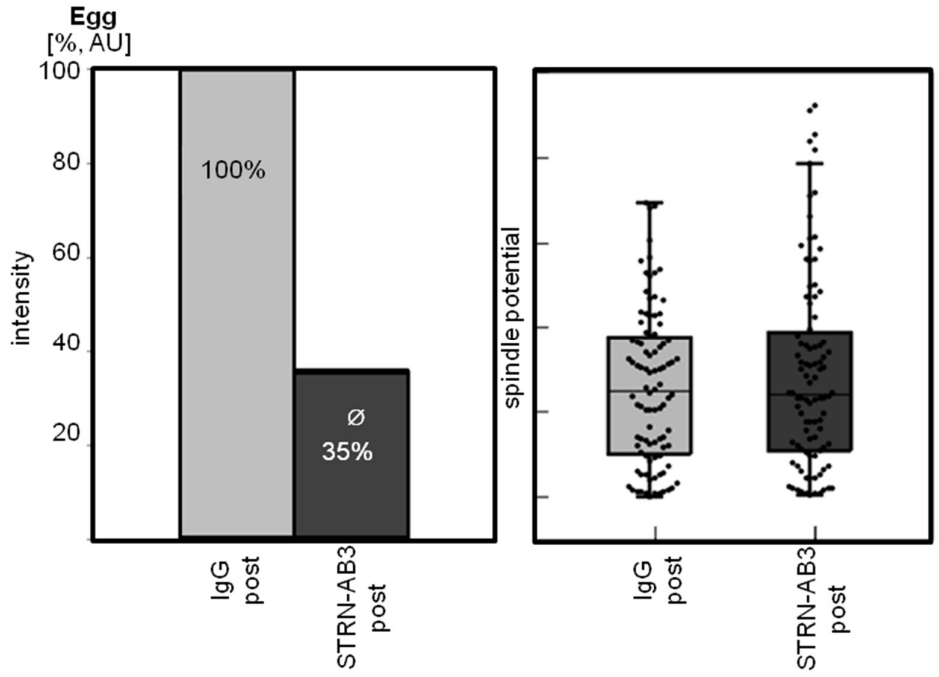

Figure 17: Efficiency of immunodepletion and changes in spindle forming potential. The left graph shows the reduced STRN blot signal averaged from all immunodepletion blots. The protein was depleted with STRN-AB3 while the blots were analyzed with STRN-AB0. On average, the depleted lysates contained about 3x less STRN. The right blot shows the results from the corresponding microscopy analysis. Cy3-labeled tubulin indicates bipolar spindles in M-phase arrested frog egg extract.

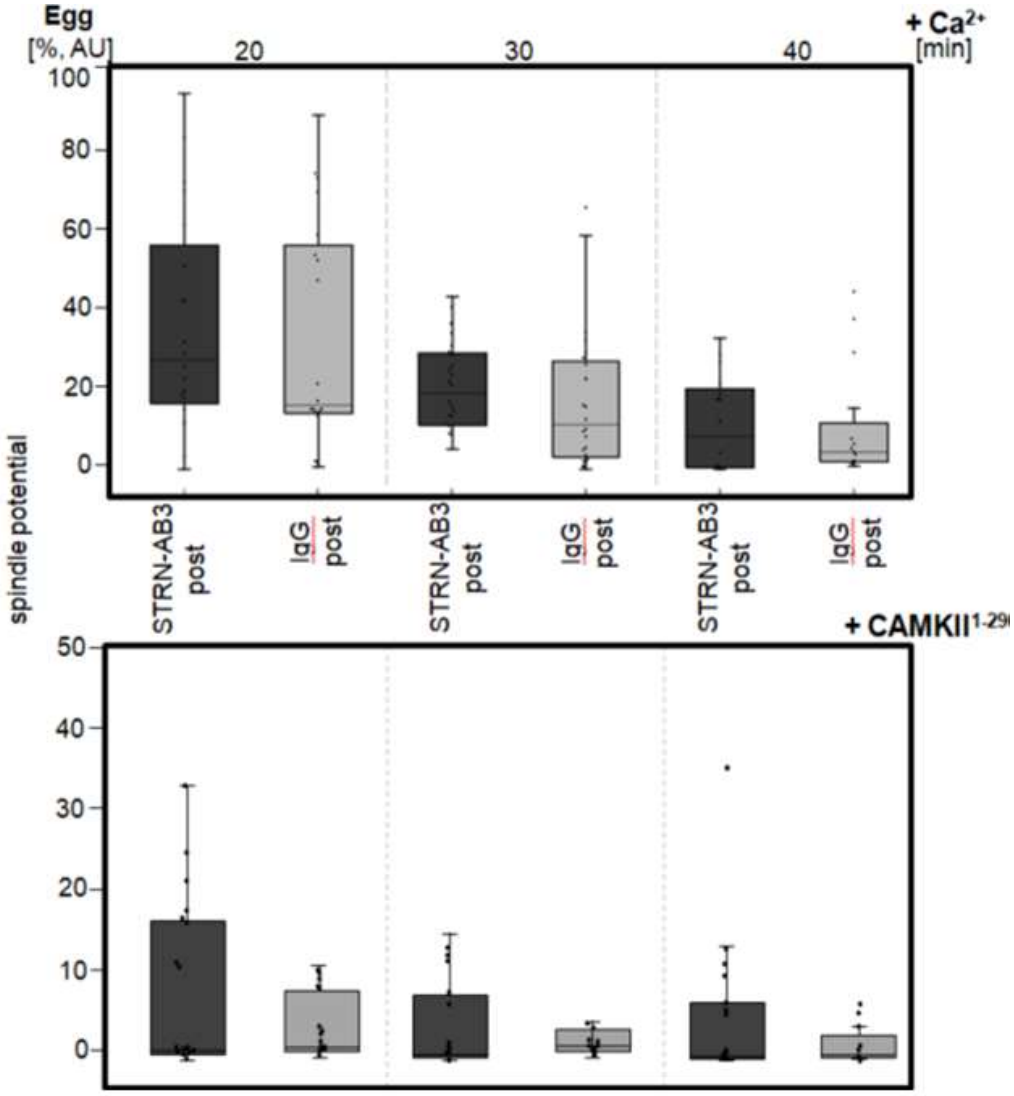

Figure 18: Numbers of formed spindles during the first mitotic cell cycle and upon chromatid segregation. The experiment shows the outcome of cycled meiotic egg extract that contain bipolar spindle structures (visible by supplemented fluorescent Cy3 labeled tubulin). The columns show a comparison between STRN-depleted (ΔSTRN) and unspecific IgG (Δmock)-depleted extract. The amount of spindle structures is calculated relative to the amount of added sperm nuclei. Upper plot shows the result of addition of 0,6 mM $CaCl_2$ and lower plot shows the result of addition of 3 µM CAMKII (wt amino acid 1-290, constitutively active[245]).

The plot in figure 17 shows the non-treated condition with stably arrested spindles in the first mitosis after activation. The following graphs in figure 18 show two treatments to stimulate chromatid segregation. Both had similar effects but with different kinetics. The effect of calcium ions is seen after a short lag phase of 20 min. Similar to untreated stable spindles, the direct comparison between the control and the STRN lacking extract showed no significant differences.

This is true for all time points. All graphs from figure 17 and 18 suggest more stable structures during STRN shortage. The statistical difference over the here presented three time points is either not normal distributed or not significant. For Ca^{2+} treatment the difference between Δmock and ΔSTRN cell free lysate is p = 0,477. The $CAMKII^{aa1-290}$ treatment in the first 20 min shows a trend of different behavior. Further analysis might provide a proof of STRN deficiency regarding M-phase exit.

The addition of 3 µM kinase starts sister chromatid segregation after 10 min. Later time points show hardly any structures. As in previous graphs the STRN depleted sample has a higher 25% quartile and maximum whisker. The counted structures summarize four independent experiments with a total of average 16 spindle/sperm ratios per time point. In this pilot experiment each graph shows a trend of higher spindle stability in the ΔSTRN lysates. More experiments are recommended to verify the suggestion of this pilot experiment that STRN destabilizes mitotic spindles in *Xenopus laevis* embryonic extract.

Apart from the statistics and the total number of structures, the corresponding fluorescence figures show no overall morphological discrepancies. Figure 19 and 20 start with fully cycled complete bipolar spindles arrested at metaphase. The condensed DNA is positioned in the metaphase plate. As statistics show, when treated with calcium the structures stay stable also for 20 min. The segregation has a lag phase due to the slow enzymatic cascade activation.

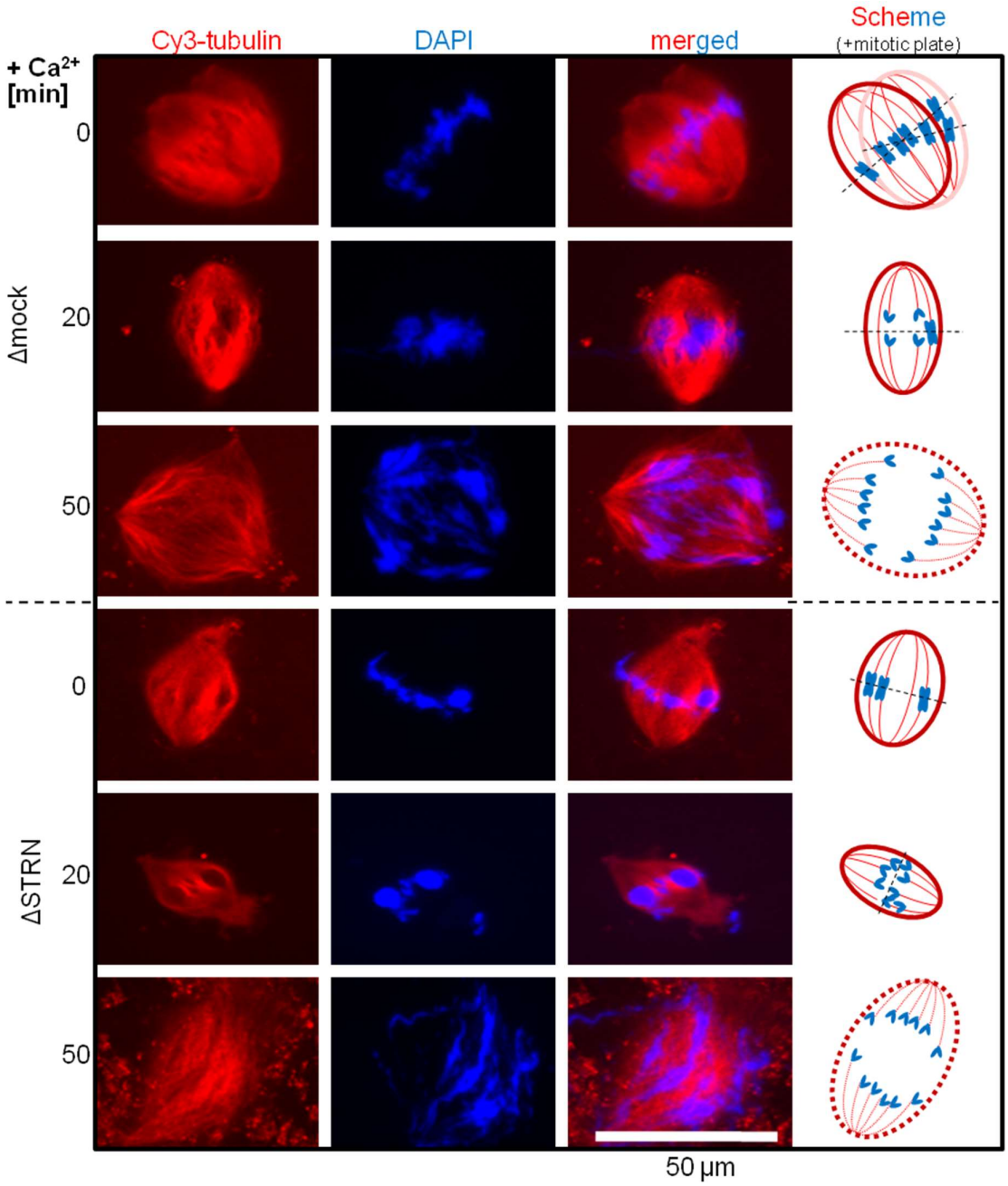

Figure 19: Examples of *Xenopus laevis* egg extract spindles upon Ca^{2+} addition. Examples of 3 different mitotic stages for both IgG control and STRN-AB3-depleted lysates are shown: First, fully aligned condensed chromatids (DAPI) at the mitotic plate during metaphase and, second and third, 2 time points after 0,6 mM Ca^{2+} addition. Upper series show the condition with IgG (Δmock) treated extract, while lower images show STRN-deficient egg extract. The spindle structures (shape and size) are morphologically comparable. The scheme images show the orientation of the spindle and include the metaphase plate position. Scale = 50 µm.

Late time points of figure 19 and 20 are exceptional rather rare pictures, since the steps after metaphase-anaphase transition are short-lived. The kinase induced M-phase exit is significantly faster in comparison to the ion-addition. I only find putative leftovers of spindles but no transient states due to the relatively fast effect of the kinase. Such disperse MT polymers can be observed already at early time points of 10 min.

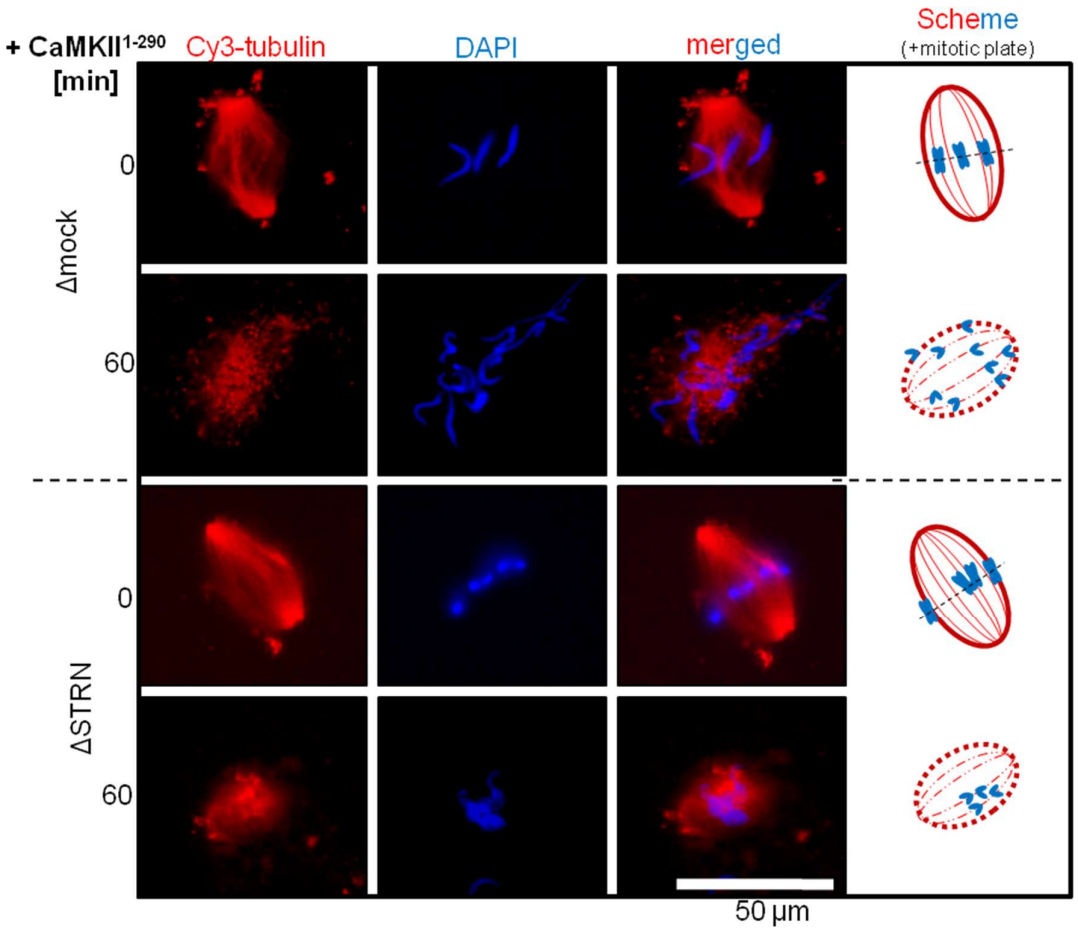

Figure 20: Examples of *Xenopus laevis* egg extract spindles upon CAMKII addition. Since STRN itself is Ca^{2+}sensitive due to its calmodulin binding domain, the experiment was alternatively performed with constitutively active CaMKII$^{aa1-290}$, which is used for this purpose in previous literature[179,245]. As in the previous figure 19 the red channel shows Cy3 labeled tubulin and the blue channel the DNA/DAPI. Scale = 50 µm.

A stimulus of Ca^{2+} addition to M-phase arrested egg lysates initiates metaphase-anaphase transition *in vitro* with the activation of APC/C and degradation of Cyclin B. The following blot shows the kinetics of putative M-phase associated proteins every 10 min in a time range from 0 to 70 min. The blot of anti-Cyclin B, the mitosis specific cyclin, served as a control.

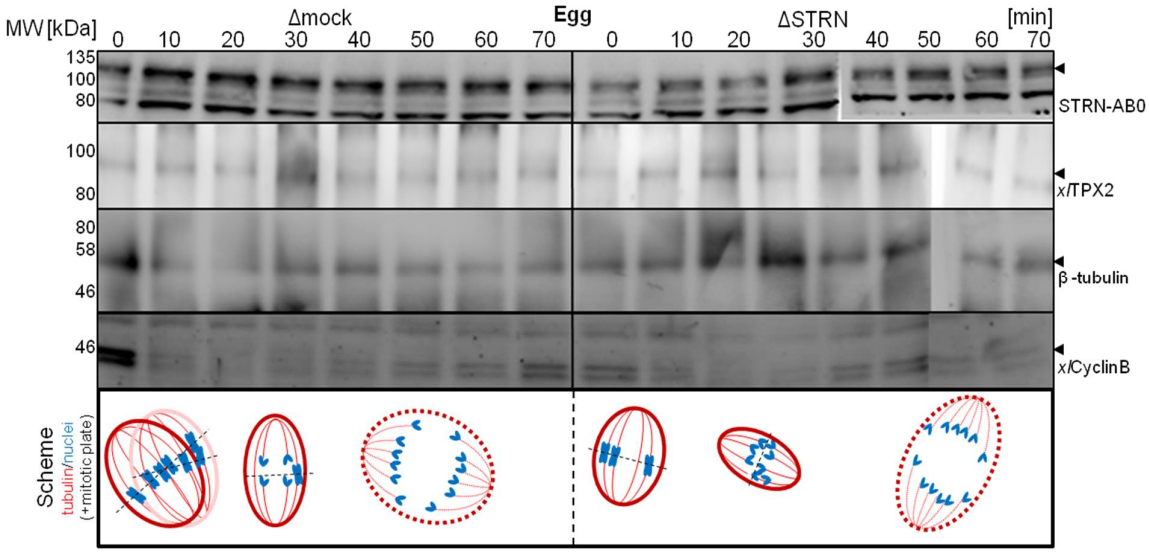

Figure 21: Addition of 0,6 mM Ca^{2+}does not have any visible effect onto STRN expression or modification in Western blot. The Western blots depicted here show no visible effect of STRN deficient extract. The kinetics show the levels of indicated proteins after calcium induction in the non-depleted (ΔIgG) and STRN-depleted (ΔSTRN) extract. Starting point (0 min) refers to the CSF mitotic arrested extract and end point (70 min) the interphasic state. The black arrows indicate the individual protein masses, STRN at 110 kDa, TPX2 at 100 kDa, β-tubulin at 50 kDa, Cyclin B at 45 kDa.

The M-phase specific protein Cyclin B forms the maturation promoting factor together with CDK1[251]. A high Cyclin B concentration is a marker for M-Phase arrest and can be observed during the starting condition of 0 min. This rapidly decreases after calcium addition. The anti-TPX2 blot serves as control. *In vivo,* when the nuclear envelope breaks down during mitosis or meiosis, TPX2 allows RANGTP-induced MT nucleation[322]. There is no visible change within the TPX2 signal, similar to the tubulin loading control. Also, the pattern of M-phase phosphorylation sites, which can be observed with the anti-MPM2 antibody, shows no visible kinetics (not shown here). The antibody labels M-phase specific phosphorylation epitopes.

Typical signals for M-phase marker antibody anti-MPM2 are MAP2 (*X. laevis* 205 kDa), HSP70 (*X. laevis* 71 kDa), CDC25 (*X. laevis* CDC25A 60 kDa) and DNA topoisomerase IIα (*X. laevis* TOPO2A 179 kDa)[329].

3.4 STRN antibody co-IP MS result explains its putative function

The anti-STRN antibody is an effective tool not only to immunodeplete the egg extract but also for the immunoprecipitation. The bead coupled antibody binds to endogenous STRN. Every interaction partner bound to STRN will be co-purified in this experiment. The STRN-AB3 immunoprecipitate is separated on an SDS gel and divided into high molecular mass and low molecular mass samples (upper and lower gel piece to lower complexity).

After tryptic digest the LC-MS/MS analysis was done by the core facility for mass spectrometry & proteomics (CFMP) at the Zentrum für Molekulare Biologie at the Heidelberg University (ZMBH) and the core facility for mass spectrometry from Institute of Biochemistry and Molecular Biology at the Bonn University (IBMB).

Potential M-phase interactions are listed in table 15. The list contains 3 different experiments. From experiment to experiment, I increased either antibody specificity (first assay STRN-AB2, second and third with STRN-AB3) or washing stringency. The first column of each result's table contains the gene name (HUGO/EntrezID). The genes are sorted by their hit frequency in identification. All listed candidates are not identified in the control anti-IgG immunoprecipitates.

After subtracting the anti-IgG candidates STRN-AB2 yielded 121 specific protein entries with 776 counted peptides. The optimized STRN-AB3 pull down identified 79 specific entries with 267 peptides. In the third co-IP I find 5 candidates with a total number of 28 peptides after background subtraction. The corresponding column to each gene consists of the number of counted peptides, the native complete protein mass in kDa and the protein ID to its RefSeq entry (if available and curated for *Xenopus laevis*). In all measurements STRN was readily detectable although not with the highest score. The entries highlighted in grey are promising candidates that are reproducible in different measurements, can be verified via a different technique or are already known STRN interaction partners from previous papers.

Table 15: Mass spectrometry analysis of anti-STRN immunoprecipitation of *Xenopus laevis* egg extracts. The list shows candidates after subtracting proteins from the anti-IgG precipitation control as background. The coloring of the first column is a coarse interpretation of function with its legend on the right side. The grey marking in the second column highlights proteins that came up as potential interaction partners for STRN multiple times with different verification techniques.

MS STRN-AB2	PeptideNo-kDa-*ProtID*	MS STRN-AB3	PeptideNo-kDa-*ProtID*	MS STRN-AB3strin gend	PeptideNo-kDa-*ProtID*
DNM1	**38**-95-*NP_001361772.1*	RIF1	**55**-257-*NP_001267578.1*	ZNF638	**12**-259-*XP_018098451.1*
CPSF1	**35**-156-*XP_018122441.1*	THOC2	**22**-182-*XP_018088431.1*	RHAMM	**8**-137-*NP_001087936.1*
SYMPK	**33**-134-*Q7ZYV9*	PLEC	**17**-529-*XP_018079502.1*	**STRN**	**4**-87-*NP_001087621.1*
CPSF2	**30**-89-*Q9W799*	CSE1L	**16**-110-*NP_001086035.1*	THOC1	**2**-75-*NP_001082490.1*
STRN	**25**-87-*NP_001087621.1*	RHAMM	**15**-137-*NP_001087936.1*	THOC2	**2**-182-*XP_018088431.1*
MYCBP2	**21**-516-*XP_018102752.1*	**STRN**	**13**-87-*NP_001087621.1*		
KATNB1	**21**-72-*Q4V7Y7*	THOC1	**9**-75-*NP_001082490.1*		
SSX2IP	**20**-65-*Q6NRK1*	PFK	**6**-88-*NP_001086921.1*		
KLHL11	**18**-77-*XP_018090175.1*	PPP2R1A	**6**-65-*NP_001081031.1*		
KATNAL1	**17**-60-*XP_018103188.1*	DNM1	**5**-95-*NP_001361772.1*		
ARHGEF1	**17**-121-*XP_018081772.1*	RANGAP1	**5**-63-*NP_001165668.1*		
DDX41	**16**-70-*XP_018107720.1*	POLD1	**4**-125-*NP_001087694.1*		
LUZP1	**16**-120-*NP_001086680.1*	THOC7	**4**-23-*NP_001080651.1*		
KATNA1	**16**-56-*NP_001084226.1*	THOC3	**4**-36-*XP_018107685.1*		
LARP4	**15**-81-*NP_001121273.1*	CAPN1	**3**-81-*NP_001080485.1*		
GTF2IRD1	**14**-111-*B7ZQJ9*	ECH	**3**-31-*NP_001086341.1*		
FXR1	**14**-76-*Q7ZTQ5*	COPG1	**3**-98-*NP_001083575.1*		
PABPC1	**14**-70-*P20965*	THOC6	**3**-37-*NP_001089841.1*		
APOB	**13**-51-*NP_001089224.1*	KCC2	**3**-122-*XP_018090659.1*		
WDR33	**13**-183-*XP_018121304.1*	HDAC	**2**-55-*NP_001079396.1*		
RCC1	**11**-45-*NP_001085384.1*	KIF20A	**2**-101-*NP_001088540.1*		
NONO	**11**-53-*NP_001080735.1*	RFC2	**2**-38-*NP_001084837.1*		
ELMSAN1	**10**-128-*XP_018087743.1*	DDX6	**2**-54-*XP_018097503.1*		
SFPQ	**10**-66-*XP_018105000.1*	GSN	**2**-81-*NP_001081527.1*		
PKC	**10**-77-*NP_001087142.1*	PKM	**2**-57-*NP_001080582.1*		
FMR1	**9**-64-*Q2KHP9*	DDX3X	**2**-77-*NP_001080283.1*		
CCDC61	**8**-58-*XP_017952369.2*	EEF1G	**2**-50-*NP_001079766.1*		
ASCC3	**7**-205-*XP_018118856.1*	UBE2V1	**2**-17-*NP_001084304.1*		
CSTF2	**7**-55-*NP_001080179.1*	CDC37	**2**-43-*NP_001015912.1*		
CUL3	**7**-89-*Q6GPF3*	EIF4G2	**1**-79-*NP_001106324.1*		

RNA/DNA modulators
MT modulators
STRIPAK proteins
THOC proteins

CHD4	**7**-215-*NP_001080504.1*	EIF2S1	**1**-36-*Q7ZTK4*
UPF1	**7**-122-*NP_001085862.1*	CAND1	**1**-136-*NP_001085373.1*
RBBP8	**7**-97-*XP_018079149.1*	CLTC	**1**-191-*NP_001085860.1*
STRIP1	**7**-61-*NP_001121347.1*	KPNA2	**1**-58-*NP_001080433.1*
SH3KBP1	**7**-47-*XP_018104557.1*	KIF2C	**1**-83-*Q91636*
XRN2	**7**-53-*NP_001091411.1*	XRCC5	**1**-82-*NP_001081127.1*
PCM1	**6**-228-*Q9PVV4*	EXOC4	**1**-39-*AAH72283.1*
CENPE	**6**-340-*NP_001080954.1*	TEX11	**1**-110-*XP_018086249.1*
TSNARE1	**6**-69-*XP_018124413.1*	MELK	**1**-74-*Q91821*
PIWIL1	**6**-98-*XP_002940227.2*	COPBI	**1**-107-*NP_001090083.1*
SNRNP200	**5**-245-*XP_002932581.2*	H4C1	**1**-11-*P62799*
CPSF6	**5**-59-*Q6DDW4*	FEN1	**1**-43-*NP_001080984.1*
EIF4ENIF1	**5**-86-*NP_001086710.1*	PAN2	**1**-72-*NP_001086001.1*
FIP1L1	**5**-64-*NP_001088083.1*	CTPS1	**1**-67-*NP_001088219.1*
ASCC2	**5**-84-*NP_001080879.1*	LRRC47	**1**-63-*NP_001079842.1*
CTTNBP2	**5**-181-*XP_018108053.1*	CYP1B1	**1**-63-*XP_018120646.1*
YBX2	**5**-36-*P45441*	H2AX	**1**-15-*Q6GM86*
ZNF598	**5**-101-*NP_001089231.2*	MGA	**1**-337-*XP_018086529.1*
ASCC1	**5**-39-*XP_018080883.1*	PTH	**1**-11-*CAW30788.1*
CACTIN	**5**-94-*XP_018099013.1*	ACVR2A	**1**-58-*NP_001088256.1*
PRMT5	**5**-72-*Q6NUA1*	DST	**1**-861-*XP_018118962.1*
HDAC1	**5**-55-*NP_001079396.1*	ITGB1	**1**-88-*NP_001084331.1*
CPEB1	**4**-63-*Q52KN7*	PPFIA1	**1**-137-*NP_001088956.1*
DNAJC7	**4**-56-*XP_018093427.1*	BRD4	**1**-151-*Q08D75*
DHX35	**4**-78-*XP_018093906.1*	DHX15	**1**-86-*XP_018098562.1*
KLHL24	**4**-68-*XP_018121341.1*	SEC14	**1**-82-*XP_018089816.1*
XIAB	**4**-55-*A5D8Q0*	RPS5	**1**-23-*NP_001079800.1*
CIT	**3**-194-*XP_018097396.1*	UBE2D3	**1**-17-*NP_001084434.1*
CNOT1	**3**-271-*XP_018116117.1*	IPO4	**1**-120-*XP_018114829.1*
PRRC2A	**3**-223-*XP_018088742.1*	MCM9	**1**-127-*NP_001084773.1*
PRPF6	**3**-109-*NP_001087374.2*	PHB2	**1**-33-*NP_001086635.1*
PSPC1	**3**-59-*XP_018103230.1*	ADAM15	**1**-90-*AAI46627.1*
PHF14	**3**-101-*XP_018122822.1*	SGCD	**1**-20-*XP_018109995.1*
RNF123	**3**-134-*XP_018115370.1*	CRY1	**1**-70-*NP_001081129.1*
DDB1	**3**-127-*Q6P6Z0*	ZRANB2	**1**-38-*NP_001084142.1*
DDX4	**3**-79-*XP_018096464.1*	PRRC2B	**1**-241-*XP_018088147.1*
RBM26	**3**-119-*Q2T9I5*	SYT1	**1**-45-*NP_001087607.1*
WDR8	**3**-52-*NP_001089991.1*	ANXA7	**1**-55-*NP_001087675.1*

NUP107	**3**-105-*NP_001091312.1*	MFSD5	**1**-50-*NP_001121281.1*
DHX15	**3**-86-*XP_018098562.1*	ECI2	**1**-40-*NP_001089808.1*
ATX2	**3**-118-*XP_018099700.1*	SARM1	**1**-79-*XP_018104264.1*
RHAMM	**3**-137-*NP_001087936.1*	SLC22	**1**-62-*NP_001087673.1*
GATAD2A	**3**-61-*NP_001121310.1*	GBX2	**1**-37-*NP_001083900.1*
NCAPG	**3**-116-*Q9YHB5*	SERPINE1	**1**-45-*NP_001090520.1*
STAU1	**3**-78-*XP_018093622.1*	LRRTM4	**1**-68-*XP_031755134.1*
SOGA1	**3**-179-*XP_018093959.1*	PPFIA2	**1**-142-*XP_031754748.1*
TDRD3	**3**-73-*Q6NRP6*	GPX1	**1**-22-*NP_001088896.3*
DHX16	**2**-104-*XP_018088758.1*	EDA	**1**-39-*XP_004916866.1*
MTOR	**2**-288-*XP_031761370.1*	THOC5	**1**-78-*NP_001080668.1*
CSPP1	**2**-150-*XP_018123546.1*		
TCF20	**2**-205-*XP_018114230.1*		
SMC2	**2**-15-*XP_018095460.1*		
IGF2BP3	**2**-65-*O57526*		
UPF2	**2**-147-*NP_001089661.1*		
VPS13C	**2**-421-*XP_018108373.1*		
ARVCF	**2**-102-*XP_018099619.1*		
CLUH	**2**-147-*Q0IHW8*		
KIF5B	**2**-110-*ABG74914.1*		
CPSF3	**2**-78-*NP_001088278.1*		
KIF20A	**2**-101-*NP_001088540.1*		
KARS1	**2**-70-*NP_001080050.1*		
PLAA	**2**-88-*NP_001121253.1*		
STRN3	**2**-81-*NP_001086983.1*		
DDX23	**2**-94-*XP_018105478.1*		
ACIN1	**2**-73-*NP_001089912.1*		
STAU2	**2**-75-*NP_001080784.1*		
SYNCRIP	**2**-69-*NP_001084953.1*		
TARS1	**2**-83-*NP_001087812.1*		
AKAP8L	**2**-51-*XP_018109096.1*		
IMMT	**2**-85-*XP_018098488.1*		
DDX43	**2**-75-*XP_018096093.1*		
ORC3	**2**-81-*NP_001079397.1*		
NDUFS1	**2**-80-*XP_018094504.1*		
RCBTB1	**2**-66-*NP_001084549.2*		
SLC25A13	**2**-75-*XP_018124682.1*		
FAM114A1	**2**-57-*XP_018084612.1*		
RPN2	**2**-69-*NP_001079661.1*		
SQSTM1	**1**-50-*NP_001079920.1*		
MIB1	**1**-111-*XP_018079145.1*		
STRIP2	**1**-90-*XP_018108284.1*		
RICTOR	**1**-191-*XP_018100001.1*		
ZNF326	**1**-56-*A2RV70*		
DUSP11	**1**-38-*XP_018110694.1*		
SRRM2	**1**-94-*AAH76812.1*		
CNOT2	**1**-60-*AAH73075.1*		
TRIM3	**1**-81-*XP_018105997.1*		
MTA1	**1**-71-*NP_001087897.1*		
CD2BP2	**1**-46-*NP_001080561.1*		
KIF23	**1**-90-*NP_001088544.1*		
DHX34	**1**-130-*XP_018085690.1*		
SF3B3	**1**-136-*XP_018116130.1*		

The raw data from the MS results were sorted in the open source program tool Scaffold 5 according to their peptide frequency. All candidates that were found in the IgG-precipitate control got subtracted from the shown list.
STRN-antibody-precipitate specific identifications were then inserted into the DAVID online tool for characterization and categorization of their molecular functions (seen in table 16). DAVID is a database for annotation, visualization and integrated discovery and provides functional interpretation of large lists of genes derived from genomic studies, *e. g*. microarray and proteomics studies.

The coloring of table 15, table 16, the map in figure 22, 23 and later in human cells seen table 17 and the map in figure 42 refers to the DAVID database characterization. Furthermore, each individual gene entry, its categorization and characterization got double-checked by looking up the GeneCard database summary.

The most frequent category is the orange one, which is defined as DNA/RNA-associated proteins. This includes proteins that play a role in transcription, translation, splicing and related functions. The list shows proteins from both upstream (transcription) DNA-related and downstream (splicing, translation) mRNA-related processing.

The second common category is the light and dark-blue category. Light blue includes proteins that are already described MAPs, centrosomal proteins or play a role in MT modulation. Dark blue are STRN and already known STRN interactors (including STRIPAK complex components). A third category comes up with the STRN-AB3 immunoprecipitate, but not with STRN-AB2: The green-stained mitotic cell cycle and growth relevant THOC-proteins, known as transcription factor/nuclear export (THO)-complex[330].

Apart from that, a high scoring protein of the STRN-AB2-list is the polyadenylation machinery protein SYMPK (Symplekin) found with a 33 peptides[331]. Symplekin cannot be found with STRN-AB3. The dark-grayish staining of the second column indicates MS findings that come up redundantly within this thesis. Some of them can be verified as true STRN interactors with independent methods (like previous proofed in Western blot and later seen in BIOID).

The listed candidates from table 15 are pasted into STRING database. STRING evaluates the list by checking recorded results from gene ontology (GO) terms. It compares data from different sources like Western blots, immunofluorescent co-staining or does text mining for proteins described together. In both maps of figure 22 STRN-AB2 1st MS and figure 23 STRN-AB3 2nd MS I excluded free floating candidates that did not exhibit any connection to the network (putative known interactions).

Table 16: The interpreted pathways (gene list categorization) from DAVID database. As in previous lists the orange label indicates DNA/RNA-associated interpretation of protein pathways and the light blue labels MAP or centrosomal associated pathways.

MS IP STRN-AB2			MS IP STRN-AB3		
Gene ontology term	**raw *p*-value**	**FDR**	**Gene ontology term**	**raw *p*-value**	**FDR**
mRNA metabolic process (GO:0016071)	$2{,}98\times10^{-25}$	$4{,}70\times10^{-21}$	viral mRNA export from host cell nucleus (GO:0046784)	$6{,}95\times10^{-12}$	$1{,}10\times10^{-7}$
mRNA processing (GO:0006397)	$1{,}89\times10^{-24}$	$1{,}49\times10^{-20}$	translocation of molecules into host (GO:0044417)	$1{,}16\times10^{-11}$	$9{,}11\times10^{-8}$
RNA splicing (GO:0008380)	$8{,}12\times10^{-22}$	$4{,}27\times10^{-18}$	establishment of localization in cell (GO:0051649)	$3{,}32\times10^{-11}$	$1{,}75\times10^{-7}$
nucleic acid metabolic process (GO:0090304)	$1{,}43\times10^{-21}$	$5{,}64\times10^{-18}$	cellular localization (GO:0051641)	$1{,}57\times10^{-10}$	$6{,}18\times10^{-7}$
RNA metabolic process (GO:0016070)	$6{,}65\times10^{-21}$	$2{,}10\times10^{-17}$	cellular nitrogen compound metabolic process (GO:0034641)	$1{,}97\times10^{-8}$	$6{,}21\times10^{-5}$
mRNA splicing, via spliceosome (GO:0000398)	$4{,}18\times10^{-20}$	$1{,}10\times10^{-16}$	nucleobase-containing compound metabolic process (GO:0006139)	$2{,}27\times10^{-8}$	$5{,}97\times10^{-5}$
RNA splicing, via transesterification reactions with bulged adenosine as nucleophile (GO:0000377)	$4{,}18\times10^{-20}$	$9{,}42\times10^{-17}$	cellular protein localization (GO:0034613)	$2{,}59\times10^{-8}$	$5{,}84\times10^{-5}$
RNA splicing, via transesterification reactions (GO:0000375)	$5{,}18\times10^{-20}$	$1{,}02\times10^{-16}$	cellular macromolecule localization (GO:0070727)	$2{,}77\times10^{-8}$	$5{,}46\times10^{-5}$
nucleobase-containing compound metabolic process (GO:0006139)	$3{,}13\times10^{-19}$	$5{,}48\times10^{-16}$	biological process involved in interaction with host (GO:0051701)	$3{,}40\times10^{-8}$	$5{,}96\times10^{-5}$
RNA processing (GO:0006396)	$2{,}60\times10^{-18}$	$4{,}11\times10^{-15}$	cellular aromatic compound metabolic process (GO:0006725)	$3{,}61\times10^{-8}$	$5{,}69\times10^{-5}$
heterocycle metabolic process (GO:0046483)	$6{,}42\times10^{-18}$	$9{,}21\times10^{-15}$	nucleocytoplasmic transport (GO:0006913)	$6{,}81\times10^{-8}$	$9{,}76\times10^{-5}$
cellular aromatic compound metabolic process (GO:0006725)	$1{,}27\times10^{-17}$	$1{,}67\times10^{-14}$	biological process involved in symbiotic interaction (GO:0044403)	$7{,}45\times10^{-8}$	$9{,}80\times10^{-5}$
cellular nitrogen compound metabolic process (GO:0034641)	$7{,}34\times10^{-17}$	$8{,}90\times10^{-14}$	nuclear transport (GO:0051169)	$7{,}55\times10^{-8}$	$9{,}16\times10^{-4}$
organic cyclic compound metabolic process (GO:1901360)	$8{,}83\times10^{-17}$	$9{,}95\times10^{-14}$	macromolecule localization (GO:0033036)	$9{,}29\times10^{-8}$	$1{,}05\times10^{-4}$
gene expression (GO:0010467)	$2{,}92\times10^{-14}$	$3{,}07\times10^{-14}$	heterocycle metabolic process (GO:0046483)	$1{,}01\times10^{-7}$	$1{,}06\times10^{-4}$
macromolecule metabolic process (GO:0043170)	$8{,}19\times10^{-14}$	$8{,}08\times10^{-14}$	intracellular protein transport (GO:0006886)	$1{,}27\times10^{-7}$	$1{,}25\times10^{-4}$
nitrogen compound metabolic process (GO:0006807)	$4{,}82\times10^{-11}$	$4{,}47\times10^{-8}$	macromolecule metabolic process (GO:0043170)	$1{,}60\times10^{-7}$	$1{,}48\times10^{-4}$
RNA localization (GO:0006403)	$7{,}72\times10^{-11}$	$6{,}77\times10^{-8}$	organic cyclic compound metabolic process (GO:1901360)	$2{,}22\times10^{-7}$	$1{,}94\times10^{-4}$
mRNA polyadenylation (GO:0006378)	$1{,}07\times10^{-10}$	$8{,}89\times10^{-8}$	nucleic acid metabolic process (GO:0090304)	$4{,}15\times10^{-7}$	$3{,}45\times10^{-4}$
RNA polyadenylation (GO:0043631)	$1{,}30\times10^{-10}$	$1{,}03\times10^{-7}$	organic substance metabolic process (GO:0071704)	$4{,}97\times10^{-7}$	$3{,}92\times10^{-4}$
RNA transport (GO:0050658)	$2{,}84\times10^{-10}$	$2{,}14\times10^{-7}$	nitrogen compound transport (GO:0071705)	$6{,}17\times10^{-7}$	$4{,}63\times10^{-4}$
nucleic acid transport (GO:0050657)	$2{,}84\times10^{-10}$	$2{,}04\times10^{-7}$	cellular component organization (GO:0016043)	$7{,}30\times10^{-7}$	$5{,}24\times10^{-4}$
establishment of RNA localization (GO:0051236)	$3{,}19\times10^{-10}$	$2{,}19\times10^{-7}$	localization (GO:0051179)	$7{,}88\times10^{-7}$	$5{,}40\times10^{-4}$
protein-containing complex localization (GO:0031503)	$4{,}78\times10^{-10}$	$3{,}14\times10^{-7}$	protein localization (GO:0008104)	$8{,}77\times10^{-7}$	$5{,}77\times10^{-4}$
regulation of translation (GO:0006417)	$5{,}95\times10^{-10}$	$3{,}75\times10^{-7}$	regulation of DNA damage checkpoint (GO:2000001)	$1{,}07\times10^{-6}$	$6{,}74\times10^{-4}$
DNA-templated transcription, termination (GO:0006353)	$1{,}82\times10^{-9}$	$1{,}10\times10^{-6}$	metabolic process (GO:0008152)	$1{,}25\times10^{-6}$	$7{,}57\times10^{-4}$
cellular metabolic process (GO:0044237)	$2{,}00\times10^{-9}$	$1{,}17\times10^{-6}$	cellular metabolic process (GO:0044237)	$1{,}39\times10^{-6}$	$8{,}12\times10^{-4}$
organelle organization (GO:0006996)	$2{,}67\times10^{-9}$	$1{,}51\times10^{-6}$	mRNA 3'-end processing (GO:0031124)	$1{,}48\times10^{-6}$	$8{,}36\times10^{-4}$
primary metabolic process (GO:0044238)	$3{,}40\times10^{-9}$	$1{,}85\times10^{-6}$	protein transport (GO:0015031)	$1{,}81\times10^{-6}$	$9{,}83\times10^{-4}$
mRNA transport (GO:0051028)	$3{,}69\times10^{-9}$	$1{,}94\times10^{-6}$	cellular component organization or biogenesis (GO:0071840)	$2{,}08\times10^{-6}$	$1{,}09\times10^{-3}$
nucleobase-containing compound transport (GO:0015931)	$4{,}04\times10^{-9}$	$2{,}06\times10^{-6}$	protein export from nucleus (GO:0006611)	$2{,}33\times10^{-6}$	$1{,}19\times10^{-3}$
mRNA 3'-end processing (GO:0031124)	$4{,}36\times10^{-9}$	$2{,}15\times10^{-6}$	peptide transport (GO:0015833)	$2{,}41\times10^{-6}$	$1{,}19\times10^{-3}$
regulation of cellular amide metabolic process (GO:0034248)	$5{,}43\times10^{-9}$	$2{,}60\times10^{-6}$	anion transport (GO:0006820)	$2{,}46\times10^{-6}$	$1{,}17\times10^{-3}$
termination of RNA polymerase II transcription (GO:0006369)	$8{,}47\times10^{-9}$	$3{,}93\times10^{-6}$	intracellular transport (GO:0046907)	$2{,}58\times10^{-6}$	$1{,}20\times10^{-3}$
mRNA cleavage (GO:0006379)	$1{,}02\times10^{-8}$	$4{,}61\times10^{-6}$	transport (GO:0006810)	$2{,}78\times10^{-6}$	$1{,}25\times10^{-3}$
organic substance metabolic process (GO:0071704)	$1{,}12\times10^{-8}$	$4{,}90\times10^{-6}$	amide transport (GO:0042886)	$3{,}34\times10^{-6}$	$1{,}46\times10^{-3}$
mRNA export from nucleus (GO:0006406)	$2{,}86\times10^{-8}$	$1{,}22\times10^{-5}$	telomere maintenance (GO:0000723)	$3{,}53\times10^{-6}$	$1{,}50\times10^{-3}$
mRNA-containing ribonucleoprotein complex export from nucleus (GO:0071427)	$2{,}86\times10^{-8}$	$1{,}19\times10^{-5}$	cell cycle (GO:0007049)	$3{,}74\times10^{-6}$	$1{,}55\times10^{-3}$
pre-mRNA cleavage required for polyadenylation (GO:0098789)	$4{,}45\times10^{-8}$	$1{,}80\times10^{-5}$	nuclear export (GO:0051168)	$4{,}08\times10^{-6}$	$1{,}65\times10^{-3}$
mitotic nuclear division (GO:0140014)	$5{,}35\times10^{-8}$	$2{,}11\times10^{-5}$	telomere organization (GO:0032200)	$4{,}13\times10^{-6}$	$1{,}63\times10^{-3}$
mRNA cleavage involved in mRNA processing (GO:0098787)	$6{,}01\times10^{-8}$	$2{,}31\times10^{-5}$	response to stress (GO:0006950)	$4{,}15\times10^{-6}$	$1{,}59\times10^{-3}$
RNA phosphodiester bond hydrolysis (GO:0090501)	$6{,}36\times10^{-8}$	$2{,}39\times10^{-5}$	negative regulation of DNA damage checkpoint (GO:2000002)	$4{,}27\times10^{-6}$	$1{,}60\times10^{-3}$
nuclear export (GO:0051168)	$6{,}71\times10^{-8}$	$2{,}46\times10^{-5}$	establishment of localization (GO:0051234)	$4{,}50\times10^{-6}$	$1{,}65\times10^{-3}$
metabolic process (GO:0008152)	$7{,}90\times10^{-8}$	$2{,}83\times10^{-5}$	establishment of protein localization (GO:0045184)	$4{,}51\times10^{-6}$	$1{,}62\times10^{-3}$

ribonucleoprotein complex export from nucleus (GO:0071426)	$8,48x10^{-8}$	$2,97x10^{-5}$	mRNA export from nucleus (GO:0006406)	$5,32x10^{-6}$	$1,87x10^{-3}$
ribonucleoprotein complex localization (GO:0071166)	$9,04x10^{-8}$	$3,10x10^{-5}$	mRNA-containing ribonucleoprotein complex export from nucleus (GO:0071427)	$5,32x10^{-6}$	$1,83x10^{-3}$
mitotic cell cycle process (GO:1903047)	$9,44x10^{-8}$	$3,17x10^{-5}$	DNA repair (GO:0006281)	$5,68x10^{-6}$	$1,91x10^{-3}$
regulation of mRNA metabolic process (GO:1903311)	$1,14x10^{-7}$	$3,75x10^{-5}$	cellular response to stress (GO:0033554)	$6,55x10^{-6}$	$2,15x10^{-3}$
posttranscriptional regulation of gene expression (GO:0010608)	$1,29x10^{-7}$	$4,16x10^{-5}$	DNA metabolic process (GO:0006259)	$7,87\ x10^{-6}$	$2,53x10^{-3}$
RNA export from nucleus (GO:0006405)	$1,39x10^{-7}$	$4,38x10^{-5}$	negative regulation of cell cycle checkpoint (GO:1901977)	$8,34x10^{-6}$	$2,63x10^{-3}$
chromosome organization (GO:0051276)	$1,78x10^{-7}$	$5,49x10^{-5}$	cellular response to DNA damage stimulus (GO:0006974)	$8,53x10^{-6}$	$2,64x10^{-3}$
cell cycle process (GO:0022402)	$2,05x10^{-7}$	$6,21x10^{-5}$	biological process involved in interspecies interaction between organisms (GO:0044419)	$8,76x10^{-6}$	$2,66x10^{-3}$
RNA 3'-end processing (GO:0031123)	$2,08x10^{-7}$	$6,20x10^{-5}$	ribonucleoprotein complex export from nucleus (GO:0071426)	$1,11x10^{-5}$	$3,31x10^{-3}$
nucleic acid phosphodiester bond hydrolysis (GO:0090305)	$2,51x10^{-7}$	$7,34x10^{-5}$	regulation of cell cycle checkpoint (GO:1901976)	$1,13x10^{-5}$	$3,29x10^{-3}$
organelle fission (GO:0048285)	$2,91x10^{-7}$	$8,34x10^{-5}$	ribonucleoprotein complex localization (GO:0071166)	$1,16x10^{-5}$	$3,33x10^{-3}$
cell cycle (GO:0007049)	$3,20x10^{-7}$	$9,02x10^{-5}$	mRNA metabolic process (GO:0016071)	$1,26x10^{-5}$	$3,56x10^{-3}$
protein export from nucleus (GO:0006611)	$3,59x10^{-7}$	$9,94x10^{-5}$	organic substance transport (GO:0071702)	$1,29x10^{-5}$	$3,56x10^{-3}$
cellular macromolecule metabolic process (GO:0044260)	$3,80x10^{-7}$	$1,03x10^{-4}$	double-strand break repair (GO:0006302)	$1,40x10^{-5}$	$3,76x10^{-3}$
mitotic cell cycle (GO:0000278)	$4,29x10^{-7}$	$1,15x10^{-4}$	primary metabolic process (GO:0044238)	$1,40x10^{-5}$	$3,80x10^{-3}$
cellular component organization (GO:0016043)	$5,26x10^{-7}$	$1,38x10^{-4}$	RNA export from nucleus (GO:0006405)	$1,55x10^{-5}$	$4,08x10^{-3}$
regulation of mRNA catabolic process (GO:0061013)	$6,30x10^{-7}$	$1,63x10^{-4}$	nitrogen compound metabolic process (GO:0006807)	$1,74x10^{-5}$	$4,50x10^{-3}$
mitotic sister chromatid segregation (GO:0000070)	$7,50x10^{-7}$	$1,91x10^{-4}$	RNA 3'-end processing (GO:0031123)	$2,04x10^{-5}$	$5,20x10^{-3}$
nuclear division (GO:0000280)	$8,17x10^{-7}$	$2,05x10^{-4}$	RNA splicing (GO:0008380)	$2,65x10^{-5}$	$6,64x10^{-3}$
negative regulation of metabolic process (GO:0009892)	$1,02x10^{-6}$	$2,52x10^{-4}$	regulation of response to DNA damage stimulus (GO:2001020)	$2,67x10^{-5}$	$6,59x10^{-3}$
gene silencing by RNA (GO:0031047)	$1,11x10^{-6}$	$2,68x10^{-4}$	mRNA transport (GO:0051028)	$3,77x10^{-5}$	$9,15x10^{-3}$
cellular component organization or biogenesis (GO:0071840)	$1,15x10^{-6}$	$2,75x10^{-4}$	regulation of cell cycle (GO:0051726)	$4,02x10^{-5}$	$9,61x10^{-3}$
negative regulation of mRNA metabolic process (GO:1903312)	$1,19x10^{-6}$	$2,80x10^{-4}$	chromosome organization (GO:0051276)	$4,40x10^{-5}$	$1,04x10^{-2}$
negative regulation of mRNA catabolic process (GO:1902373)	$1,72x10^{-6}$	$4,00x10^{-4}$	protein localization to organelle (GO:0033365)	$4,47x10^{-5}$	$1,04x10^{-2}$
negative regulation of translation (GO:0017148)	$1,82x10^{-6}$	$4,15x10^{-4}$	cell cycle process (GO:0022402)	$4,81x10^{-5}$	$1,10x10^{-2}$
cellular process (GO:0009987)	$2,71x10^{-6}$	$6,10x10^{-4}$	secretion by cell (GO:0032940)	$5,81x10^{-5}$	$1,31x10^{-2}$
negative regulation of macromolecule metabolic process (GO:0010605)	$3,25x10^{-6}$	$7,21x10^{-4}$	protein-containing complex localization (GO:0031503)	$6,24x10^{-5}$	$1,39x10^{-2}$
nucleocytoplasmic transport (GO:0006913)	$3,28x10^{-6}$	$7,20x10^{-4}$	response to stimulus (GO:0050896)	$6,86x10^{-5}$	$1,50x10^{-2}$
sister chromatid segregation (GO:0000819)	$3,29x10^{-6}$	$7,11x10^{-4}$	negative regulation of gene expression (GO:0010629)	$6,87x10^{-5}$	$1,48x10^{-2}$
nuclear transport (GO:0051169)	$3,62x10^{-6}$	$7,73x10^{-4}$	cellular macromolecule metabolic process (GO:0044260)	$8,54x10^{-5}$	$1,82x10^{-2}$
negative regulation of RNA catabolic process (GO:1902369)	$4,40x10^{-6}$	$9,25x10^{-4}$	stress granule assembly (GO:0034063)	$8,67x10^{-5}$	$1,82x10^{-2}$
negative regulation of cellular amide metabolic process (GO:0034249)	$5,20x10^{-6}$	$1,08x10^{-3}$	base-excision repair (GO:0006284)	$8,86x10^{-5}$	$1,84x10^{-2}$
cellular macromolecule biosynthetic process (GO:0034645)	$7,16x10^{-6}$	$1,47x10^{-3}$	positive regulation of cellular component organization (GO:0051130)	$9,00x10^{-5}$	$1,84x10^{-2}$
negative regulation of cellular metabolic process (GO:0031324)	$8,32x10^{-6}$	$1,68x10^{-3}$	regulation of DNA metabolic process (GO:0051052)	$9,42x10^{-5}$	$1,90x10^{-2}$
macromolecule biosynthetic process (GO:0009059)	$1,09x10^{-5}$	$2,17x10^{-3}$	export from cell (GO:0140352)	$9,52x10^{-5}$	$1,90x10^{-2}$
negative regulation of gene expression (GO:0010629)	$1,11x10^{-5}$	$2,19x10^{-3}$	mRNA processing (GO:0006397)	$9,83x10^{-5}$	$1,94x10^{-2}$
negative regulation of RNA metabolic process (GO:0051253)	$1,45x10^{-5}$	$2,82x10^{-3}$			
microtubule-based process (GO:0007017)	$1,66x10^{-5}$	$3,19x10^{-3}$			
negative regulation of nitrogen compound metabolic process (GO:0051172)	$1,67x10^{-5}$	$3,17x10^{-3}$			
regulation of gene expression (GO:0010468)	$1,81x10^{-5}$	$3,40x10^{-3}$			
cytoskeleton organization (GO:0007010)	$1,84x10^{-5}$	$3,41x10^{-3}$			
regulation of mRNA stability (GO:0043488)	$1,94x10^{-5}$	$3,56x10^{-3}$			
negative regulation of cellular biosynthetic process (GO:0031327)	$2,51x10^{-5}$	$4,56x10^{-3}$			
regulation of biosynthetic process (GO:0009889)	$2,68x10^{-5}$	$4,81x10^{-3}$			
regulation of RNA stability (GO:0043487)	$2,75x10^{-5}$	$4,88x10^{-3}$			
rhythmic process (GO:0048511)	$3,10x10^{-5}$	$5,43x10^{-3}$			
macromolecule catabolic process (GO:0009057)	$3,23x10^{-5}$	$5,60x10^{-3}$			
gene silencing (GO:0016458)	$3,28x10^{-5}$	$5,62x10^{-3}$			
negative regulation of biosynthetic process (GO:0009890)	$3,45x10^{-5}$	$5,85x10^{-3}$			

negative regulation of cellular macromolecule biosynthetic process (GO:2000113)	$3{,}84 \times 10^{-5}$	$6{,}44 \times 10^{-3}$	
regulation of cellular biosynthetic process (GO:0031326)	$3{,}93 \times 10^{-5}$	$6{,}52 \times 10^{-3}$	
microtubule-based movement (GO:0007018)	$4{,}10 \times 10^{-5}$	$6{,}74 \times 10^{-3}$	
regulation of cell cycle process (GO:0010564)	$4{,}13 \times 10^{-5}$	$6{,}72 \times 10^{-3}$	
negative regulation of macromolecule biosynthetic process (GO:0010558)	$4{,}28 \times 10^{-5}$	$6{,}90 \times 10^{-3}$	
intracellular protein transport (GO:0006886)	$4{,}55 \times 10^{-5}$	$7{,}25 \times 10^{-3}$	
DNA metabolic process (GO:0006259)	$4{,}70 \times 10^{-5}$	$7{,}41 \times 10^{-3}$	
nitrogen compound transport (GO:0071705)	$4{,}78 \times 10^{-5}$	$7{,}46 \times 10^{-3}$	
regulation of metabolic process (GO:0019222)	$4{,}82 \times 10^{-5}$	$7{,}46 \times 10^{-3}$	
chromosome segregation (GO:0007059)	$4{,}92 \times 10^{-5}$	$7{,}53 \times 10^{-3}$	
DNA dealkylation involved in DNA repair (GO:0006307)	$4{,}94 \times 10^{-5}$	$7{,}50 \times 10^{-3}$	
regulation of cytoplasmic mRNA processing body assembly (GO:0010603)	$4{,}94 \times 10^{-5}$	$7{,}43 \times 10^{-3}$	
negative regulation of nucleobase-containing compound metabolic process (GO:0045934)	$5{,}01 \times 10^{-5}$	$7{,}46 \times 10^{-3}$	
regulation of organelle organization (GO:0033043)	$5{,}07 \times 10^{-5}$	$7{,}48 \times 10^{-3}$	
regulation of cellular macromolecule biosynthetic process (GO:2000112)	$5{,}21 \times 10^{-5}$	$7{,}62 \times 10^{-3}$	
nuclear chromosome segregation (GO:0098813)	$6{,}10 \times 10^{-5}$	$8{,}83 \times 10^{-3}$	
regulation of macromolecule metabolic process (GO:0060255)	$7{,}76 \times 10^{-5}$	$1{,}11 \times 10^{-2}$	
microtubule severing (GO:0051013)	$7{,}80 \times 10^{-5}$	$1{,}11 \times 10^{-2}$	
regulation of macromolecule biosynthetic process (GO:0010556)	$8{,}42 \times 10^{-5}$	$1{,}19 \times 10^{-2}$	
negative regulation of intracellular steroid hormone receptor signaling pathway (GO:0033144)	$8{,}61 \times 10^{-5}$	$1{,}20 \times 10^{-2}$	
protein transport (GO:0015031)	$9{,}07 \times 10^{-5}$	$1{,}25 \times 10^{-2}$	
transcription, DNA-templated (GO:0006351)	$9{,}32 \times 10^{-5}$	$1{,}28 \times 10^{-2}$	
nucleic acid-templated transcription (GO:0097659)	$9{,}47 \times 10^{-5}$	$1{,}29 \times 10^{-2}$	
DNA conformation change (GO:0071103)	$9{,}61 \times 10^{-5}$	$1{,}30 \times 10^{-2}$	

A second cluster within the GO term list is the centrosomal and MT associated interaction network (light blue labeling in table 16). Both, STRN-AB2 and STRN-AB3 antibody pull downs exhibit several proteins that play a role in MT related pathways like MT growth and shrinkage (KATNA1, KIF2C), cell cycle (PPP2R1A, SMC2[68,332]), cell division (RHAMM[333]), centrosome (SSX2IP[102]) and cilia signaling (WDR8[272]). Everything that belongs to this category is highlighted in blue in the maps of figure 22 and 23. Interestingly, the STRN-AB2-IP mass spectrometry results contain STRIPAK candidates. Among them I find STRIP1, STRIP2, CTTNBP2 and STRN3 (also known as SG_2NA). The STRN-AB3 pull down shows only one STRIPAK protein:

This is PPP2R1A also known as PP2A (Serine/threonine-protein phosphatase 2A) 65 kDa regulatory subunit Aα. Proteins that can be verified with both (STRN-AB2 and STRN-AB3) antibody precipitate MS experiments are STRN itself, RHAMM, DNM1, DHX15 and KIF20A. The latter protein is a well described MAP, or more specifically, a kinesin family member with known cell cycle and M-phase regulating functions[334]. The Hyaluronan-mediated motility receptor (HMMR), known as XRHAMM in *Xenopus*, can be verified in all three MS experiments, and with both types of antibodies. Similar to KIF20A, RHAMM is known to play a M-phase modulating role[333].

The stringently washed 3rd co-IP MS result contains a limited number of identifications to form the STRINGdb interaction network (like in figure 22 and 23) but confirms the previously found proteins from the THO complex also with the STRN-AB3. The THO protein complex components cannot be verified with STRN-AB2.

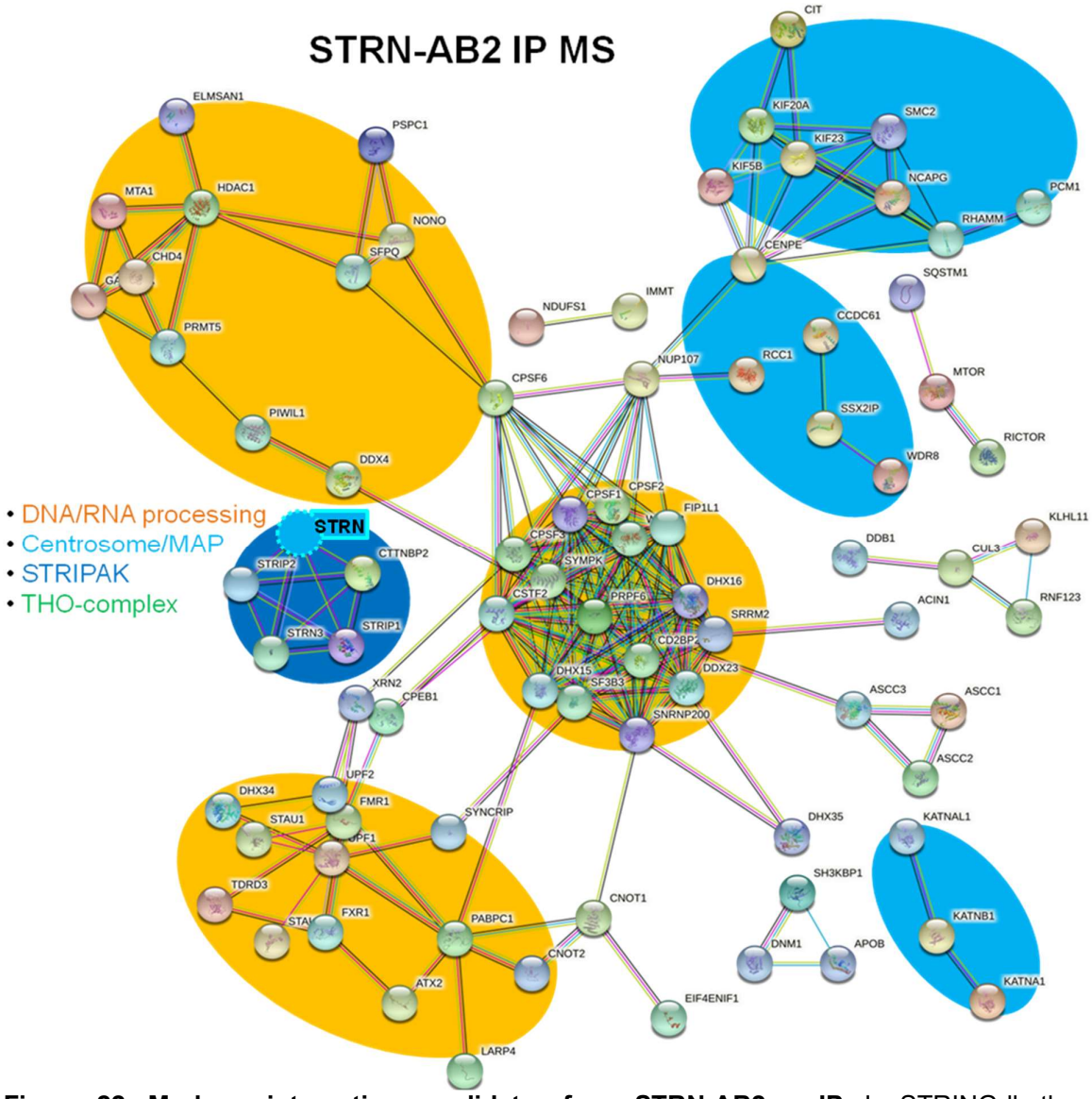

Figure 22: M-phase interaction candidates from STRN-AB2 co-IP. In STRINGdb the candidates can be analyzed regarding known interactions. The links between the nodes resemble different sources and evaluation strategies (text mining, experiments, databases, co-expression, neighborhood, gene fusion, co-occurrence). Disconnected nodes are removed in this view and the nodes only show the query input. The indicated molecular function is related to GO-term analysis.

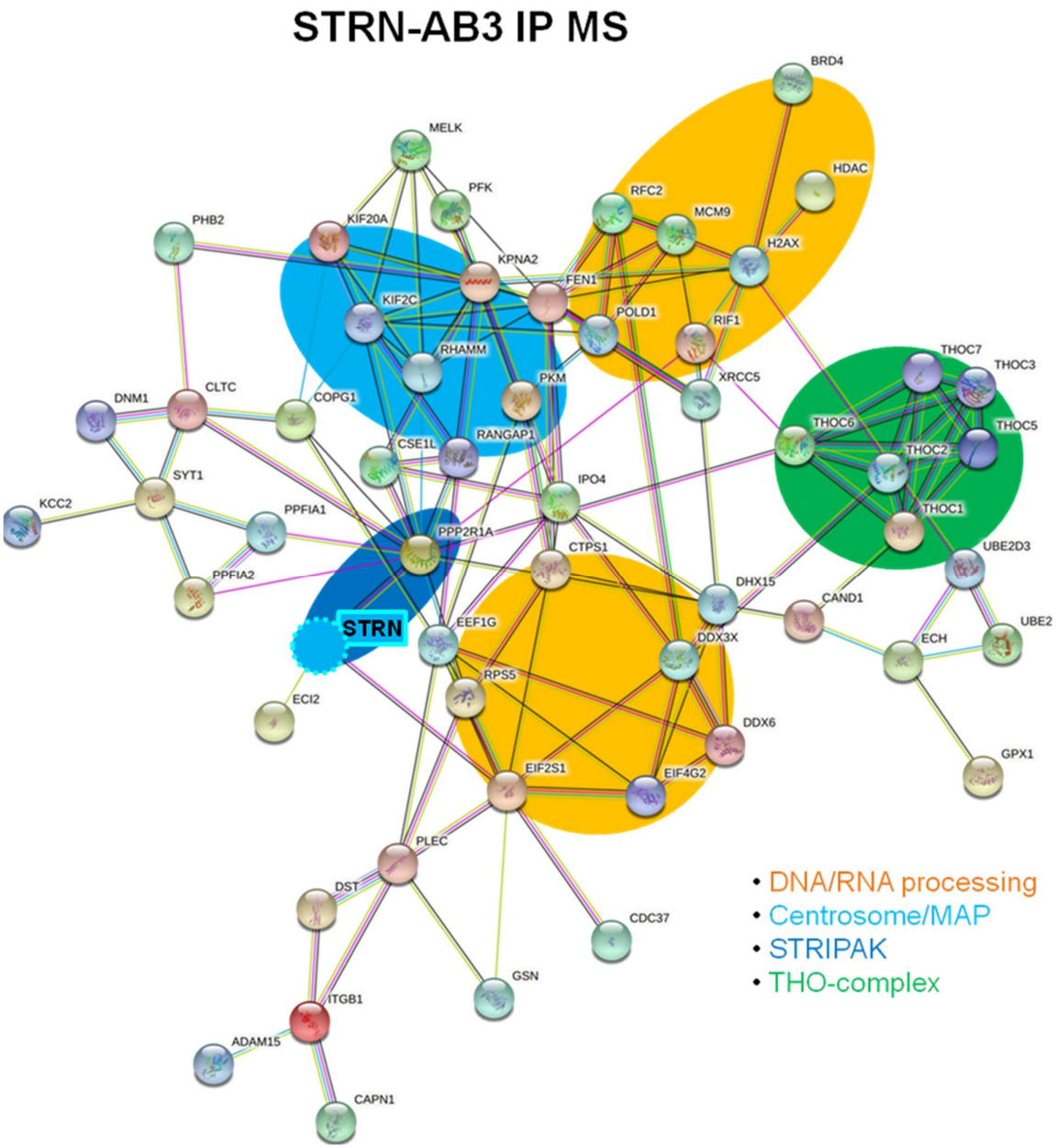

Figure 23: The M-phase interaction candidates from STRN-AB3 co-IP. The highlighted internal networks represent centrosome or MT associated proteins in blue, STRIPAK components in dark blue, mRNA/DNA processing proteins in orange and the THO complex in green.

Every candidate within the co-IP can be checked via different methodology and different model systems. I verify the depleted lysates and the purified anti-STRN pull down with antibodies which our lab has in stock (blot of fig. 24). These are CSPP1, XRHAMM and SSX2IP. The used antibodies are yielded using *Xenopus laevis* specific peptides.

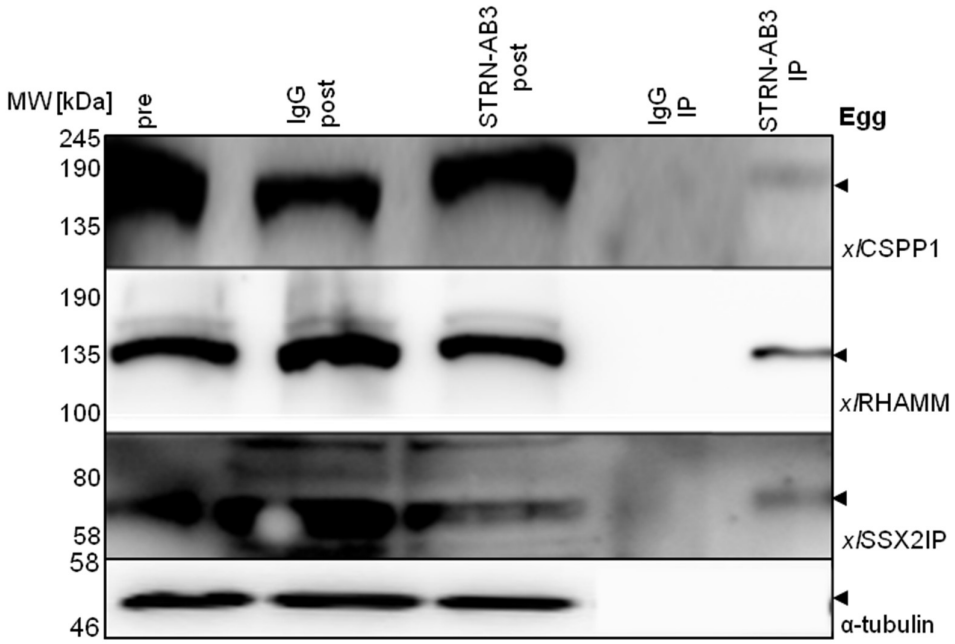

Figure 24: Western blot evidence of protein candidates that came together within MS co-IP result. The *Xenopus laevis* peptide-specific antibodies for Western blot detection are stocks from our lab. The blots are similar to previously shown STRN-antibody Western blots. The STRN-precipitation was performed with STRN-AB3. The MS findings give reason to perform blot analysis with the putative STRN-interactors shown here. The black arrows refer to the protein masses of 146 kDa for CSPP1, 137 kDa for XRHAMM, 65 kDa for SSX2IP.

The Western blot in figure 24 shows that none of the candidates can be reduced within the lysates by anti-STRN immunodepletion. The immunoprecipitation confirms CSPP1, XRHAMM and SSX2IP in the STRN-AB3 immunoprecipitates. This is interesting because CSPP1 and SSX2IP are listed within the STRN-AB2 MS result, but not in the STRN-AB3 result. This could be due to different antibody affinity between STRN-AB2 and STRN-AB3 or concentration issues.

Furthermore, I try to verify STRN-antibody co-IP with Western blot for GRP78, α-tubulin and PP2A subunit c. GRP78, an ER marker protein co-localized with STRN in human cell lines. No GRP78 can be found in the STRN-AB3 IP pull down. Previous analysis shows that tubulin co-IP is only possible with taxol hyperstabilized tubulin and co-sedimented MAPs (see blot in figure 14). A STRIPAK or PP2A complex-associated STRN protein would have been verified when the STRN-AB3 precipitate resulted in a signal with the anti-*xl*PP2Ac antibody. However, this antibody results in an obscure signal in Western blot and I only use it for immunofluorescence in human cell lines (figure 29).

One advantage in contrast to the cell free *Xenopus* embryonal system is the possibility to analyze the sub cellular localization using immunofluorescence staining. For highly specific antibodies that are directly coupled to a fluorescent dye (without a secondary antibody being necessary) and that bind with high affinity to distinct points/compartments (like the centrosome) an immunostaining is possible for the cell free extract. However, most antibodies lead to a cloudy signal in lysates since the cytosol is strongly mixed and organization is disrupted.

Each result so far should be treated carefully and double-checked, and is just a fraction of the true protein interaction framework. However, double checking should not be limited to one model system. Therefore, I characterize STRN in human embryonal fibroblast cell line IMR-90 aside from the *Xenopus laevis* cell free system.

○ 3.5 STRN localization phenotype in human cell lines

In order to clarify the conserved function of STRN I make use of an additional experimental system, *i. e*. the human cell culture model. Each of the antibodies used here for immunofluorescence staining has different epitope specificity. Alternatively molecular cloning and transfection is used to generate stable cell lines with tagged STRN variants. The STRN localization can be peeled out from all represented staining methods.

Figure 25 shows PFA fixed IMR-90 cells in interphase. Different antibody-based stainings of STRN and cells stably expressing STRN-EGFP are depicted. The IMR-90 wild type cells in figures 25 show conventional primary anti-STRN and secondary fluorescent dye coupled antibody labeling. In blue the DNA labeling of DAPI signal shows condensed DNA. The majority of immunofluorescence staining shows a disperse localization within the cytoplasm. An accumulated signal can be observed surrounding the nucleus while it fades out towards the cell periphery. In rare cases, like the STRN-TurboID anti-BirA staining, the tagged STRN shows nuclear and cytosolic staining.

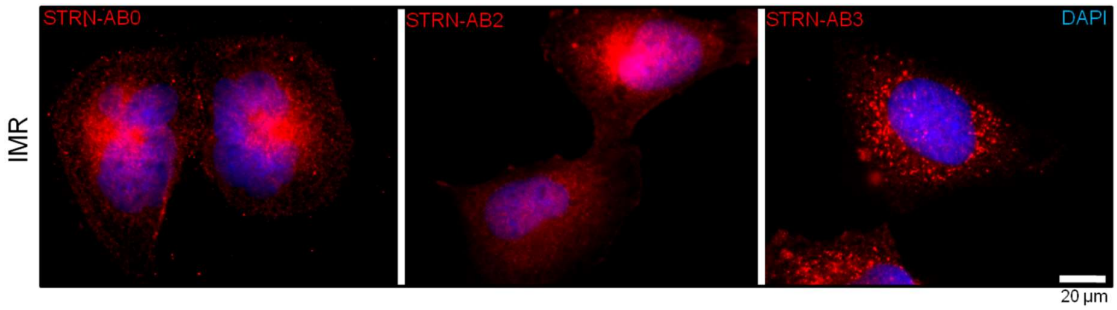

Figure 25: PFA-fixed IMR-90 cells stained with different STRN-antibodies. The immunofluorescence microscopy images show detection using STRN-AB0, *i. e.* the commercial anti-STRN antibody, and two newly generated STRN-antibodies, STRN-AB2 and STRN-AB3. The images show merged signals of the secondary antibody anti-rabbit Cy3 and DAPI. All show a dispersed signal within the cytosol with condensed particles surrounding the nucleus. The STRN signal does not cover the nucleus, and the red nuclear signal comes from out-of-focus cytosolic signal surrounding the nucleus.

In order to detect endogenous STRN, besides indirect immunofluorescence from figure 25, I make use of IMR-90 cells stably expressing STRN-EGFP. These cells give a robust, accurate signal without off-target effects (see figure 26, 27, 28). This can then be verified with anti-STRN antibody co-staining. A restaining with anti-GFP antibodies resulted in the same signal pattern as the live cell view of the GFP signal (yellow signal when aligned).

Figure 26 (interphase), 27 (early M-phase), and 28 (late M-phase) show consistent stainings during different cell cycle stages. Three different STRN-tagged stable cell lines (on top of endogenous STRN-standalone protein) are portrayed in figure 26. The BIOID-constructs have an additional bi-cistronic reporter signal (mKate2) which is used for the screening for positive clones. The reporter has no intrinsic known side effects and is independently translated from the BIOID fusion protein. Biotinylation assays are highly depending on kinetics. Substrate concentration, incubation temperature and incubation time are the screws which have to be optimized. Prior to immunofluorescence I perform a Western blot analysis (later seen in the blot of figure 40) in order to optimize the best biotinylation conditions.

For fluorescent staining I verify biotinylation/streptavidin signal saturation and no further incensement after 10 min of incubation with 150 µM biotin. This is true for MiniID, TurboID, STRN-TurboID and STRN-MiniID. The difference between the TurboID tagged STRN and the MiniID tagged one is that the STRN-Turbo cells show higher variability for a signal within the nucleus than the STRN-MiniID cells. The fading signal towards the cell periphery is not as visible in contrast to other stainings. Total STRN localizes in a higher concentration around the nucleus and decreases in a gradient like pattern towards the cell edges.

Methanol fixation results in a more punctual, dotted signal within the cytoplasm. Previous literature described STRN being cytosolic and membrane-bound, which is why the majority of stainings are performed with PFA fixation[319,335,336]. Cellular subfractionation in IMR-90 cells shows STRN in a membrane bound fraction. This can be verified and controlled by a digitonin based protocol and Western blot (not shown here)[337].

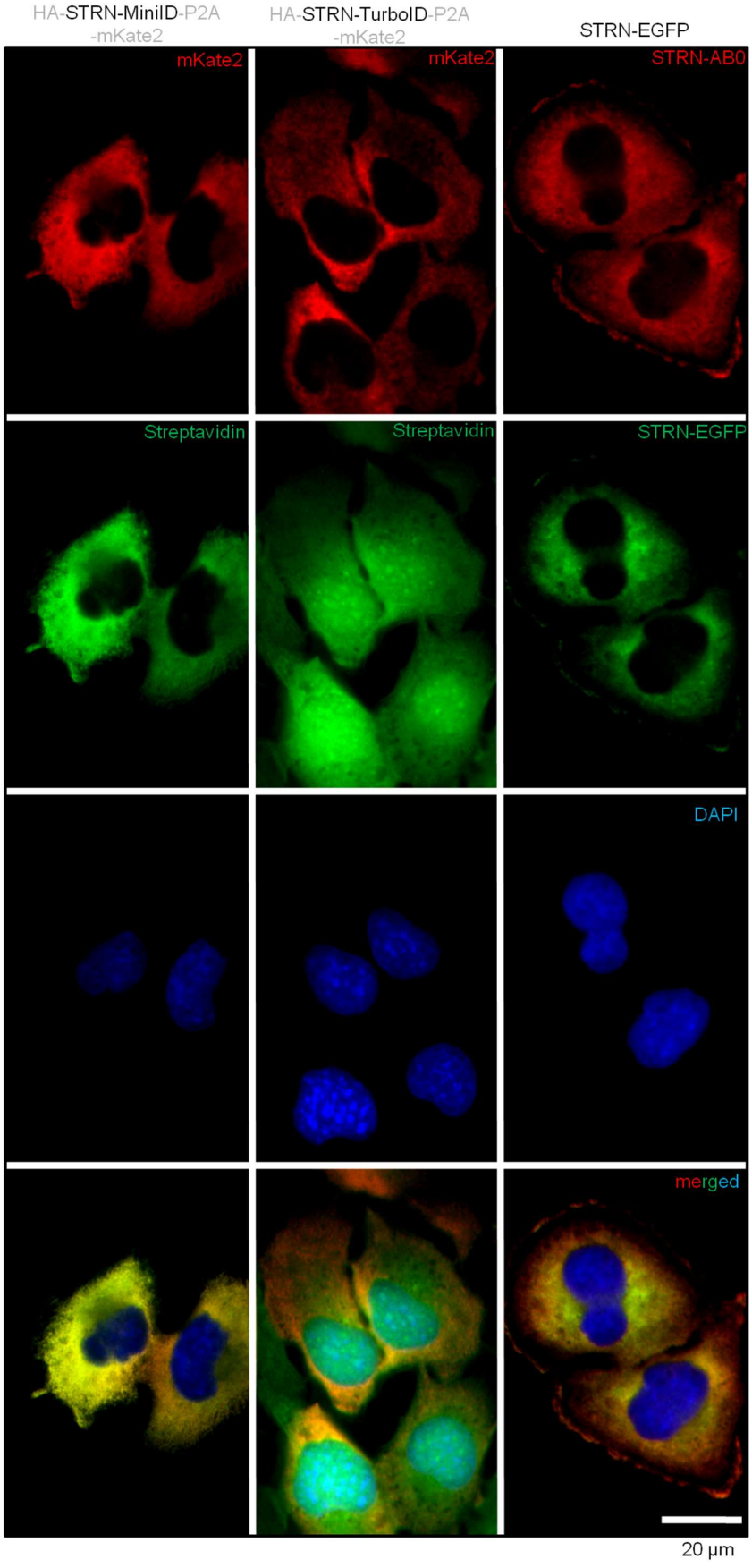
HA-STRN-MiniID-P2A
-mKate2
HA-STRN-TurboID-P2A
-mKate2
STRN-EGFP
mKate2
mKate2
STRN-AB0
Streptavidin
Streptavidin
STRN-EGFP
DAPI
merged
20 µm

Figure 26: IMR-90 cells stable expressing tagged STRN variants in interphase. The human embryonal lung fibroblasts are transfected and selected for stable expression of two BIOID constructs, STRN-MiniID and STRN-TurboID with bi-cistronic tag mKate2 as well as a STRN-EGFP fusion construct. All three cell lines show dispersed cytosolic STRN-specific signal. The STRN-TurboID cells additionally pinpoint STRN to the nucleus. This can be a specific effect of the fusion tag, since it is not reproduced with the other tagged variants.

In early M-phase (depictured in figure 27) I can observe accumulated signal at the spindle poles. This effect is only visible with the indirect STRN-antibody stainings, but not with the cell lines stably expressing tagged STRN variants.

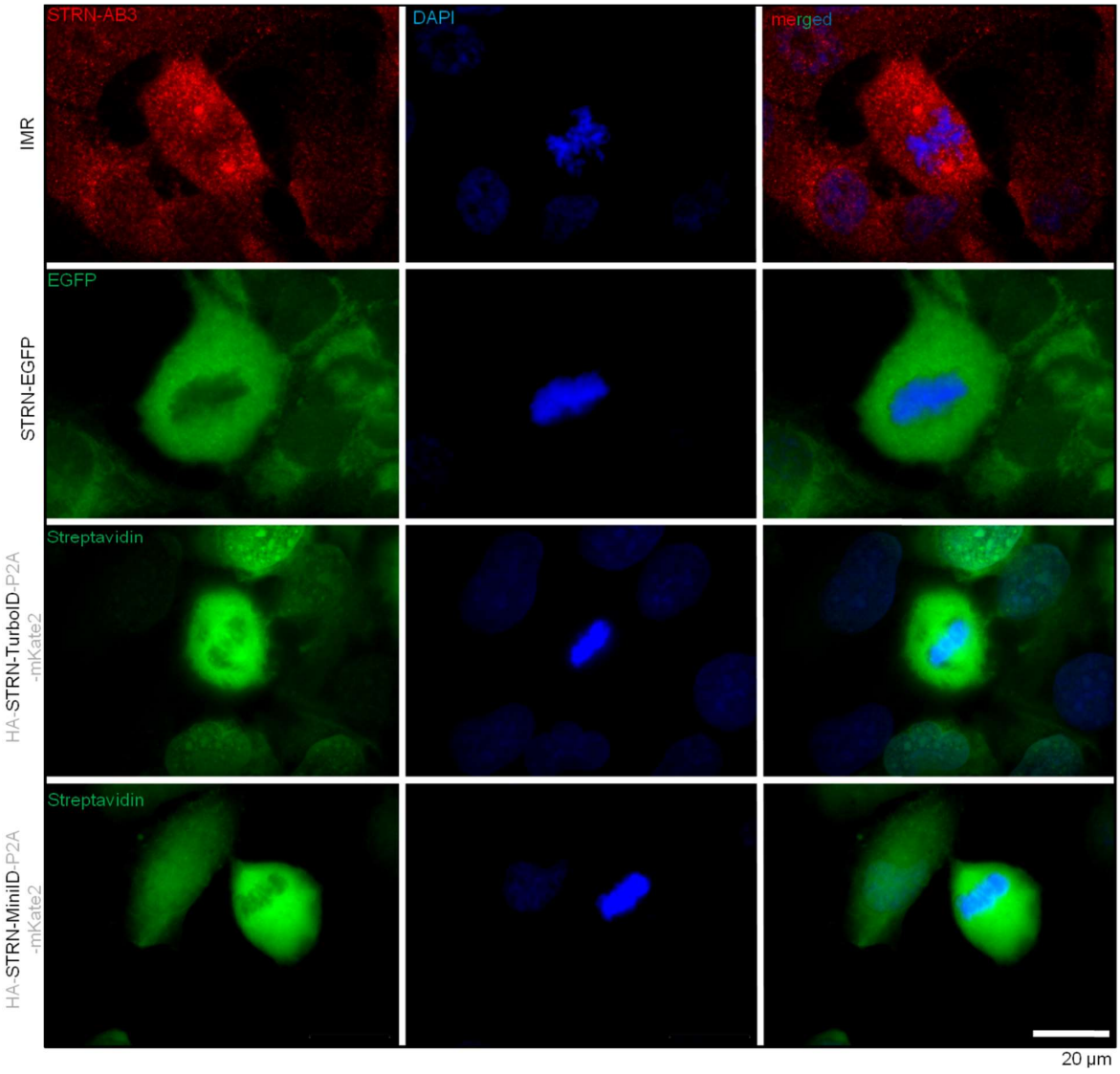

Figure 27: IMR-90 cells, wt, or stably expressing tagged STRN variants in early M-phase. As in interphase the STRN signal in M-phase is a blurry cell-filling signal. After NEB the only delimitation within the rounded mitotic cell is the signal displacement of the compact DNA signal. An exceptional observation comes up with antibody stainings: STRN-AB3 exhibits an accumulation around the spindle poles in metaphase. This signal can be found in the STRN KO and KD cells with this antibody (seen later in figure 33).

A dividing cell has no compartimenzation through a nuclear membrane, it rounds off and condeses cellular material to a smaller area. Therefore, the signal becomes less specific. The only signal-free gap is the condensed DNA. DNA is a macromolecular structure, that can displace cytosolic material in cells rounding up during division.

Both the monoclonal STRN-AB0 and polyclonal STRN-AB3 antibody reveal accumulated signal close to the centrosome. Later division steps (*i. e*. anaphase in figure 28) do not show pole-accumulation. This might suggest transient localisation at centrosomes. However, the bipolar signal also came up in siRNA STRN KD cells and in a stable biallelic IMR-90 STRN KO cell line (see figure 33).

This observation might indicate unspecific binding of the antibodies to centrosomes. During cell division STRN, ubiquitous localizes in the cell but excludes the chromatin. The BIOID constructs show a fiber like pattern along the spindle structure. Figure 27 displays this pattern during mitotic entry and figure 28 during mitotic exit.

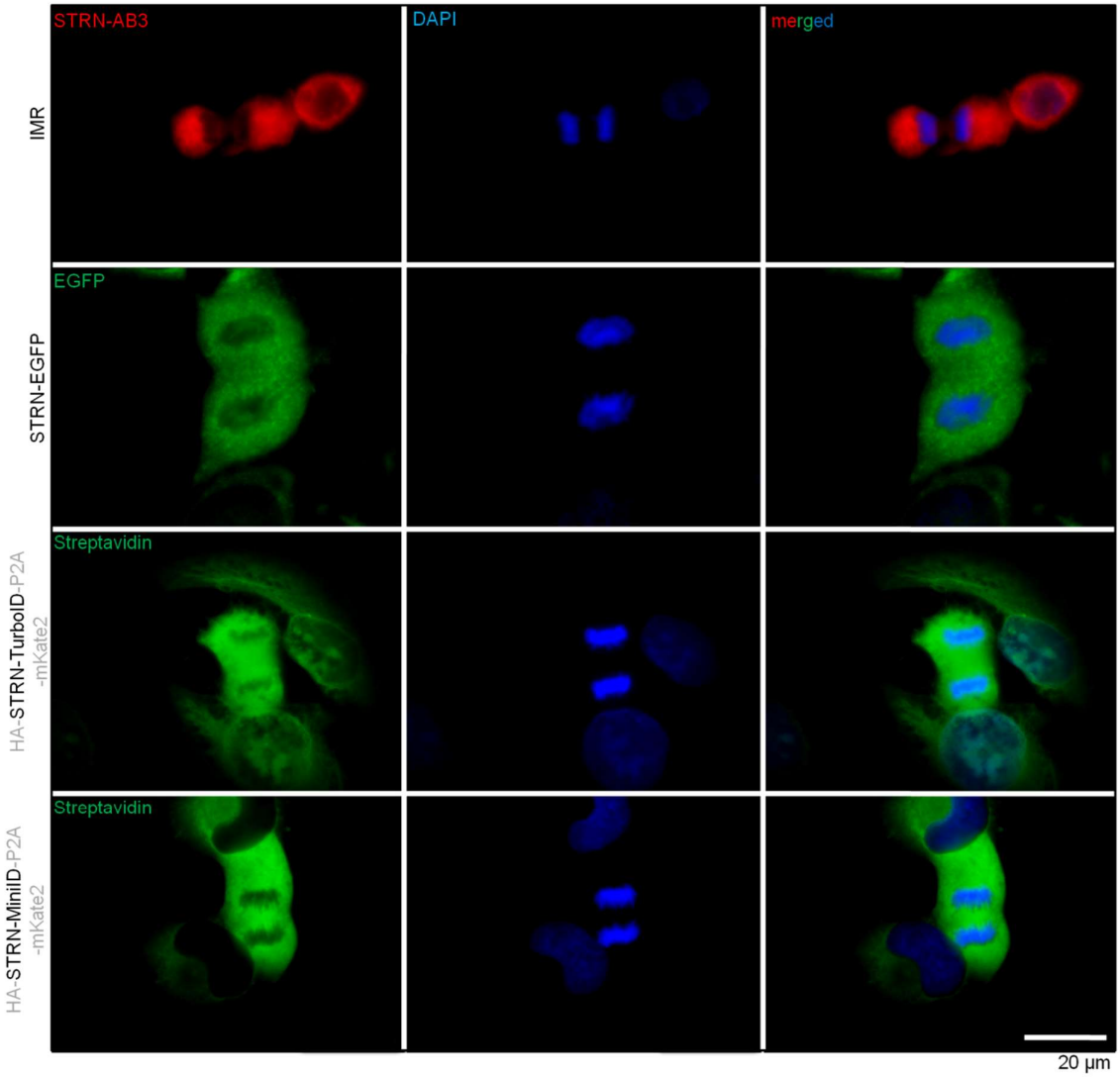

Figure 28: IMR-90 cells, wt, or stably expressing tagged STRN variants in late M-phase. Within these cell cycle stages all staining methods result in the same detection pattern: Similar to early mitotic steps, the rounded cell has an ubiquitous cell-filling signal without any accumulation dots. There is no visible differece between the individual cell lines during M-phase exit.

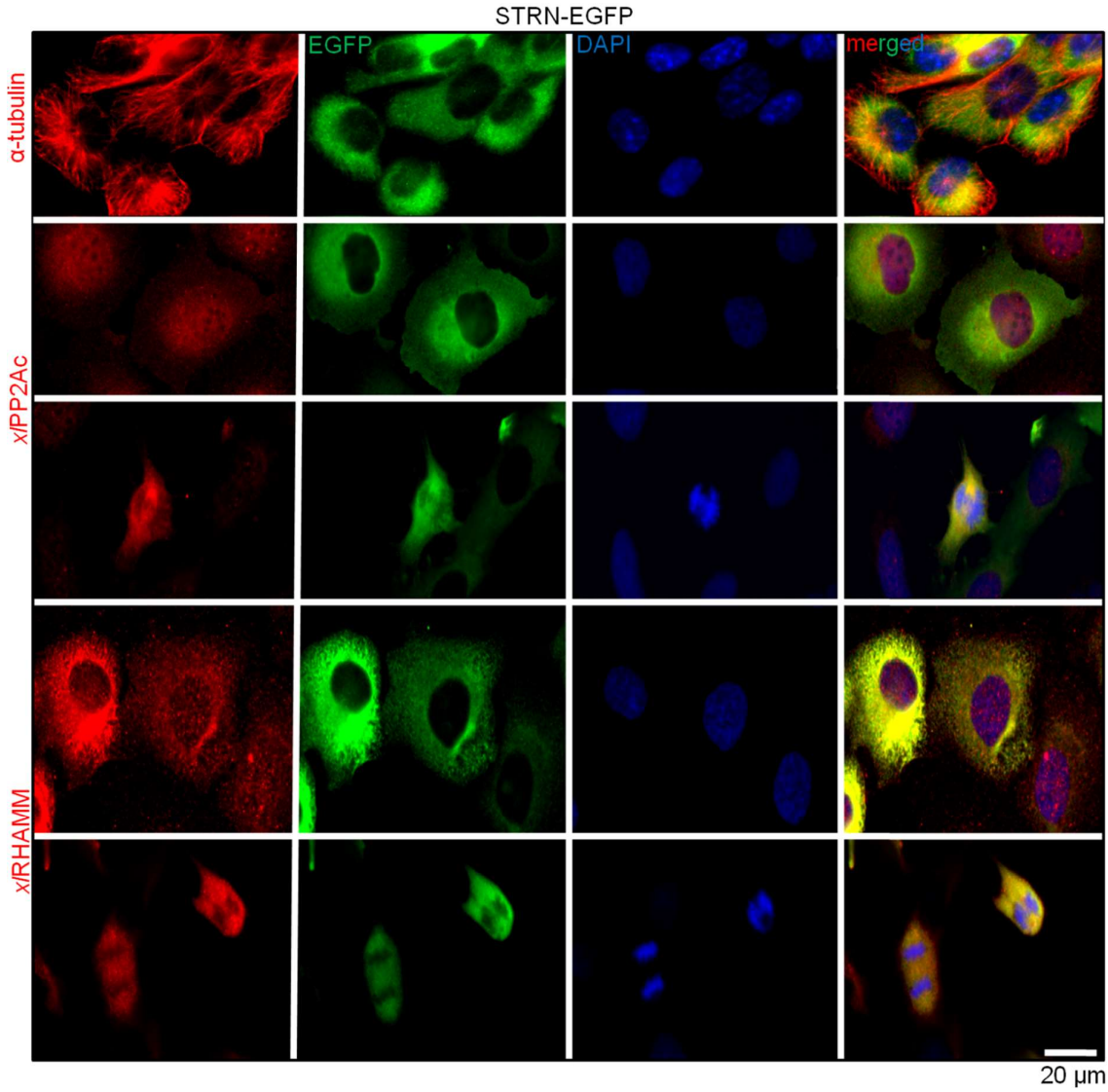

Figure 29: Different types of immunofluorescence co-stainings of STRN during interphase and mitosis. The anti-tubulin IF is the only MeOH fixed sample while all others are PFA fixed. Tubulin co-localization might suggest a MT modulating function of STRN. If STRN function is STRN-complex formation dependent is checked via an anti-*xl*PP2A catalytic subunit co-stain. Because of previous MS findings of the *Xenopus* embryonal system an anti-*xl*RHAMM costaining can be meaningful.

An anti-α-tubulin indirect immunofluorescence staining represents the cytoskeleton with fibers passing through the cytosol as a network that starts at the MTOC. The sample of figure 29 is a methanol fixed one, since tubulin and related MAP proteins usually result in clear fibre like structures under these conditions. A PFA fixed anti-α-tubulin co-staining with STRN-EGFP cells can be observed later (see figure37) . The co-staining of STRN does not show a similar structure or local accumulation. The anti-α-tubulin signal in mitosis resembles a defined bipolar spindle, while STRN remains ubiquitous distributed.

Except the tubulin staining, all co-stainings in figure 29 are performed on PFA fixed samples. Recent research shows STRN to play a role in focal adhesion or cell-cell connection (like HEK293T and HUH7 human cell line)[319]. I also check the co-staining with an anti-paxillin antibody (not shown here).

No co-localization can be verified in this case. Another not presented staining is performed with anti-GRP78. The protein GRP78 is a marker of the endoplasmic reticulum. In immunofluorescence the co-localization of STRN to ER marker GRP78 reflects a vesicle-organelle-like phenotype, which confirms STRN association to membranes. This fits to the result of cellular subfractionation in IMR-90 cells. The digitonin based protocol shows STRN in the membrane fraction when analysed by Western blot[337].

The last two stainings of figure 29 show STRN-EGFP co-stainings with anti-*X. laevis* RHAMM antibody. The protein RHAMM is a well known centrosomal protein that promotes integrity for the mitotic spindle[333,338]. A RHAMM-STRN interaction is not describedso far. The proteomic co-IP analysis with an anti-PP2A catalytic subunit antibody revealed an interaction to RHAMM (HMMR) in pancreatic β-cells. With a STRN-PP2A association, which is well known from literature, a STRN-RHAMM asscociation can make sense most likely, and thereby it supports the findings by Zhang *et al*. in 2016[339]. Both proteins are sensitive for phosphorylation. In my work RHAMM can be found in all proteomic results with the anti-STRN antibody co-IP of the *Xenopus laevis* extract. The NCBI alignment between human and frog RHAMM protein displayed 52% identity, 98% query coverage and an e-value of 10^{-58}. This relatively low identity value gives reasons to interpret the signal carefully. According to literature RHAMM co-localizes with MT during mitosis and represents a bipolar spindle structure[333]. The *xl*RHAMM antibody used here in human cells gives an idea of a spindle like structure but has a high background with accumulation in tubulin-rich parts.

The major anti-*xl*RHAMM signal resembles a random distribution within the cell, so a co-localization with STRN by chance is more likely. Cells in anaphase show a specific localization along the mitotic spindle to the spindle poles. The spindle-to-background/cytosol ratio is comparable to the STRN signal. The yellow spindle signal in the merged picture show a co-localization during anaphase.

The IFs I analyse here indicate a co-localization of STRN to GRP78, RHAMM and partially PP2Ac. The anti-CSPP1 and anti-SSX2IP antibody that worked with the *Xenopus laevis* egg extract Western blot co-IP from figure 24 resemble a centrosomal-specific punctual signal and no STRN-colocalization canbe verified. An alternative to untreated IMR-90 cells canbe provided by the stable STRN-EGFP IMR-90 cell line.

I performe an immunodepletion and immunoprecipitation with an anti-GFP antibody in clarified human cell lysates. In order to clarify STRN's interaction, I prepare a Western blot analysis of the immunoprecipitation with an anti-GFP from the IMR-90 STRN-EGFP cell lysates.

- **3.6 The concentration level of STRN controls the cell cycle**

The previously depicted immunofluorescence stainings show the phenotypes of each stable cell line during different stages of interphase and M-phase. The following plots of figure 30 and figure 31 show the statistical relationship, first between interphase and M-phase, and, second between the single M-phase stages (presented in figure 31). This analysis is performed under different conditions: Non-treated, nocodazol synchronized and reverted (MT disassably and following reassambly), Aurora A inhibitor MK5108 synchronized and reverted (M-phase entry lag and following M-phase exit), and last but not least Aurora A inhibitor synchronized, reverted and, additionally, MAD2 siRNA depleted (M-phase entry lag with unfunctional SAC criteria checkpoint) . The reason for the synchronization is to get a homogenous result and countable number of deviding cells.

This task is necessary for valid statistics. Graph A1 of figure 30 shows the different treated cell lines in interphase without addition of synchronizing supplements. The differece between non-treated IMR-90 wild type cells and stable STRN knock out cells is p = 0,000 and thereby highly significant.

This is also true for the same cell types regarding their behavior in cell division. This strong different behavior of IMR-90 wild type and STRN KO cells is not visible when the cells are synchronized under MT disrupting coditions and following reverted with reassambly (figure 30 B1 and B2). It becomes visible again during interphase and cell division under less toxic treatment and Aurora A inhibition synchronization and reverted (figure 30 C1 and C2).

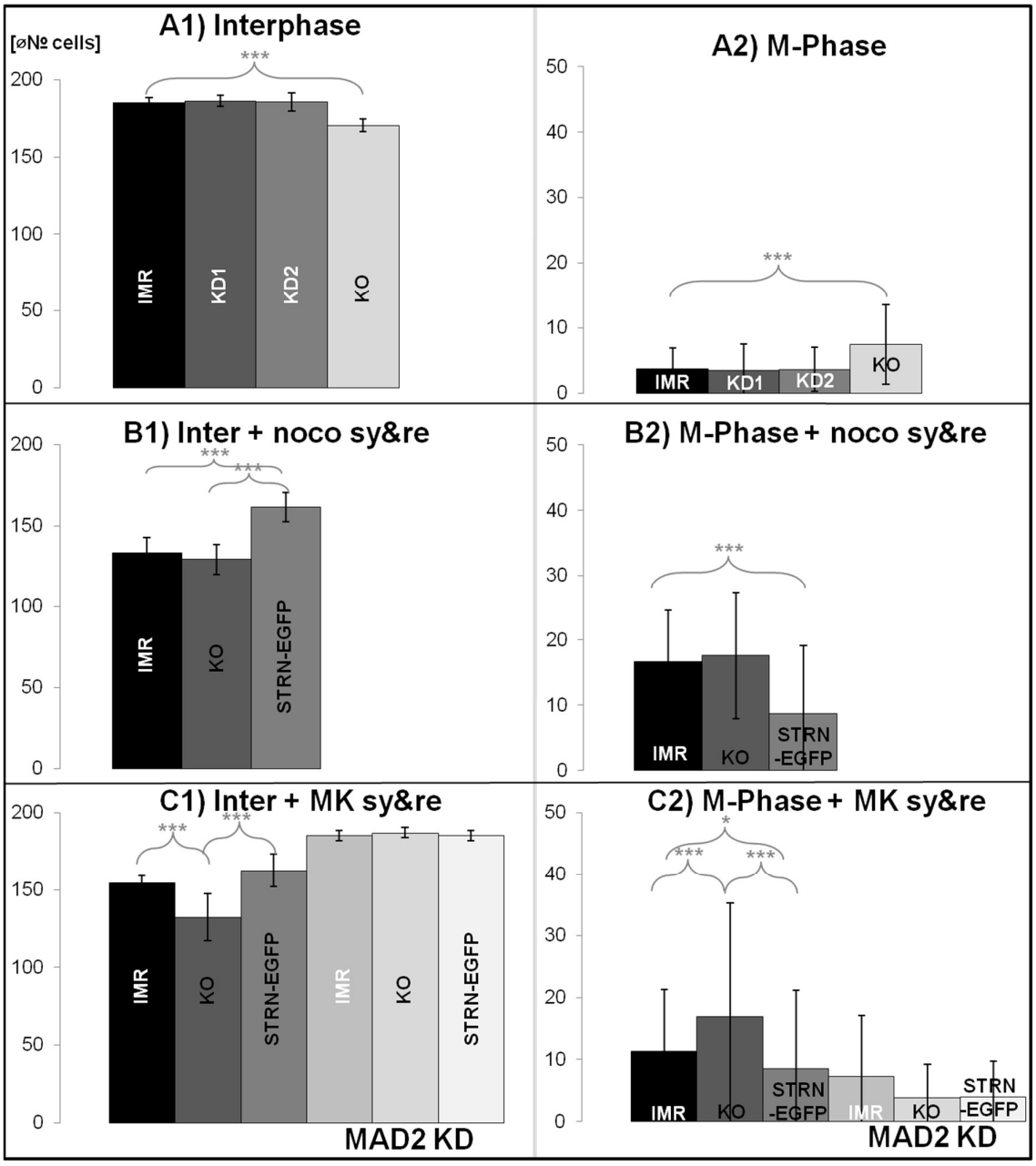

Figure 30: Plotting of Interphase to M-phase ratio of different IMR-90 cell lines. In this analysis the cell cycle stage of a total number of n = 2400 (12x 200) cells per condition is defined. Some conditions (KD and STRN-EGFP) are still pending for this experiment. The y-axis shows the averages from the different slides. In the first row without any chemical treatment, in the second row after 8 h of synchronization with 100 nM nocodazole[340], and, third, with 4 µM of Aurora A kinase inhibitor MK5108[341] (also known as VX-689) treatment for 24 h. In order to get a less toxin-affected phenotype and to trigger G_2-M-phase transition the chemicals are replaced with pure media for 80 min at 37 °C. In the case of Aurora A inhibition an extensive analysis was performed with a siRNA KD of spindle assembly checkpoint protein MAD2. The KD overcomes the checkpoint function, M-phase arrest is reverted, and the cells end up primarily in interphase.

The graphs shown in figure 30 give information about the different behaviors between the cells or cell lines used here. The fixed immunofluorescence observations show untreated stable cells in interphase in plot A1. In case of the KD cells there are still experiments pending to get a total number of n = 2400 cells (always within 3 independent experiments with 4 fixed slides = 12 slides with 200 cells each). The STRN deleted KO cells have a higher rate of division:

For example, during the Aurora inhibition IMR-90 wild type compared to STRN KO cells correspond to a difference of p = 0,001 in interphase and M-phase. On the other hand, there seems to be a shift to interphase for the STRN-EGFP cells: The IMR-90 wild type during MT disrupting conditions has significantly (p = 0,000) less cell division. If this is due to division being slower and cells are slowed down in M-phase, and thus interphase is relatively shorter, or if the cells are pushed to divide more often, is not clear.

It cannot be ruled out that STRN can also have functions in individual rate limiting steps such as like G_1 and G_2 checkpoint. The plots might give evidence of a cell cycle control function of STRN since a STRN oversupply has the opposite effect of a STRN deletion: This graph represents the data for chemically synchronized cells while untreated STRN-EGFP analysis is still pending. However, the current data is already conclusive.

The MK5108 treatment inhibits Aurora A and leads to synchronization in late G_2-phase. This synchronization turned out to be the most gentle and specific method for synchronization at entry into cell division. Therefore, on top of the MK5108 synchronization, I perfom a MAD2 KD with transiently transfected siRNA. During M-phase entry spindle checkpoint proteins MAD1 and MAD2 form a complex and are recruited to the outer kinetochore.

MAD2 binds to unattached kinetochores and induces mitotic arrest signal amplification. The complex of both catalyses the conformational change of a highly dynamic pool of target proteins. Only one unattached kinetochore is sufficient to generate a signal from the kinetochore to prevent anaphase onset. The checkpoint function is maintained, APC/C is not activated and no M-phase proteins are degraded[342,343]. The usage of MAD2 siRNA depletes the protein by silencing its mRNA.

Thereby the MAD1-MAD2 complex cannot form, the binding of MT +-end to the kinetochore is not reviewed correctly and metaphase-anaphase transition can proceed in a checkpoint-uncoupled way[344]. In order to get a statistical more evident answer about the M-phase behavior, the cells were synchronized with Aurora inhibitor after 2 days of transfection.

Consistently, I see that STRN KO lines increase the number of mitotic cells while showing fewer interphase cells. *Vice versa* STRN excess such as in IMR-90 STRN-EGFP cells increases the fraction of interphase cells and decreased cells in mitotic stages. In figure 30 C1 and C2 the last three columns show each stable cell lines (wildtype, STRN deletion and STRN oversupply) with MAD2 KD.

The columns show that removing SAC function also uncouples the dependency of the STRN-levels. All three conditions show more or less similar levels of interphase and M-phase after MAD2 depletion. This suggests a STRN dependend function in M-phase control the loss of which provokes M-phase delay due to non-satisfied SAC signalling.

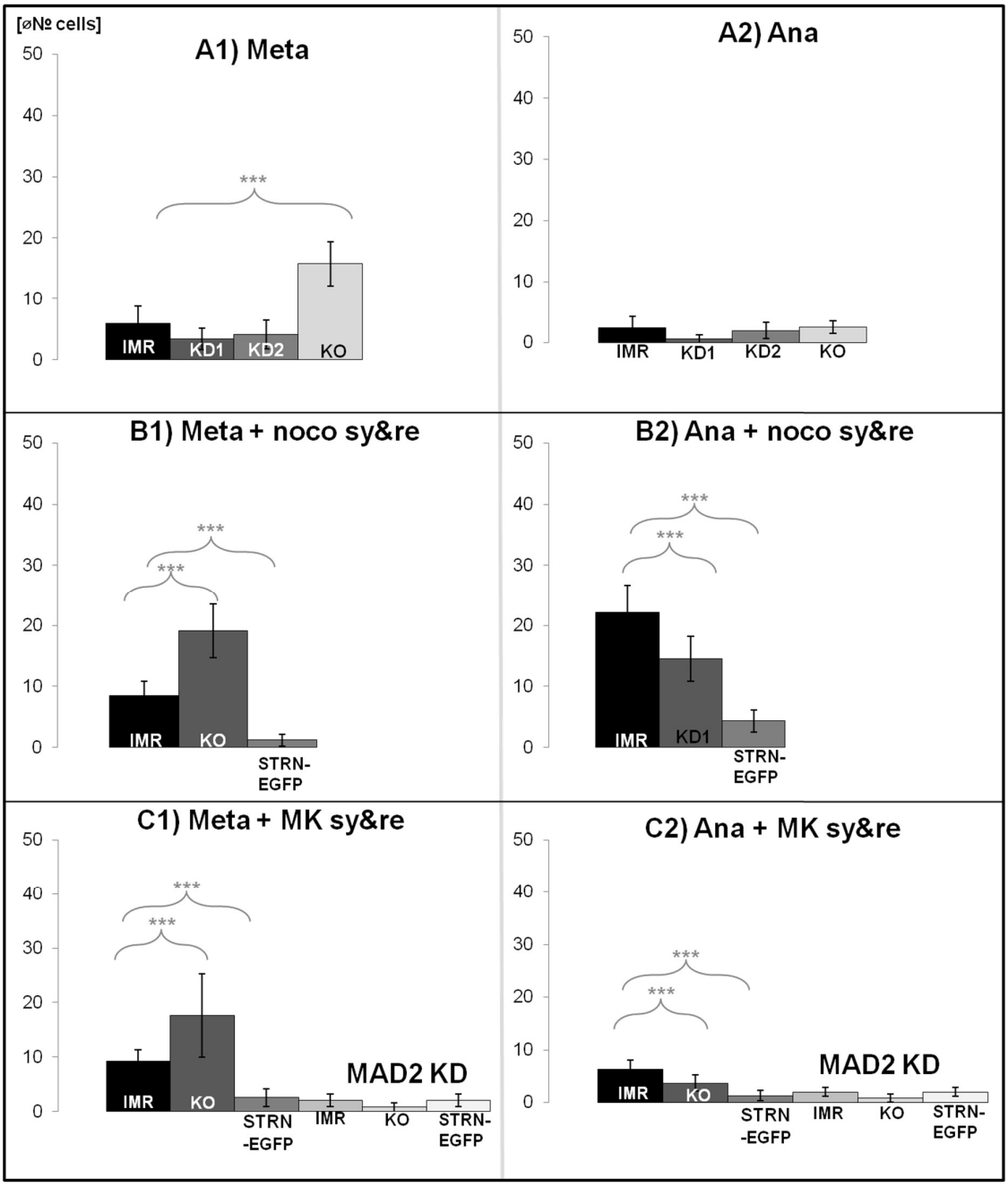

Figure 31: Graph of detailed M-phase ratios of different IMR-90 cell lines. The plots give insights of M-phase states from figure 30. Some conditions and cell treatments are still pending for this pilot experiment. For each condition the total number of counted cells was n = 2400 (12x 200). For statistics the different cell types are synchronized to M-phase with nocodazole (8 h 100 nM) and MK5108 (24 h 4 µM). The toxic effect is reduced by replacing the toxin-containing media with fresh media and releasing the stationary synchronized state for 80 min at 37 °C.

The plots in figure 31 show a more detailed view of the M-phase than in figure 30. In this analysis I focus on meta- and anaphase because observation of these phases is more frequent than prophase and telophase. The plots described here resemble mitosis entry with metaphase arrested cells and mitosis exit with anaphase-passing cells. The plots show a significant metaphase increase for the STRN KO cell line, the KO column under all different conditions (untreated, nocodazole synchronized *i. e*. MT disassembly and reverted for reassembly and MK5108 synchronized *i. e*. Aurora A inhibition and release for M-phase progression).

The metaphase-anaphase transition seems altered for STRN deficient cells, which is why higher M-phase ratios (like in figure 30) make sense. The cells cannot transcend the step to chromatid segregation but, once they overcome the delay, they go through anaphase normally. On the other hand, STRN-EGFP shows both, less meta- and less anaphase ratios. The whole M-phase seems accelerated for cells with endogenous STRN and CMV-overexpressed STRN-EGFP on top.

Regarding previous analysis with M-phase *Xenopus* embryonal extract from figure 17 and 18 (spindle forming potential in STRN-IP depleted extract), this result in human IMR-90 cells fits because I see in both cases higher metaphase stability during STRN shortage.

So which role could STRN play for cell cycle kinetics? The STRN protein is a putative PP2A regulating subunit of the PPase complex. The phosphatase PP2A is known as master regulator of the cell cycle. The protein catalyzeses dephosphorylations specific in time and space on a broad range of substrates. The anti-*xl*PP2Ac antibody used here is a mixed serum against the catalytic subunit of *Xenopus laevis* PP2A. A protein alignment of human and frog ‘PP2A catalytic subunit α’ with NCBIs blastp shows a 99% identity, 100% query coverage and an e-value of 0. Nonspecific background signal with the anti-*xl*PP2Ac antibody should be due to the underrepresented different antibodies within the serum mixture and can be neglected.

The co-staining in interphase reveals cytosolic distribution for PP2A and STRN. Additionaly, PP2A shows a blurry signal within the nucleus. Both proteins show disperse nucleus-surrounding accumulation in interphase. This ring-like structure around the nucleus suggests a co-localization of STRN and PP2Ac. A disperse signal always comes with the probablity of a co-localization by chance. The blot signal of the PP2Ac antibody results in no clear answer in the anti-STRN co-IP either.

The PP2A co-staining in M-phase shown here corresponds to a prometaphase stage. The cell is not completely rounded and the DNA is not fully aligned to the metaphase plate. Both the PP2Ac and the STRN signal seem co-aligned and the pattern gives reason to suspect a spindle structure. This apparent behaviour can also occur due to the exclusion from the space consuming condensed chromosomes.

The Western blot (figure 32) shows a depletion with anti-GFP antibody in STRN-EGFP stable cells. Prior to the experiment the cells are treated with two different chemicals: First thymidine, a pyrimidine deoxynucleoside, which blocks DNA replication during S-phase. And second with MK5108 an Aurora A inhibitor that prevents the cell from M-phase entry. When the cells are synchronized the cell lysate shows a reduced STRN-EGFP signal on Western blot. The endogenous STRN level is not affaceted after anti-GFP IP (anti-STRN blot was performed subsequently in an experiment apart from the here presented blots).

Interestingly, I am able to verify a reduction of the SSX2IP signal within the lysate. The co-IP showed both STRN-EGFP and SSX2IP pull down from interphase arrested (thymidine treated) and mitotically arrested (Aurora A inhibitor MK5108 treated) cells. I can detect a more than 20 kDa mass shift for STRN-EGFP and the SSXIP pull down. This observation of the IP fractions might be treated carefully.

The Western blot is performed under denaturing conditions (SDS) and no complex or protein oligomerization is left. One possible reason of a mass shift can be PTMs or covalent protein bindings, pH differences or salt concentrations of the loaded samples. The signal in both blots from anti-GFP and anti-SSX2IP show similar migration and shift behaviour, which is why the difference of salt concentration in lysate and IP might be most likely.

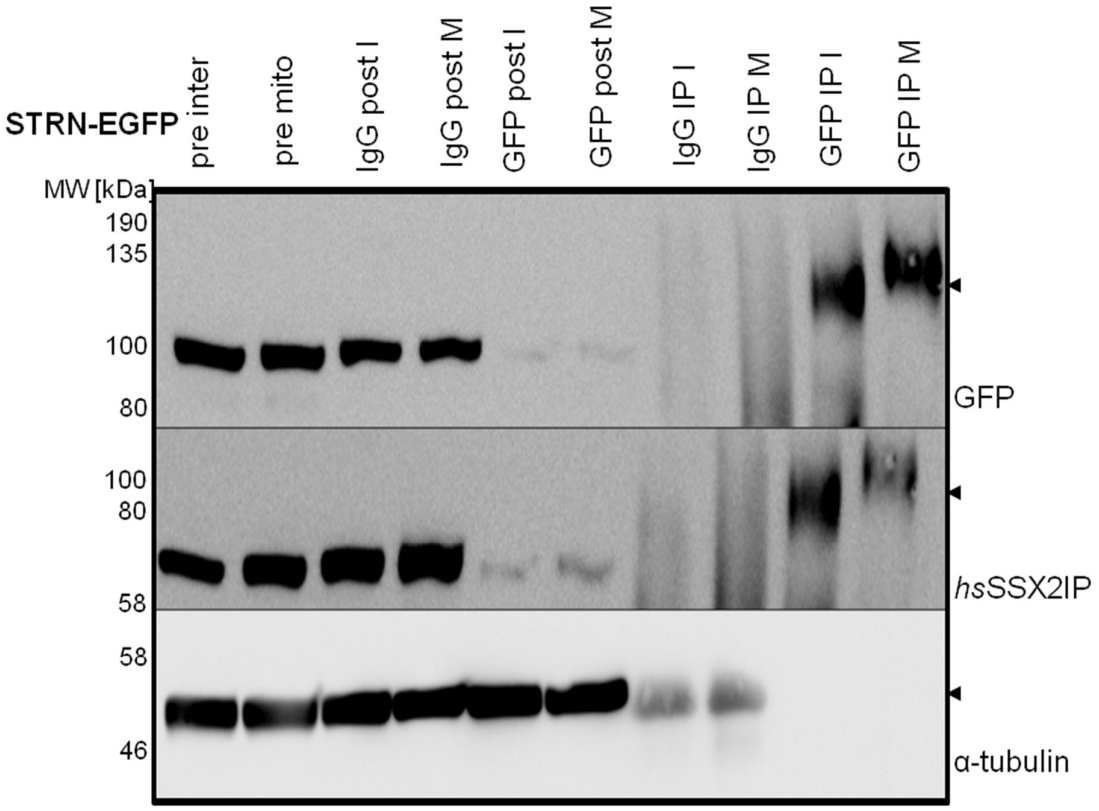

Figure 32: Anti-GFP immunoprecipitation Western blot of the IMR-90 STRN-EGFP stable cells. The anti-GFP are coupled to Dynabeads and mixed with the cell lysate. Anti-GFP binds to the STRN-EGFP tag and everything what is interacting with STRN-EGFP in the RIPA lysates. The GFP antibody pull down contains the centrosomal protein SSX2IP. A mass shift of STRN (anti-STRN blot not presented here), STRN-EGFP (GFP) and SSX2IP can be verified in the co-IP fractions. The analysis is performed in synchronized interphase (thymidine treatment) and synchronized mitosis (MK5108 treatment). A difference between both becomes visible in the purified immunoprecipitates.

The same experiment can be done with an anti-STRN, anti-RHAMM and the pending CSPP1 antibody. The Western blot for both results in a questionable disperse signal in human lysate in contrast to the samples from cell free frog egg extract.

All STRN specific antibodies used here are also tested for immunofluorescence of STRN KD and KO. Unexpectedly, the total signal is not reduced for both KD and KO. This can mean high background recognition of the antibody and that this is not a suitable method to verify STRN reduction via IF. Figure 33 shows that STRN-AB3 exhibits more spindle pole oriented signal during mitosis as STRN-AB0. This pole accumulation remains in KD and KO.

Staining artifacts cannot be excluded and make antibody signals more questionable, while stable STRN-EGFP signal is the more reliable method for STRN localization. The two STRN antibodies STRN-AB0 and STRN-AB3 produce a dot like signal at the mitotic poles. This might indicate a centrosomal localization with these antibodies even without STRN being expressed. The blot indicates that STRN is reduced or gone in these samples so an unspecific centrosomal recognition by the anti-STRN antibody is more likely.

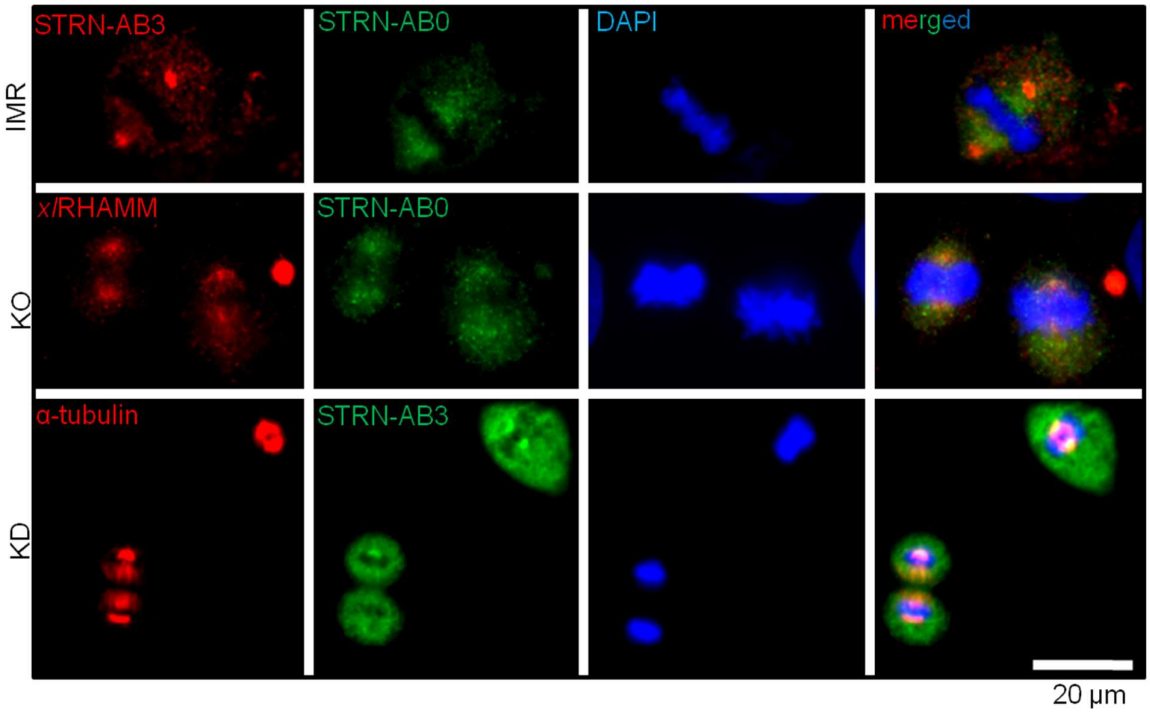

Figure 33: STRN antibodies show a centrosomal signal in mitosis even in the KO and KD situations. Both the commercial monoclonal anti-STRN antibody of STRN-AB0 and the polyclonal purified STRN-AB3 antibody produce a centrosomally accumulated signal at the spindle poles in IMR-90 cells. This signal is stronger for the STRN-AB3. When this is a specific STRN localization, the signal should be gone in the KO and KD staining.

So how to verify if the STRN KO has a MT related effect? This can be done by manipulation of the tubulin within the different cell lines used here. The blot in figure 34 A shows no altered STRN expression levels with the different treatment and synchronization methods. The blot adds evidence that MT stabilizing and disrupting conditions do not have an effect onto STRN expression levels for endogenous STRN and for stable STRN-EGFP.

The anti-MPM2 blot of figure 34 B gives a hint to the mitosis specific phosphorylation as it shows decreased phosphorylation in the STRN oversupply cell line of STRN-EGF. The monoclonal MPM2 antibody binds to a phospho amino acid-containing epitope (LTPLK and FTPLQ motifs) present on more than 50 proteins of M-phase eukaryotic cells. Prominent signals of MPM2 include MAP2 (*H. sapiens* 200 kDa), HSP70 (*H. sapiens* 70 kDa), CDC25 (*H. sapiens* CDC25A 55 kDa) and DNA topoisomerase IIα (*H. sapiens* TOPO2A 174 kDa).

The blot gives reason to assume that normal STRN expression and STRN shortage have no effect on the M-phase specific phosphorylation pattern according to the MPM2 blot signal. This changes under STRN oversupply conditions of endogenous STRN together with CMV-promoter overrepresented STRN-EGFP. The (here not presented) MPM2 blot suggests that the specific phosphorylation of the LTPLK and FTPLQ epitope does not take place, or the target proteins are not even translated in a normal level.

- **3.7 Different cell treatment has effects onto the MT kinetics of STRN stable IMR-90 cells**

As a potential MT modulator STRN can be manipulated via pharmacologically active substances affecting MTs such as the MT depolymerizing nocodazole or the MT hyperstabilizing taxol (figure 34 A). In contrast to nocodazole, a less toxic and more selective M-phase synchronization can be done with the Aurora A inhibitor MK5108[341]. Nocodazole is a high affinity ligand, which not only binds to β-tubulin, but also kinases, like ABL, c-KIT, BRAF, and MEK[340]. In contrast, MK5108 is a highly selective Aurora A kinase inhibitor. The protein levels of this serine/threonine kinase increase during M-phase. Native Aurora A associates with the mitotic spindle poles and the adjacent spindle microtubules.

One Aurora A phosphorylation target for MT modulation already mentioned here is TPX2[273]. Both nocodazole and MK5108 stop the cell cycle during late G_2/M-phase entry. A comparison between both M-phase synchronizing chemicals with the IMR-90 wildtype, STRN deficiency (KO) and STRN oversupply (STRN-EGFP) is depicted in figure 34 B. All STRN-AB0 blot signals so far, including figure 36 A) are evaluated by ImageJ integrals. In order to get an idea, the plot in figure 36 B) serves as pilot result, gives a trend for interpretation and shows the summarized resulting peaks of the STRN-AB0 antibody blot signal.

The anti-tubulin loading control suggests a different loading amount in this case and therefore this observation might be checked by repeating this experiment (furthermore to get a solid statistics). I load similar amounts of cellular material on each lane so a compensatory effect of the STRN KO might indicate a higher expression rates of tubulin. IMR-90 wildtype cells with endogenous STRN levels and STRN overexpressing STRN-EGFP cells do not show any altered expression pattern in Western blot after addition of these chemicals, or after cold treatment to depolymerize MT (figure 34 A and 35 A).

In this case I expose the cells to 4 °C for 1 h of incubation time. Low temperatures promote tubulin depolymerization *in vitro* and *in vivo*[345,346]. This depolymerization is reversible. In figure 35 A) I plot the differences in MT regrowth between the individual stable IMR cells. The cold-treated cells are placed onto a 37 °C plate for 4 min and are directly MeOH fixed. This pilot experiment's data is based on immunofluorescence stainings of MTs. The distance between the reforming MTOC and the longest tubulin fiber is measured. This result is directly linked to MT nucleation and growth rate. Plot A from figure 35 suggests a significantly slower MT regrowth after cold treatment for the STRN KO cells.

The IMR-90 cells compared to the STRN KO cells reach a difference of p = 0,015 and the STRN-EGFP cells compared to the STRN KO cells result in a significance of p = 0,000.

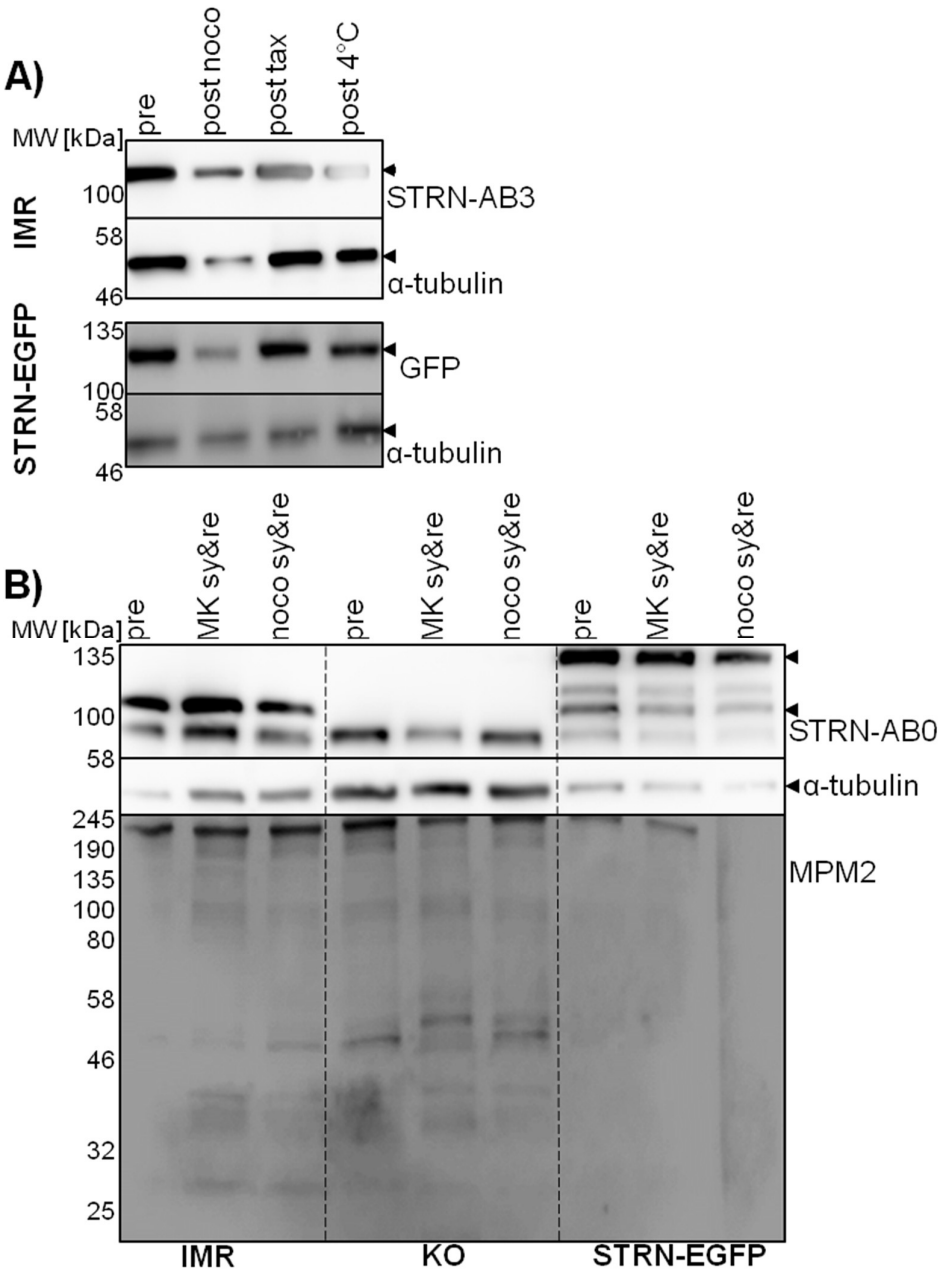

Figure 34: IMR-90 cells upon different treatment with MT (de)stabilizing conditions. The Western blot in A) shows the levels of STRN do not change under treatment of MT affecting factors like chemicals and temperature. The treatment with taxol hyperstabilize the MT polymers. Nocodazole and low temperature depolymerize the MT polymers. In blot B) the different STRN stable cells are shown with different synchronization chemicals. The label &re means additional 3 h of treatment without the chemical to recover from toxic treatment. The varying tubulin and MPM2 signals between different cell line experiments give reason to repeat this pilot experiment.

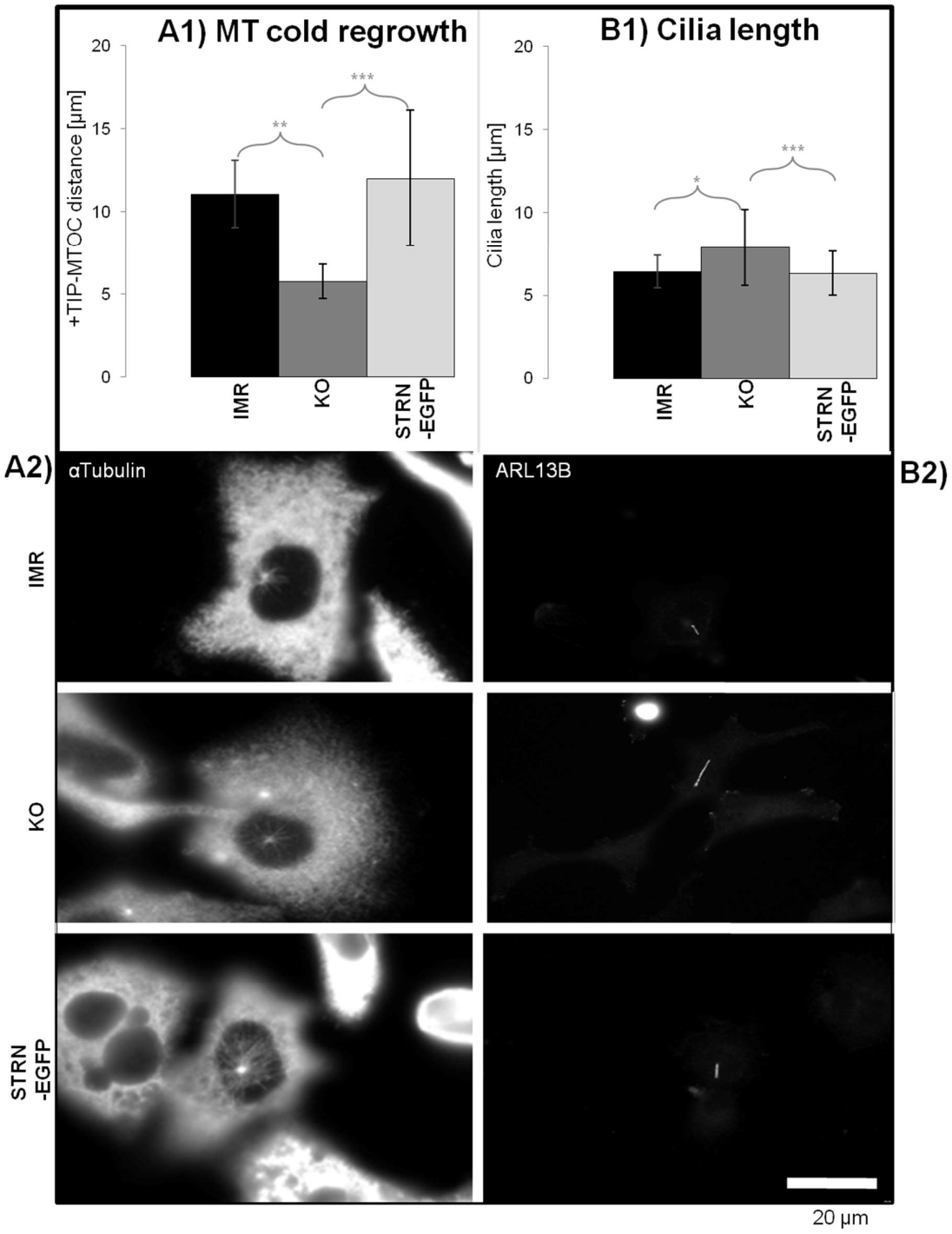

Figure 35: MT regrowth after depolymerization and ciliogenesis under starvation conditions. The plots shown here describe different kinetics of MT polymerization within n = 2400 cells. Plot A) regrowth after cold treatment (1 h 2 °C MT depolymerization and 4 min 37 °C repolymerization). Plot B) shows the different cell lines after 72 h of serum-free cultivation. In both cases MT lengths were measured: In A1) the length between the MTOC and the three longest MT fibers (A2 shows the corresponding anti-α-tubulin staining). In B1) the length of the axonemal MTs in cilia (B2 shows the corresponding anti-ARL13B cilia marker staining).

As a second method for investigating STRN-dependent function or disorders in MT dynamics, I also have a look onto ciliogenesis. Serum starvation of many human cell lines can drive the cells to cell cycle arrest in G_0. The formation of primary cilia plays a role for the transition from G_0/G_1 to S phase[347].

A starvation experiment of 72 h is depictured in figure 35 B). Discrepancies in cilia duplication, positioning or length can lead to errors in extracellular signal sensing or responses to mechanical forces. The ciliary signal is detected with a specific cilia marker protein (ARL13B). The plot shows disturbed ciliogenesis for the STRN KO cell line. The cilia are significantly longer when IMR-90 cells are compared to STRN KO cells p = 0,023. The STRN KO compared to STRN-EGFP cells results in an even higher significant difference of p = 0,000.

Defects in ciliogenesis can lead to ciliopathies. Multiple ciliopathies are linked to altered cilia length. This includes retinitis pigmentosa, renal cystic disease, polydactyly, *situs inversus*, mental retardation, hypoplasia of *corpus callosum*, dandy-walker malformation, posterior encephalocoele, and hepatic disease[348].

- **3.8 Osmotic stress results in a different STRN phenotype**

Recent research found proteins that form numerous foci within the cytosol in close correlation with osmotic stress[349]. The particles appear and disappear depending on the cell volume. Conditions like a salt shock forces the cell to shrink and proteins become tightly packed. Highly complex networks form condensates in the surrounding cytosol or nucleus [350]. Supramolecular complexes have a high potential to phase separate. I suspect STRN to play a role as a platform for supramolecular complexes. If this is the case can be analyzed with the here presented osmotic assays. First, I want to check if the morphology and phenotype of the STRN immunofluorescence change under osmotic stress.

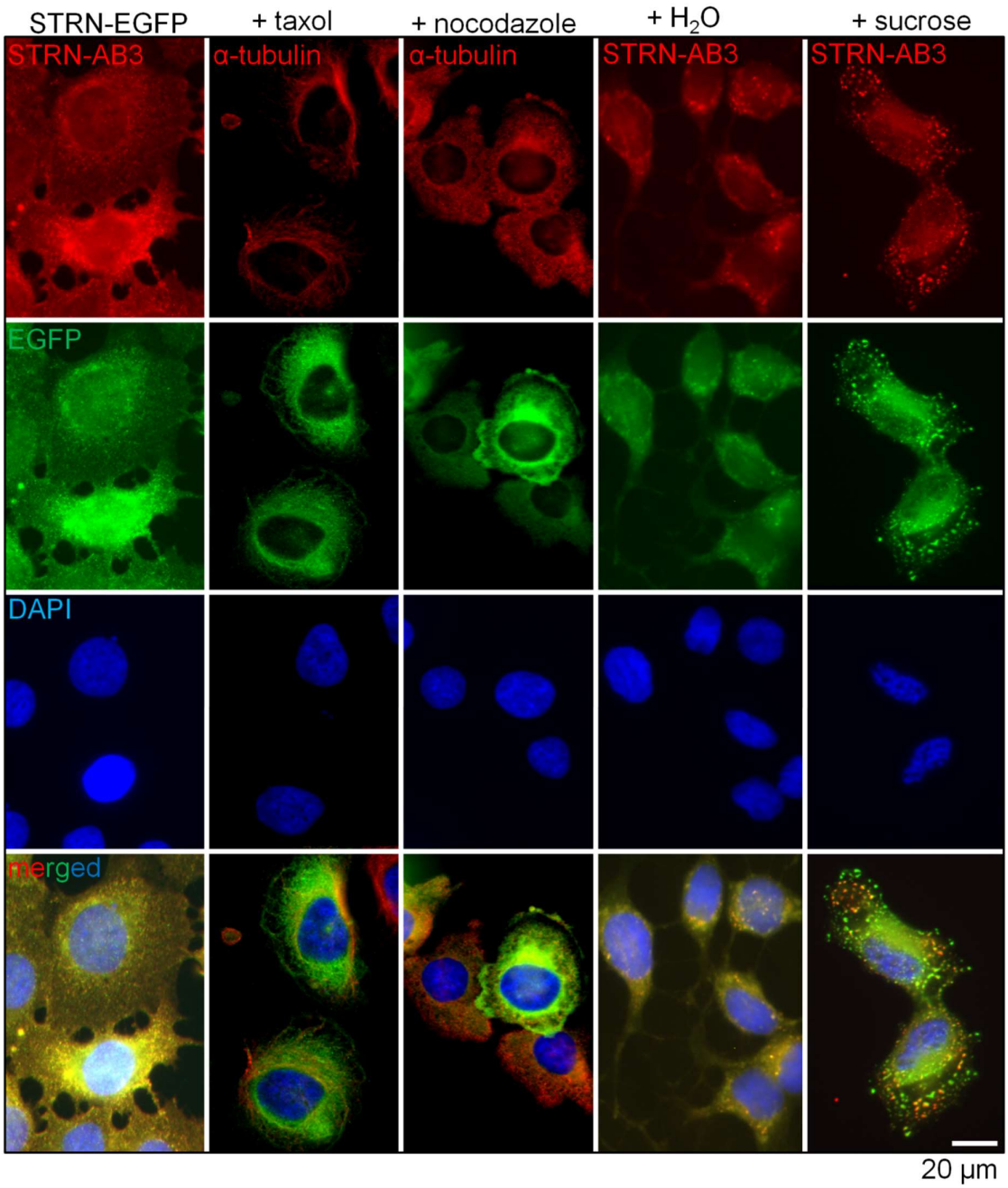

Figure 36: Subcellular localization of STRN-EGFP under different cellular conditions. All pictures show IMR-90 STRN-EGFP stable cells. First untreated, second with taxol, third with nocodazole (both 3 h, 3 µM), fourth with hypoosmotic H_2O dilution (3 h 50%), fifth supplemented with hyperosmotic sucrose (3 h 400 mM). A possible explanation for this phenotype might be sucrose induced liquid-liquid phase separation and thereby formation of condensates that have a certain size (from 200 nm – 2 µm) and are mainly localized in the cellular periphery.

In figure 36 I present stable STRN-EGFP cells with different co-stainings and chemical treatments. While the hypoosmotic H_2O treatment generates a more diffuse less accumulated STRN signal, the hyperosmotic sucrose sample has the opposite effect: It has the highest impact onto the STRN signal and exhibits a dotted granule-like accumulation. One explanation for this can be liquid-liquid phase separation. This can mean formation of STRN-EGFP condensates by exposition to hyperosmotic stress. The red channel shows re-staining with the STRN-AB3 antibody, and the green channel the EGFP signal directly.

The yellow signal reflects a perfect match between the STRN antibody signal and the GFP antibody signal. In hypo- and hyperosmotic treatment the cellular volume reduces by 50% and the cells tended to detach during the treatment. A slight signal shift between anti-STRN and STRN-EGFP can be observed in the 400 mM sucrose treated cells. This might imply a different cellular translocalization of endogenous STRN and STRN-EGFP. Both in the hypoosmotic and the hyperosmotic condition the samples; fully recover when this treatment is reverted. Taxol and nocodazole treated samples maintain MT defects after release over the following generations.

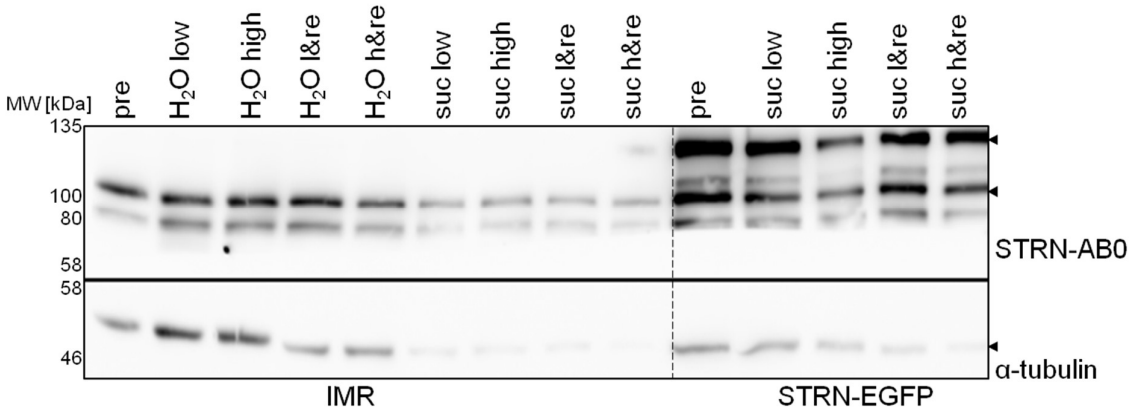

Figure 37: The STRN expression pattern under osmotic stress. The left blot shows the effect in IMR-90 wild type cells and the right blot in STRN-EGFP cells. All samples shown here result from a 10 cm culture dish with 80% confluence. The cells are incubated for 3 h. Pre is equivalent to untreated condition, H_2O low is a 25% dilution, H_2O high a 50% dilution, sucrose low is equivalent to 200 mM, sucrose high is equivalent to 400 mM sucrose, and the &re samples have additional 3 h incubation under normal conditions.

The blot in figure 37 verifies that hypoosmotic stress does not have any effect onto the IMR-90 wild type expression pattern. The loading control of the endogenous STRN shows a reduced cell concentration under sucrose treatment. This reduced Western

blot signal is not visible in the STRN overexpressing STRN-EGFP cells. In both cases cell detachment can be observed.

A quantitative verification of the aggregates is seen in the plot of figure 38. Therefore, I calculate Fiji/ImageJ integrals of the STRN-EGFP signal. The columns divide into pixel area per cell, pixel area per granule and pixel intensity per granule. For the cell area I average in total 50 different cells. From these 10 cells I measure 3 different particle positions (=30 values for granule area and granule intensity). The brackets show significant differences between the pixel area per granule and the pixel intensity per granule. Hyperosmotic cells show 4 times bigger particle sizes within the cytosol with a significance of p = 0,000. The signal intensity is increased by these cells due to overexposed accumulation within the condensates. A green signal proportion increase by 29% can be verified with 400 mM sucrose addition.

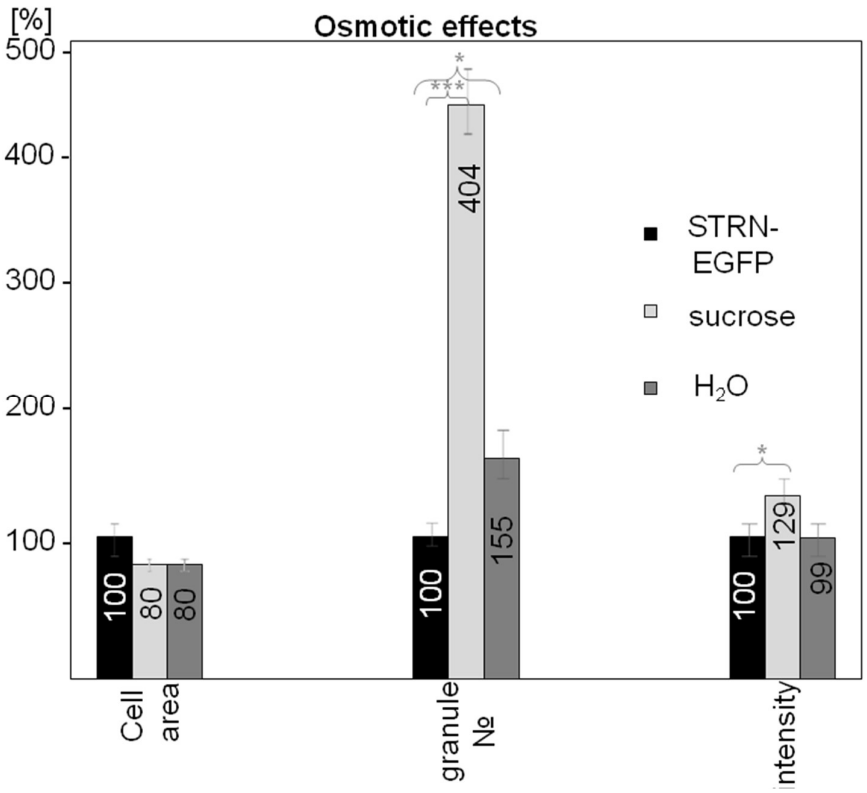

Figure 38: Quantitative verification of STRN condensates analyzed by immunofluorescence. For this analysis I observe 50 single cells per condition. Osmotic stress had similar effect onto the cellular area and reduced the size by 20%. The number of condensates (or here granule) is dramatically increased with sucrose treatment. I separate the stress granules-background signal with Fiji in this case. Overall intensity is apparently increased by sucrose treatment. Accumulated condensates form bright spots of STRN-signal.

○ 3.9 Proximity-dependent biotinylation in stable STRN-BIOID cells reveal transient interaction clouds

So far, all previous data is mostly dependent on specific antibodies. An alternative is delivered by recently introduced proximity-dependent biotinylation assays, a method to first bypass this antibody dependency and, second, to additionally increase the possible interaction range by detecting also transient interactors. Since it is a time, temperature and substrate concentration specific method, a careful optimization of signal to background has to be made. The longer the incubation or the higher the substrate concentration, the more proteins get biotinylated.

Therefore, controls were made such as cell lines with standalone BIOID tags (here IMR-90 HA-TurboID-P2A-mKate2 and IMR-90 HA-MiniID-P2A-mKate2). Previously presented immunofluorescence stainings already show biotinylation in intact cells. In PFA fixed samples the red channel is always the bi-cistronic reporter mKate2. This indicates the stably introduced gene fragment also in living cells. The green channel is occupied with either biotinylation/streptavidin signal or, anti-BIOID or anti-STRN staining. In the control cells with the standalone BIOID tag, differences between even the TurboID and the MiniID can be observed. Both controls show biotinylation streptavidin-Alexa488 signal within the nucleus and in the cytosol, while for the STRN-tagged stable cells this is only the case for STRN-MiniID and not STRN-TurboID. Further differences can be observed when looking at the antibody staining of the HA-tag.

In the case of MiniID and TurboID the tagged ligases produced HA-signal within the nucleus. For the STRN-MiniID and STRN-TurboID stable cells only STRN-TurboID produces signal within the nucleus. Therefore, the TurboID-tag can lead to an altered localization for the protein of interest. The signal specificity for streptavidin in immunofluorescence is way higher compared to Western blot. In both cases, 150 µM biotin is used as standard substrate concentration for the biotin ligases. In Western blot saturation comes up after 80 min of incubation time.

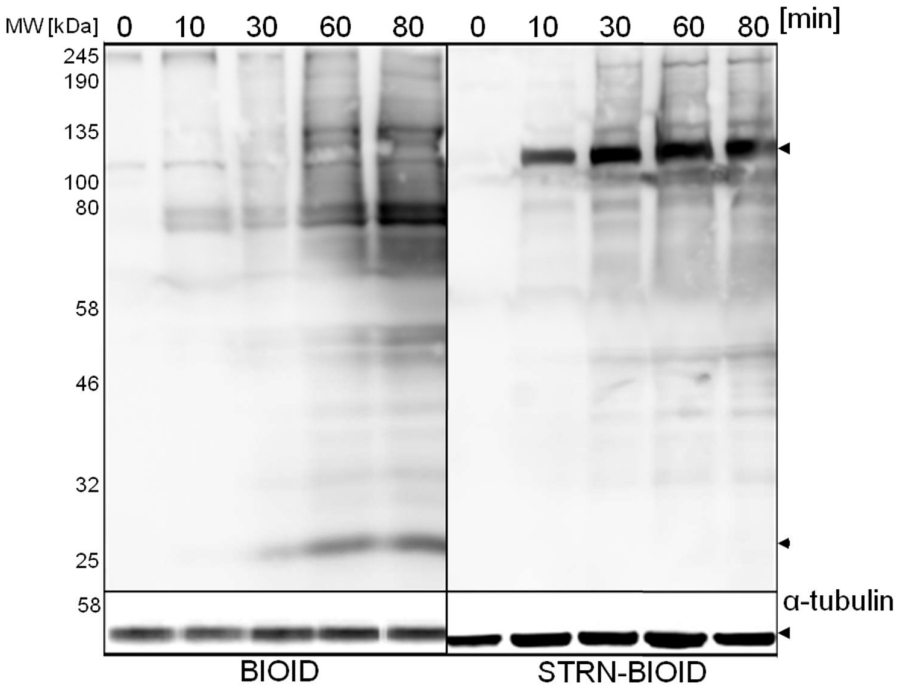

Figure 39: Streptavidin-HRP blot with kinetics and bead purification of control cells BIOID and STRN-BIOID. The cells are selected with 500 µg/mL G418. The blot displays the product of proximity labeling within stable IMR-90 HA-MiniID-mKate2 and HA-STRN-MiniID-mKate2. Stable clones are cultivated in 15 cm plates to 80% confluence. The cell lines generate different biotinylation signal intensities. For MS samples, the cells are incubated with 150 µM biotin for 80 min, while for IF samples no further signal improvement can be verified already after 10 min at 150 µM biotin. The upper black arrow indicates the signal of the self-biotinylated fusion protein STRN-BIOID, and the lower one of BIOID.

In figure 39, I analyze the basic kinetics of a BIOID biotinylation assay in IMR-90 cells with HA-MiniID-mKate2 and HA-STRN-MiniID-mKate2. The literature approves a less active but more specific proximity labeling for the MiniID ligase. The kinetics of 80 min seems adequate for observation of mitotic exit after releasing synchronized cells from their chemical additives. The Western blot in figure 40 shows the stepwise purification of the biotinylated proteins from the STRN-MiniID lysates.

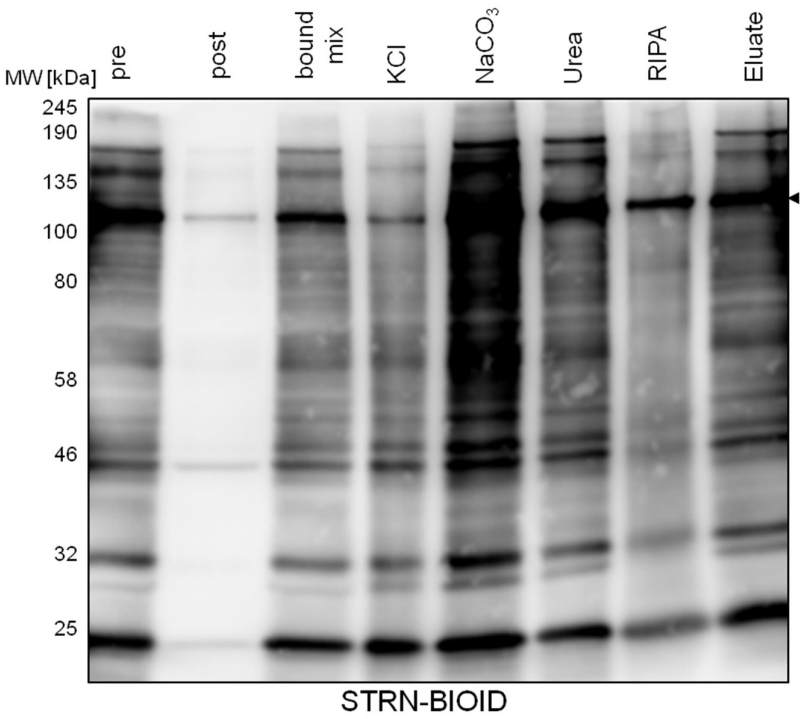

Figure 40: Preparation of MS samples for BIOID biotinylated proteins. The streptavidin-bead purification are performed with the protocol from Branon *et al*[288]. The $NaCO_3$-washing step lane has an excess of protein loaded. The post-lysate indicates almost all biotinylated protein get bound for purification. Within each washing step, weakly bound molecules are reduced, and the final eluate is analyzed by mass spectrometry analysis.

The streptavidin paramagnetic beads represent a highly specific method to purify biotinylated proximate and transient interactions. The streptavidin-HRP blot of figure 40 shows that almost every biotinylated candidate can be bound to the beads. During the stringent washing protocol, the overall yield is still high enough for mass spectrometry identification. The biotin concentration of choice is 150 µM over a time range of 80 min. Within this time period, an adequate amount of targets can be labeled. After optimizing the bead purification of biotinylated proteins both the control and the STRN-MiniID samples are verified via mass spectrometry.

Similar to the *Xenopus laevis* proteomics for the human BIOID screening I use a LC-MS/MS identification performed by the core facility for mass spectrometry & proteomics (CFMP) at the Zentrum für molekulare Biologie at the Heidelberg University (ZMBH) and the core facility for mass spectrometry from Institute of Biochemistry and Molecular Biology at the Bonn University (IBMB). In a first attempt, I screen lysates with mixed cell cycle stages of biotinylated proteins. The sample for the mitotically arrested and the released sample are imminent. The standalone MiniID screen results in a list of 222 different protein entries and 1246 peptides in total. The biotinylation analysis of the fusion protein STRN-MiniID results in 282 different protein entries and 1558 peptides in total.

The list in table 17 includes all proteins (or their HUGO gene name) which can be verified in the STRN-MiniID but not in the MiniID background. Typical background candidates like human keratin and the bead streptavidin are subtracted. Both, the MiniID control and the STRN-Mini protein list contain several isoforms of tubulin and actin peptides that get subtracted. Similar to previous screenings STRN does not reach the highest score but a total number of 16 STRN peptides can be verified.

Table 17: Mass spectrometry results from STRN-MiniID biotinylation assay. The biotinylation labeling is performed in human embryonal lung fibroblast IMR-90. The proteins listed here are filtered for proteins that do not occur in the MiniID standalone list, or are not typical background proteins like the keratin or streptavidin from the purification protocol.

Gene name STRN-Mini MS (BIOID) not arrested	PeptideNo	kDa	proteinID
CCT8	36	**60**	NP_006576.2
CDK5RAP2	24	**215**	NP_060719.4
DBNL	21	48	NP_001014436.1
STRN	**16**	**81**	**NP_003153.2**
SMC2	16	136	NP_006435.2
CACYBP	11	26	NP_055227.1
NUDC	9	63	NP_006591.1
ANXA1	7	39	NP_000691.1
STRN4	6	26	NP_037535.2
DDX3Y	4	73	NP_004651.2
ACTG2	3	42	NP_001606.1
SERPINH1	3	46	NP_001226.2
NOP58	2	60	NP_057018.1
DSG1	2	114	NP_001933.2

NOP56	2	66	NP_006383.2
ZYX	2	61	NP_003452.1

The first high scoring candidates from that list are CCT8 with 36 found peptides (T-complex protein 1 subunit theta) and CDK5RAP2 (CDK5 Regulatory Subunit Associated Protein 2) with 24 found peptides. Both of them play a role in ciliogenesis. CCT8 is a chaperonin in the so called BBS-CCT complex[351]. Several databases already show PP2A and even STRN (family member) interaction with CCT8[352]. CDK5RAP2 is an essential protein of the centrosome that anchors the γ-tubulin ring complex (γTuRC)[229].

In the slime mold *Dictyostelium discoideum,* the CDK5RAP2 orthologue (CEP161) show an interaction to the PP2A orthologue (phr2AB) of the B55 regulatory subunit[353]. A direct interaction between STRN and CDK5RAP2 is not described so far. An STRN equivalent score is achieved by SMC2. The SMC2 protein is the only found protein from BIOID, which is redundant for *Xenopus* egg extract co-IP MS using STRN-AB2. The screening result of table 17 verifies STRN4 (Zinedin) consistent with STRN family members known to form hetero- and homooligomers in STRIPAK complexes. The protein list contains DNA/RNA processing related candidates and MAP MT modulating ones. In contrast to the MS co-IP with STRN-AB3 in *Xenopus laevis* egg extract, no THOC proteins can be identified.

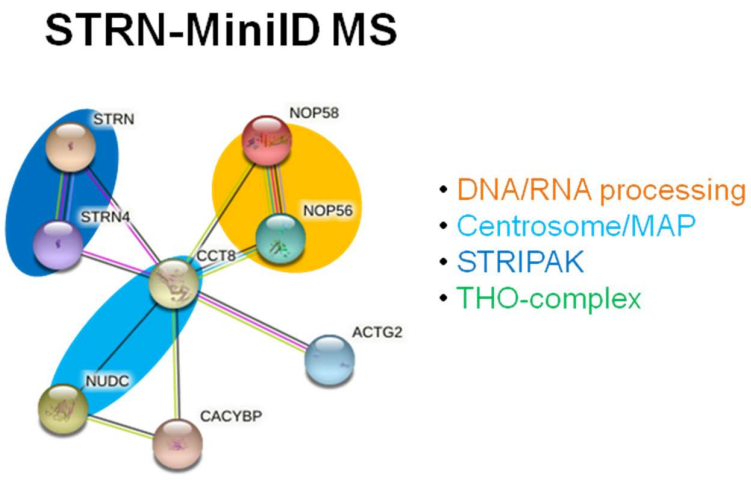

Figure 41: The mixed cell cycle BIOID screening candidates from human IMR-90 mass spectrometry. In STRINGdb links in between nodes resemble evaluation from GO terms, including text mining, experiments, databases, co-expression, neighborhood, gene fusion and co-occurrence. After query input, the map gets adjusted in order to remove free floating proteins. The proteins here do not occur in the MiniID standalone control assay and are STRN-MiniID exclusive candidates.

Beside proteomics, functional analysis can give further information of STRN's mode of operation within the cell. The here described methods give insight into STRN's role during cell cycle regulation as MT modulator. There is still data missing to finalize the pilot experiments. But the results so far are arguments in favor of the hypothesis STRN having a MAP-like function and being a MT modulating protein.

4 Discussion

The protein STRN is one of the variable PP2A regulatory B sub domains and is known to serve as a platform for the superordinate assembly of the so called STRIPAK complex[140]. There is little known, about the primary functions of STRN, its (phospho)-modifications, how STRN protein levels are regulated and which proteins interact to STRN. This is mainly due to a lack of STRN-specific tools, such as the highly specific STRN antibody which I generated for this purpose.

4.1 STRN is a cell division regulator

Understanding the importance of STRN in cellular processes helps to decode complex pathway networks in the cell. As the data presented here indicates, STRN promises new insights into the fast regulation of MT dynamics during the cell cycle: First and foremost, STRN comprises interactions with known kinases and phosphatases. A proximate fine tuning of phosphorylation and dephosphorylation is a key strategy for functional switches of proteins. Phospho-modification is the most rapid and flexible way for on/off switches, which are required for precise cell cycle progression. In context of this thesis I characterize STRN regarding its putative role as a MT modulator.

Observation from previous literature shows higher STRN levels in M-phase compared to late G_2 MT co-sediments. Our comparable MT interactome analysis of embryonal *Xenopus laevis* stage VI oocyte lysate and mature egg extract served as motivation and foundation stone for my work[102].

With the here presented tools I am able to verify known STRN interaction partners, such as STRIP1, STRIP2 and CTTNBP2. This verification describes STRIPAK proteins in an embryonal model system (in this case *Xenopus laevis*) for the first time. Furthermore, I verify PP2A phosphatase subunits as interaction partners. My data suggests that STRN might undergo mobility shifts in western blot when treated with cell cycle manipulating drugs or when looking at different arrested cell cycle stages. Mobility discrepancies in the western blots, lane shifts in the sucrose gradient and the fact that I find PP2A and STRIPAK interactors in mass spectrometry imply STRN modulation and assembly of a protein complex. These are first indications that a post translational modification of STRN, like *e. g*. phosphorylation is associated with cell cycle progression.

Recent literature describes STRN depletion in human HeLa cell line and overexpression of STRN in MCF-7 cells. Researchers postulate STRN might be a marker for apoptosis. Apoptosis and proliferation are depending on cell division (or mitosis) and are tightly linked: Apoptosis destroys unwanted cells, proliferation increases the number of cells. For both pathways similar set screws (putative STRN interaction proteins) are turned and adjusted depending on the current situation.

The same paper lines out a caspase induced proteolytic cleavage of 110 kDa STRN into smaller fragments, is linked to apoptosis. The authors, however, do not discuss cell cycle correlated observations in their experiments[335]. In the context of apoptosis, the STRIPAK components and associated proteins MST1/2 (the mammalian Hippo kinase), CCM3 and MAP4K4 kinase are known to regulate apoptosis[354–356]. So, *vice versa,* first, this could also be true for STRN and, second, this might also be the case for cell division.

A PP2A-STRN dependent fine-tuning mechanism for checkpoint functions is conceivable and likely to control MT modulation during the cell cycle. Depletion of STRN4 in cancer cell lines reduced proliferation, inhibited cell cycle progression and induced apoptosis[357]. Silencing of STRN4 significantly reduces the invasion and migration of the cancer cell lines.

Vice versa STRN4 upregulation leads to increased invasiveness by activating STRIPAK kinase MINK1 and its downstream transcription factors[358]. Taken together, as STRN family members within the STRIPAK complex have a large interchangeability, STRN might behave similar as STRN4 and can also be a putative oncogene.

In my immunofluorescence of STRN manipulated cells I do not observe any differences in cell number, the phenotype of single cells or an increase in apoptotic cells. This might require more determined analysis. But reduced invasiveness and migration can also be a result of altered cell cycle progression. In fact, my data shows a shift in cell cycle progression for the STRN dysregulated cell lines. Human IMR-90 cells with STRN KO have a slower cell division compared to the endogenous STRN and STRN-EGFP cell line. *Vice versa* STRN-EGFP shows less dividing cells compared to endogenous STRN. This fits to the findings in *Xenopus laevis* STRN-depleted egg extracts: The bipolar spindle structures remain longer with lower STRN levels. The presented data suggests a faster cell cycle with STRN shortage and a slower cell cycle with STRN oversupply.

The experiment of bipolar spindle formation and subsequently induced chromatid segregation in *Xenopus laevis* egg extracts show that STRN might stabilize bipolar spindles in the first mitosis after fertilization, but overall STRN shortage leads to a slower and more chaotic segregation. The question if STRN has a spindle-stabilizing or a segregation hindering function might be clarified by the following set up: A rescue experiment with the addition of soluble recombinant STRN or addition of a STRN mRNA to produce new protein by *in vitro* translation directly in the system.

The cell free system is a model with its limitations. The main difference between calcium and CAMKII$^{aa1\text{-}290}$ induced anaphase-metaphase transition is a faster impact of the CAM kinase. Moreover, calcium will stimulate a broader range of cascade downstream activated proteins, kinases and phosphatases that play a role in mitosis[359]. In the very first cell division after fertilization, the sperm enters the egg and a calcium influx triggers progression from metaphase II to anaphase II. Ca^{2+} sensitive and calmodulin-binding proteins, like CAMKII are activated. Calcium is a second messenger that has multiple functions in the cell[326]. In order to guarantee cell cycle

progression, it binds to calmodulin (CAM). This binding activates ion channels, protein kinases, adenylyl cyclases, protein phosphatases and phosphodiesterases[328].

One crucial limitation of the cell free extract is that STRN itself is calcium sensitive and its depletion can lower the contraction rate of cardiomyocytes[360]. The spindle disassembly of MT structures or the destabilization of central MTs in complete spindles can be induced by recombinant, constitutively active CAMKII and independent of CDK1 inactivation. PP2A with its regulatory subunit B55 dephosphorylates CAMKII in order to suppress apoptosis in *Xenopus laevis* egg extracts and human 293T cell line[361]. In human breast cells the dephosphorylation of CAMKII by PP2A occurs during the G_2 and/or M-phases and is essential for metaphase-anaphase transition[362]. It is not clear which B subunit controls this dephosphorylation. The trend I observe in my work, *i. e*. lagging chromatid segregation in the *Xenopus laevis* M-phase egg extracts, suggest a delayed mitotic exit. Whether this delay originates from early or late mitosis can be answered with experiments in human cell lines.

My immunofluorescence data suggests incomplete chromatid segregation. The pictures might imply chromatin bridges or lagging segregation. A similar phenotype can be found in the IgG-depleted control images, which is why this seems to be a standard observation due to the handling and the disruption because of pipetting steps. The transition states during chromatid segregation are rare observations, and this short-termed process is depending on a perfectly timed fixation. The number of cells entering anaphase and going further to interphase is higher for STRN KO human embryonal fibroblasts. In contrast, the cell line with STRN excess is either stuck directly in interphase without going into mitosis or cannot overcome the metaphase-anaphase transition. In the future, one should check if STRN-depleted extract, STRN-deleted cells or STRN-EGFP overexpressing cells behave different during M-phase or chromatid segregation steps. A clearer answer might be given by life cell imaging approaches.

Altered cell cycle ratios or different segregation behavior might be an indication of an affected spindle assembly checkpoint (SAC). The SAC protein complex is the guardian of faithful chromosome segregation. In cell division the SAC prevents chromatid segregation when the MTs are not fully attached to the kinetochore complexes. An incorrectly working SAC can explain the observation of irregular M-phase ratios

because of altered cell cycle velocity. The SAC is signal sensitive and the rate-limiting factor of cell division progression.

This protein complex has the main function to prevent premature chromatid segregation. Being robust, there are rarely malfunctions of the SAC, which, when disturbed, might lead to different proliferation rates and thereby malignant cells. One group of the SAC-associated proteins consists of conserved kinases that lead to protein signaling cascades in eukaryotes. When k-fibers are stably attached, the SAC criteria are fulfilled, the checkpoint is inactivated, chromosome can segregate, and the cell can divide.

Beside other SAC components premature chromatid segregation or loss of sister chromatid cohesion is inhibited by the MAD1-MAD2 protein complex. MAD1 and CDC20 are APC/C coactivators[363]. The phosphatase PP2A-B56 dephosphorylates CDC20. Active APC/C ubiquinylates a broad range of cell division proteins and thereby metaphase-anaphase transition can proceed. Besides the MAD2 KD a different strategy to proof STRN SAC regulation would make sense. Because the cells undergo a harsh mRNA transfection and a major fraction of cells die during this procedure and the rate of dividing cells is low. One of several alternatives to a transfection dependent depletion of MAD2 could be specific chemical inhibition of SAC proteins. For instance, a selective SAC inhibitor that disrupts MAD2 CDC20 binding would be M2I-1[364].

Depletion of the PP2A B55 regulatory subunit in *X. laevis* egg extracts maintained the meiotic metaphase arrest. The addition of a specific CDK inhibitor ($P27^{KIP1}$) failed to promote metaphase-anaphase transition in the PP2A-B55 deficient lysate[68]. However, this mechanism is not observed in human cells [62]. Even if the PP2A B subunit itself was conserved between orthologues it could still have different roles. The regulatory B subunits differentiate into several isoforms: For PP2A B55 α, β, γ, δ and for PP2A B56 α, β, γ, δ and ε. Instead of the PP2A B56 or PP2A B55 regulatory subunit, a STRN related function of SAC-control might be possible.

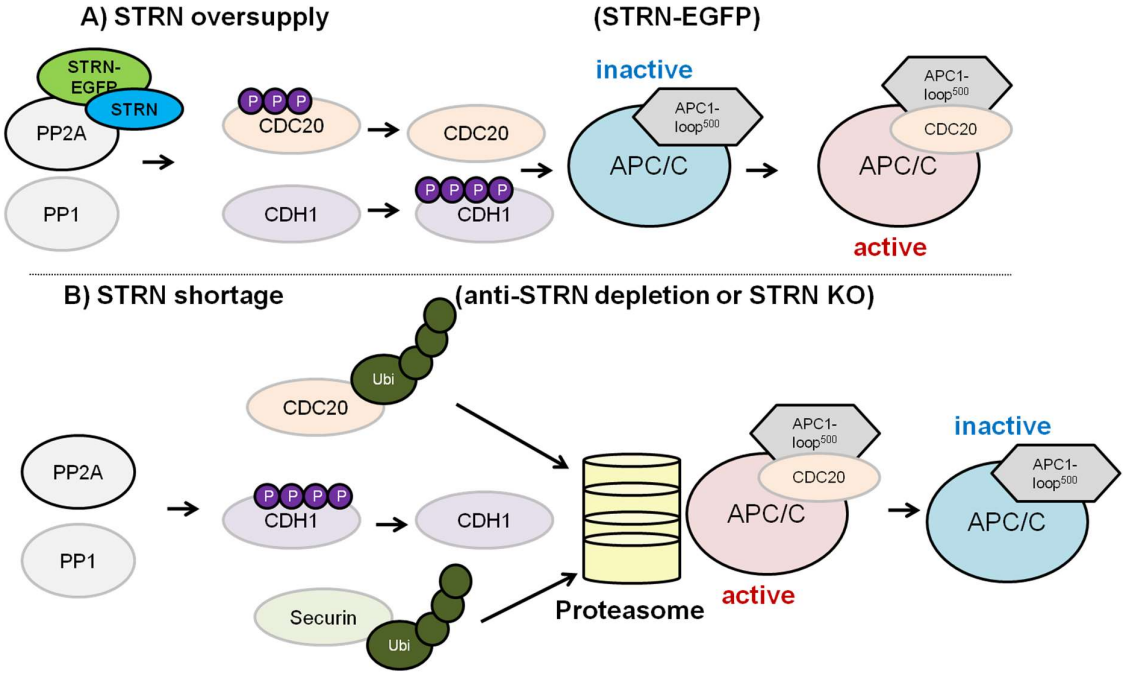

Figure 42: A hypothetical model on the basis of my own results and literature how PP2A STRN regulatory subunits might control cell division progression. Graph A) describes a more PP2A B56-like function while B) a PP2A B55-like function of STRN, whereby a strict separation of both is not possible (explained in continuous text).Depending on the STRN concentration (or modification-depending binding affinity) the protein STRN can have M-phase impact.

Since there are just a few phosphatases in comparison to the large number of kinases, they have wide substrate spectra and a defined interplay. The phosphatase PP1 functions in both the first and in the last steps of mitosis[365–369]. PP1 and PP2A share several targets as dephosphorylation substrates but targeting different positions. It has to be checked if PP2A STRN can replace the dephosphorylation regulation of PP2A B55 and PP2A B56, or if PP2A STRN has different distinct dephosphorylation destinations in terms of mitotic progression.

When speaking of the PP2A regulatory subunit, a clear separation between PP2A B55 and PP2A B56 function and localization is not possible since previous work showed that both can play a role in the different phases of the M-phase and are distributed ubiquitous in the cell with some accumulation at kinetochores and centrosomes. In *C. elegans* embryos, PP2A B55 is known to have a function even in mitotic entry[70].

The PP2A B56 phosphatase dephosphorylates PLK1 and regulates spindle organization during mitotic entry[370]. While distinct isoforms of PP2A B56 (γ and ε) are known to counteract Aurora B kinase activity in anaphase during mitotic exit[371]. A separation which role STRN plays in M-phase might have the same difficulty as separating the role of PP2A B55 and PP2A B56. Two hypothetical explanations how STRN can regulate PP2A dephosphorylation are shown in figure 42. The upper pathway A) can explain why STRN oversupply leads to a higher number of cells being stationary in interphase: In this case the APC/C stays active and no M-phase proteins (like M-phase marker Cyclin B) can accumulate. Figure 42 picture B) might describe the STRN deficient situation: The APC/C co-activator CDH1 is dephosphorylated by PP2A and cannot bind to the E3 ligase. Thereby APC/C becomes inactive, and M-phase is delayed. The MPF will not be degraded.

Taken together, my results suggest a direct link between STRN and cell cycle and cell division regulation, which was not known so far. We still do not know which PP2A B-regulatory subunit is required for which function. They might be organism-specific, tissue-specific, hormone-regulated, time-dependent and there might be many more challenges in order to verify the true function of STRN, PP2A STRN or STRIPAK. Another point of view to answer STRN's true function can be elucidated by the protein's interaction partners. Previous research shows, the SAC is a well-described protein network machinery. A putative checkpoint related function of STRN might be verified, when looking at the STRN interactome.

4.2 The STRN proteasome shows evidence of a MAP-like character and MT modulating function

The results of my proteomics experiments show that STRN binds to multiple proteins during interphase and mitosis. My experiments focus on embryonal systems of *Xenopus* oocytes, eggs and human embryonal lung fibroblast cells. I verify the STRN interactome within my work. With regard to this a direct support of SAC correlated cell cycle control by function of the STRN associated STRIPAK complex is still enigmatic. The SAC interaction network is closely positioned to the kinetochore protein complex interaction network and *vice versa*. My MS results show interaction of STRN with CENP-E in *Xenopus laevis* egg lysate.

The kinetochore can be separated into the outer MT-sided KMN network, named after its protein complex of KNL1, MIS12, and NDC80, and the inner centromere-sided CCAN (constitutive centromere-associated network), with *e. g*. CENP-C and CENP-T[372]. The protein CENP-E connects MT +-end tips to the kinetochore and directs other proteins to the kinetochore, like BUB1B, MAD1 and MAD2[373]. The phosphatase subunit PP2A B56 is known to bind and to direct dephosphorylate the leading SAC multi-domain pseudo kinase BUBR1, which promotes chromosome congression at the kinetochore[38,374,375]. A similar function for STRN is conceivable.

STRN family members tend to form homo- and heterooligomers due to α-helices assembling in the coiled-coil domain[36,376,377]. Consistently I am able to verify the known interaction of STRN to other STRN family members STRN3 in frog eggs and STRN4 in human cells. The STRN family member STRN3 (SG_2NA) is known to control the cell cycle and to be STRIPAK associated. A siRNA depletion of STRN3 extends G_1 phase, and stable overexpression extends G_2[121]. The authors of these findings do not describe, however, if there is an impact upon cell division.

Studies of the proteomics elucidate the crucial factors of oogenesis and embryonal development: It is known that different PP2A regulatory B subunits have specialized responsibilities in cell division processes. Previous data from the *Xenopus* model system showed that the complex of CDK1 and Cyclin B phosphorylates Greatwall kinase (together with ARPP19 and ENSA feedback loop mechanism) and PP2A B55 inhibition is maintained until Cyclin B is degraded. Thereby PP2A B55 can control mitotic exit[235,236,378,379].

Another study showed a siRNA depletion of PP2A regulatory subunit STRN in *C. elegans* caused smaller oocytes and nuclear mislocalization[380]. Since STRN family members do not carry catalytic activity, the cell cycle control is likely to work as a PP2A associated mechanism. A cell cycle regulation by PP2A regulation through STRN association might explain the complex temporal behavior of mitotic progression and fine-tuning. Similar recognition determinants are regulated at widely different rates by a single pathway.

A STRN KD with primary striatal neurons from rat embryos resulted in increased dendritic complexity and an increased density of dendritic spines. The experiments show a PP2A STRN phospho-regulation and the author suspect dendritic development depends on the STRIPAK complex assembly. As before, the author did not discuss cell cycle discrepancies (since they used primary neural cells). STRN depleted striatal neurons might degenerate into earlier developmental phase[125]. STRN might play a different role in embryonal cell division compared to fully develop adult cell division.

We know from mammals and amphibians that, upon meiotic oocyte and follicle maturation, gonadotropin induces steroid hormone production like progesterone, testosterone and estradiol[381–383]. *In vivo* the process of folliculogenesis in response to hormonal stimulation, which produces mature, follicle-free (after germinal vesicle breakdown), fertilization-competent meiotic oocytes, is termed ’ovulation‘. This process includes translation (or upregulation) of all proteins necessary for proper spindle organization and chromosome alignment for correct chromosome segregation.

Likewise, the foundation stone to my thesis is a comparative co-sedimentation experiment with hyperstabilized MT within *Xenopus laevis* oocyte (late Interphase G_2) and egg (M-phase arrested) lysates. Natively bound MAPs are co-sedimented with the MT. Five experiments independently of each other show, one prominent protein candidate of the M-phase upregulated fraction is STRN.

Oocytes lose their centrosomes regularly before meiosis[193]. Given eliminated centrosomes, ovulation requires maturation or upregulation of associated proteins that are essential for cell division forming a dense interaction cloud, *i. e.* a PCM without centrioles.

In this aspect STRN might be involved in complementing the eliminated centrosomes, and thereby be essential for the first rapid divisions of the zygote after fertilization. It

would be interesting to see if STRN has a high mRNA concentration and protein concentration right after fertilization. A decrease after a view cell divisions (zygote-blastula transition), would mean STRN is translated from maternal mRNA stocks and the zygote will not maintain STRN upregulation. Furthermore, one could test if STRN absence leads to defects or lethality in early embryogenesis.

Recently, in fruit fly, researchers identified STRN in association with zygotic lethal mutations. The fast cell division during embryogenesis is highly dependent on tightly controlled cell division. The flies with maternal and zygotic mutated STRN die during embryogenesis with a dorsal-open phenotype[108]. Since the very first cell divisions of embryogenesis are very fast, deficiencies of regulating proteins (such as STRN as part of the STRIPAK complex) can lead to dramatic changes.

The early embryo consists of totipotent cells, *i. e.* embryonic stem cells that can develop into every kind of cell type. After a fast division phase the cells lose their totipotency and develop into pluripotent inner cell mass, trophoblasts and blastocoele of the blastocyst's embryonal morula stage. During this stage cell division slows down. Differences between these developmental stages are in cell signaling (like WNT) and individual protein levels.

In humans there are two known STRN isoforms: An 86 kDa (STRN1-1) and an 80 kDa (STRN1-2) protein. From the proteomics result, it is not clear which isoform was in the co-IP, but the WB suggests my data predominantly shows the 86 kDa STRN1-1 variant. The signal after SDS-PAGE runs higher as calculated from the amino acid sequence, *i. e.* at 110 kDa. Previous literature showed that this 110 kDa isoform signal is the predominant STRN isoform in mammals.

A cre-conditional KO mouse of the PP2A scaffold subunit A did not affect spindle formation but compromised spindle shape and cytokinesis in meiosis II. The mutated and cre-flipped mothers produced similar amounts of mature oocytes although in 84% fertilization failed. The scaffold subunit PP2A A is essential for the formation of the trimolecular PP2A complex. Without PP2A, dephosphorylation of CDK1 is abolished during meiotic resumption[384].

The PP2A A scaffold and C catalytic subunit are the fixed functional subunits for dephosphorylation, while the B subunit is highly variable and the responsible factor for the predetermined working environment and substrate specificity of the catalytic subunit. The PP2A trimolecular complex can dephosphorylate independently of STRIPAK interactors, but some functions can only be accomplished when it assembles to the superordinate STRIPAK complex.

Prior to embryonal development, STRIPAK components can have an impact onto gametes. Studies in *C. elegans* show a centrosomal accumulation of the STRIP orthologue in meiotic metaphase oocytes. STRIP depletion results in infertile worms[107]. The coiled-coil domain of the STRN protein plays a role in recruiting binding partners like the verified STRIPAK components STRIP1/2, CTTNBP2 and PP2A scaffold subunit A (PPP2R1A).

Due to its role as major regulator of the cell cycle, PP2A and all its subunits are suspected to play a role in cancer diseases. When STRN mutation, lack or disorder would lead to altered chromatid segregation, it was a putative novel oncogene. This would make STRN a possible candidate for drug treatment or gene therapy. A high throughput screening of mitotic proteins revealed that STRN silencing resulted in mitotic mistakes like misalignment and lagging[385]. The scientists combined potent gene silencing using STRN targeting siRNA with time-lapse microscopy and computational image processing[385]. The publication describes errors in chromatid segregation, the appearance of binuclear cells and induced cell death.

The PP2A-STRN complex assembly and phospho-modification functionality might depend on the cell cycle stage. STRN deficiency could lead to missing phospho-regulation. Thereby, defects in chromatid segregation and lagging chromosomes could lead to aneuploid cells and mutations could accumulate with time. In the human HEK293 cell line, PP2A STRN is known to dephosphorylate STE20-like kinases (MST3, MST4 and STK25[144]). The targeted MST3 kinase is linked to mitotic chromosome alignment and mitotic exit[386]. It is most likely that STRN is the phosphatase regulating protein and dephosphorylation of the kinase is crucial for late cell division steps.

As the name already suggests, STRIP1 and STRIP2 are a major STRN interacting protein. STRN, in turn, is suspected to stabilize STRIP proteins[220].

In my analysis I am able to verify STRIP1 and STRIP2 as STRN interactor in *Xenopus laevis* egg extracts. Earlier literature consistently shows STRIP binding to STRN is very frequent in different tissues and organisms[23,61,126–128,130,138,139,142,144,147,149,70,218,220,233,240,74,84,86,91,97,102,115].

Earlier analysis in fruit fly shows STRIP co-localization and stability integration of MTs in *Drosophila* olfactory projection neurons[387]. The STRIP antibody used in this paper generates a more defined IF signal as all STRN antibodies used here. It might be interesting to see if STRIP signal looks different in the here used STRN KO and STRN-EGFP cell line. Regarding my research, a meaningful next step can be a control tool allowing the analysis of interactors using STRIP itself as bait, in order to confirm STRN. Furthermore, it would be interesting to see how STRIP behaves in the STRN-manipulated systems, like the IMR-90 STRN KO and the IMR-90 STRN-EGFP cell line. Apart from STRIP1/2 such an analysis would make sense for all here discussed putative STRN interactors.

Besides STRIP, I am able to verify the STRIPAK component CTTNBP2. The protein CTTNBP2 is known as cortactin binding protein and F-actin regulator. It also associates with MT in neurons. CTTNBP2 can be co-pelleted together with polymerized tubulin and regulates dendritic arborization *in vivo*[388]. The close interaction of CTTNBP2 to moesin has an essential role during repolarization processes of the cytoskeleton during mitotic onset. Similar to CTTNBP2, moesin is a linker of the actin cytoskeleton with the plasma membrane and thereby regulates the structure and function of specific domains of the cell cortex. Regarding the STRIPAK complex, a paper from 2020 found decreased moesin phosphorylation after STRN depletion and PP2A inhibition[220].

Mitotic entry requires activation of moesin[389]. The scientists De Jamblinne *et al*. found that this activation is missing when either STRN is depleted or PP2A inhibited in *D. melanogaster* S2 embryonal cells[220]. The authors observed epithelial-mesenchymal-transition (EMT) and increased apoptosis in the STRN depleted or PP2A inhibited cells, but aspects of cell cycle or division regulation were not quantified or discussed within their findings.

This work also suspected missing dephosphorylation of STRIPAK associated STK10 STE20-like kinase. The kinase is not activated and phosphorylation of moesin is lost[220]. The STE20-like kinases of the STRIPAK complex are flexible and have a tightly controlled phospho-regulation. Similar to STE20 family of serine/threonine protein kinases STK10, STK3 and STK25 can phosphorylate moesin, and, together with STRIPAK component CCM3, these kinases can inhibit actin stress fiber formation to regulate endothelial cell junctions[390].

My experiments do not directly verify CCM3 or the GCKIII kinase as STRN interactors. The protein GCKIII (or STE20 family STK25/26 kinase) is the most frequently described kinase within the STRIPAK complex. It might be possible that STRN assembles only transiently to a multiprotein complex and that the complexation from a PP2A to a STRIPAK supramolecular complex is a step-by-step time-dependent process during distinct development stages or phases of the cell cycle.

Most of the different STRIPAK components are ubiquitously found in cells of different tissue types. Some are already known to play a role in mitosis. During mitosis the *Drosophila* orthologue of STRIPAK protein MOB4 plays a role in spindle focusing, centrosome separation and focusing of k-fibers[151]. Depletion of MOB4 resulted in a loss of crosslinking activity between k-fibers and centrosomal MTs. The STRIPAK components seem to be omnipresent. They are found in organelles, the nuclear envelope and the centrosome. Therefore, Frost *et al*. suggested that STRIPAK might play a role as a bridge between organelle and cell division signaling processes[391].

Another analysis showed a STRIPAK protein complex assembly is linked to mitotic exit. This analysis proofed a STRN4-MINK1 interaction. The STRN family member mediates the association of substrates with phosphatase holo-enzymes, while binding to the kinase MINK1. The scientists saw that this interaction is essential for the last step of mitosis, cellular abscission[143]. A similar function might be true for STRN and would have been suspected with MINK1 protein verification during my interactome analysis. However, verification of further STRIPAK components it might need other conditions or analysis methods.

Currently known published data and the STRIPAK proteins I find within my experiments put a focus on the function of STRN being involved in congression of chromosomes during metaphase. The DNA is compacted and winded by cohesion (with the responsible proteins SMC1, SMC3) and condensin (SMC2, SMC4). The protein SMC2 is one of the core components of the condensin ring and essential during mitosis. The condensin complex is crucial for the correct compaction of chromosomes during mitosis.

SMC proteins regulate chromosomal dynamics during cell division, localize to primary cilia of photoreceptors and are postulated to be involved in ciliary transport[392]. In the MS proteomics of the STRN interaction network a remarkable score was achieved with SMC2. Both frog (metaphase synchronized) and human (BIOID assay with mixed cell cycle stages) MS screenings contained SMC2 as putative STRN interacting protein. An interaction of SMC2 to STRN is not described so far, but a paper from 2018 shows PP2A B55 (isoform β but not α) dephosphorylation of SMC2 in embryonal *Xenopus laevis* egg extracts[393].

The PP2A B subunit is not only variable within the STRN family but for all possible B subunits. A similar interaction as PP2A B55 to SMC2 might be possible for STRN as well. SMC2 and additional proteins from STRN interaction screenings discussed here suggest STRN as a conceivable regulator of cell division progression. Previous literature shows a WNT signaling regulated control of the DNA condensation by SMC2[394]. This fits to the suggestion of the STRIPAK complex, being involved in WNT signaling[395]. STRN as regulating protein within the STRIPAK complex might play a similar role as the superior pathway regulator of WNT.

The WNT pathway is well-known for the regulation of differentiation, cell migration and proliferation during embryogenesis and in adult tissues. A close linkage to subordinate processes like individual cell division phases makes sense.

In the case of STRN BIOID and EGFP fusion tag the signal implies an ellipse shape but does not accumulate at the poles. Both SSX2IP and RHAMM interaction to STRN can be verified by mass spectrometry, western blot co-IP, or more or less immunofluorescence co-localization. SSX2IP is a centriolar satellite protein and one of the first centrosomal component identified so far whose expression rises in meiosis[102].

The latter is also true for STRN. Together with other candidates, SSX2IP forms granules that cluster around the centrosome in a MT-dependent manner[208,263]. Several mitosis specific phosphorylation sites are known for SSX2IP[167,396,397]. A kinase that targets SSX2IP during mitosis is PLK1. Phosphorylated SSX2IP is either inactivated by degradation, dephosphorylation (for instance by PP2A STRN), downregulation or a combination of these.

A PP2A-dependent dephosphorylation of SSX2IP might be important for PCM disassembly after cell division. If SSX2IP is an interactor for STRN, might become visible by controlling the centrosome signal of SSX2IP in the STRN KO cells compared to the endogenous STRN IMR-90 cell line.

A poorly characterized or even until now unknown STRN interaction is the interaction to the MAP RHAMM[398]. Similar to CTTNBP2, RHAMM is known to link the MT to the actin cytoskeleton[399]. Proteins that share microfilaments and intermediate filament interaction are a small family and might play a crucial role for the cytoskeletal interplay. In mitosis, RHAMM is spindle pole and chromosomally located, and functions in the maintenance of spindle integrity[338].

In previous literature, a PP2A catalytic subunit C co-IP pull down and mass spectrometry screening verified PP2A-RHAMM interaction in pancreatic β-cells[339]. The authors identified RHAMM as a glucose responsive PP2Ac interactor, while PP2Ac-STRN could be identified in a glucose independent co-IP. The PP2A subunit assembly (or the STRN interactome) might be not only depending on the cell cycle but also on other parameters like nutrient content in the cytosol.

Further evidence for centrosomal STRN localization is the high interaction score in the human cell line BIOID screening of CDK5RAP2. This highly conserved protein plays a role in ciliogenesis, associates with the γ-TURC and might drive its conformational change during mitotic spindle formation[217,400,401]. Regarding my work CDK5RAP2 generates the 2nd highest score in the BIOID screening in human cells while it cannot be verified with antibody-based methods.

It is unclear if the STRN interaction to CDK5RAP2 might play a role during amphibian embryogenesis or mitosis, since this cannot be verified with the results I generated with the CSF extract. The interaction of CDK5RAP2 to STRN could be a transient but plentiful interaction and therefore caught by the BIOID assay.

Transient interactions make sense for the fast and short intervals during cell cycle progression. In *Dictyostelium discoideum* the orthologue of PP2A B55 is known to be responsible for specific dephosphorylation of CDK5RAP2[353]. A direct interaction between STRN and CDK5RAP2 is not described so far.

In general, both cilia and the mitotic spindle require the activity of centrosomes (or MTOCs) and therefore share an overlapping proteome (MAP interactome).

The process of ciliogenesis is tightly linked to the cell cycle. In mammals, almost every cell type can assemble cilia in interphase, *i. e*. in G_1- or G_0-phase, and disassemble them prior to mitosis. The daughter centriole is assembled in a previous cell cycle to

the mother centriole. The mother centriole has an additional appendix, consisting of molecules specific to mother centrioles[402].

CDK5RAP2 is not only an important protein for the γ-TURC and mitotic spindle assembly but also plays a role in ciliogenesis. Another protein from the mass spectrometry results important for ciliogenesis is CCT8. Similar to CDK5RAP2 this protein generates a high score but is only visible in the human STRN BIOID assay. CCT8 is a chaperonin in the so called BBS-CCT complex, a complex regulating transport of vesicles to the cilia[351]. Several screenings from previous literature already show PP2A, and even STRN interaction to the ciliary protein CCT8[139,352]. STRN is known to interact with further candidates from the BBS-CCT complex (CCT2, CCT3, CCT4, CCT5, CCT6A/B and CCT7[139]). In my case I only find one protein candidate, *i. e.* CCT8. An anti-PP2A B56 IP and mass screening implied a function of PP2A to cilium assembly[403,404].

Previous research found that PP2A dephosphorylation of KIF7 translocates the protein to the cilia tip. The responsible PP2A B regulatory subunit for this process is not known. The kinesin KIF7 regulates MT dynamics, localization of the cilia and organization of the ciliary tip[405]. In my proteomics I do not find KIF7 but different kinesin family members, which have diverse roles including recruitment of PLK1 to the central spindle, MT cargo transport, MT plus-end depolymerizing activity and centrosome and nuclear positioning during mitotic entry (KIF20A, KIF23, KIF2C, and KIF5B). Mice pups with a conditional STRN KO showed deficiencies in epithelial sensing cells in the organ of Corti (cochlea maturation).

STRN is important for cell-cell junction integrity of the sensory epithelium, which is why these mice have a deaf phenotype[319,406]. This research was done with mouse embryos but if these mice showed any altered cell cycle was not mentioned. However, the sensory epithelium is based on specialized MT modulation of so called stereo-cilia. The authors suggested also STRN as a PP2A regulatory subunit and phospho-modulating protein as the responsible factor that makes the formation of stereo-cilia possible.

The cilium is the cells' sensory antenna. The STRIPAK associated kinase STK4 (also known as MST1) is a hippo pathway component that localizes to the basal body of cilia and promotes ciliogenesis[407]. STRN might play a role in cilia formation, since I am able to find cilia-related proteins like CCT8 and I observe significantly shorter cilia in STRN deleted cells. When the mechanism how STRN affects ciliogenesis can be deciphered, the protein might be a novel reference point for the treatment of ciliopathies.

In 2012, Frost *et al.* showed siRNA depletion for the closely related protein STRN3 (SG_2NA) and the STRN interaction partner STRIP1. This paper describes an altered ploidy measured by DNA content analysis and binuclear to horseshoe- and torus-shaped nuclei or fragmented nuclear remnants in microscopy. They observed that Golgi stacks and centrosomes were found within the cavity of abnormal shaped nuclei[391].

As introduced, the cell cycle is controlled by up- and downregulation of cyclins. For interphase to M-phase transition the cytoskeleton is completely restructured. This is managed by MAPs and MTs. The screening by Bärenz *et al*. of pelleted MTs found STRN associated to the MT and MAP pellet[102]. In my own experiments, I verified STRN upregulation in mature egg lysates compared to stage VI oocytes. Bärenz *et al*. showed five independent MS screenings from polymerized MT pellets of *Xenopus laevis* mitotic egg extract[102].

In cell culture experiments STRN shortage by siRNA depletion resulted in hyperphosphorylation of MAP2 and MT depolymerization[131]. In my experiments, the STRN fluorescent signal in cell lines does not show any changes after chemical treatment with cytoskeleton modulating drugs. However, the proteomics from STRN co-IP and proximity labeling suggest an interaction of STRN to described MAPs. If STRN directly binds to tubulin or just modulates MAPs (regulates their phosphorylation) is still questionable.

In interphase the de- and repolymerization of MT filaments is altered without STRN. The STRN deleted cells are significantly smaller in size compared to IMR-90 wild type cells. It is not clear if the MT dynamics is different directly due to loss of STRN, extension limitations due to an altered cell size (KO cells are smaller) or mutations that formed during the passaging. Shorter polymerized MT in the regrowth assay indicate a slowed down polymerization dynamics. This might provide an explanation why the cells without STRN have a slower cell cycle or M-phase lag.

Finally, two out of three MS experiments from frog identify THO complex component THOC1, THOC2, THOC3, THOC5, THOC6 and THOC7 bound to the anti-STRN antibody. The THO complex is involved in transcription, transport of spliced mRNAs to the cytoplasm and genome stability in mitosis and meiosis[330]. High throughput mass spectrometry screening of PP2A interactions could already identify a THOC2 PP2A correlation in earlier publications[408]. The corresponding B regulatory subunit is not known so far and STRN might be a promising candidate according to my findings. The THO complex is one essential protein complex for embryogenesis[409].

THOC2 mutated worm embryos showed abnormal mitosis[330]. The mechanism behind this are not elucidated so far. THOC2 is located to the nucleus in interphase. The association of STRN to the THO complex in M-phase after nuclear envelope breakdown can be an explanation why a major part of identified proteins in frog are associated with mRNA processing.

This observation would be an explanation why no THOC to STRN association can be verified in interphasic human cells. As major regulator of the cell cycle PP2A-mediated dephosphorylation has wide spectra of targets. Already early research found a PP2A-controled transcription[410] and translation[411] mechanism. The only known direct link of STRN to mRNA processing from literature is the MS-found binding partner ELF2S1. Similar to the THO complex, ELF2S1 links transcription with translation by promoting the binding of the initiator tRNA to 40S ribosomal subunits[412].

As the paper of Frost *et al*. suggests, STRIPAK could bridge mitosis to the membrane stacks close to the nucleus. The paper hypnotizes a bridge to the Golgi apparatus, but regarding my findings of STRN being associated with translation machinery a bridge to the ER is more likely. STRN might play a role in the mRNA processing machinery[391]. In the very first fast cell division steps of embryogenesis proteins translate from a pool of remarkably stable maternal mRNAs. These rapid divisions are enabled because of transcriptional quiescence[413,414]. The embryonal interaction between THOC2 and STRN could play a role in transcription repression or translation of the highly concentrated stocks of maternal mRNA. A linkage between membrane-compartments and MT modulation during mitosis is already known for other proteins like STIM1, REEP3, REEP4[415,416]. For example, the ER protein STIM1 connects membranes and MT.

Similar to STRN, STIM1 is phosphorylated during mitosis and is calcium sensitive[415,417,418]. After translation the proteins are directed to the Golgi apparatus and their location of destination within the cell. In the Golgi they can mature and get PTMs. MOB4 is a STRIPAK candidate that associates with the Golgi apparatus. In my experiments I find STRN membrane associated in human cells sub-fractionated extracts and cytosolic soluble during the CSF MAP pelleting. As Frost *et al*. already postulated, this could be due to STRN's exclusive interaction with the nuclear membrane. This membrane-association would then be lost after the nuclear envelope breakdown during cell division[391].

5 Conclusion

With the results I present in this thesis I am able to show the many facets of the protein STRN. I analyzed this protein because a prior mass screening of potential M-phase upregulated MT modulating proteins contained STRN as a high scoring candidate. STRN has a different behavior in different developmental stages *e. g.* embryonal and adult cell stage. The here presented figure 43 shows a putative model how STRN serves as binding platform for multiple proteins with regard to the cell cycle. The data I produced give reason to assume a STRN KO leads to a decelerated cell cycle while STRN oversupply (in form of STRN-EGFP on top of endogenous STRN) accelerates the cell cycle. In interphase the PP2A catalytic subunit maintains the dephosphorylated state for multiple proteins of the centrosome and in M-phase the PP2A B subunit STRN associated kinases (hyper) phosphorylated broad spectra of cell division relevant proteins.

I limited my discussion onto proteins that are absent in the control sample, or proteins that were reproducibly identified in different measurements or with different techniques.

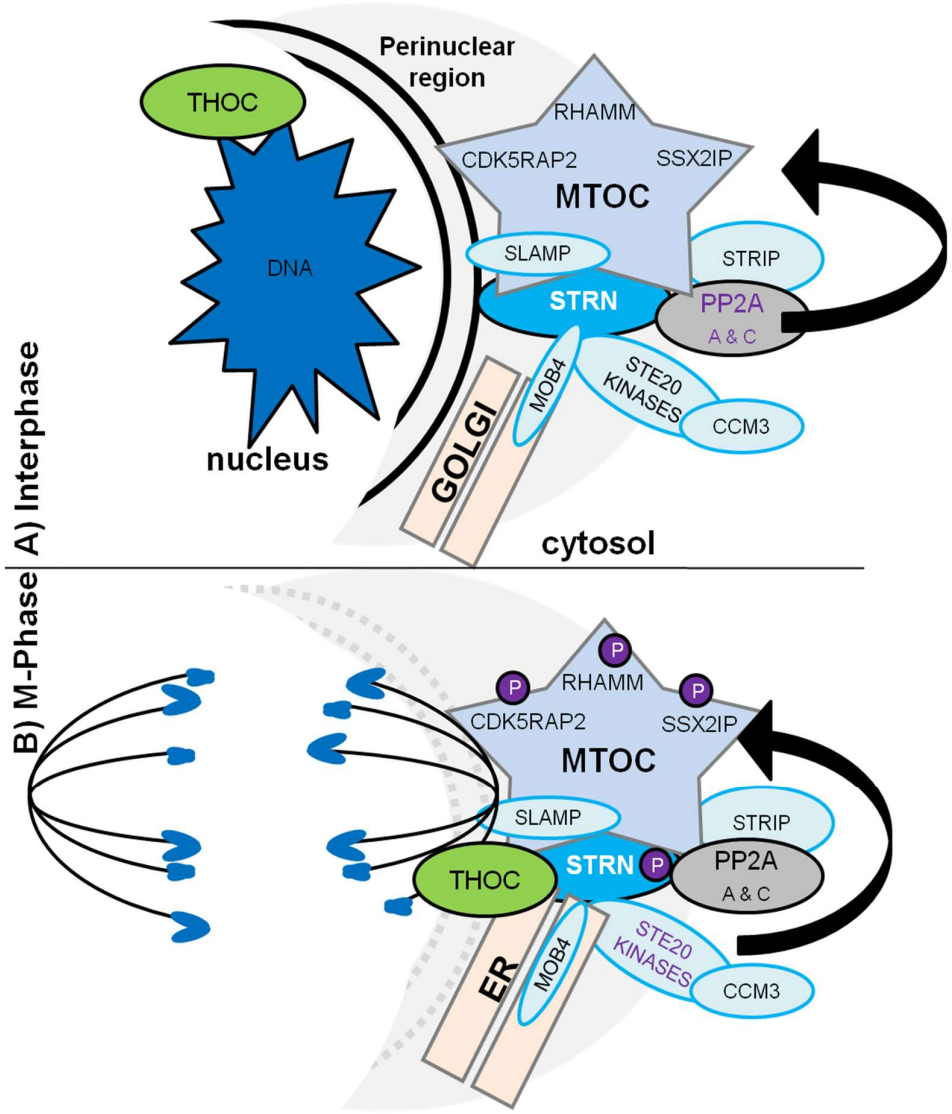

Figure 43: Hypothetical model for the MAP interplay and STRIPAK phospho-regulation during interphase and mitosis. The STRN interaction network discussed in this thesis verified a STRN centrosomal interaction network. This can explain phospho-regulation of MAPs (by PP2A dephosphorylation and STE20 kinase phosphorylation) for mitotic remodeling and tight control of mitotic progression.

The characterization of putative new MAPs can be meaningful in order to decipher early oogenesis and embryogenesis. During oogenesis the centrosomes are eliminated and the high protein concentration of the matured PCM matrix is suspected to play a major role for the fast cell divisions after fertilization. STRN could be involved in the story how the centrosomal functions are replaced during this early developmental stage.

My MS results from STRN antibody co-IP and BIOID assays verify MT related proteins from pathways like MT growth and shrinkage (KATNA1[419], KIF2C/MCAK[420]), cell cycle progression (PPP2R1A, SMC2[68,332]), cell division (RHAMM[333]), centrosome functions (SSX2IP[102]), ciliary signaling (SMC2[392], CCT8), mRNA transcription and/or translation (THOC). This work is the first thesis that is able to identify and redundantly characterize these STRN interaction partners. The interaction to RHAMM can explain the altered cell cycle and M-phase speed when STRN is manipulated. RHAMM is responsible for spindle integrity and it might be interesting if the RHAMM protein is affected during STRN manipulation. Together with the interaction to CDK5RAP2 and CTT8 a centrosomal or centrosome-compensating function for the STRN protein is most likely.

The THO-complex binds to STRN after nuclear breakdown disassembly, which might be important for M-phase protein translation from maternal mRNAs. The bridge between the STRIPAK complex and the ER might only occur during the very fast cell cycle steps of early embryogenesis. This would have the benefit that fine tuning of phosphorylation-state and protein biosynthesis would be in a time and space dependent close distance. The THO-STRN interaction can be the reason why my co-IP putative interaction proteins result in a majority of mRNA modulating proteins. One part of this protein interaction network plays a role during transcription repression and how only the current mRNA pool is used during the fast early embryonal cell divisions.

The here presented results and quoted literature suggests STRN might have different roles in cellular processes, including oocyte maturation, cell cycle regulation, especially cell division, MT dynamics and ciliogenesis. A more determined and detailed look into each individual process might be meaningful and might decode the wide spectra and functional role of the PP2A B regulatory subunit STRN.

6 Literature

1. von Mohl, H. & Winter, A. W. Über die Vermehrung der Pflanzenzellen durch Teilung. *Bayer. Staatsbibliothek* (**1835**).

2. Flemming, W. Beiträge zur Kenntniss der Zelle und Ihrer Lebenserscheinungen: Teil II. *Archiv für mikroskopische Anatomie* (**1880**)

3. Basto, R. *et al.* Flies without Centrioles. *Cell* (**2006**).

4. Bustamante-Marin, X. M. & Ostrowski, L. E. Cilia and mucociliary clearance. *Cold Spring Harb. Perspect. Biology* 9, (**2017**).

5. Nigg, E. A. & Raff, J. W. Centrioles, Centrosomes, and Cilia in Health and Disease. *Cell* (**2009**)

6. Yamashita, Y. M., Mahowald, A. P., Perlin, J. R. & Fuller, M. T. Asymmetric inheritance of mother versus daughter centrosome in stem cell division. *Science* (80). (**2007**)

7. Lüders, J. The microtubule cytoskeleton: Organisation, function and role in disease. (**2016**)

8. Pelletier, L. *et al.* The *Caenorhabditis elegans* centrosomal protein SPD-2 is required for both pericentriolar material recruitment and centriole duplication. *Curr. Biol.* (**2004**)

9. Varmark, H. *et al*. Asterless Is a Centriolar Protein Required for Centrosome Function and Embryo Development in *Drosophila*. *Curr. Biol*. (**2007**)

10. Vaizel-Ohayon, D. & Schejter, E. D. Mutations in centrosomin reveal requirements for centrosomal function during early *Drosophila* embryogenesis. *Curr. Biol*. (**1999**)

11. Hamill, D. R., Severson, A. F., Carter, J. C. & Bowerman, B. Centrosome maturation and mitotic spindle assembly in *C. elegans* require SPD-5, a protein with multiple coiled-coil domains. *Dev. Cell* (**2002**)

12. Andersen, J. S. *et al*. Proteomic characterization of the human centrosome by protein correlation profiling. *Nature* (**2003**)

13. Bonaccorsi, S., Giansanti, M. G. & Gatti, M. Spindle self-organization and cytokinesis during male meiosis in asterless mutants of *Drosophila melanogaster*. *J. Cell Biol.* (**1998**)

14. Gache, V. *et al. Xenopus* meiotic microtubule-associated interactome. *PLoS One* (5) (**2010**).

15. Hughes, J. R. *et al*. A microtubule interactome: Complexes with roles in cell cycle and mitosis. *PLoS Biol*.(6) 785–795 (**2008**).

16. Mitchison, T. & Kirschner, M. Dynamic instability of microtubule growth. *Nature* (312) 237–42 (**1984**).

17. Lindwall, G. & Cole, R. D. Phosphorylation affects the ability of tau protein to promote microtubule assembly. *J. Biol. Chem.* (**1984**).

18. Mandelkow, E. M. *et al*. Tau domains, phosphorylation, and interactions with microtubules. *Neurobiol. Aging* (**1995**)

19. Ramkumar, A., Jong, B. Y. & Ori-McKenney, K. M. ReMAPping the microtubule landscape: How phosphorylation dictates the activities of microtubule-associated proteins. *Developmental Dynamics* (**2018**)

20. Hunter, T. The Age of Crosstalk: Phosphorylation, Ubiquitination, and Beyond. *Molecular Cell* (28) (**2007**).

21. Hunter, T. Why nature chose phosphate to modify proteins. Philosophical Transactions of the Royal Society B: *Biological Sciences* (367) (**2012**).

22. Kataria, M. & Yamano, H. Interplay between Phosphatases and the Anaphase-Promoting Complex/Cyclosome in Mitosis. *Cells* (**2019**)

23. Manning, G., Whyte, D. B., Martinez, R., Hunter, T. & Sudarsanam, S. The protein kinase complement of the human genome. *Science* (**2002**)24. Chen, M. J., Dixon, J. E. & Manning, G. Genomics and evolution of protein phosphatases. *Sci. Signal.* (**2017**)

25. Torrent, L. & Ferrer, I. PP2A and Alzheimer Disease. *Curr. Alzheimer Res.* (**2012**)

26. Remmerie, M. & Janssens, V. PP2A: A promising biomarker and therapeutic target in endometrial cancer. *Frontiers in Oncology* (**2019**)27. Kobayashi, Y., Mercado, N., Barnes, P. J. & Ito, K. Defects of protein phosphatase 2A causes corticosteroid insensitivity in severe asthma. *PLoS One* (**2011**)

28. Nader, C. P., Cidem, A., Verrills, N. M. & Ammit, A. J. Protein phosphatase 2A (PP2A): A key phosphatase in the progression of chronic obstructive pulmonary disease (COPD) to lung cancer. *Respiratory Research* (**2019**)

29. Smith, R. J. *et al.* PP1 and PP2A Use Opposite Phospho-dependencies to Control Distinct Processes at the Kinetochore. *Cell Rep.* (**2019**).

30. Vallardi, G., Allan, L. A., Crozier, L. & Saurin, A. T. Division of labour between pp2a-b56 isoforms at the centromere and kinetochore. *Elife* (**2019**)

31. Saurin, A. T. Kinase and phosphatase cross-talk at the kinetochore. *Frontiers in Cell and Developmental Biology* (**2018**).

32. Hunter, T. Protein kinases and phosphatases: The Yin and Yang of protein phosphorylation and signaling. *Cell* (**1995**).

33. Shi, Y. Serine/Threonine Phosphatases: Mechanism through Structure. *Cell* (**2009**).

34. Virshup, D. M. & Shenolikar, S. From Promiscuity to Precision: Protein Phosphatases Get a Makeover. *Molecular Cel*l (**2009**)

35. Hiraga, A. & Tamura, S. Protein phosphatase 2A is associated in an inactive state with microtubules through 2A1-specific interaction with tubulin. *Biochem. J*. (Mar 1) 433–439 (**2000**).

36. Moreno, C. S., Lane, W. S. & Pallas, D. C. A Mammalian Homolog of Yeast MOB1 is Both a Member and a Putative Substrate of Striatin Family-Protein Phosphatase 2A Complexes. *J. Biol. Chem*. (276), 24253–24260 (**2001**).

37. Joukov, V. & De Nicolo, A. Aurora-PLK1 cascades as key signaling modules in the regulation of mitosis. *Science Signaling* (**2018**)

38. Ditchfield, C. *et al*. Aurora B couples chromosome alignment with anaphase by targeting BubR1, Mad2, and Cenp-E to kinetochores. *J. Cell Biol.* (**2003**).

39. Ahonen, L. J. *et al*. Polo-like kinase 1 creates the tension-sensing 3F3/2 phosphoepitope and modulates the association of spindle-checkpoint proteins at kinetochores. *Curr. Biol.* (**2005**)

40. Elia, A. E. H., Cantley, L. C. & Yaffe, M. B. Proteomic screen finds pSer/pThr-binding domain localizing Plk1 to mitotic substrates. *Science* (80). (**2003**).

41. Dorée, M. Leland H. Hartwell, R. Timothy Hunt, Paul M. Nurse. Key regulators of the cell cycle. *Medecine/Sciences* (**2001**)42. Samejima, K. *et al*. Mitotic chromosomes are compacted laterally by KIF4 and condensin and axially by topoisomerase IIα. J. *Cell Biol.* (**2012**)

43. Hagstrom, K. A., Holmes, V. F., Cozzarelli, N. R. & Meyer, B. J. *C. elegans* condensin promotes mitotic chromosome architecture, centromere organization, and sister chromatid segregation during mitosis and meiosis. *Genes Dev*. (**2002**)

44. Kaitna, S., Pasierbek, P., Jantsch, M., Loidl, J. & Glotzer, M. The aurora B kinase AIR-2 regulates kinetochores during mitosis and is required for separation of homologous chromosomes during meiosis. *Curr. Biol*. (**2002**)

45. Hudson, D. F., Vagnarelli, P., Gassmann, R. & Earnshaw, W. C. Condensin is required for nonhistone protein assembly and structural integrity of vertebrate mitotic chromosomes. *Dev. Cell* (**2003**)

46. Kelly, A. E. *et al*. Survivin reads phosphorylated histone H3 threonine 3 to activate the mitotic kinase Aurora B. *Science* (80). (**2010**)47. Collins, E., Mann, B. J. & Wadsworth, P. Eg5 restricts anaphase B spindle elongation in mammalian cells. *Cytoskeleton* (71), (**2014**).

48. Saunders, A. M., Powers, J., Strome, S. & Saxton, W. M. Kinesin-5 acts as a brake in anaphase spindle elongation. *Current Biology* (**2007**)49. Brust-Mascher, I., Sommi, P., Cheerambathur, D. K. & Scholey, J. M. Kinesin-5-dependent poleward flux and spindle length control in *Drosophila* embryo mitosis. *Mol. Biol. Cell* (**2009**).

50. Straight, A. F., Sedat, J. W. & Murray, A. W. Time-lapse microscopy reveals unique roles for kinesins during anaphase in budding yeast. *J. Cell Biol.* (**1998**)

51. DeLuca, J. G. *et al*. Kinetochore Microtubule Dynamics and Attachment Stability Are Regulated by Hec1. *Cell* (**2006**)

52. Welburn, J. P. I. *et al*. Aurora B Phosphorylates Spatially Distinct Targets to Differentially Regulate the Kinetochore-Microtubule Interface. *Mol. Cell* (**2010**)

53. Dobrynin, G. *et al*. Cdc48/p97-Ufd1-Npl4 antagonizes Aurora B during chromosome segregation in HeLa cells. *J. Cell Sci.* (**2011**)54. Wlodarchak, N. & Xing, Y. PP2A as a master regulator of the cell cycle. *Critical Reviews in Biochemistry and Molecular Biology* (**2016**)

55. Afonso, O. *et al.* Feedback control of chromosome separation by a midzone Aurora B gradient. *Science* (80). (**2014**)

56. Chen, C. *et al*. Striatins contain a noncanonical coiled coil that binds protein phosphatase 2A A subunit to form a 2:2 heterotetrameric core of striatin-interacting phosphatase and kinase (STRIPAK) complex. *J. Biol. Chem*. (289) 9651–9661 (**2014**).

57. Sontag, E., Nunbhakdi-Craig, V., Bloom, G. S. & Mumby, M. C. A novel pool of protein phosphatase 2A is associated with microtubules and is regulated during the cell cycle. *J. Cell Biol*. (128) 1131–1144 (**1995**).

58. Xu, Y. *et al*. Structure of the Protein Phosphatase 2A Holoenzyme. *Cell* (**2006**)

59. Janssens, V. & Goris, J. Phosphatases Implicated in Cell Growth and Signalling. *Biochem. J*. (**2001**).

60. Lechward, K., Awotunde, O. S., Świątek, W. & Muszyńska, G. Protein phosphatase 2A: Variety of forms and diversity of functions. *Acta Biochim. Pol*. (**2001**)61. Tsuchiya, Y. *et al*. Distinct B subunits of PP2A regulate the NF-κB signalling pathway through dephosphorylation of IKKβ, IκBα and RelA. *FEBS Letters* (**2017**)

62. Schmitz, M. H. A. *et al*. Live-cell imaging RNAi screen identifies PP2A-B55α and importin-β 21 as key mitotic exit regulators in human cells. *Nat. Cell Biol*. (**2010**)

63. Thompson, L. J., Bollen, M. & Fields, A. P. Identification of protein phosphatase 1 as a mitotic lamin phosphatase. *J. Biol. Chem*. (**1997**)

64. Watanabe, N. *et al.* Cyclin-dependent kinase (CDK) phosphorylation destabilizes somatic Wee1 via multiple pathways. *Proc. Natl. Acad. Sci.* (**2005**).

65. Harvey, S. L. *et al.* A phosphatase threshold sets the level of Cdk1 activity in early mitosis in budding yeast. *Mol. Biol. Cell* (**2011**)

66. Hégarat, N. *et al.* PP2A/B55 and Fcp1 Regulate Greatwall and Ensa Dephosphorylation during Mitotic Exit. *PLoS Genet.* (**2014**).

67. Játiva, S., Calabria, I., Moyano-Rodriguez, Y., Garcia, P. & Queralt, E. Cdc14 activation requires coordinated Cdk1-dependent phosphorylation of Net1 and PP2A–Cdc55 at anaphase onset. *Cell. Mol. Life Sci.* (**2019**)

68. Mochida, S., Ikeo, S., Gannon, J. & Hunt, T. Regulated activity of PP2A-B55 is crucial for controlling entry into and exit from mitosis in *Xenopus* egg extracts. *EMBO J*. (**2009**).

69. Wurzenberger, C. & Gerlich, D. W. Phosphatases: Providing safe passage through mitotic exit. *Nature Reviews Molecular Cell Biology* (**2011**).

70. Boudreau, V., Chen, R., Edwards, A., Sulaimain, M. & Maddox, P. S. PP2A-B55/SUR-6 collaborates with the nuclear lamina for centrosome separation during mitotic entry. *Mol. Biol. Cell* (**2019**)

71. Song, M. H., Liu, Y., Anderson, D. E., Jahng, W. J. & O'Connell, K. F. Protein Phosphatase 2A-SUR-6/B55 Regulates Centriole Duplication in *C. elegans* by Controlling the Levels of Centriole Assembly Factors. *Dev. Cell* (**2011**)

72. Enos, S. J., Dressler, M., Gomes, B. F., Hyman, A. A. & Woodruff, J. B. Phosphatase PP2A and microtubule-mediated pulling forces disassemble centrosomes during mitotic exit. *Biol. Open* (**2018**)

73. Sudakin, V. *et al.* The cyclosome, a large complex containing cyclin-selective ubiquitin ligase activity, targets cyclins for destruction at the end of mitosis. *Mol. Biol. Cell* (**1995**) 74. King, R. W. *et al*. A 20s complex containing CDC27 and CDC16 catalyzes the mitosis-specific conjugation of ubiquitin to cyclin B. *Cell* (**1995**) 75. Enserink, J. M. & Kolodner, R. D. An overview of Cdk1-controlled targets and processes. *Cell Division* (5) (**2010**).

76. Peter, M., Nakagawa, J., Dorée, M., Labbé, J. C. & Nigg, E. A. Identification of major nucleolar proteins as candidate mitotic substrates of cdc2 kinase. *Cell* (**1990**)

77. Masui, Y. & Markert, C. L. Cytoplasmic control of nuclear behavior during meiotic maturation of frog oocytes. *J. Exp. Zool.* (**1971**)78. Zou, H., McGarry, T. J., Bernal, T. & Kirschner, M. W. Identification of a vertebrate sister-chromatid separation inhibitor involved in transformation and tumorigenesis. *Science* (80). (**1999**) .

79. Heim, A., Tischer, T. & Mayer, T. U. Calcineurin promotes APC/C activation at meiotic exit by acting on both XErp1 and Cdc20. *EMBO Rep*. (**2018**) 80. Chung, E. & Chen, R. H. Phosphorylation of Cdc20 is required for its inhibition by the spindle checkpoint. *Nature Cell Biology* (**2003**)

81. Poenie, M., Alderton, J., Steinhardt, R. & Tsien, R. Calcium rises abruptly and briefly throughout the cell at the onset of anaphase. Science (80). (**1986**)82. Burke, D. J. & Stukenberg, P. T. Linking Kinetochore-Microtubule Binding to the Spindle Checkpoint. *Developmental Cell* (**2008**)83. Visintin, R. *et al*. The phosphatase Cdc14 triggers mitotic exit by reversal of Cdk-dependent phosphorylation. *Mol. Cell* (**1998**)

84. Breitkreutz, A. *et al*. A global protein kinase and phosphatase interaction network in yeast. *Science* (80). (**2010**) .

85. Ho, Y. *et al.* Systematic identification of protein complexes in *Saccharomyces cerevisiae* by mass spectrometry. *Nature* (**2002**).

86. Visintin, R., Hwang, E. S. & Amon, A. Cfi 1 prevents premature exit from mitosis by anchoring Cdc14 phosphatase in the nucleolus. *Nature* (**1999**) .

87. Ah-Fong, A. M. V. & Judelson, H. S. New role for Cdc14 phosphatase: Localization to basal bodies in the oomycete *Phytophthora* and its evolutionary coinheritance with eukaryotic flagella. *PLoS One* (**2011**).

88. Vigneron, S. *et al*. Kinetochore localization of spindle checkpoint proteins: Who controls whom? *Mol. Biol. Cell* (15), (**2004**).

89. Mapelli, M. & Musacchio, A. MAD contortions: conformational dimerization boosts spindle checkpoint signaling. *Current Opinion in Structural Biology* (17) (**2007**).

90. De Antoni, A. *et al.* The Mad1/Mad2 complex as a template for Mad2 activation in the spindle assembly checkpoint. *Curr. Biol.* (15), (**2005**).

91. Kulukian, A., Han, J. S. & Cleveland, D. W. Unattached Kinetochores Catalyze Production of an Anaphase Inhibitor that Requires a Mad2 Template to Prime Cdc20 for BubR1 Binding. *Dev. Cell* (16), (**2009**).

92. Simonetta, M. *et al.* The influence of catalysis on Mad2 activation dynamics. *PLoS Biol.* (7) (**2009**).

93. Xu, P., Raetz, E. A., Kitagawa, M., Virshup, D. M. & Lee, S. H. BUBR1 recruits PP2A via the B56 family of targeting subunits to promote chromosome congression. *Biol. Open* (**2013**)

94. Suijkerbuijk, S. J. E., Vleugel, M., Teixeira, A. & Kops, G. J. P. L. Integration of Kinase and Phosphatase Activities by BUBR1 Ensures Formation of Stable Kinetochore-Microtubule Attachments. *Dev. Cell* (**2012**)

95. Tang, Z. *et al.* PP2A Is Required for Centromeric Localization of Sgo1 and Proper Chromosome Segregation. *Dev. Cel*l (10) 575–585 (**2006**).

96. Kitajima, T. S. *et al.* Shugoshin collaborates with protein phosphatase 2A to protect cohesin. *Nature* (441) (**2006**).

97. Okumura, E. *et al*. Cyclin B-Cdk1 inhibits protein phosphatase PP2A-B55 via a greatwall kinase-independent mechanism. *J. Cell Biol.* (**2014**)

98. Decker, M. *et al.* Limiting amounts of centrosome material set centrosome size in *C. elegans* embryos. *Curr. Biol.* (**2011**)99. Littlepage, L. E. *et al.* Identification of phosphorylated residues that affect the activity of the mitotic kinase Aurora-A. *Proc. Natl. Acad. Sci. U. S. A.* (**2002**) 100. Schlaitz, A. L. *et al.* The *C. elegans* RSA Complex Localizes Protein Phosphatase 2A to Centrosomes and Regulates Mitotic Spindle Assembly. *Cell* (**2007**) 101. Wueseke, O. *et al*. The *Caenorhabditis elegans* pericentriolar material components SPD-2 and SPD-5 are monomeric in the cytoplasm before incorporation into the PCM matrix. *Mol. Biol. Cell* (**2014**).

102. Bärenz, F. *et al*. The centriolar satellite protein SSX2IP promotes centrosome maturation. *J. Cell Biol*. (202) 81–95 (**2013**).

103. Wasserman, W. J., Houle, J. G. & Samuel, D. The maturation response of stage IV, V, and VI *Xenopus* oocytes to progesterone stimulation *in vitro*. *Dev. Biol*. (**1984**)

104. Castets, F. *et al.* Zinedin, SG_2NA, and striatin are calmodulin-binding, WD repeat proteins principally expressed in the brain. *J. Biol. Chem*. (275) 19970–19977 (**2000**).

105. Moreno, C. S. *et al*. WD40 repeat proteins striatin and S/G_2 nuclear autoantigen are members of a novel family of calmodulin-binding proteins that associate with protein phosphatase 2A. *J. Biol. Chem.* (275) 5257–5263 (**2000**).

106. Wang, C. L., Shim, W. B. & Shaw, B. D. *Aspergillus nidulans* striatin (StrA) mediates sexual development and localizes to the endoplasmic reticulum. *Fungal Genet. Biol.* (**2010**)

107. Maheshwari, R., Pushpa, K. & Subramaniam, K. A role for post-transcriptional control of endoplasmic reticulum dynamics and function in *C. elegans* germline stem cell maintenance. *Dev.* (**2016**)

108. Chen, H.-W. *et al.* CKA, a Novel Multidomain Protein, Regulates the JUN N-Terminal Kinase Signal Transduction Pathway in *Drosophila. Mol. Cell. Biol*. (**2002**).

109. Petrovic, A. *et al*. The MIS12 complex is a protein interaction hub for outer kinetochore assembly. *J. Cell Biol*. (**2010**)

110. Musacchio, A. & Desai, A. A molecular view of kinetochore assembly and function. *Biology* (**2017**)

111. Neer, E. J., Schmidt, C. J., Nambudripad, R. & Smith, T. F. The ancient regulatory-protein family of WD-repeat proteins. *Nature* (371) 297–300 (**1994**).

112. Sanghamitra, M. *et al.* WD-40 repeat protein SG_2NA has multiple splice variants with tissue restricted and growth responsive properties. *Gene* (**2008**) 113. Jain, B. P. *et al.* Tissue specific expression of SG_2NA is regulated by differential splicing, RNA editing and differential polyadenylation. *Gene* (**2015**)

114. Tang, Y. *et al*. Architecture, substructures, and dynamic assembly of STRIPAK complexes in Hippo signaling. *Cell Discov*. (**2019**)

115. Benoist, M., Gaillard, S. & Castets, F. The striatin family: A new signaling platform in dendritic spines. *Journal of Physiology Paris* (99) 146–153 (**2006**).

116. Breitman, M., Zilberberg, A., Caspi, M. & Rosin-Arbesfeld, R. The armadillo repeat domain of the APC tumor suppressor protein interacts with Striatin family members. *Biochim. Biophys. Acta - Mol. Cell Res.* (1783) 1792–1802 (**2008**).

117. Landberg, G. & Tan, E. M. Characterization of a DNA-binding nuclear autoantigen mainly associated with S phase and G2 cells. *Exp. Cell Res*. (212) 255–261 (**1994**).

118. Muro Y, Chan Ek, Landberg G & Tan Em. A cell-cycle nuclear autoantigen containing WD-40 motifs expressed mainly in S and G_2 phase cells. *Biochem. Biophys. Res. Commun*. (207) 1029–1037 (**1995**).

119. Jain, B. P. *et al.* SG_2NA is a regulator of endoplasmic reticulum (ER) homeostasis as its depletion leads to ER stress. *Cell Stress Chaperones* (22) 853–866 (**2017**).

120. Tanti, G. K. & Goswami, S. K. SG_2NA recruits DJ-1 and Akt into the mitochondria and membrane to protect cells from oxidative damage. *Free Radic. Biol. Med*. (75) 1–13 (**2014**).

121. Pandey, S., Talukdar, I., Jain, B. P. & Goswami, S. K. GSK3β and ERK regulate the expression of 78 kDa SG_2NA and ectopic modulation of its level affects phases of cell cycle. *Sci. Rep.* (**2017**)

122. Lin, L., Lo, L. H. Y., Lyu, Q. & Lai, K. O. Determination of dendritic spine morphology by the striatin scaffold protein STRN4 through interaction with the phosphatase PP2A. *J. Biol. Chem*. (**2017**)

123. Castets, F. *et al.* A novel calmodulin-binding protein, belonging to the WD-repeat family, is localized in dendrites of a subset of CNS neurons. *J. Cell Biol.* (134) 1051–1062 (**1996**).

124. Bartoli, M. *et al.* Down-regulation of striatin, a neuronal calmodulin-binding protein, impairs rat locomotor activity. *J. Neurobiol.* (**1999**).

125. Li, D., Musante, V., Zhou, W., Picciotto, M. R. & Nairn, A. C. Striatin-1 is a B subunit of protein phosphatase PP2A that regulates dendritic arborization and spine development in striatal neurons. *J. Biol. Chem.* (**2018**)

126. Moqrich, a *et al.* Cloning of human striatin cDNA (STRN), gene mapping to 2p22-p21, and preferential expression in brain. *Genomics* (51) 136–139 (**1998**).

127. Neisch, A. L., Neufeld, T. P. & Hays, T. S. A STRIPAK complex mediates axonal transport of autophagosomes and dense core vesicles through PP2A regulation. *J. Cell Biol*. (Jan 18), 1–21 (**2017**).

128. Wei, L. *et al.* Identification of key genes, transcription factors and MicroRNAs involved in intracranial aneurysm. *Mol. Med. Rep.* (**2018**) 129. Garza, A. E. *et al.* Variants in striatin gene are associated with salt-sensitive blood pressure in mice and humans. *Hypertension* (**2015**)

130. Meurs, K. M. *et al.* Association of dilated cardiomyopathy with the striatin mutation genotype in boxer dogs. *J. Vet. Intern. Med*. (**2013**).

131. Kaźmierczak-Barańska, J., Pęczek, Ł., Przygodzka, P. & Cieślak, M. J. Downregulation of striatin leads to hyperphosphorylation of MAP2, induces depolymerization of microtubules and inhibits proliferation of HEK293T cells. *FEBS Lett.* (589) 222–230 (**2015**).

132. Sánchez, C., Díaz-Nido, J. & Avila, J. Phosphorylation of microtubule-associated protein 2 (MAP2) and its relevance for the regulation of the neuronal cytoskeleton function. *Progress in Neurobiology* (61) 133–168 (**2000**).

133. Vasquez, R. J., Howell, B., Yvon, A. M., Wadsworth, P. & Cassimeris, L. Nanomolar concentrations of nocodazole alter microtubule dynamic instability *in vivo* and *in vitro. Mol. Biol. Cell (*8) 973–985 (**1997**).

134. Niceta, M. *et al.* Mutations impairing GSK3-mediated MAF phosphorylation cause cataract, deafness, intellectual disability, seizures, and a down syndrome-like facies. *Am. J. Hum. Genet.* (**2015**) 135. Xie, W. R. *et al*. An Atoh1-S193A phospho-mutant allele causes hearing deficits and motor impairment. *J. Neurosci.* (**2017**)

136. Zhai, X., Liu, C., Zhao, B., Wang, Y. & Xu, Z. Inactivation of cyclin-dependent kinase 5 in hair cells causes hearing loss in mice. *Front. Mol. Neurosci.* (**2018**) 137.Nunbhakdi-Craig, V. *et a*l. Protein phosphatase 2A associates with and regulates atypical PKC and the epithelial tight junction complex. *J. Cell Biol*. (158) (**2002**).

138. Schuhmacher, D., Sontag, J. M. & Sontag, E. Protein phosphatase 2A: More than a passenger in the regulation of epithelial cell-cell junctions. *Frontiers in Cell and Developmental Biology* (7) (**2019**).

139. Goudreault, M. *et al.* A PP2A phosphatase high density interaction network identifies a novel striatin-interacting phosphatase and kinase complex linked to the cerebral cavernous malformation 3 (CCM3) protein. *Mol. Cell. proteomics* (8) 157–171 (**2009**).

140. Hwang, J. & Pallas, D. STRIPAK complexes: structure, biological function, and involvement in human diseases. *Int J Biochem Cell Biol* (Feb) 118–148 (**2014**).

141. Shi, Z., Jiao, S. & Zhou, Z. STRIPAK complexes in cell signaling and cancer. *Oncogene* (35) 1–9 (**2016**).

142. Pöggeler, S. & Kück, U. A WD40 Repeat Protein Regulates Fungal Cell Differentiation and Can Be Replaced Functionally by the Mammalian Homologue Striatin A WD40 Repeat Protein Regulates Fungal Cell Differentiation and Can Be Replaced Functionally by the Mammalian Homologue Striat. *Eukaryot Cell* (3), 232–240 (**2004**).

143. Hyodo, T. *et al*. Misshapen-like kinase 1 (MINK1) is a novel component of striatin-interacting phosphatase and kinase (STRIPAK) and is required for the completion of cytokinesis. *J. Biol. Chem.* (**2012**)

144. Gordon, J. *et al*. Protein phosphatase 2a (PP2A) binds within the oligomerization domain of striatin and regulates the phosphorylation and activation of the mammalian Ste20-Like kinase Mst3. *BMC Biochem*. (**2011**).

145. Havugimana, P. C. *et al*. A census of human soluble protein complexes. *Cell* (**2012**).

146. McNally, K. P., Bazirgan, O. A. & McNally, F. J. Two domains of p80 katanin regulate microtubule severing and spindle pole targeting by p60 katanin. *J. Cell Sci.* (**2000**).

147. Schulte, J. *et al.* DMob4/Phocein regulates synapse formation, axonal transport, and microtubule organization. *J Neurosci* (30) 5189–5203 (**2010**).

148. Baillat, G. *et al*. Molecular cloning and characterization of phocein, a protein found from the Golgi complex to dendritic spines. *Mol. Biol. Cell* (12) 663–673 (**2001**).

149. Baillat, G., Gaillard, S., Castet, F. & Monneron, A. Interactions of phocein with nucleoside-diphosphate kinase, Eps15, and dynamin I. *J. Biol. Chem.* (277) 18961–18966 (**2002**).

150. Luca, F. C. & Winey, M. Mob1, an essential yeast gene required for completion of mitosis and maintenance of ploidy. *Mol. Biol. Cell* (**1998**)151. Trammell, M., Mahoney, N., Agard, D. & Vale, R. Mob4 plays a role in spindle focusing in *Drosophila* S2 cells. *J Cell Sci* (Apr) 1284–1292 (**2008**).

152. Sugden, P. H., McGuffin, L. J. & Clerk, A. SOcK, MiSTs, MASK and STicKs: The GCKIII (germinal centre kinase III) kinases and their heterologous protein-protein interactions. *Biochemical Journal* (**2013**).

153. Delpire, E. The mammalian family of sterile 20p-like protein kinases. *Pflugers Archiv European Journal of Physiology* (**2009**)

154. Ribeiro, P. S. *et al.* Combined Functional Genomic and Proteomic Approaches Identify a PP2A Complex as a Negative Regulator of Hippo Signaling. *Mol. Cell* (39) 521–534 (**2010**).

155. Couzens, A. L. *et al.* Protein Interaction Network of the Mammalian Hippo Pathway Reveals Mechanisms of Kinase-Phosphatase Interactions. *Sci. Signal.* 6(302): (**2013**).

156. Kean, M. *et al.* Structure-function analysis of core STRIPAK Proteins: a signaling complex implicated in Golgi polarization. *J Biol Chem* (Jul 15) 25065–25075 (**2011**).

157. Frey, S. The STRIPAK complex and its role in fruiting-body development of the filamentous fungus *Sordaria macrospora*. (*Georg-August-Universität Göttingen*, **2015**).

158. Bastos, R. N. & Barr, F. A. Plk1 negatively regulates Cep55 recruitment to the midbody to ensure orderly abscission. *J. Cell Biol.* (**2010**)

159. Steigemann, P. *et al.* Aurora B-Mediated Abscission Checkpoint Protects against Tetraploidization. *Cell* (**2009**)

160. Kim, J. W. *et al.* STRIPAK directs PP2A activity toward MAP4K4 to promote oncogenic transformation of human cells. *Elife* (**2020**).

161. Yao, Z. *et al*. A novel human STE20-related protein kinase, HGK, that specifically activates the c-Jun N-terminal kinase signaling pathway. *J. Biol. Chem*. (**1999**)

162. Meng, Z. *et al.* MAP4K family kinases act in parallel to MST1/2 to activate LATS1/2 in the Hippo pathway. *Nat. Commun.* (**2015**).

163. Mack, G. J. & Compton, D. A. Analysis of mitotic microtubule-associated proteins using mass spectrometry identifies astrin, a spindle-associated protein. *Proc. Natl. Acad. Sci. U. S. A.* (**2001**)

164. Liska, A. J. *et al.* Homology-based functional proteomics by mass spectrometry: Application to the *Xenopus* microtubule-associated proteome. *Proteomics* (**2004**).

165. Tegha-Dunghu, J. *et al*. EML3 is a nuclear microtubule-binding protein required for the correct alignment of chromosomes in metaphase. *J. Cell Sci.* (**2008**)

166. Sauer, G. *et al*. Proteome analysis of the human mitotic spindle. *Mol. Cell. Proteomics* (**2005**)

167. Malik, R. *et al*. Quantitative analysis of the human spindle phosphoproteome at distinct mitotic stages. *J. Proteome Res.* (**2009**) .

168. Nousiainen, M., Silljé, H. H. W., Sauer, G., Nigg, E. A. & Körner, R. Phosphoproteome analysis of the human mitotic spindle. *Proc. Natl. Acad. Sci. U. S. A.* (**2006**)

169. Reber, S. B. *et al.* XMAP215 activity sets spindle length by controlling the total mass of spindle microtubules. *Nat. Cell Biol.* (15) 1116–1122 (**2013**).

170. Hatch, E. M., Kulukian, A., Holland, A. J., Cleveland, D. W. & Stearns, T. Cep152 interacts with Plk4 and is required for

centriole duplication. *J. Cell Biol*. (191) 721–729 (**2010**).

171. Gilbert, S. F. & Barresi, M. J. F. d*Am. J. Med. Genet. Part A* (**2017**).

172. Murray, A. W. Cell cycle extracts. *Methods Cell Biol*. (**1991**).

173. Tunquist, B. J. & Maller, J. L. Under arrest: cytostatic factor (CSF)-mediated metaphase arrest in vertebrate eggs. *Genes Dev* (Mar 15) 683–710 (**2003**).

174. Schmidt, A., Rauh, N. R., Nigg, E. A. & Mayer, T. U. Cytostatic factor: An activity that puts the cell cycle on hold. *J. Cell Sci.* (119) 1213–1218 (**2006**).

175. Tischer, T., Hörmanseder, E. & Mayer, T. U. The APC/C inhibitor Xerp1/Emi2 is essential fo*r Xenopus* early embryonic divisions. *Science* (80). (**2012**).

176. Hansen, D. V., Tung, J. J. & Jackson, P. K. CaMKII and Polo-like kinase 1 sequentially phosphorylate the cytostatic factor Emi2/XErp1 to trigger its destruction and meiotic exit. *Proc. Natl. Acad. Sci. U. S. A*. (**2006**)

177. Rauh, N. R., Schmidt, A., Bormann, J., Nigg, E. A. & Mayer, T. U. Calcium triggers exit from meiosis II by targeting the APC/C inhibitor XErp1 for degradation. *Nature* (**2005**).

178. Liu, J. & Maller, J. L. Calcium elevation at fertilization coordinates phosphorylation of XErp1/Emi2 by Plx1 and CaMK II to release metaphase arrest by cytostatic factor. *Curr. Biol.* (15) (**2005**).

179. Reber, S., Over, S., Kronja, I. & Gruss, O. J. CaM kinase II initiates meiotic spindle depolymerization independently of APC/C activation. *J. Cell Biol.* (183) 1007–1017 (**2008**).

180. Levasseur, M. *et al.* Release from meiotic arrest in ascidian eggs requires the activity of two phosphatases but not CAMKII. *Dev.* (**2013**).

181. Shoji, S. *et al*. Mammalian Emi2 mediates cytostatic arrest and transduces the signal for meiotic exit via Cdc20. *EMBO J*. (**2006**).

182. Madgwick, S., Levasseur, M. & Jones, K. T. Calmodulin-dependent protein kinase II, and not protein kinase C, is sufficient for triggering cell-cycle resumption in mammalian eggs. *J. Cell Sci*. (**2005**).

183. Suzuki, T. *et al*. Mouse Emi2 as a distinctive regulatory hub in second meiotic metaphase. *Development* (**2010**).

184. Blow, J. J. & Laskey, R. A. Initiation of DNA replication in nuclei and purified DNA by a cell-free extract of *Xenopus* eggs. *Cell* (**1986**).

185. Cavazza, T., Peset, I. & Vernos, I. From meiosis to mitosis - the sperm centrosome defines the kinetics of spindle assembly after fertilization in *Xenopus. J. Cell Sci.* (**2016**).

186. Cavazza, T., Malgaretti, P. & Vernos, I. The sequential activation of the mitotic microtubule assembly pathways favors bipolar spindle formation. *Mol. Biol. Cell* (27) (**2016**).

187. Manandhar, G., Schatten, H. & Sutovsky, P. Centrosome Reduction During Gametogenesis and Its Significance1. *Biol. Reprod.* (**2005**)

188. Szollosi, D., Calarco, P. & Donahue, R. P. Absence of centrioles in the first and second meiotic spindles of mouse oocytes. *J. Cell Sci.* (**1972**).

189. Delattre, M. & Gönczy, P. The arithmetic of centrosome biogenesis. *Journal of Cell Science* (**2004**)

190. Borrego-Pinto, J. *et al*. Distinct mechanisms eliminate mother and daughter centrioles in meiosis of starfish oocytes. *J. Cell Biol.* (**2016**)

191. Mikeladze-Dvali, T. *et al*. Analysis of centriole elimination during *C. elegans* oogenesis. *Development* (**2012**).

192. Pimenta-Marques, A. *et al.* A mechanism for the elimination of the female gamete centrosome in *Drosophila melanogaster. Science* (80). (**2016**)

193. Gruss, O. Animal Female Meiosis: The Challenges of Eliminating Centrosomes. *Cells* (**2018**).

194. Wueseke, O. *et al.* Polo-like kinase phosphorylation determines *Caenorhabditis elegans* centrosome size and density by biasing SPD-5 toward an assembly-competent conformation. *Biol. Open* (5) (**2016**).

195. Choi, Y. K., Liu, P., Sze, S. K., Dai, C. & Qi, R. Z. CDK5RAP2 stimulates microtubule nucleation by the γ-tubulin ring complex. *J. Cell Biol.* (**2010**).

196. Gomez-Ferreria, M. A. *et al.* Novel NEDD1 phosphorylation sites regulate γ-tubulin binding and mitotic spindle assembly. *J. Cell Sci.* (**2012**)

197. Cota, R. R. *et al.* MZT1 regulates microtubule nucleation by linking γTuRC assembly to adapter-mediated targeting and activation. *J. Cell Sci.* **(2017)**

198. Lin, T. C. *et al.* MOZ ART1 and γ-tubulin complex receptors are both required to turn γ-TuSC into an active microtubule nucleation template. *J. Cell Biol*. (**2016**)

199. Job, D., Valiron, O. & Oakley, B. Microtubule nucleation. *Current Opinion in Cell Biology* (**2003**) 200. Kollman, J. M., Polka, J. K., Zelter, A., Davis, T. N. & Agard, D. A. Microtubule nucleating γ 3-TuSC assembles structures with 13-fold microtubule-like symmetry. *Nature* (**2010**).

201. Schatz, C. A. *et al*. Importin α-regulated nucleation of microtubules by TPX2. *EMBO J*. (**2003**).

202. Scrofani, J., Sardon, T., Meunier, S. & Vernos, I. Microtubule nucleation in mitosis by a RanGTP-dependent protein complex. *Curr. Biol*. (**2015**).

203. Gruss, O. J. O. . *et al.* Ran induces spindle assembly by reversing the inhibitory effect of importin α on TPX2 activity. *Cell* (104) 83–93 (**2001**).

204. Clarke, P. R. & Zhang, C. Spatial and temporal coordination of mitosis by Ran GTPase. *Nature Reviews Molecular Cell Biology* (**2008**).

205. Nakamura, M. *et al*. When overexpressed, a novel centrosomal protein, RanBPM, causes ectopic microtubule nucleation similar to γ-tubulin. J. Cell Biol. (1998) doi:10.1083/jcb.143.4.1041.

206. Zierhut, C., Jenness, C., Kimura, H. & Funabiki, H. Nucleosomal regulation of chromatin composition and nuclear assembly revealed by histone depletion. *Nat. Struct. Mol. Biol*. (21) 617–625 (**2014**).

207. Carazo-Salas, R. E. *et al*. Generation of GTP-bound ran by RCC1 is required for chromatin-induced mitotic spindle formation. *Nature* (**1999**).

208. Kubo, A., Sasaki, H., Yuba-Kubo, A., Tsukita, S. & Shiina, N. Centriolar satellites: Molecular characterization, ATP-dependent movement toward centrioles and possible involvement in ciliogenesis. *J. Cell Biol.* (147) 969–979 (**1999**).

209. Dobbelaere, J. *et al.* A genome-wide RNAi screen to dissect centriole duplication and centrosome maturation in *Drosophila*. *PLoS Biol*. (**2008**)

210. Lee, K. & Rhee, K. PLK1 phosphorylation of pericentrin initiates centrosome maturation at the onset of mitosis. *J. Cell Biol.* (**2011**).

211. Conduit, P. T. *et al*. The centrosome-specific phosphorylation of Cnn by Polo/Plk1 drives Cnn scaffold assembly and centrosome maturation. *Dev. Cell* (**2014**).

212. Feng, Z. *et al.* Structural Basis for Mitotic Centrosome Assembly in Flies. *Cell* (**2017**)

213. Woodruff, J. B. *et al*. Regulated assembly of a supramolecular centrosome scaffold *in vitro. Science* (80). (**2015**).

214. Woodruff, J. B. *et a*l. The Centrosome Is a Selective Condensate that Nucleates Microtubules by Concentrating Tubulin. *Cell* (**2017**)

215. Liu, Q., Yu, J., Zhuo, X., Jiang, Q. & Zhang, C. Pericentrin contains five NESs and an NLS essential for its nucleocytoplasmic trafficking during the cell cycle. *Cell Res.* (**2010**).

216. Kim, S. & Rhee, K. Importance of the CEP215-pericentrin interaction for centrosome maturation during mitosis. *PLoS One* (**2014**)

217. Liu, P. *et al.* Insights into the assembly and activation of the microtubule nucleator γ-TuRC. *Nature Dec (*19) (**2019**).

218. Lüders, J., Patel, U. K. & Stearns, T. GCP-WD is a γ-tubulin targeting factor required for centrosomal and chromatin-mediated microtubule nucleation. *Nat. Cell Biol.* (**2006**) .

219. Sdelci, S. *et al*. Nek9 phosphorylation of NEDD1/GCP-WD contributes to Plk1 control of γ-tubulin recruitment to the mitotic centrosome. *Curr. Biol.* (**2012**) 220. De Jamblinne, C. V. *et al.* STRIPAK regulates Slik localization to control mitotic morphogenesis and epithelial integrity. *J. Cell Biol.* (219) (**2020**).

221. Pinyol, R., Scrofani, J. & Vernos, I. The role of NEDD1 phosphorylation by aurora a in chromosomal microtubule nucleation and spindle function. *Curr. Biol.* (**2013**) 222. Özlü, N. *et al.* An essential function of the *C. elegans* ortholog of TPX2 is to localize activated Aurora A Kinase to Mitotic Spindles. *Dev. Cell* (**2005**).

223. Hannak, E., Kirkham, M., Hyman, A. A. & Oegema, K. Aurora-A kinase is required for centrosome maturation in *Caenorhabditis elegans*. *J. Cell Biol.* (**2001**).

224. Vasquez, R. J., Gard, D. L. & Cassimeris, L. Phosphorylation by CDK1 regulates XMAP215 function *in vitro. Cell Motil. Cytoskeleton* (43) (**1999**).

225. Brouhard, G. J. *et al.* XMAP215 Is a Processive Microtubule Polymerase. *Cell* (132) (**2008**).

226. Hernández-Vega, A. *et al*. Local Nucleation of Microtubule Bundles through Tubulin Concentration into a Condensed Tau Phase. *Cell Rep*. (20) (**2017**).

227. King, M. R. & Petry, S. Phase separation of TPX2 enhances and spatially coordinates microtubule nucleation. *Nat. Commun*. (11) (**2020**).

228. Conduit, P. T. *et al*. Centrioles regulate centrosome size by controlling the rate of Cnn incorporation into the PCM. *Curr. Biol.* (**2010**).

229. Fong, K. W., Choi, Y. K., Rattner, J. B. & Qi, R. Z. CDK5RAP2 is a pericentriolar protein that functions in centrosomal attachment of the γ-tubulin ring complex. *Mol. Biol. Cell* (**2008**)

230. Fong, K. W. *et al*. Interaction of CDK5RAP2 with EB1 to track growing microtubule tips and to regulate microtubule dynamics. *Mol. Biol. Cell* (**2009**)

231. Su, L. K. *et al*. APC Binds to the Novel Protein EB. *Cancer Res*. (**1995**).

232. Kronja, I., Kruljac-Letunic, A., Caudron-Herger, M., Bieling, P. & Karsenti, E. XMAP215-EB1 interaction is required for proper spindle assembly and chromosome segregation in *Xenopus* egg extract. *Mol Biol Cell* (Jun 20) 2684–2696 (**2009**).

233. Pesin, J. A. & Orr-Weaver, T. L. Regulation of APC/C Activators in Mitosis and Meiosis. *Annu. Rev. Cell Dev. Biol.* (**2008**)

234. Castro, A., Bernis, C., Vigneron, S., Labbé, J. C. & Lorca, T. The anaphase-promoting complex: A key factor in the regulation of cell cycle. *Oncogene* (**2005**)

235. Gharbi-Ayachi, A. *et al*. The substrate of Greatwall kinase, Arpp19, controls mitosis by inhibiting protein phosphatase 2A. *Science* (80). (**2010**).

236. Mochida, S., Maslen, S. L., Skehel, M. & Hunt, T. Greatwall phosphorylates an inhibitor of protein phosphatase 2A that is essential for mitosis. *Science* (80). (**2010**) .

237. Willems, E. *et al*. The functional diversity of Aurora kinases: A comprehensive review. *Cell Division* (**2018**)

238. Liu, Q. & Ruderman, J. V. Aurora A, mitotic entry, and spindle bipolarity. *Proc. Natl. Acad. Sci. U. S. A*. (**2006**)

239. Reboutier, D., Benaud, C. & Prigent, C. Aurora A's functions during mitotic exit: The guess who game. *Frontiers in Oncology* (**2015**)

240. Afonso, O. *et al*. Spatiotemporal control of mitotic exit during anaphase by an aurora B-Cdk1 crosstalk. *Elife* (**2019**)

241. Krenn, V. & Musacchio, A. The Aurora B kinase in chromosome bi-orientation and spindle checkpoint signaling. *Frontiers in Oncology* (**2015**)

242. Bolanos-Garcia, V. M. & Blundell, T. L. BUB1 and BUBR1: Multifaceted kinases of the cell cycle. *Trends in Biochemical Sciences* (**2011**) 243.Xu, P., Virshup, D. M. & Lee, S. H. B56-PP2A regulates motor dynamics for mitotic chromosome alignment. *J. Cell Sci.* 127 4567–4573 (**2014**).

244. Skelding, K. A., Rostas, J. A. P. & Verrills, N. M. Controlling the cell cycle: The role of calcium/calmodulin-stimulated protein kinases I and II. *Cell Cycle* (**2011**) 245. Lorca, T. *et al.* Calmodulin-dependent protein kinase II mediates inactivation of MPF and CSF upon fertilization of *xenopus* eggs. *Nature* (**1993**).

246. Beauman, S. R., Campos, B., Kaetzel, M. A. & Dedman, J. R. CyclinB1 expression is elevated and mitosis is delayed in HeLa cells expressing autonomous CaMKII. *Cell. Signal.* (**2003**).

247. Voss, K. *et al.* CCM3 interacts with CCM2 indicating common pathogenesis for cerebral cavernous malformations. *Neurogenetics* (8) 249–256 (**2007**).

248. Amos, L. A. & Schlieper, D. Microtubules and maps. *Adv. Protein Chem*. (71) 257–298 (**2005**).

249. Nunbhakdi-Craig, V. *et al.* Expression of protein phosphatase 2A mutants and silencing of the regulatory B alpha subunit induce a selective loss of acetylated and detyrosinated microtubules. *J. Neurochem*. (101) 959–971 (**2007**).

250. Frey, S., Reschka, E. J. & Pöggeler, S. Germinal center kinases SmKIN3 and SmKIN24 are associated with the *Sordaria macrospora* striatin-interacting phosphatase and kinase (STRIPAK) complex. *PLoS One* (**2015**).

251. Gavet, O. & Pines, J. Progressive Activation of CyclinB1-Cdk1 Coordinates Entry to Mitosis. *Dev. Cell* (**2010**)

252. Popov, A. V. *et al.* XMAP215 regulates microtubule dynamics through two distinct domains. *EMBO J.* (**2001**) 253. Pereira, A. L. *et al.* Mammalian CLASP1 and CLASP2 cooperate to ensure mitotic fidelity by regulating spindle and kinetochore function. *Mol. Biol. Cell* (**2006**)254. Bieling, P. *et al*. Reconstitution of a microtubule plus-end tracking system *in vitro. Nature* (450) 1100–1105 (**2007**).

255. Gupta, K. K. *et al*. Probing Interactions between CLIP-170, EB1, and Microtubules. *J. Mol. Biol.* (**2010**)

256. Hung, L. Y., Chen, H. L., Chang, C. W., Li, B. R. & Tang, T. K. Identification of a novel microtubule-destabilizing motif in CPAP that binds to tubulin heterodimers and inhibits microtubule assembly. *Mol. Biol. Cell* (**2004**)

257. Home, H. *et al.* MAPRE1 (Microtubule-associated protein, RP/EB family, member 1). (1), 1–7 (**2017**).

258. Tirnauer, J. S. & Bierer, B. E. EB1 proteins regulate microtubule dynamics, cell polarity, and chromosome stability. *Journal of Cell Biology* (149) 761–766 (**2000**).

259. Zimniak, T., Stengl, K., Mechtler, K. & Westermann, S. Phosphoregulation of the budding yeast EB1 homologue Bim1p by Aurora/Ipl1p. *J. Cell Biol*. (186) 379–391 (**2009**).

260. Camlin, N. J., McLaughlin, E. A. & Holt, J. E. Motoring through: The role of kinesin superfamily proteins in female meiosis. H*um. Reprod. Update* (**2017**)261. Chen, G. Y. *et al.* Eg5 Inhibitors Have Contrasting Effects on Microtubule Stability and Metaphase Spindle Integrity. *ACS Chem. Biol.* (**2017**)

262. Tanenbaum, M. E. *et al.* A complex of Kif18b and MCAK promotes microtubule depolymerization and is negatively regulated by aurora kinases. *Curr. Biol*. (**2011**).

263. Hori, A. & Toda, T. Regulation of centriolar satellite integrity and its physiology. *Cellular and Molecular Life Sciences* (**2016**)

264. Dammermann, A. & Merdes, A. Assembly of centrosomal proteins and microtubule organization depends on PCM-1. *J. Cell Biol.* (**2002**).

265. Kim, J., Kim, J. & Rhee, K. PCNT is critical for the association and conversion of centrioles to centrosomes during mitosis. *J. Cell Sci*. (**2019**).

266. Kleylein-Sohn, J. *et al.* Plk4-Induced Centriole Biogenesis in Human Cells. *Dev. Cell* (13) 190–202 (**2007**).

267. Tournebize, R. *et al.* Distinct roles of PP1 and PP2A-like phosphatases in control of microtubule dynamics during mitosis. *EMBO J*. (16) 5537–5549 (**1997**).

268. Hastie, C. J. & Cohen, P. T. W. Purification of protein phosphatase 4 catalytic subunit: Inhibition by the antitumour drug fostriecin and other tumour suppressors and promoters. *FEBS Lett.* (431) 357–361 (**1998**).

269. Kutay, U., Izaurralde, E., Bischoff, F. R., Mattaj, I. W. & Görlich, D. Dominant-negative mutants of importin-β block multiple pathways of import and export through the nuclear pore complex. *EMBO J*. (**1997**) 270. Dumont, J. *et al*. A centriole- and RanGTP-independent spindle assembly pathway in meiosis I of vertebrate oocytes. *J. Cell Biol*. (**2007**)

271. Inoue, D. *et al.* Expression of the novel maternal centrosome assembly factor Wdr8 is required for vertebrate embryonic mitoses. *Nat. Commun*. (8) (**2017**).

272. Kurtulmus, B. *et al.* WDR8 is a centriolar satellite and centriole-associate protein that promotes ciliary vesicle docking during ciliogenesis. *J. Cell Sci.* (8) 621–636 (**2015**).

273. Gruss, O. J. *et al*. Chromosome-induced microtubule assembly mediated by TPX2 is required for spindle formation in HeLa cells. *Nat. Cell Biol.* (**2002**) 274. Alfaro-Aco, R., Thawani, A. & Petry, S. Structural analysis of the role of TPX2 in branching microtubule nucleation. *J. Cell Biol*. (216) 983–997 (**2017**).

275. Li, W. *et al.* EB1 promotes microtubule dynamics by recruiting Sentin in *Drosophila* cells. *J. Cell Biol.* (**2011**).

276. Bakhoum, S. F., Genovese, G. & Compton, D. A. Deviant Kinetochore Microtubule Dynamics Underlie Chromosomal Instability. *Curr. Biol*. (**2009**) .

277. Domnitz, S. B., Wagenbach, M., Decarreau, J. & Wordeman, L. MCAK activity at microtubule tips regulates spindle microtubule length to promote robust kinetochore attachment. *J. Cell Biol*. (**2012**)

278. Zanic, M., Widlund, P. O., Hyman, A. A. & Howard, J. Synergy between XMAP215 and EB1 increases microtubule growth rates to physiological levels. *Nat. Cell Biol.* (15) 688–693 (**2013**).

279. Akhmanova, A. & Steinmetz, M. O. Tracking the ends: A dynamic protein network controls the fate of microtubule tips. *Nature Reviews Molecular Cell Biology* (**2008**) 280. Kline-Smith, S. L., Khodjakov, A., Hergert, P. & Walczak, C. E. Depletion of Centromeric MCAK Leads to Chromosome Congression and Segregation Defects Due to Improper Kinetochore Attachments. *Mol. Biol. Cell* (**2004**) 281. Laemmli, U. K. Cleavage of Structural Proteins during the Assembly of the Head of Bacteriophage T4. *Nature* (227) 680–685 (**1970**).

282. Brinkley, B. R. Microtubule organizing centers. Annual review of cell biology (**1985**).

283. Moses, R. M. & Masui, Y. Cytostatic factor (CSF) activity in cytosols extracted from *Xenopus laevis* eggs. *Exp. Cell Res*. (**1990**)

284. Sezonov, G., Joseleau-Petit, D. & D'Ari, R. *Escherichia coli* physiology in Luria-Bertani broth. *J. Bacteriol. (*189), 8746–

8749 (**2007**).

285. Bertani, G. The Mode of Phage Liberation by Lysogenic *Escherichia coli*1. *J. Bacteriol*. (**1951**).

286. Hanahan, D. & Harbor, C. S. Studies on transformation of *Escherichia coli* with plasmids. *J. Mol. Bio.* (166) 557–580 (**1983**).

287. Studier, F. W. & Moffatt, B. A. Use of bacteriophage T7 RNA polymerase to direct selective high-level expression of cloned genes. *J. Mol. Bio.* (189) 113–130 (**1986**).

288. Branon, T. C. *et al.* Efficient proximity labeling in living cells and organisms with TurboID. *Nature Biotechnology* (**2018**)

289. Stewart, M., Kent, H. M. & McCoy, A. J. The structure of the Q69L mutant of GDP-Ran shows a major conformational change in the switch II loop that accounts for its failure to bind nuclear transport factor 2 (NTF2). *J. Mol. Biol.* (**1998**).

290. Kim, D. *et al.* An improved smaller biotin ligase for BioID proximity labeling. *J. Chem. Inf. Model*. (Apr 15) 1188–1196 (**2016**).

291. Gökirmak, T. *et al.* Localization and substrate selectivity of sea urchin multidrug (MDR) efflux transporters. *J. Biol. Chem.* (**2012**)

292. Husedzinovic, A. *et al.* Phosphoregulation of the human SMN complex. *Eur. J. Cell Biol.* (93), 106–117 (**2014**).

293. Bimboim, H. C. & Doly, J. A rapid alkaline extraction procedure for screening recombinant plasmid DNA. *Nucleic Acids Res.* (**1979**).

294. Porath, J., Carlsson, J., Olsson, I. & Belfrage, G. Metal chelate affinity chromatography, a new approach to protein fractionation. *Nature* (Dec 18), 598–599 (**1975**).

295. Box, J. F. Guinness, gosset, fisher, and small samples. *Stat. Sci.* (**1987**).

296. Kuge, H. & Richter, J. D. Cytoplasmic 3′ poly(A) addition induces 5′ cap ribose methylation: implications for translational control of maternal mRNA. *EMBO J.* (**1995**)

297. Gurdon, J. B. Changes in somatic cell nuclei inserted into growing and maturing amphibian oocytes. *J. Embryol. Exp. Morphol.* (**1968**).

298. Sawin, K. E. & Mitchison, T. J. Mitotic spindle assembly by two different pathways *in vitro*. *J. Cell Biol*. (**1991**)

299. Heald, R. *et al*. Self-organization of microtubules into bipolar spindles around artificial chromosomes in *Xenopus* egg extracts. *Nature* (**1996**)300. Philpott, A., Leno, G. H. & Laskey, R. A. Sperm decondensation in *Xenopus* egg cytoplasm is mediated by nucleoplasmin. *Cell* (**1991**) 301. Hyman, A. *et al*. Preparation of modified tubulins. *Methods Enzymol.* (**1991**)

302. Desai, A., Verma, S., Mitchison, T. J. & Walczak, C. E. Kin I kinesins are microtubule-destabilizing enzymes. *Cell* (96) 69–78 (**1999**).

303. Maresca, T. J. & Heald, R. Methods for studying spindle assembly and chromosome condensation in *Xenopus* egg extracts. *Methods in molecular biology* (**2006**) 304. Kaboord, B. & Perr, M. Isolation of proteins and protein complexes by immunoprecipitation. *Methods in molecular biology* (**2008**)

305. Miernyk, J. A. & Thelen, J. J. Biochemical approaches for discovering protein-protein interactions. *Plant J*. (**2008**) 306. Kerényi, L. & Gallyas, F. Über probleme der quantitativen auswertung der mit physikalischer entwicklung versilberten agarelektrophoretogramme. *Clin. Chim. Acta (*47) (**1973**).

307. Gaudernack, G., Leivestad, T., Ugelstad, J. & Thorsby, E. Isolation of pure functionally active CD8+ T cells positive selection with monoclonal antibodies directly conjugated to monosized magnetic microspheres. *J. Immunol. Methods* (**1986**)

308. Sloboda, R. D. Isolation of microtubules and microtubule-associated proteins using paclitaxel. *Cold Spring Harb. Protoc*. (**2015**).

309. Harrington, E. A. *et al.* VX-680, a potent and selective small-molecule inhibitor of the Aurora kinases, suppresses tumor growth *in vivo*. *Nat. Med.* (**2004**)

310. Roux, K. J., Kim, D. I., Raida, M. & Burke, B. A promiscuous biotin ligase fusion protein identifies proximal and interacting proteins in mammalian cells. *J. Cell Biol*. (196) 801–810 (**2012**).

311. Tong, L. Structure and function of biotin-dependent carboxylases. *Cellular and Molecular Life Sciences* (**2013**).

312. Chomczynski, P. & Sacchi, N. Single-step method of RNA isolation by acid guanidinium thiocyanate-phenol-chloroform extraction. *Anal. Biochem*. (**1987**) 313. Altschul, S. F., Gish, W., Miller, W., Myers, E. W. & Lipman, D. J. Basic local alignment search tool. *J. Mol. Biol.* (**1990**)

314. Bateman, A. *et al.* UniProt: The universal protein knowledgebase. *Nucleic Acids Res*. (**2017**).

315. Kronja, I., Kruljac-Letunic, A., Caudron-Herger, M., Bieling, P. & Karsent, E. XMAP215-EB1 interaction is required for proper spindle assembly and chromosome segregation in *Xenopus* egg extract. *Mol. Biol. Cell* (**2009**)

316. Goshima, G. Identification of a TPX2-like microtubule-associated protein in *Drosophila*. *PLoS One* (**2011**)

317. Baumgarten, T. *et al.* Isolation and characterization of the *E. coli* membrane protein production strain Mutant56(DE3). *Sci. Rep.* (7) (**2017**).

318. Ferrer, M., Chernikova, T. N., Yakimov, M. M., Golyshin, P. N. & Timmis, K. N. Chaperonins govern growth of *Escherichia coli* at low temperatures. *Nat. Biotechnol.* (**2003**).

319. Lahav-Ariel, L. *et al.* Striatin is a novel modulator of cell adhesion. *FASEB J.* (**2019**)

320. Schultz, R. M., Stein, P. & Svoboda, P. The oocyte-to-embryo transition in mouse: Past, present, and future. *Biology of Reproduction* (99) (**2018**).

321. Masui, Y. & Wang, P. Cell cycle transition in early embryonic development of *Xenopus laevis*. *Biol. Cell* (90) (1998).

322. Gruss, O. J. *et al*. Ran induces spindle assembly by reversing the inhibitory effect of importin α on TPX2 activity. *Cell* (**2001)**

323. Sulimenko, V. *et al.* Association of brain γ-tubulins with αβ-tubulin dimers. *Biochem. J.* (365) (**2002**).

324. Paul Chang & Tim Stearns. δ-Tubulin and ε-tubulin: two new human centrosomal tubulins reveal new aspects of centrosome structure and function. *Nat. Cell Biol*. (2) 30–35 (**1999**).

325. Schilling, M. *et al*. TOR signaling regulates liquid phase separation of the SMN complex governing snRNP biogenesis. *Cell Rep*. (35) (**2021**).

326. Kahl, C. R. & Means, A. R. Regulation of Cell Cycle Progression by Calcium/Calmodulin-Dependent Pathways. *Endocrine Reviews* (24) (**2003**).

327. Tokmakov, A. A., Stefanov, V. E., Iwasaki, T., Sato, K. I. & Fukami, Y. Calcium signaling and meiotic exit at fertilization in *Xenopus* egg. *International Journal of Molecular Sciences* (**2014**)

328. Chin, D. & Means, A. R. Calmodulin: A prototypical calcium sensor. *Trends in Cell Biology* (10) (**2000**).

329. Taagepera, S., Dent, P., Her, J. H., Sturgill, T. W. & Gorbsky, G. J. The MPM-2 antibody inhibits mitogen-activated protein kinase activity by binding to an epitope containing phosphothreonine-183. *Mol. Biol. Cell* (5) (**1994**).

330. Castellano-Pozo, M., García-Muse, T. & Aguilera, A. The *Caenorhabditis elegans* THO Complex Is Required for the Mitotic Cell Cycle and Development. *PLoS One* (7) (**2012**).

331. Kolev, N. G. & Steitz, J. A. Symplekin and multiple other polyadenylation factors participate in 3-end maturation of histone mRNAs. (**2005**)

332. Yeong, F. M. *et al.* Identification of a Subunit of a Novel Kleisin-β/SMC Complex as a Potential Substrate of Protein Phosphatase 2A. *Curr. Biol.* (13) (**2003**).

333. Tolg, C. *et al*. RHAMM promotes interphase microtubule instability and mitotic spindle integrity through MEK1/ERK1/2 activity. *J. Biol. Chem*. (285) (**2010**).

334. Wu, W. Da, Yu, K. W., Zhong, N., Xiao, Y. & She, Z. Y. Roles and mechanisms of Kinesin-6 KIF20A in spindle organization during cell division. *European Journal of Cell Biology* (98) (**2019**).

335. Nader, M., Khalil, B., Kattuah, W., Dzimiri, N. & Bakheet, D. Striatin translocates to the cytosol of apoptotic cells and is proteolytically cleaved in a caspase 3-dependent manner. *Heliyon 6*, (**2020**).

336. Bartoli, M., Monneron, A. & Ladant, D. Interaction of calmodulin with striatin, a WD-repeat protein present in neuronal dendritic spines. *J. Biol. Chem*. (273) (**1998**).

337. Holden, P. & Horton, W. A. Crude subcellular fractionation of cultured mammalian cell lines. *BMC Res. Notes* (**2009**)
338. Maxwell, C. A. *et al.* RHAMM is a centrosomal protein that interacts with dynein and maintains spindle pole stability. *Mol. Biol. Cell* (14) (2003).

339. Zhang, X. *et al.* Quantitative proteomics reveals novel protein interaction partners of PP2A catalytic subunit in pancreatic β-cells. *Mol. Cell. Endocrinol.* (424) (**2016**).

340. Park, H., Hong, S. & Hong, S. Nocodazole is a high-affinity ligand for the cancer-related kinases ABL, c-KIT, BRAF, and MEK. *ChemMedChem* (7) (**2012**).

341. Shimomura, T. *et al*. MK-5108, a Highly Selective Aurora-A Kinase Inhibitor, Shows Antitumor Activity Alone and in

Combination with Docetaxel. (**2010**) 342. Musacchio, A. & Salmon, E. D. The spindle-assembly checkpoint in space and time. *Nature Reviews Molecular Cell Biology* (8) (**2007**).

343. Yu, H. Structural activation of Mad2 in the mitotic spindle checkpoint: The two-state Mad2 model versus the Mad2 template model. *Journal of Cell Biology* (173) (**2006**).

344. Homer, H. A., McDougall, A., Levasseur, M., Murdoch, A. P. & Herbert, M. Mad2 is required for inhibiting securin and cyclin B degradation following spindle depolymerisation in meiosis I mouse oocytes. *Reproduction* (130) (**2005**).

345. Lange, g., mandelkow, e. -m, jagla, a. & mandelkow, e. Tubulin oligomers and microtubule oscillations: Antagonistic role of microtubule stabilizers and destabilizers. *Eur. J. Biochem.* (178) (**1988**).

346. Bordas, J., Mandelkow, E. M. & Mandelkow, E. Stages of tubulin assembly and disassembly studied by time-resolved synchrotron X-ray scattering. *J. Mol. Biol*. (164) (**1983**).

347. Goto, H., Inoko, A. & Inagaki, M. Cell cycle progression by the repression of primary cilia formation in proliferating cells. Cellular and Molecular Life Sciences vol. 70 (2013).

348. Van der Heiden, K., Egorova, A. D., Poelmann, R. E., Wentzel, J. J. & Hierck, B. P. Role for Primary Cilia as Flow Detectors in the Cardiovascular System. *International Review of Cell and Molecular Biology* (290) (**2011**).

349. Alexandrov, A. I. *et al*. Analysis of novel hyperosmotic shock response suggests 'beads in liquid' cytosol structure. (**2019**).

350. Li, J. *et al*. Protein phase separation and its role in chromatin organization and diseases. *Biomedicine and Pharmacotherapy* (138) (**2021**).

351. Seo, S. *et al*. BBS6, BBS10, and BBS12 form a complex with CCT/TRiC family chaperonins and mediate BBSome assembly. *Proc. Natl. Acad. Sci. U. S. A*. (107) (**2010**).

352. Wang, D. Y., Kamuda, K., Montoya, G. & Mesa, P. The TRiC/CCT Chaperonin and Its Role in Uncontrolled Proliferation. *Advances in Experimental Medicine and Biology* (1243) (**2020**).

353. Müller, R. *et al.* The regulatory subunit phr2AB of *Dictyostelium discoideum* phosphatase PP2A interacts with the centrosomal protein CEP161, a CDK5RAP2 ortholog. *Genes to Cells* (23) (**2018**).

354. Qin, F., Tian, J., Zhou, D. & Chen, L. Mst1 and Mst2 kinases: Regulations and diseases. *Cell and Bioscience* (3) (**2013**).

355. Chen, L. *et al.* Apoptotic functions of PDCD10/CCM3, the gene mutated in cerebral cavernous malformation 3. *Stroke* (40) (**2009**).

356. Chen, S. *et al.* SOX2 regulates apoptosis through MAP4K4-Survivin signaling pathway in human lung cancer cells. *Carcinogenesis* (35) (**2014**).

357. Wong, M. *et al*. Silencing of STRN4 suppresses the malignant characteristics of cancer cells. *Cancer Sci*. (105) (**2014**).

358. Řezníčková, E. *et al.* Activity of 2,6,9-trisubstituted purines as potent PDGFRα kinase inhibitors with antileukaemic activity. *Eur. J. Med. Chem.* (182) (**2019**).

359. Hepler, P. K. The role of calcium in cell division. *Cell Calcium* (16) (**1994**).

360. Nader, M. *et al*. Cardiac striatin interacts with caveolin-3 and calmodulin in a calcium sensitive manner and regulates cardiomyocyte spontaneous contraction rate. *Can. J. Physiol. Pharmacol*. (95) (**2017**).

361. Huang, B. *et al.* Metabolic control of Ca2+/calmodulin-dependent protein kinase II (CaMKII)-mediated caspase-2 suppression by the B55β/protein phosphatase 2A (PP2A). *J. Biol. Chem*. (289) (**2014**).

362. Hoffman, A. *et al*. Dephosphorylation of CaMKII at T253 controls the metaphase-anaphase transition. *Cell. Signal*. (26), (**2014**).

363. Sudakin, V., Chan, G. K. T. & Yen, T. J. Checkpoint inhibition of the APC/C in HeLa cells is mediated by a complex of BUBR1, BUB3, CDC20, and MAD2. *J. Cell Biol.* (154) (**2001**).

364. Kastl, J. *et al*. Mad2 Inhibitor-1 (M2I-1): A Small Molecule Protein-Protein Interaction Inhibitor Targeting the Mitotic Spindle Assembly Checkpoint. *ACS Chem. Biol*. (10) (**2015**).

365. Grallert, A. *et al.* A PP1-PP2A phosphatase relay controls mitotic progression. *Nature* (517) (**2015**).

366. Margolis, S. S. *et al*. PP1 control of M phase entry exerted through 14-3-3-regulated Cdc25 dephosphorylation. *EMBO J*. (22) (**2003**).

367. Rogers, S. *et al.* PP1 initiates the dephosphorylation of MASTL, triggering mitotic exit and bistability in human cells. *J. Cell Sci.* (129) (**2016**).

368. Holder, J., Poser, E. & Barr, F. A. Getting out of mitosis: spatial and temporal control of mitotic exit and cytokinesis by

PP1 and PP2A. *FEBS Letters* (593) (**2019**).

369. Wu, J. Q. *et al*. PP1-mediated dephosphorylation of phosphoproteins at mitotic exit is controlled by inhibitor-1 and PP1 phosphorylation. *Nat. Cell Biol.* (11) (**2009**).

370. Nilsson, J. Protein phosphatases in the regulation of mitosis. *Journal of Cell Biology* (218) (**2019**).

371. Bastos, R. N., Cundell, M. J. & Barr, F. A. KIF4A and PP2A-B56 form a spatially restricted feedback loop opposing Aurora B at the anaphase central spindle. *J. Cell Biol*. (207) (**2014**).

372. Hara, M. & Fukagawa, T. Critical Foundation of the Kinetochore: The Constitutive Centromere-Associated Network (CCAN). *Progress in molecular and subcellular biology* (**2017**)

373. Gudimchuk, N. *et al.* Kinetochore kinesin CENP-E is a processive bi-directional tracker of dynamic microtubule tips. *Nat. Cell Biol.* (15) (**2013**).

374. Lampson, M. A. & Kapoor, T. M. The human mitotic checkpoint protein BubR1 regulates chromosome-spindle attachments. *Nat. Cell Biol*. (7) (**2005**).

375. Wang, J. *et al.* Crystal structure of a PP2A B56-BubR1 complex and its implications for PP2A substrate recruitment and localization. *Protein Cell* (7) (**2016**).

376. Burkhard, P., Stetefeld, J. & Strelkov, S. V. Coiled coils: A highly versatile protein folding motif. *Trends in Cell Biology* (11) (**2001**).

377. Gaillard, S. *et al*. Targeting of proteins of the striatin family to dendritic spines: Role of the coiled-coil domain. *Traffic 7,* (**2006**).

378. Castilho, P. V., Williams, B. C., Mochida, S., Zhao, Y. & Goldberg, M. L. The M phase kinase greatwall (Gwl) promotes inactivation of PP2A/B55δ, a phosphatase directed against CDK phosphosites. *Mol. Biol. Cell* (**2009**).

379. Rangone, H. *et al.* Suppression of scant identifies endos as a substrate of greatwall kinase and a negative regulator of protein phosphatase 2a in mitosis. *PLoS Genet*. (7) (**2011**).

380. Pal, S. *et al.* CCM-3 Promotes *C. elegans* Germline Development by Regulating Vesicle Trafficking Cytokinesis and Polarity. *Curr. Biol.* (27) (**2017**).

381. Fortune, J. E. & Tsang, P. C. Production of androgen and estradiol-17β by *Xenopus* ovaries treated with gonadotropins *in vitro. Gen. Comp. Endocrinol.* (43) (**1981**).

382. Fortune, J. E. Steroid production by *Xenopus* ovarian follicles at different developmental stages. *Dev. Biol*. (99) (**1983**).

383. El-Zein, G., Boujard, D., Garnier, D. H. & Joly, J. The dynamics of the steroidogenic response of perifused *Xenopus* ovarian explants to gonadotropins. *Gen. Comp. Endocrinol.* (71) (**1988**).

384. Hu, M. W. *et al.* Scaffold subunit aalpha of PP2A is essential for female meiosis and fertility in mice. *Biol. Reprod.* (91), (**2014**).

385. Neumann, B. *et al*. Phenotypic profiling of the human genome by time-lapse microscopy reveals cell division genes. *Nature* (464), (**2010**).

386. Cornils, H., Kohler, R. S., Hergovich, A. & Hemmings, B. A. Human NDR Kinases Control G1/S Cell Cycle Transition by Directly Regulating p21 Stability. *Mol. Cell. Biol*. (31), (**2011**).

387. Sakuma, C., Okumura, M., Umehara, T., Miura, M. & Chihara, T. A STRIPAK component Strip regulates neuronal morphogenesis by affecting microtubule stability. *Sci. Rep*. (5), 17769 (**2015**).

388. Shih, P. Y., Lee, S. P., Chen, Y. K. & Hsueh, Y. P. Cortactin-binding protein 2 increases microtubule stability and regulates dendritic arborization. *J. Cell Sci.* (127) (**2014**).

389. Ramkumar, N. & Baum, B. Coupling changes in cell shape to chromosome segregation. *Nature Reviews Molecular Cell Biology* (17) (**2016**).

390. Zheng, X. *et al.* CCM3 signaling through sterile 20-like kinases plays an essential role during zebrafish cardiovascular development and cerebral cavernous malformations. *J. Clin. Invest.* (120) (**2010**).

391. Frost, A. *et al.* Functional repurposing revealed by comparing *S. pombe* and *S. cerevisiae* genetic interactions. *Cell* (**2012**)

392. Khanna, H. *et al.* RPGR-ORF15, which is mutated in retinitis pigmentosa, associates with SMC1, SMC3, and microtubule transport proteins. *J. Biol. Chem*. (280) (**2005**).

393. Wang, F. *et al.* Protein interactomes of protein phosphatase 2A B55 regulatory subunits reveal B55-mediated regulation of replication protein A under replication stress. *Sci. Rep*. (8) (**2018**).

394. Dávalos, V. *et al*. Human SMC2 protein, a core subunit of human condensin complex, is a novel transcriptional target of the WNT signaling pathway and a new therapeutic target. *J. Biol. Chem.* (287) (**2012**).

395. Schad, E. G. & Petersen, C. P. STRIPAK Limits Stem Cell Differentiation of a WNT Signaling Center to Control Planarian Axis Scaling. *Curr. Biol.* (30) (**2020**).

396. Dephoure, N. *et al.* A quantitative atlas of mitotic phosphorylation. *Proc. Natl. Acad. Sci. U. S. A.* (105) (**2008**).

397. Santamaria, A. *et al.* The Plk1-dependent phosphoproteome of the early mitotic spindle. *Mol. Cell. Proteomics* (10) (**2011**).

398. Nickel, A. geb. P. Entstehung und Morphogenese des Vorderhirns - Die Rolle des mit Mikrotubuli assoziierten Proteins Hmmr in *Xenopus laevis.* (*Universität Hohenheim*, **2020**).

399. Assmann, V., Jenkinson, D., Marshall, J. F. & Hart, I. R. The intracellular hyaluronan receptor RHAMM/IHABP interacts with microtubules and actin filaments. *J. Cell Sci.* (112) (**1999**).

400. Fong, K.-W., Choi, Y.-K., Rattner, J. B. & Qi, R. Z. CDK5RAP2 Is a Pericentriolar Protein That Functions in Centrosomal Attachment of the-Tubulin Ring Complex. *Mol. Biol. Cell* (19) 115–125 (**2008**).

401. Joseph, N. *et al*. Disease-Associated Mutations in CEP120 Destabilize the Protein and Impair Ciliogenesis. *Cell Rep.* (23) (**2018**).

402. Piel, M., Meyer, P., Khodjakov, A., Rieder, C. L. & Bornens, M. The respective contributions of the mother and daughter centrioles to centrosome activity and behavior in vertebrate cells. *J. Cell Biol.* (149) (**2000**).

403. Ko, J. Y., Lee, E. J. & Park, J. H. Interplay between primary cilia and autophagy and its controversial roles in cancer. *Biomolecules and Therapeutics* (27) (**2019**).

404. Taschner, M., Bhogaraju, S. & Lorentzen, E. Architecture and function of IFT complex proteins in ciliogenesis. *Differentiation* (83) (**2012**).

405. Liu, Y. C. *et al*. The PPFIA1-PP2A protein complex promotes trafficking of Kif7 to the ciliary tip and Hedgehog signaling. *Sci. Signal*. (7) (**2014**).

406. Ponniah, P. *et al.* Striatin is required for hearing and affects inner hair cells and ribbon synapses. *biorxiv* (March 11), (**2020**).

407. Kim, M., Kim, M., Lee, M. S., Kim, C. H. & Lim, D. S. The MST1/2-SAV1 complex of the Hippo pathway promotes ciliogenesis. *Nat. Commun*. (5) (**2014**).

408. Mezarino, V. M. S. Characterization of Protein Interactions by Mass Spectrometry and Bioinformatics. (*Ludwig–Maximilians–Universität München*, **2019**).

409. Wang, X., Chang, Y., Li, Y., Zhang, X. & Goodrich, D. W. Thoc1/Hpr1/p84 Is Essential for Early Embryonic Development in the Mouse. *Mol. Cell. Biol*. (26) (**2006**).

410. Alberts, A. S. *et al*. Protein phosphatase 2A potentiates activity of promoters containing AP-1-binding elements. *Mol. Cell. Biol.* (13) (**1993**).

411. Buss, W. C., Stepanek, J. & Queen, S. A. Association of tissue-specific changes in translation elongation after cyclosporin with changes in elongation factor 2 phosphorylation. *Biochem. Pharmacol*. (48) (**1994**).

412. Bohlen, J., Fenzl, K., Kramer, G., Bukau, B. & Teleman, A. A. Selective 40S Footprinting Reveals Cap-Tethered Ribosome Scanning in Human Cells. *Mol. Cell* (79) (**2020**).

413. Moore, G. P. M., Lintern-Moore, S., Peters, H. & Faber, M. RNA synthesis in the mouse oocyte. *J. Cell Biol.* (60) (**1974**).

414. Oakberg, E. F. Relationship between stage of follicular development and RNA synthesis in the mouse oocyte. *Mutat. Res. - Fundam. Mol. Mech. Mutagen*. (6) (**1968**).

415. Smyth, J. T., Beg, A. M., Wu, S., Putney, J. W. & Rusan, N. M. Phosphoregulation of STIM1 leads to exclusion of the endoplasmic reticulum from the mitotic spindle. *Curr. Biol*. (22) (**2012**).

416. Schlaitz, A. L., Thompson, J., Wong, C. C. L., Yates, J. R. & Heald, R. REEP3/4 ensure endoplasmic reticulum clearance from metaphase chromatin and proper nuclear envelope architecture. *Dev. Cell* (26) (**2013**).

417. Olsen, J. V *et al.* Quantitative Phosphoproteomics Reveals Widespread Full Phosphorylation Site Occupancy During Mitosis *Science Signaling* (3) (**2010**).

418. Kettenbach, A. N. *et al.* Quantitative phosphoproteomics identifies substrates and functional modules of Aurora and Polo-like kinase activities in mitotic cells. *Sci. Signal.* (4) (**2011**).

419. McNally, F. J. & Thomas, S. Katanin is responsible for the M-phase microtubulesevering activity in *Xenopus* eggs. *Mol.*

Biol. Cell (9) (**1998**).

420. Gardner, M. K., Zanic, M., Gell, C., Bormuth, V. & Howard, J. Depolymerizing kinesins Kip3 and MCAK shape cellular microtubule architecture by differential control of catastrophe. *Cell* (147) (**2011**).